



Applications of Density Functional Theory (DFT) in Organic and Inorganic Reactions

by

Ali Gouranourimi

School of Natural Sciences - Chemistry

Submitted in fulfilment of the requirements for the Doctor of Philosophy

University of Tasmania

March 2019

Declaration of Originality

This thesis contains no material which has been accepted for a degree or diploma by the University or any other institution, except by way of background information and duly acknowledged in the thesis, and to the best of my knowledge and belief no material previously published or written by another person except where due acknowledgement is made in the text of the thesis, nor does the thesis contain any material that infringes copyright.

Ali Gouranourimi

21 March 2019

Authority of Access

This thesis is not to be made available for loan or copying for two years following the date this statement was signed. Following that time, the thesis may be made available for loan and limited copying and communication in accordance with the Copyright Act 1968.

Statement of Co-Authorship

The following people and institutions contributed to the publication of work undertaken as part of this thesis:

Candidate: Ali Gouranourimi (University of Tasmania)

Author 1: Alireza Ariafard (University of Tasmania)

Author 2: Brian F. Yates (University of Tasmania)

Author 3: Antony Chipman (University of Tasmania)

Author 4: Rasool Babaahmadi (University of Tasmania)

Author 5: Angus Olding (University of Tasmania)

Author 6: Jianwen Jin (Monash University)

Author 7: Yichao Zhao (Monash University)

Author 8: Philip Wai Hong Chan (Monash University)

Contribution of work by Co-authors for each paper:

Paper 1: Located in Chapter 4

1. **A. Gouranourimi**; A. Chipman; R. Babaahmadi; A. Olding; B. F. Yates; A. Ariafard, *Nazarov Cyclisation Initiated by DDQ-Oxidized Pentadienyl Ether: A Mechanistic Investigation from the DFT Perspective*, *Org. Biomol. Chem.* **2018**, *16*, 9021-9029. (**Hot Paper, Chapter 4**)

Author contributions:

Conceived and designed experiment: Candidate, Alireza Ariafard, Brian F. Yates

Performed the experiments: Candidate

Analysed the data: Candidate, Alireza Ariafard, Brian F. Yates

Wrote the manuscript: Candidate, Alireza Ariafard, Brian F. Yates

Paper 2: Located in chapter 5

2. J. Jin; Y. Zhao; **A. Gouranourimi**; A. Ariafard; P. W. H. Chan, *Mechanistic Investigation of Chiral Brønsted Acid Catalyzed Enantioselective Dehydrative Nazarov-type Electrocyclization (DNE) of Aryl and 2-Thienyl Vinyl*

Alcohols, J. Am. Chem. Soc. 2018, 140, 5834-5841. (Chapter 5)

Author contributions:

Conceived and designed experiment: Philip Wai Hong Chan

Performed the experimental section: Jianwen Jin

Performed the computational section: Candidate

Analysed the computational data: Candidate, Alireza Ariaferd

Wrote the computational section of the manuscript: Candidate, Alireza Ariaferd

Paper 3: Located in chapter 6

3. A. Chipman; A. Gouranourimi; K. Farshadfar; A. Olding; B. F. Yates; A. Ariaferd,
*A Computational Mechanistic Investigation into Reduction of Gold(III) Complexes
by Amino Acid Glycine: A New Variant for Amine Oxidation*, Chem. Eur. J. 2018,
24, 8361-8368. (Hot Paper, Chapter 6)

Conceived and designed experiment: Candidate, Alireza Ariaferd, Brian F. Yates

Performed the experiments: Candidate, Antony Chipman

Analysed the data: Candidate, Alireza Ariaferd, Brian F. Yates

Wrote the manuscript: Candidate, Antony Chipman, Alireza Ariaferd, Brian F. Yates

We, the undersigned, endorse the above stated contribution of work undertaken for each of
the published (or submitted) peer-reviewed manuscripts contributing to this thesis:

Signed: _____

Ali
Gouranourimi
Candidate
<School of Natural
Sciences> University
of Tasmania

Brian F. Yates
Primary Supervisor
<School of Natural
Sciences > University
of Tasmania

Simon Ellingsen
Head of School
<School of Natural
Sciences > University
of Tasmania

Date: _____

27/09/2019

Sep 30, 2019

30/9/2019

Acknowledgment

Many people need to be thanked for all the kindness and support I received during my PhD candidature period. First of all, to my supervisors Assoc. Prof. Alireza Ariaferd and Prof. Brian F. Yates. I owe a lot to both for leading and mentoring me throughout. To all the other PhD and Honours students as well as other academics and postdocs within the synthesis group for all their help in many aspects of research, coursework, presentations and companionship. Special thanks to Prof. Allan Canty, Dr. Alex Bissember, Assoc. Prof. Jason Smith, Rasool Babaahmadi, and Anthony Chipman for helping me during my PhD. And finally, to my friends and family for their unconditional love and support.

Publications and Presentation Resulting from Research Described in this Thesis:

Peer-Reviewed Journals:

1. **A. Gouranourimi**; A. Chipman; R. Babaahmadi; A. Olding; B. F. Yates; A. Ariafard, *Nazarov Cyclisation Initiated by DDQ-Oxidized Pentadienyl Ether: A Mechanistic Investigation from the DFT Perspective*, *Org. Biomol. Chem.* **2018**, 16, 9021-9029. (**Hot Paper, Chapter 4**)
2. J. Jin; Y. Zhao; **A. Gouranourimi**; A. Ariafard; P. W. H. Chan, *Mechanistic Investigation of Chiral Brønsted Acid Catalyzed Enantioselective Dehydrative Nazarov-type Electrocyclization (DNE) of Aryl and 2-Thienyl Vinyl Alcohols*, *J. Am. Chem. Soc.* **2018**, 140, 5834-5841. (**Chapter 5**)
3. A. Chipman; **A. Gouranourimi**; K. Farshadfar; A. Olding; B. F. Yates; A. Ariafard, *A Computational Mechanistic Investigation into Reduction of Gold(III) Complexes by Amino Acid Glycine: A New Variant for Amine Oxidation*, *Chem. Eur. J.* **2018**, 24, 8361-8368. (**Hot Paper, Chapter 6**)
4. **Ali Gouranourimi**; Alex Bissember, *Development of a Novel Application of Amino-Cope Rearrangement and its Anionic Variant*, **The 41st Annual Synthesis Symposium**, Melbourne, The University of Melbourne, 2016 (Poster presentation).
5. **Ali Gouranourimi**; Alireza Ariafard; Brian. F. Yates, *Nazarov Cyclization Initiated by DDQ-Oxidized Pentadienyl Ether: A Mechanistic Investigation from the DFT Perspective*, **Organic 18 RACI Organic Division National Conference**, Perth, WA, 2018 (Poster presentation).

Abbreviations

The following abbreviations have been used throughout this thesis:

°	degree(s)
°C	degrees Celsius
δ	chemical shift (parts per million)
λ	wavelength (nm)
Å	Ångstrom
ACR	Amino Cope Rearrangement
Ar	unspecified aryl group
BDE	bond dissociation energy
Boc	<i>tertiary</i> butoxycarbonyl
bpy	2,2-bipyridine
br	broad
Bu	butyl
B3LYP	DFT functional
BOX	bis(oxazoline)
BQ	benzoquinone
BS1	basis set one
BS2	basis set two
cm	centimetre(s)
CDC	cross-dehydrogenative coupling
CPCM	conductor-like polarized continuum model
d	doublet
DFT	Density Functional Theory
DMDT	N,N-dimethylthiocarbamate
DNE	dehydrative Nazarov-type electrocyclisation
DDQ	2,3-dichloro-5,6-dicyano-1,4-benzoquinone
DEF2-TZVP	basis set

EI	electron impact (mass spectrometry)
Et	ethyl
ESDT	ethylsarcosinedithiocarbamate
EtOAc	ethyl acetate
ee	enantiomeric excess
g	grams(s)
G09	Gaussian 09 program
G16	Gaussian 16 program
GBS	general basis set
GSH	glutathione
Gly	glycine
GA	glyoxylate
h	hour(s)
HOMO	highest occupied molecular orbital
HPLC	high performance liquid chromatography
IRC	intrinsic reaction coordinate
LUMO	lowest unoccupied molecular orbital
LANL2DZ	basis set
m	multiple
<i>m</i>	<i>meta</i>
Me	methyl
min	minute(s)
MECP	minimum energy crossing point
mmol	millimole(s)
mg	milligram
mL	millilitre(s)
mmol	millimole(s)
MPA-MB-231	density functional
nm	nanometer(s)
NBO	natural bond orbital
NMR	nuclear magnetic resonance

NHC	N-heterocyclic carbene
o	<i>ortho</i>
ORTEP	Oak Ridge Thermal-Ellipsoid Plot Program
OMe	Methoxy
<i>p</i>	<i>para</i>
Ph	Phenyl
pK _a	acid dissociation constant
ppm	parts per million
<i>i</i> Pr	isopropyl
<i>q</i>	quartet
R	unspecified alkyl group
r.t.	room temperature
s	singlet
SET	single electron transfer
SMD	solvation model based on density
t	triplet
TPP	tripolyphosphate
THF	tetrahydrofuran
TLC	thin layer chromatography
TMS	trimethylsilyl
UV	ultra violet

Abstract

The first chapter provides a brief introduction to the computational methods used in this thesis.

The second and third chapters of this thesis, "Amino-Cope Rearrangement and its anionic form: a mechanistic study from the DFT perspective" and "Development of a Novel Application of the Amino-Cope Rearrangement", outline the development of an original, unified synthetic strategy that will provide conspicuous and distinctive access to a range of structurally diverse lycopodium, cylindricine, and lepadiformine alkaloids and their derivatives. Specifically, this is achieved by establishing an unprecedented method for the efficient preparation of annulated medium-size *N*-heterocycles *via* the novel application of an anionic Amino-Cope Rearrangement (ACR). In addition to identifying and defining new synthetic strategies, the results in these chapters will improve the ability to construct complex biologically significant compounds, enhance fundamental understanding of organic molecules and explore key principles of chemical reactivity and mechanism. The Amino-Cope Rearrangement and its anionic form have been investigated mechanistically and experimentally in these chapters. Progress in synthesis is a few steps away from making the Amino-Cope Rearrangement substrate required to provide the product after the rearrangement. From a mechanistic point of view, different kinds of this rearrangement were explored: Neutral ACR, metallated ACR, and naked ACR, finding that while the neutral ACR proceeds *via* a concerted pathway, metallated and naked ACR goes through the step-wise mechanism. With the information from the DFT results, it is anticipated that the rearrangement on the substrate will be able to be performed in the future in order to investigate this area more deeply.

In the fourth and fifth chapters of this thesis, an important organic reaction called Nazarov cyclization is explored. In the fourth chapter, DFT has been utilised to study the mechanism of Nazarov cyclisations initiated by oxidation of pentadienyl ethers by a benzoquinone derivative (DDQ), as recently reported experimentally by West et al. (Angew. Chem. Int. Ed., **2017**, 56, 6335). It was found that the reaction is most likely initiated by a hydride transfer from the pentadienyl ether to an oxygen of DDQ through a concerted pathway and not a single electron transfer mechanism. Interestingly, an excellent correlation

between the hydride transfer activation energy and the gap between the ether HOMO and the benzoquinone LUMO ($R^2=0.99$) was found. Based on this correlation, a formula for predicting the activation energy of the oxidation process mediated by DDQ is provided.

In the fifth chapter, an efficient chiral Brønsted acid-catalyzed enantioselective Dehydrative Nazarov-type Electrocyclization (DNE) of electron-rich aryl- and 2-thienyl- β -amino-2-en-1-ols is described. The 4π conrotatory electrocyclization reaction affords access to a wide variety of the corresponding 1H-indenes and 4H-cyclopenta[b]thiophenes in excellent yields of up to 99% and enantiomeric excess (ee) values of up to 99%. Computational studies based on a proposed intimate contact ion-pair species that is further assisted by hydrogen bonding between the amino group of the substrate cation and chiral catalyst anion provide insight into the observed product enantioselectivities.

Since cancer remains among the most widespread and difficult to cure diseases, and often involves problems due to the use of cisplatin, the most common drug for cancer treatment currently, finding an alternative drug which shows the same properties of cisplatin without side effects is highly desirable. Recently, gold complexes, especially in the oxidation state of +III, have enjoyed renewed interest in this field, mainly because platinum(II) and gold(III) have the same isoelectronic configuration (d^8). As a result, the last chapter of this thesis, which talks about gold chemistry, provides a mechanistic exploration of the reduction of gold(III) complexes by the amino acid glycine. Interestingly, when the nitrogen atom of glycine coordinates to the gold(III) centre, its C^α -hydrogen atom becomes so acidic that it can be easily deprotonated. This deprotonation, that can be facilitated by a mild base, converts the amino acid into a potent reductant by which gold(III) is reduced to gold(I) with a moderate activation energy. Apparently, this is the first investigation suggesting that primary amines are oxidized to imines via direct α -carbon deprotonation. This work also provides a rationalization behind why gold(III) complexes with amine-based polydentate ligands are reluctant to undergo a redox process.

Table of Contents

Chapter One

Introduction to Density-Functional Theory (DFT) 1

1.1	Introduction	1
1.2	The Rise of Density-Functional Theory	2
1.3	Methods in Density-Functional Theory	3
1.4	Advantages of Density-Functional Theory	3
1.5	Application of Density-Functional Theory	4
1.6	Challenges for Density-Functional Theory	4
1.7	Hybrid Methods in Density-Functional Theory	5
1.8	Basis sets in density-Functional Theory	6
1.9	Diffuse Functions	7
1.10	Summary	8
1.11	References	9

Chapter Two

Amino-Cope Rearrangement and its Anionic Variant: A Mechanistic Study from the DFT Perspective 11

2.1	Introduction	11
2.1.1	Pericyclic reactions in organic synthesis	11
2.1.2	[3,3] Sigmatropic rearrangement	12
2.1.3	Cope rearrangement	13
2.2	Amino-Cope Rearrangement and its Anionic Variant	14

2.2.1	<i>The neutral Amino-Cope Rearrangement</i>	14
2.2.2	<i>The Amino-Cope Rearrangement with a metal counterion</i>	15
2.3	Computational Study	19
2.4	Results and Discussion	20
2.4.1	<i>Neutral Amino-Cope Rearrangement</i>	20
2.4.2	<i>Amino-Cope Rearrangement with a metal counterion</i>	24
2.4.3	<i>Anionic Amino-Cope Rearrangement (Naked ACR)</i>	27
2.5	Conclusions	28
2.6	References	30

Chapter Three

<i>Development of a Novel Synthetic Application of the Anionic Amino-Cope Rearrangement</i>		32
3.1	Introduction	32
3.2	Development of the Amino-Cope Rearrangement	33
3.3	Synthetic Applications of the Amino-Cope Rearrangement	36
3.4	Results and Discussion	40
3.4.1	<i>Synthesis of compound 25</i>	41
3.4.2	<i>Synthesis of compound 25a</i>	42
3.4.3	<i>Generation of compound 26</i>	43
3.4.4	<i>Formation of vinyl borinane 27</i>	43
3.4.5	<i>Formation of compound 28</i>	44
3.4.6	<i>Generation of compound 29b</i>	45
3.4.7	<i>Formation of compound 29</i>	45
3.4.8	<i>Formation of compound ACRS31</i>	48
3.4.9	<i>Formation of compound 35</i>	49
3.5	Conclusion	50
3.6	Experimental Procedures and Data	51
3.7	References	56

Chapter Four

Nazarov Cyclisations Initiated by DDQ-Oxidised Pentadienyl Ether: A Mechanistic Investigation from the DFT Perspective

4.1	Introduction	58
4.2	Computational Study	63
4.3	Results and Discussion	64
4.3.1	<i>Substitution effects of the dienes substrate on the ease of the C-H bond cleavage</i>	67
4.3.2	<i>Substitution effects of benzoquinone on the hydride transfer mechanism</i>	70
4.3.3	<i>A predictive formula for the reactivity of C-H bond cleavage</i>	72
4.3.4	<i>Application of predictive formula for substrates with ortho-substituted aryl rings</i>	74
4.4	Conclusion	75
4.5	References	76

Chapter Five

Mechanistic Investigation of Chiral Bronsted Acid Catalyzed enantioselective Dehydrative Nazarov-type Electrocyclisation (DNE) of Aryl and 2-Thienyl Vinyl Alcohols

5.1	Introduction	79
5.2	Enantioselective Dehydrative Nazarov-type Electrocyclization (DNE)	82
5.3	Computational Study	84
5.4	Results and Discussion	85
5.5	Conclusion	96
5.6	References	97

Chapter Six

A Computational Mechanistic Investigation into Reduction of Gold(III) Complexes by the Amino Acid Glycine: A New Variant for Amine Oxidation

6.1	Introduction	101
6.1.1	<i>The origin of gold therapy</i>	102
6.1.2	<i>Gold(III) anticancer complexes</i>	103
6.1.3	<i>Au(III) reducing agents in the human body</i>	104
6.2	Computational Details	106
6.3	Results and Discussion	110
6.3.1	<i>Can the redox reaction proceed through intermediate 6?</i>	114
6.3.2	<i>Chelate effect</i>	116
6.3.3	<i>Impact of carboxylic acid functional group on the redox activation energy</i>	119
6.3.4	<i>An alternative mechanism for amino acid oxidation via decarboxylation</i>	119
6.3.5	<i>Hydrolysis of protonated imine</i>	121
6.3.6	<i>Oxidative decarboxylation of glyoxylic acid</i>	123
6.3.7	<i>Summary of the novel proposed mechanism for reduction of Au(III)</i>	126
6.4	Conclusion	126
6.5	References	128

Appendix

A.1	Publications	133
------------	---------------------	------------

Chapter One

Introduction to Density-Functional Theory (DFT)

1.1 Introduction

Density Functional Theory (DFT) is a popular computational modelling method that derives characteristics of the molecule depending on a determination of the electron density of the molecule.^{1,2,3} Although its formal beginning was in 1964, when it was discovered by Kohn and Sham, the formative years were 1980–2010.³ It is widely accepted that Kohn-Sham density-functional theory (KS-DFT) is the most popular electronic method in computational chemistry, which stems from its favourable computational cost to accuracy ratio.³

The intuitive roots of DFT predate the primitive Kohn-Sham publications in 1964 by many years.⁴ Fermi and Thomas suggested that the exchange and kinetic energies of a system with many electrons can be locally modelled by the uniform electron gas energy densities.^{5,6} Their discoveries led to an approximate theory of electronic structure named Thomas-Fermi-Dirac Theory (TFD) which is based only on the total electronic density $\varphi(\mathbf{r})$. Although the TFD method is remarkably simple, it fails quantitatively which is mainly because it is not able to self-consistently reproduce atomic shell structure. TFD energies have errors of about 10%, which is too high for computational purposes.³ Following this, Teller proposed that Thomas-Fermi theory cannot explain molecular interactions and it is only useful for determining atomic features.⁷

Shell structure is an outcome of the Pauli exclusion rule and derives from electron pairs in orthonormal orbitals organized in Slater determinants. Hartree-Fock (HF) theory is a straightforward implementation of this. HF theory is considerably more useful than TFD, however it still suffers from inaccurate predictions in chemistry.⁸ For example, molecules such as F_2 are not bound at the Hartree-Fock level. To address these problems, it was suggested that post-HF methods, adding to the original HF method, are normally needed for viable chemical computations due to their potential to recover the correlation energy.^{9,10} Post HF theory is well established and considered as a method which is capable of great accuracy, but computationally very expensive.^{9,10} In addition, calculation of HF orbitals in condensed-matter systems was unavailable. Following this, Slater suggested a solution in which he replaced the HF exchange operator with an orbital average, named the Slater potential.¹¹ It is widely accepted that the Hartree-Fock-Slater (HFS) method can be considered as the ancestor of modern DFT.^{11,12,13}

1.2 The Rise of Density-Functional Theory:

Although the modified Hartree-Fock method (HFS) was simple and successful in many cases, in fact it was a model, not a theory, which neglects both dynamic and static correlation energies.¹¹ As a result, the HFS method cannot address dynamic correlation and its contribution to kinetic energy.³

As mentioned above, in 1964, Hohenberg, Kohn, and Sham discovered the precise and powerful theory that was able to validate the intuitive ideas of Thomas, Fermi, Dirac, and Slater.^{5,6,11} Therefore, 1964 is considered as the birth year of novel DFT.³

DFT has become very popular among computational chemists, which is mainly because it is less computationally demanding but with similar accuracy to more sophisticated methods.³ The presumption behind density functional theory is that the energy of a molecule can be calculated from the electron density.

Kohn and Hohenberg proposed that calculation of the kinetic energy of the non-interacting electron density and treatment of the correction from this energy to

that of a real system has potential to evaluate the interaction of the system approximately.¹⁴ The modified non-interacting kinetic energy is called Exchange Correlation (XC) energy and is a function of the electron density.¹⁴ Since the electron density is defined as a function, the XC energy is a function of a function which is known as a Functional.¹⁴

1.3 Methods in Density-Functional Theory:

There are three main categories of density functional methods: (a) Local density approximation (LDA) methods, which assume that the electron density is homogenous throughout the molecule,¹⁵ (b) Generalized gradient approximation (GGA) methods that are used for the non-uniformity of the electron density such as meta-GGA (rung 3) and hybrid-meta-GGA (rung 4) methods that satisfies exact constraints without empirical parameters (M06-2X functional that used in this thesis),¹⁶ and (c) Hybrid methods, which are the most popular methods in computational chemistry and attempt to combine some of the more effective properties of *ab initio* methods such as HF with some of the advances of DFT theory (B3LYP functional that used in this thesis).¹⁷ Although in some cases LDA and GGA methods perform better than hybrid methods,¹⁴ these methods are normally more expensive than hybrid methods that can be considered as a drawback.^{15,16,17} Due to the importance of hybrid methods in computational chemistry, this method will be discussed later in this section in more detail.

1.4 Advantages of Density-Functional Theory:

The most important merit of DFT is that this method is an order three function, thus scaling as N^3 (N = number of basic functions) in contrast to comparable *ab initio* methods, which scale as N^4 .¹⁸ As a result, DFT calculations are relatively faster compared to other methods of similar accuracy.¹⁸ Furthermore, DFT methods overcome one of the main downsides of *ab initio* methods, such as Hartree-Fock, which is the neglecting of electron correlation. Electron correlation can be explained as the difference between the HF energy and the complete solution of the

Schrödinger equation. DFT methods have the potential to address this difference with no significant increase in calculation time.¹⁸

1.5 Applications of Density-Functional Theory:

DFT is a robust computational theory and can be used in many systems.¹⁹ Unlike *ab initio* methods which are not ideal for systems including metals, DFT methods are very helpful for these kinds of systems.¹⁹ Furthermore, some DFT methods are constructed for specific applications. For example, hybrid methods such as B3LYP are useful for reaction calculations, while methods like MPW1K are designed to solve kinetics problems.²⁰

1.6 Challenges for Density-Functional Theory:

Although density functional theory of electronic structure has made an unprecedented impact on the application of quantum mechanics, there are still a number of challenges to be resolved as described below:²¹

- 1- “Developing a functional that performs better than B3LYP” such as GGA methods in specific cases.²¹
- 2- “The need to improve the description of reaction barriers and dispersion/van der Waals interactions” with the help of non-local functionals with short-range repulsive behaviour.²¹
- 3- “To understand the significance of $E[p]$ vs $E[\{\phi_i, \epsilon_i\}]$ and beyond”²¹
- 4- “Avoiding delocalization error and static correlation error” with the help of the wave function.²¹
- 5- “The energy of two protons separated by infinity with one and two electrons: strong correlation”²¹

Following this, in 2008 Tirado and Jorgensen have investigated the possible advantages in accuracy that could be achieved from the DFT calculations over the semi-empirical method (PM3) when they are put on an even footing for computation

of the heats of formation for 622 different molecules.²² They only considered B3LYP functional and concluded from their results that there is no major difference in performance between the DFT and the semi-empirical method for the heats of formation and isomerization energies of those 622 molecules. Thus, the results confirm that PM3, as a semi-empirical method, is a useful alternative for computation of the energetics of organic reactions.²² In addition, it is suggested that in some cases, using semi-empirical methods such as AM1 and PM3 could be more helpful rather than DFT or HF methods.²³ This is mainly because semi-empirical methods like AM1 and PM3 are widely applicable for electronic structure calculations due to their capacity to treat larger systems at lower computational cost when compared to *ab initio* methods.²³

1.7 Hybrid Methods in Density-Functional Theory:

A big step toward higher accuracy in computational chemistry was the introduction of hybrid methods.²⁴ B3LYP, as a hybrid functional, is proposed to be the major work-horse in physical chemistry.²⁵ In addition, B3LYP can be considered as the most favoured density functional in chemistry. B3LYP represents 80% of the total occurrences of density functionals in the literature between 1990–2006.²⁵ However, it is proven that B3LYP is not appropriate for all computational purposes owing to some problems such as: (A) accumulating errors on heats of formation as the size of the system is increased;²⁵ (B) increasing errors on C–X bond energies with increased alkylation;²⁵ (C) failures to give reliable energy ordering of isomers;²⁵ (D) underestimation of reaction barrier heights;²⁵ and (E) breakdown in the description of van der Waals (vdW) interactions.²⁵

In 2004, Hu et al. suggested a neural network (NN) scheme to eliminate the failures of the B3LYP method to calculate the heats of formation some organic molecules.²⁶ Interestingly, they observed that the root-mean-square deviations of ΔH_f^θ decreased considerably using the NN correction.

Following this, in 2007, Xu and co-workers proposed a composite method for the calculation of the heats of formation for some molecules in the gas phase.²⁷ They combined their results at the level of B3LYP/6-311+G (3df,2p) with a NN correction

and concluded that this new B3LYP-NN method has the potential to correct the notorious size-dependent errors of B3LYP and decrease its mean absolute deviation (MAD) remarkably. This new B3LYP method, which is known as the X1 method, gives decent performance for large molecules or more diverse chemical structures.²⁷ However, in some cases, the B3LYP-NN method is not applicable to nonequilibrium geometric systems or to bond types that have not been assigned.²⁷

In order to carry out more investigation on DFT functionals, Yanai and co-workers proposed a new hybrid exchange-correlation functional named CAM-B3LYP.²⁸ They combined the hybrid qualities of B3LYP and Tawada's long-range correction²⁹ and demonstrated that this new method gives atomization energies of similar accuracy to those from B3LYP. Unlike the B3LYP method which is not appropriate for calculating the charge transfer energies, CAM-B3LYP performs well for charge transfer excitations in different models.²⁸ Nevertheless, CAM-B3LYP diatomic harmonic vibrational wavenumbers are not as accurate as those of the B3LYP method.²⁸

In summary, although there are some challenges in using hybrid methods, they are still some of the most popular and reliable models in computational chemistry.²⁵ We will use hybrid methods such as B3LYP and a range of other functionals in this thesis.

1.8 Basis sets in Density-Functional Theory:

A basis set is the mathematical definition of the orbitals in a system used for performing the theoretical calculation.³⁰ Larger basis sets approximate the orbitals more accurately, owing to the fewer restrictions imposed on the locations of the electrons in space. Standard basis sets created by using the linear combination of Gaussian functions in order to form the orbitals can calculate electronic structures. Gaussian, a popular computational chemistry program, contains a wide range of basis sets that can be classified by the number and types of their basis functions. There are different kinds of basis sets used in computational chemistry, as described below:

Minimal Basis Sets

Minimal basis sets involve the minimum number of basis functions required for each component, as in these examples:

H: 1s

C: 1s, 2s, 2p_x, 2p_y, 2p_z

Minimal basis sets such as STO-3G use fixed-size atomic-type orbitals. STO-3G uses three Gaussian primitives per basis function.³¹

Split Valence Basis Sets

Increasing the number of basis functions per atom is the first way to make the basis sets larger. Split valence basis sets, such as 3-21G and 6-31G, contain two or more sizes of basis function for each valence orbital.^{32a} For instance, hydrogen and carbon are represented as:

H: 1s, 1s'

C: 1s, 2s, 2s', 2p_x, 2p_y, 2p_z, 2p_x', 2p_y', 2p_z'

The Dunning–Huzinaga basis set (D95), which is one of the sub-classes of double zeta basis sets, forms all molecular orbitals from linear combinations of two sizes of functions for each atomic orbital.^{32b} Equivalently, basis sets such as 6-311G use three sizes of functions for each orbital type.^{32b}

Polarized Basis Sets

In contrast to split valence basis sets, which only allow orbitals to change size, polarized basis sets allow orbitals to change shape by adding orbitals with angular momentum beyond what is needed for the ground state to the definition of each atom.³³ Following this, one of the most popular polarized basis sets is 6-31G(d).³³ This basis set has become very common among computational chemists for calculations involving up to medium-sized systems.³³ Furthermore, another popular polarized basis set is 6-31G(d,p) that can add p functions to hydrogen atoms in addition to the d functions on heavier atoms.

1.9 Diffuse Functions

Diffuse functions are considered as large-size versions of s- and p-type functions, which allow orbitals to involve a larger region of space.³⁴ Basis sets with diffuse functions are important for systems where electrons are not close to the nucleus: systems in their excited states, calculation of absolute acidities, and so on.

The 6-31+G(d) is considered as the 6-31G(d) basis set with diffuse functions added to heavy atoms. The double plus version, 6-31++G(d), adds diffuse functions to the hydrogen atoms too.^{32b} Diffuse functions on hydrogen atoms rarely make an important difference in accuracy. It is reported that diffuse functions are needed to obtain an accurate structure for the anion by comparing the two calculated geometries to that predicted by Hartree-Fock theory with a very large basis set.³⁴

1.10 Summary

This brief introduction chapter is provided to justify the aim of this thesis which is investigation of different organic and inorganic reactions in chemistry by the help of DFT. As mentioned above, DFT is the most reliable method to explore various reactions in chemistry. Since experimental investigation alone is not comprehensive enough, including many ambiguities and unanswered questions, using DFT method to further explore the results obtained in the laboratory is highly desirable. DFT is the best method to explore different aspects of the reactions which cannot be explained by experimentalist such as reactivity, rate and mechanism of the reactions. In addition, with the assistance of DFT to gain further knowledge of the mechanism of different reactions, experimental protocols can often be improved. As a result, for each chapters of this thesis, a comprehensive DFT investigation is provided along with the experimental results to explain, justify, and predict the mechanistic features of the corresponding reactions.

1.11 References

- (1) R. M. Dreizler, J. Providencia, *Density Functional Methods in Physics*, Plenum Press, New York, **1985**.
- (2) R. G. Parr, W. Yang, *Density-Functional Theory of Atoms and Molecules*, Oxford University Press, New York, **1989**.
- (3) A. D. Becke, *The Journal of Chemical Physics*, **2014**, *140*, 18A301.
- (4) W. Kohn, L. J. Sham, *Phys. Rev.* **1965**, *136*, B864.
- (5) L. H. Thomas, *Proc. Cambridge Philos. Soc.* **1927**, *23*, 542.
- (6) E. Fermi, *Rend. Accad. Lincei*, **1927**, *6*, 602.
- (7) E. Teller, *Rev. mod. Phys.* **1962**, *34*, 627.
- (8) A. D. Becke, *J. Chem. Phys.* **1993**, *98*, 1372.
- (9) A. Szabo, N. S. Ostlund, *Modern Quantum Chemistry: Introduction to Advances Electronic Structure Theory*, McGraw-Hill, New York, **1989**.
- (10) I. N. Levine, *Quantum Chemistry*, 7th ed. Pearson Education Inc., **2014**.
- (11) J. C. Slater, *Phys. Rev.* **1951**, *81*, 385.
- (12) J. C. Slater, *The Self-Consistent Field for Molecules and Solids*, McGraw-Hill, New York, **1974**.
- (13) A. D. Becke, *J. Chem. Phys.* **1982**, *76*, 6037.
- (14) K. Burke, *J. Chem. Phys.* **2012**, *136*, 150901.
- (15) S. H. Vosko, L. Wilk, M. Nusair, *Can. J. Phys.*, **1980**, *58*, 1200.
- (16) (a) J. P. Perdew, Y. Wang, *Phys. Rev. B: Condens. Matter*, **1992**, *45*, 13244. (b) J. Tao, J. P. Pedrew, V. N. Staroverov, G. E. Scuseria, *Am. Phys. Soc.*, **2003**, *91*, 146401.
- (17) P. Mori-Sanchez, A. J. Cohen, W. T. Yang, *J. Chem. Phys.*, **2006**, *124*, 091102.
- (18) F. Neese, *J. Bio. Inorg. Chem.* **2006**, *11*, 702.
- (19) A. Chong, P. Delano, *Recent Advances in Density Functional Methods*, Part 1, World Scientific, **1995**.
- (20) B. J. Lynch, D. G. Truhlar, *J. Phys. Chem.* **2001**, *105*, 2936.
- (21) A. J. Cohen, P. Mori-Sanchez, W. Yang, *Chem. Rev.* **2011**, *112*, 289.

- (22) J. Tirado-Rives, W. L. Jorgensen, *Journal of Chemical Theory and Computation*, **2008**, 4, 297.
- (23) M. Elstner, K. J. Jalkanen, M. Knapp-Mohammady, T. Frauenheim, S. Suhai, *Chem. Phys.* **2001**, 263, 203.
- (24) Y. Zhao, D. G. Truhlar, *Theor. Chem. Acc.*, **2008**, 120, 215.
- (25) (a) I. Y. Zhang, J. Wu, X. Xin, *Chem. Commun.*, **2010**, 46, 3057. (b) L. A. Curtiss, K. Raghavachari, M. J. Redfern, J. A. Pople, *J. Chem. Phys.*, **2000**, 112, 7374. (c) M. D. Wodrich, C. Corminboeuf, R. Schleyer, *Org. Lett.*, **2006**, 8, 3631. (d) C. E. Check, T. M. Gilbert, *J. Org. Chem.*, **2005**, 70, 9828. (e) E. I. Izgorodina, M. L. Coote, L. Radom, *J. Phys. Chem. A*, **2005**, 109, 7558. (f) P. R. Schreiner, A. A. Fokin, R. A. Pascal, A. De Meijere, *Org. Lett.*, **2006**, 8, 3635. (g) Y. Zhao, N. Gonzalez-Garcia, D. G. Truhlar, *J. Phys. Chem. A*, **2005**, 109, 2012.
- (26) H. X. Wang, L. Wong, G. H. Chen, *J. Chem. Phys.*, **2003**, 119, 11501.
- (27) J. Wu, X. Wu, *J. Chem. Phys.*, **2007**, 127, 214105.
- (28) T. Yanai, D. Tew, N. Handy, *Chem. Phys. Lett.*, **2004**, 393, 51.
- (29) Y. Tawada, S. Tsuneda, S. Yanagisawa, T. Yanai, K. Hirao, *J. Chem. Phys.*, **2004**, 120, 8425.
- (30) M. B. Roman, *J. Chem. Phys.*, **2010**, 132, 231101.
- (31) D. Bernard, *J. Chem. Phys.*, **1990**, 92, 508.
- (32) (a) R. C. Binning, L. A. Curtiss, *J. Comp. Chem.*, **1990**, 12, 1206. (b) Foresman, J. Frish, E., 1996. Exploring chemistry. Gaussian Inc., Pittsburg, USA.
- (33) A. J. Sadlej, *J. Theor. Chimi. Act.*, **1991**, 79, 123.
- (34) C. E. Check, *J. Phys. Chem.*, **2001**, 105, 8111.

Chapter Two

Amino-Cope Rearrangement and its Anionic variant: A Mechanistic Study from the DFT Perspective

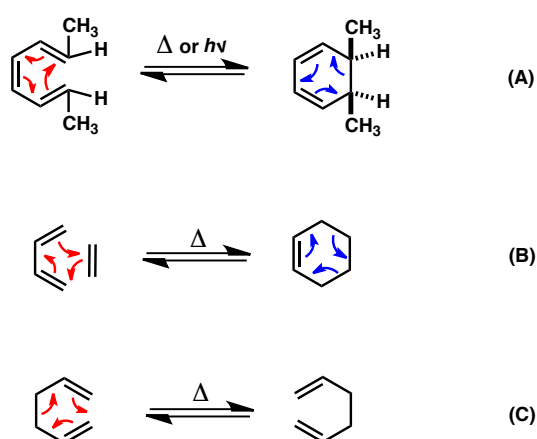
This chapter provides a mechanistic investigation of Amino-Cope Rearrangement (ACR) and its anionic variant. In recent years, these processes have been examined for use as a synthetic tool to construct carbon-carbon or carbon-heteroatom bonds. However, the mechanistic features and other applications of these interesting transformations have remained a matter of debate among chemists (12 reports in total). Therefore, this chapter focuses specifically on the mechanism of: neutral ACR, ACR with a metal counter-ion and anionic ACR of the 3-amino-1,5-diene derivatives.

2.1 Introduction: Overview of Mechanistic Features of the Cope Rearrangement

2.1.1 Pericyclic reactions in organic synthesis

In organic chemistry, there are many chemical reactions involving compounds containing multiple bonds in which the mechanism does not involve any kind of intermediate. Many of these reactions are classified by the forming and breaking of two or more bonds in a single concerted step through a cyclic transition state. These kinds of reactions are named as pericyclic reactions.¹ Electrocyclic reactions, cycloadditions, and sigmatropic rearrangements are three of the most common types of pericyclic reactions that have been studied extensively by organic chemists (Scheme 2.1.1).¹ An electrocyclization reaction is an intramolecular reaction, in which a new σ -bond is formed between the ends of a conjugated π -system, forming a cyclic product with one more ring and one less π -bond

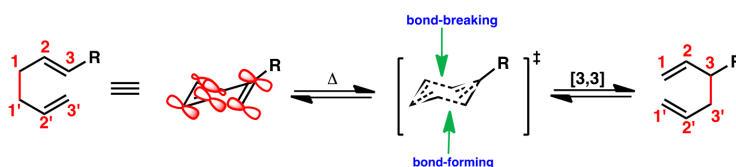
than the starting material (Scheme 2.1.1, (A)).^{2a} Another main sub-class of pericyclic reactions is cycloaddition processes, in which two or more unsaturated molecules (or parts of the same molecule) combine with the formation of a cyclic adduct with a net reduction of the bond multiplicity (Scheme 2.1.1, (B)).^{2b} The Diels-Alder reaction is a classic cycloaddition. The third major sub-class of pericyclic reactions is sigmatropic rearrangements. A sigmatropic rearrangement is a pericyclic reaction wherein one σ -bond is broken, and one σ -bond is formed in an uncatalyzed intramolecular process as shown in Scheme 2.1.1, (C).^{2c}



Scheme 2.1.1: (A): Electrocyclization process, (B): [4+2] cycloaddition, (C): [3,3]-sigmatropic rearrangement.

2.1.2 [3,3] Sigmatropic rearrangement

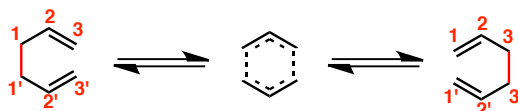
Among the fundamental chemical transformations in synthetic chemistry, the [3,3]-sigmatropic rearrangement is considered as a unique, powerful, and reliable method for the stereoselective synthesis of carbon-carbon or carbon-heteroatom bonds.³ From a mechanistic point of view, it is generally accepted that sigmatropic rearrangements proceed *via* a concerted pathway in which a σ -bond breaks and a new σ -bond forms at the same time (Scheme 2.1.2).^{2c} The most well-known of the [3,3]-sigmatropic reactions are the Cope rearrangement, Claisen rearrangement, and Fischer-indole synthesis.^{2c}



Scheme 2.1.2: [3,3]-sigmatropic rearrangement of 1,5-hexadiene.

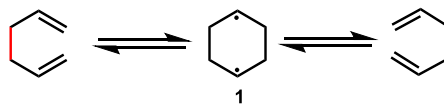
2.1.3 Cope rearrangement

The Cope rearrangement represents the simplest kind of [3,3]-sigmatropic reaction, mainly because the typical substrate for rearrangement (1,5-diene) does not contain any heteroatom substituents such as oxygen and nitrogen (Scheme 2.1.3).⁴ As shown in Scheme 2.1.3, the newly-formed σ -bond is between carbon 3 and 3'. The Cope rearrangement is considered as a concerted process and thought to progress through a cyclic transition state containing two partially bonded 3-carbon units, as shown in Scheme 2.1.3.⁴



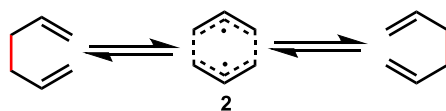
Scheme 2.1.3: The Cope rearrangement of a 1,5-diene.

A large number of investigations concerning the mechanistic features of the Cope rearrangement have been performed to find other feasible alternative transition states.⁴ Doering and co-workers were the first group to challenge the classical mechanistic proposal, suggesting an alternative pathway *via* a cyclohexane-1,4-diyil diradical intermediate **1** as shown in Scheme 2.1.4.⁵



Scheme 2.1.4: The Cope rearrangement with dyil diradical intermediate.⁵

Doering also proposed a stepwise mechanism involving the cleavage to two allyl radicals (**2**), but this was calculated to be thermodynamically unfavourable (Scheme 2.1.5).⁶



Scheme 2.1.5: The Cope rearrangement with two allyl radicals.⁶

However, Dewar and others have demonstrated that structural features, in particular the substituent on the diene, lead the Doering theory to be doubted.⁷ Dewar has shown that the location and type of the substituent can change the reaction rate. Finally, after performing a large number of computational examinations of Cope-related reactions, Schreiner proposed that biradical intermediates can be involved in the reaction route if they are stabilized by allylic resonance or aromaticity, in good agreement with previous studies, indicating that the [3,3]-sigmatropic rearrangement proceeds *via* a concerted mechanism.⁸ Previous mechanistic studies of the Cope-rearrangement suggest that, owing to the high reversibility and absence of any real thermodynamic driving force in the reaction, these rearrangements normally occur in harsh conditions such as high temperature (e.g. above 150 °C) (Scheme 2.1.1).⁹ To address these problems, it is suggested that the presence of a heteroatom such as nitrogen in the C-3 position of the 1,5-diene can make this reaction more facile, opening a new development in this field called the Amino-Cope Rearrangement (ACR).¹⁰

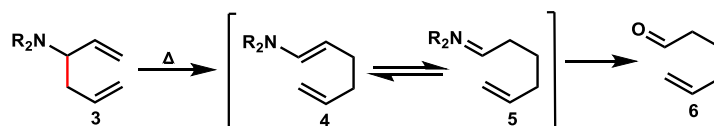
2.2 Amino-Cope Rearrangement and its Anionic Variant

2.2.1 The neutral Amino-Cope Rearrangement

The Amino-Cope Rearrangement and its anionic variant is an important sub-class of the Cope rearrangement in which its mechanism and applications are still a matter of debate.¹¹ There are very few examples of ACR in the literature (12 reports in total). The Oxy-Cope Rearrangement¹² resembles the Amino-Cope Rearrangement with an oxygen atom in place of the nitrogen atom at the C-3 position of the 1,5-diene (Scheme 2.2.1).

In 1965, Stogryn and Brios demonstrated that it is possible to improve the rate acceleration observed in the Oxy-Cope Rearrangement by replacing the hydroxyl group with a nitrogen at the 3-position of the diene (the Amino-Cope Rearrangement).^{10a} Their observations showed that, much like the Oxy-Cope Rearrangement, similar heating was required to facilitate the rearrangement. Nevertheless, by analogy to the Oxy-Cope

Rearrangement, the temperature needed is decreased when compared to the Cope rearrangement.

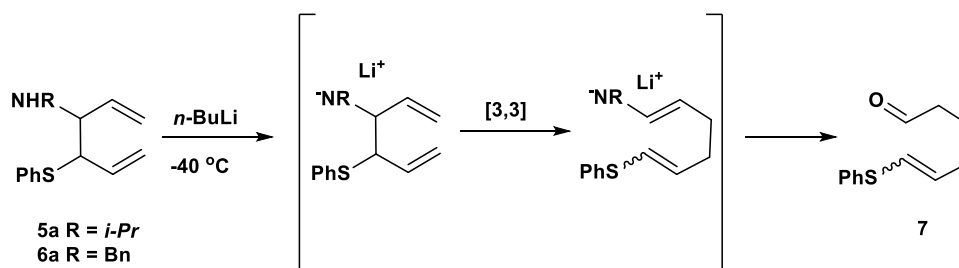


Scheme 2.2.1: Amino-Cope Rearrangement of 1,5-diene.

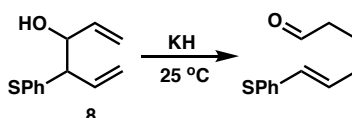
The Amino-Cope Rearrangement of 3-amino-1,5-diene **3**, gives the enamine **4**, which can be tautomerised to imine **5**, depending on the substitution of the amine, to make the final product thermodynamically more favourable. Hydrolysis of the imine then leads to aldehyde **6**, which is analogous to that obtained by the corresponding Oxy-Cope Rearrangement, and can be used for further synthetic chemistry.¹³

2.2.2 The Amino-Cope Rearrangement with a metal counterion

MacDonald was the first to report the remarkably facile charge accelerated Amino-Cope Rearrangement (Scheme 2.2.2), demonstrating similar properties to the corresponding anionic Oxy-Cope variant (Scheme 2.2.3), but at noticeably lower reaction temperatures (65°C lower).¹⁴ Amines **5a** and **6a** were constructed from the corresponding alcohol *via* tosylation, and rearrangement was achieved by deprotonation with *n*-BuLi at -40 °C, forming aldehyde **7** after acidic workup.¹⁴



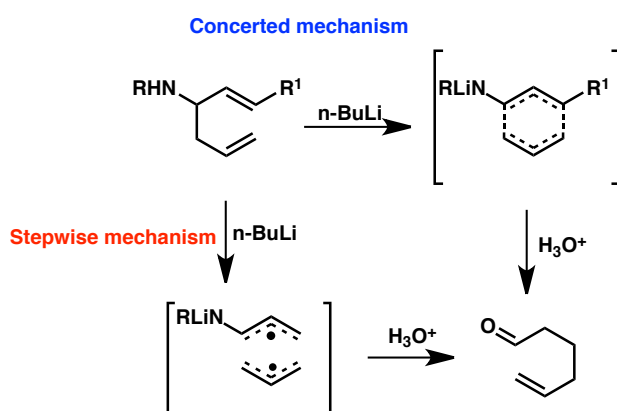
Scheme 2.2.2: Macdonald's first study of anionic Amino-Cope Rearrangement.¹⁴



Scheme 2.2.3: Charge-accelerated Oxy-Cope Rearrangement.^{12b}

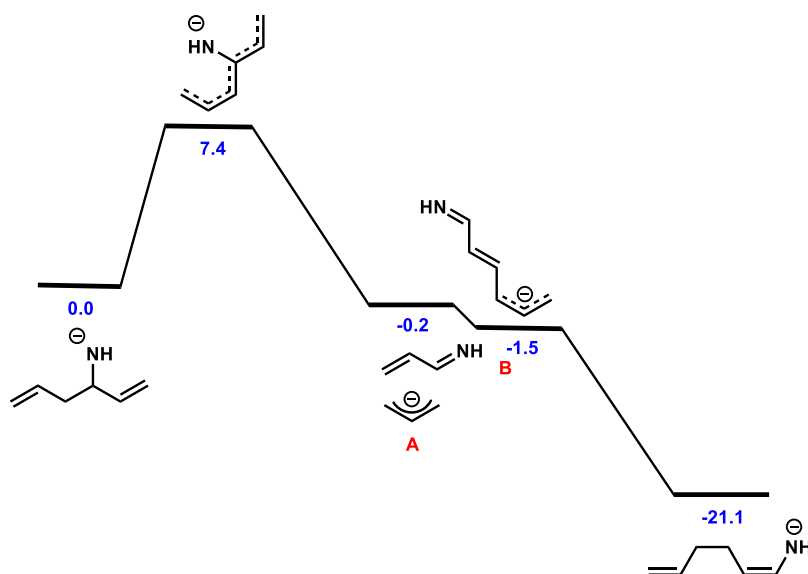
It is conspicuous that the Amino-Cope reaction of **5** and **6** (Scheme 2.2.2) takes place 65°C lower than the corresponding anionic Oxy-Cope reaction, using the potassium alkoxide formed from **8** and KH (25°C). This can be attributed to the increased basicity of the nitrogen anion compared to the oxyanion.^{13,14}

As mentioned above, mechanistic features of the ACR are not fully understood, with many ambiguities remaining. In particular, it is not clear whether the mechanism proceeds *via* a concerted or stepwise fashion (Scheme 2.2.4).



Scheme 2.2.4: Possible pathways for anionic Amino-Cope Rearrangements.

Houk and Meyers explored the rearrangement of 3-amino-1,5-dienes using *ab initio* studies, and compared them to those of the Oxy-Cope Rearrangement which is widely accepted to be concerted.¹⁵ After comparing the energies of the C-O bond dissociation in anionic Amino-Cope Rearrangements with those of the anionic oxy-Cope rearrangement, Houk and Meyers concluded that, in contrast to the oxy-Cope rearrangement pathway, the Amino-Cope mechanism is stepwise, including deallylation of the substrate *via* an imine/allyl anion intermediate and conjugate addition of the anion at the double bond terminal (Scheme 2.2.5).¹⁵ As shown in Scheme 2.2.5, the initial barrier to the rearrangement is 7.4 kcal/mol to form the intermediate stationary point **A**, containing an allyl anion and acrolein imine. Then, compound **B** gives the rearrangement product in an exothermic reaction, releasing 21.1 kcal/mol of energy.

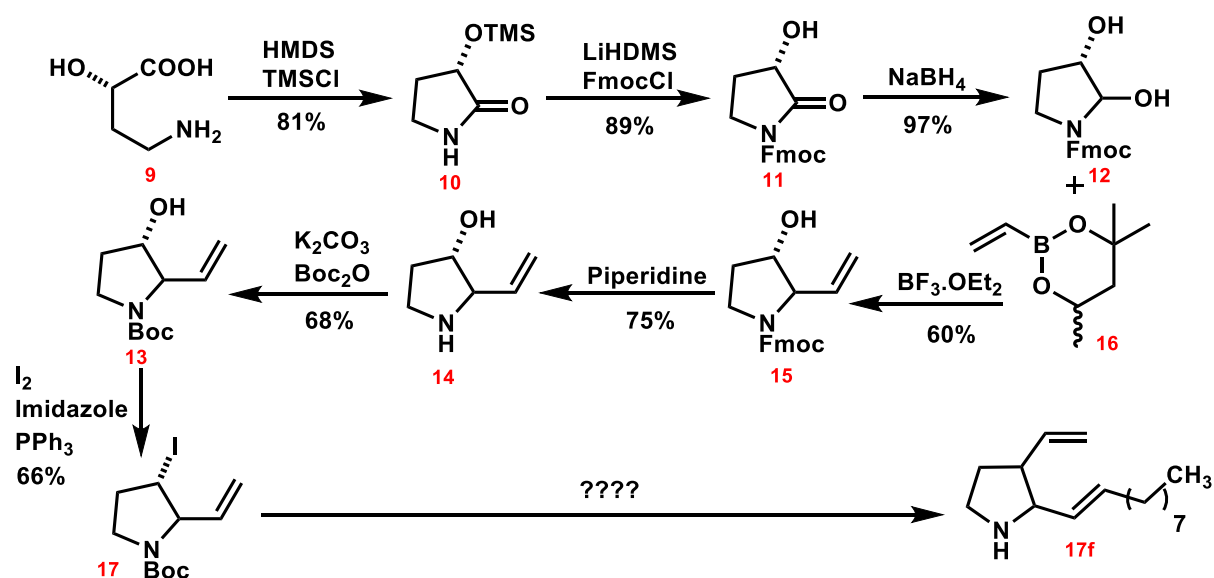


Scheme 2.2.5: Houk and co-worker's studies on Amino-Cope Rearrangement mechanism.¹⁵

Houk, in association with Haefner and Lee, has extended his original work and concluded that [3,3]-pericyclic rearrangements are promoted by heteroatom substituents such as oxygen and sulfur, which are not highly basic and therefore form more stable products.¹⁶ On the other hand, the heteroatom such as nitrogen, due to its higher basic characteristic compared to sulfur and oxygen, promotes a stepwise (cleavage/recombination) mechanism. Nevertheless, it was also suggested that the presence of a metal counterion (lithium) associated with the deprotonated compound has potential to stabilize the negative charge on the heteroatom and promote a concerted pathway.¹⁶ In contrast, Allin and co-workers examined different examples of highly stereoselective ACR, and proposed that a concerted pathway is operating.¹⁷

In conclusion, owing to limited computational studies regarding the mechanistic features of the ACR in the literature, the work described in this chapter aimed to investigate this transformation theoretically with the help of DFT. Since, theoretical or experimental studies alone are not comprehensive enough, synthesis of the Amino-Cope reaction starting material has been attempted to enable performance of the rearrangement. Scheme 2.2.6 shows progress. Further work to construct the ACR substrate will be undertaken in order to probe our computational results. This interesting synthetic pathway, which can further be

used to make different substituents of piperidine and pyrrolidine, will be discussed in detail in the next chapter of this thesis.



Scheme 2.2.6: Progress on making the ACR substrate.

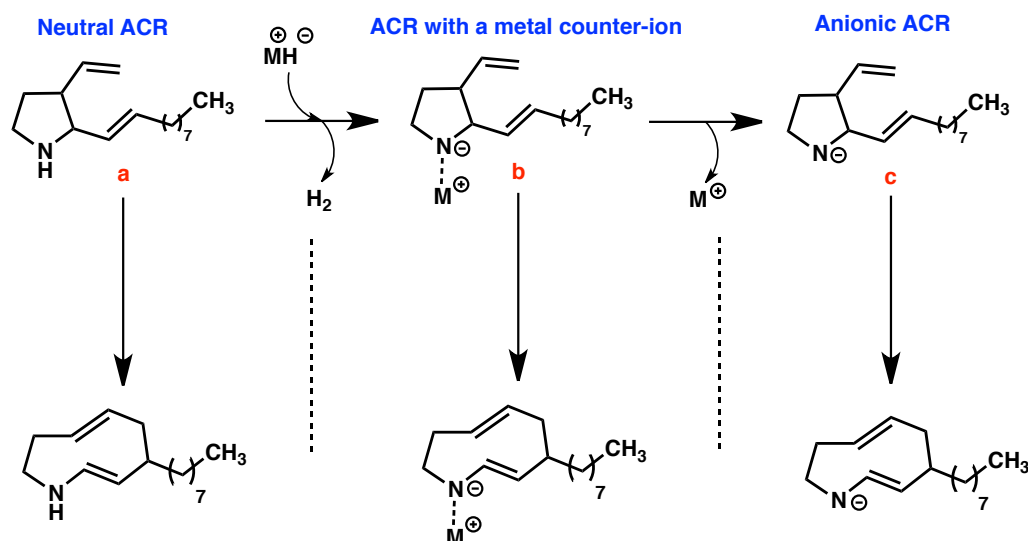
- All the calculations performed in this work have been done by the candidate in the computational chemistry laboratory (CCL) group at UTAS under supervision of Assoc. Prof. Alireza Ariafard and Prof. Brian F. Yates.

2.3 Computational Study

Gaussian 16¹⁸ was used to fully optimize all the structures involved in this study at the B3LYP level of density functional theory (DFT)¹⁹ in CH₂Cl₂ using the CPCM solvation model.²⁰ The 6-31G(d) basis set was used for all atoms.²¹ Frequency analyses were performed at the same level of theory to ensure that a minimum or transition structure was achieved. To further refine the energies obtained from the B3LYP/6-31G(d) calculations, single-point energy calculations for all of the structures with the 6-311+G(2d,p) basis set in CH₂Cl₂ using the CPCM solvation model at the M06 level were carried out to consider dispersion effect.²³ The Gibbs free energies obtained from the M06/6-311+G(2d,p)//B3LYP/6-31G(d) calculations in THF and toluene have been used throughout this chapter.

2.4 Results and Discussion

The discussion regarding the Amino-Cope Rearrangement (ACR) mechanism has been divided into three sections. In the first section, the focus is on the neutral Amino-Cope Rearrangement as depicted in Scheme 2.4, **a**. In the second section, the mechanistic features of a counterion system **b**, formed by replacing the nitrogen proton in compound **a** with an alkali metal cation (M^+) is explored. In the last part, the question of “how the ACR mechanism operates for an anionic compound such as **c**” will be answered computationally.

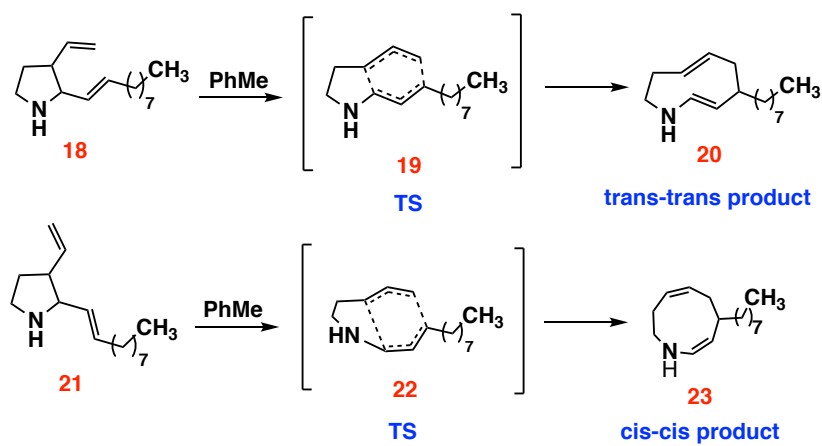


Scheme 2.4: Three different forms of Amino-Cope Rearrangement: (a) Neutral (b) metal counterion and (c) anionic.

2.4.1 Neutral Amino-Cope Rearrangement

To investigate the energy of the neutral Amino-Cope Rearrangement, two different conformers of starting material, that is **18** and **21**, were used. As shown in Scheme 2.4.1, in **18** both double bonds are positioned away from the pyrrolidine ring, whereas in **21** they are pointed toward the ring. It is inferred from the results that **18** is lower in energy than **21** by 0.8 kcal/mol (ΔG). The ACR of **18**, *via* transition structure **19**, leads to formation of the nine-membered ring product **20**, while that of **21** gives the product **23**. It is interesting to note that

the less stable substrate **21** gives the more stable product **23**. The *cis-cis* conformer product **23** is found to be lower in energy than *trans-trans* conformer **20** by 11.0 kcal/mol. This relatively huge difference in energies is probably because the ring strain in **23** is considerably decreased compared to that in product **20**. As illustrated in Figure 2.4.1, the C¹, C², C³ and H¹ atoms in **20** are not in the same plane, with a dihedral angle of 26°, whereas these atoms are nearly coplanar in **23**.



Scheme 2.4.1: Neutral Amino-Cope Rearrangement of two different conformers **18** and **21**.

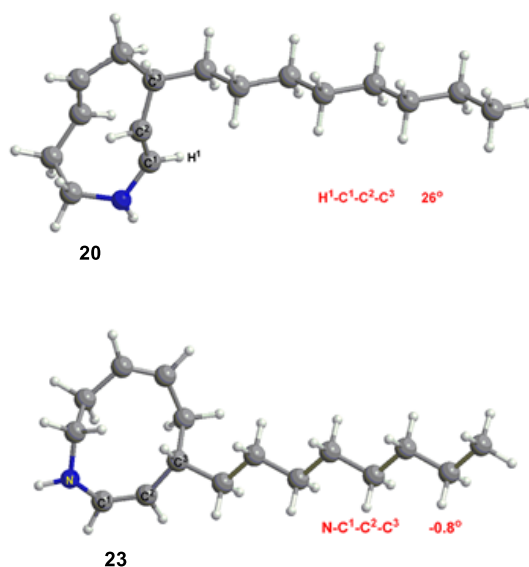


Figure 2.4.1: Ring strain and dihedral angles in the products **20** and **23**.

By looking at the frequency and vibrations of the located transition structures **19** and **22**, it can be seen that one bond is breaking, and another bond is forming at the same time. These observations confirm that the mechanism of the neutral ACR of two substrates **18** and **21** is concerted, consistent with Houk's proposal.¹⁵ As demonstrated in the ACR profile diagram, the corresponding reaction is considerably endergonic ($\Delta G > 0$) (Figure 2.4.2). Table 2.4.1 illustrates different activation energies for the ACR product obtained from different functional methods that have been used for this experiment. It is worth noting that the calculations on four different levels of theory showed the same trend as M06/6-311+G(2d,p)//B3LYP/6-31G(d), which strongly supports our results.

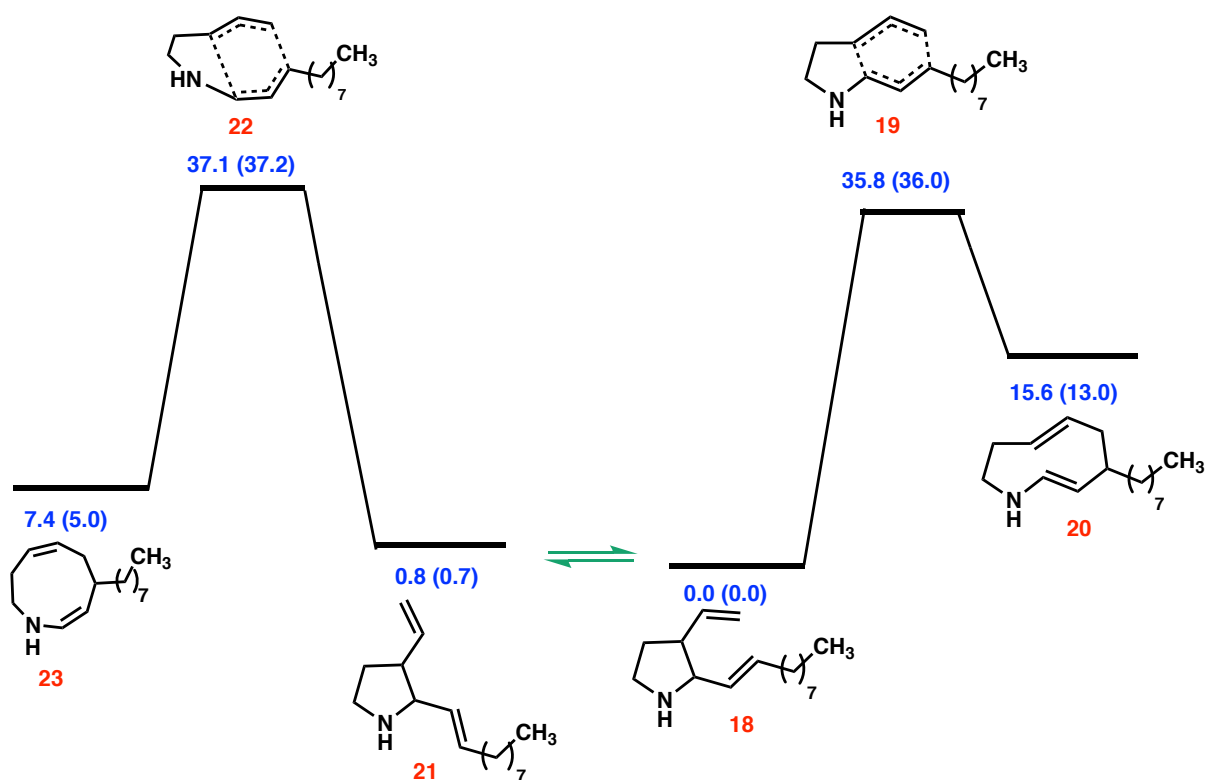


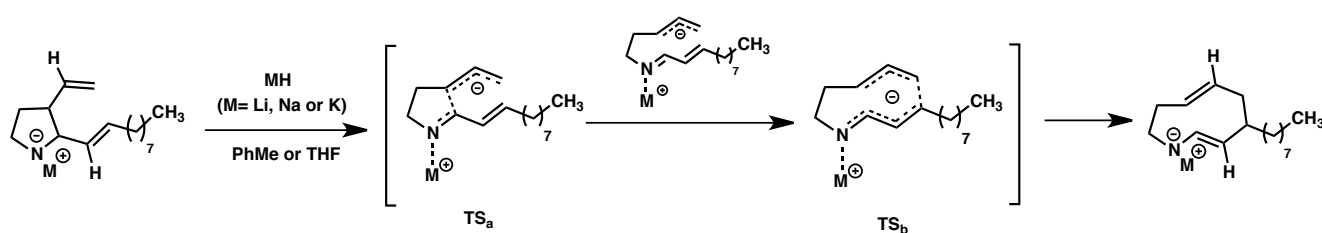
Figure 2.4.2: Energy profiles for the neutral Amino-Cope Rearrangement of substrates **18** and **21**, energies are given in kcal/mol. ($\Delta G(\Delta H)$)

Method	20	23
M06-CPCM/6-311+G(2d,p)//B3LYP-CPCM/6-31G(d)	15.6	7.4
M06-D3-CPCM/6-311+G(2d,p)//B3LYP-CPCM/6-31G(d) ²³	15	3.5
B3LYP-CPCM/6-311+G(2d,p)//B3LYP-CPCM/6-31G(d)	19.1	9.4
B3LYP-D3-CPCM/6-311+G(2d,p)//B3LYP-CPCM/6-31G(d)	18.7	6.5

Table 2.4.1: Relative Gibbs free energies (kcal/mol) of products **20** and **23** calculated with different single point methods. energies are given in kcal/mol.

2.4.2 Amino-Cope Rearrangement with a metal counterion

In 1998, Houk and co-workers explored the Amino-Cope Rearrangement with a metal counterion computationally in which they indicated that, by replacing the nitrogen proton with an alkali metal in the ACR substrate, the reaction mechanism is changed from concerted to stepwise.¹⁵ In this section, the aim is to explore the metallated ACR (Scheme 2.4, b), with different substrates to Houk's work, and report whether its mechanism proceeds *via* a concerted or stepwise pathway. To investigate the mechanistic features of ACR with a metal counterion, the same starting materials as the neutral ACR but with a metal (Li, Na or K) in place of the nitrogen proton are used (Scheme 2.4.2). A computational study is then carried out for metallated ACR to determine its mechanistic features. The general proposed pattern for these rearrangements is illustrated in Scheme 2.4.2. The rearrangement of the substrate *via* passing through the transition structures of **TS_a** and **TS_b**, gives the Amino-Cope product. Studying the frequency and vibrations of the located transition structures suggest that the rearrangement proceeds *via* a stepwise mechanism (dissociation-recombination). This is attributed to the strong π -donating ability of the nitrogen anion (Figure 2.4.3). Activation barriers and energies of different species for the rearrangement in different solvents are summarized in Table 2.4.2 and 2.4.2a.



Scheme 2.4.2: General proposed reaction of the ACR with a metal counter-ion.

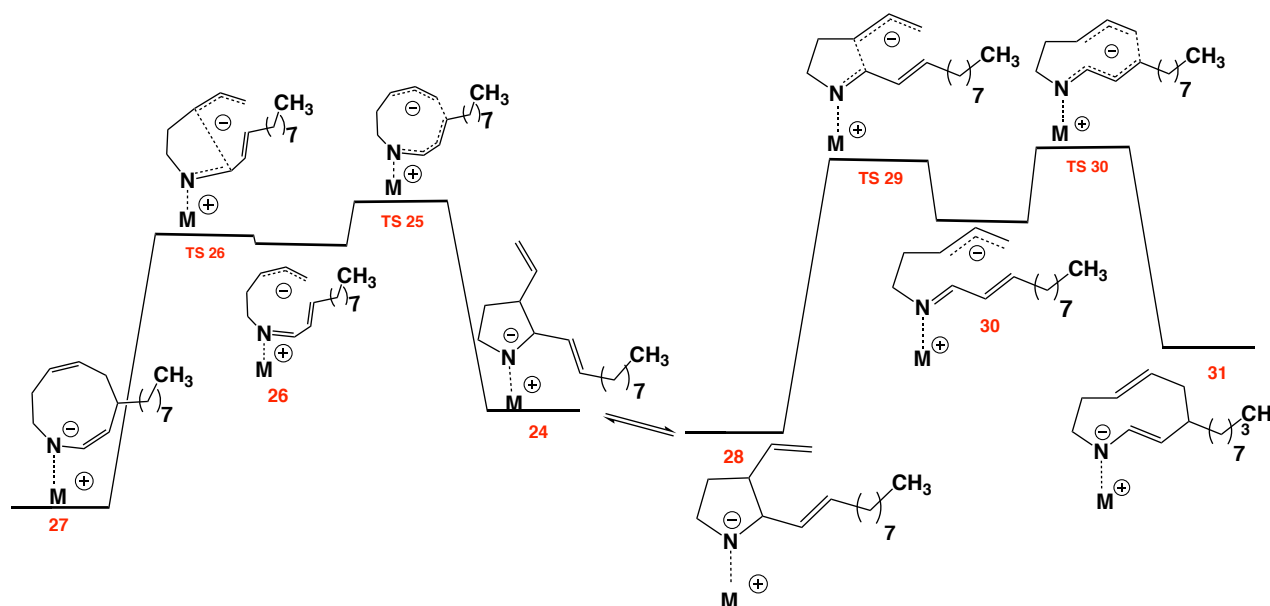


Figure 2.4.3: Energy profiles for the Amino-Cope Rearrangement with a metal counterion of substrates **24** and **28**.

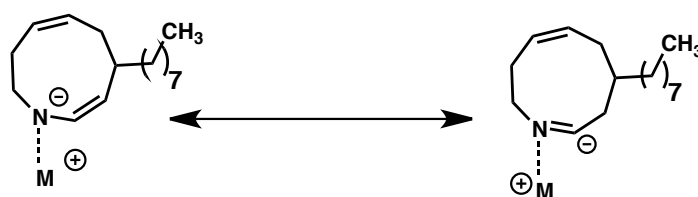
M	Solvent	24	TS 25	26	TS 26	27	28	TS 29	30	TS 30	31
Li	PhMe	2.8	26.7	24.9	27.5	-4.7	0.0	27.5	22.9	26.5	7.6
Na	PhMe	4.1	24.6	24.2	23.8	-5.5	0.0	23.8	22.2	23.8	6.5
K	PhMe	3.1	22.8	16.2	19.9	-6.6	0.0	22.0	16.0	22.5	5.8

Table 2.4.2: Relative Gibbs free energies (kcal/mol) of metallated ACR intermediates calculated in Toluene.

M	Solvent	24	TS 25	26	TS 26	27	28	TS 29	30	TS 30	31
Li	THF	3.2	23.4	22.5	22.7	-6.5	0.0	22.7	19.8	22.7	5.7
Na	THF	3.7	21.4	18.7	18.8	-7.6	0.0	20.2	19.7	19.0	4.2
K	THF	4.2	21.4	17.8	18.0	-7.8	0.0	20.1	14.2	19.5	4.1

Table 2.4.2a: Relative Gibbs free energies (kcal/mol) of metallated ACR intermediates calculated in THF.

It is inferred from the results that, as for the neutral case, the less stable substrate **24**, gives the more stable product **27**. The *cis-cis* conformer product **27** is found to be lower in energy than *trans-trans* product **31** by approximately 12.0 kcal/mol for all cases. As mentioned in the first section, the neutral ACR is noticeably endergonic whereas, in the metallated case, the corresponding reaction which leads to the *cis-cis* product **27**, is exergonic ($\Delta G < 0$) (Tables 2.4.2 and 2.4.2a). This relatively large difference in energy barriers can be attributed to the stabilizing effect of the metal positive charge and adjacent double bond in delocalizing the nitrogen negative charge (Scheme 2.4.2a).



Scheme 2.4.2a: Resonance effect in compound **27**.

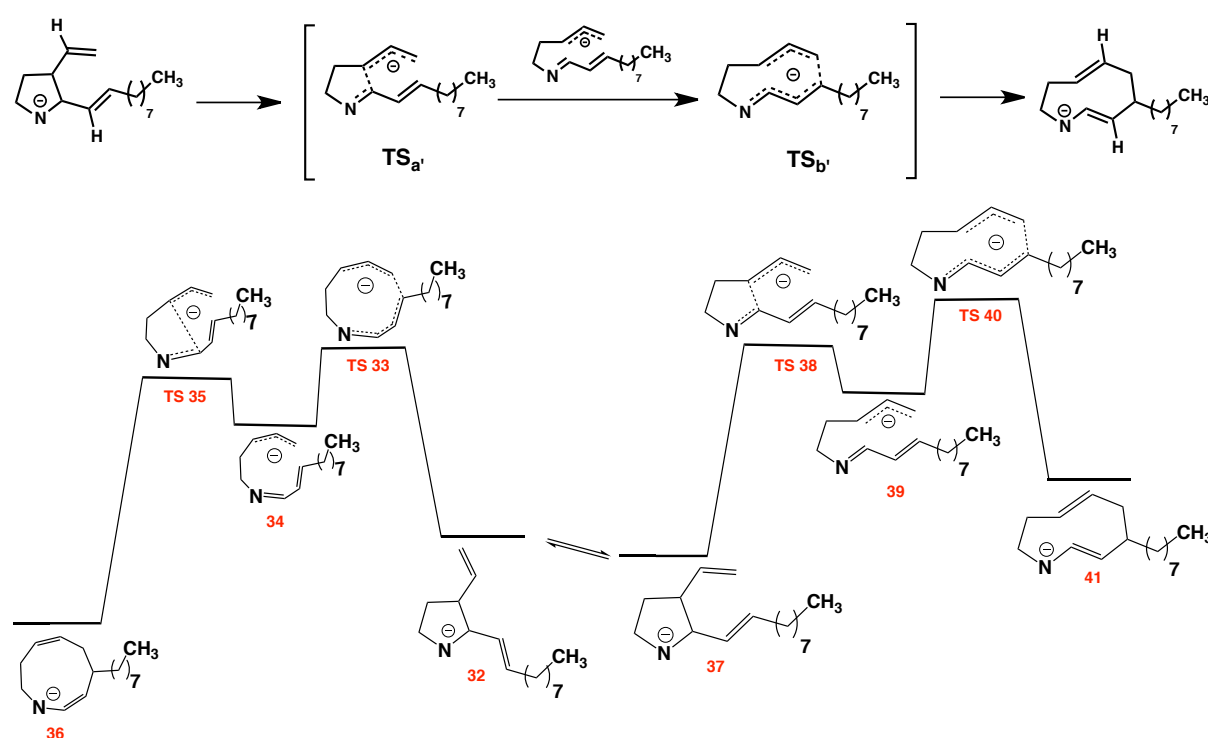
The data in Tables 2.4.2 and 2.4.2a indicate that the potential energies of different species in the rearrangement are altered by changing the metal atom from lithium to potassium. The data indicates that ACR with a lithium counterion has the highest activation barriers, and the rearrangement with a potassium counterion shows the lowest energy barriers. It is inferred from the results that activation barriers are directly dependent on the metal ion and density of the negative charge on the nitrogen atom, confirming that when the nitrogen-metal bond becomes more ionic, the stability of the intermediates increases and leads all the barriers to come down considerably. This reducing trend in the intermediate's activation barriers can favour the stepwise pathway in metallated ACR in contrast to the neutral ACR in which intermediates suffer from instability in the stepwise route. This evidence confirms that while metallated ACR undergoes the stepwise mechanism, the neutral ACR proceeds *via* a concerted pathway, which is in perfect agreement with Houk's investigations.¹⁵

To investigate the solvent effect in ACR, computational studies have been performed in the presence of THF and toluene. As illustrated in Tables 2.4.2 and 2.4.2a, activation barriers for ACR in THF are lower in energy compared to that in toluene. THF, as a polar

solvent, increases the negative charge density on the nitrogen atom, resulting in decreasing energy barriers for rearrangement. This solvent effect is in agreement with the experimental results.²²

2.4.3 Anionic Amino-Cope Rearrangement (Naked ACR)

In this section, a computational study has been carried out for the anionic Amino-Cope Rearrangement (Scheme 2.4, c) to establish the most favorable pathway for these systems. As shown in Scheme 2.4.3, the general pattern for naked ACR is similar to that in metallated ACR, indicating that its mechanism proceeds *via* a stepwise pathway in agreement with the literature.^{15,16} Activation barriers and potential energies of different species for the corresponding rearrangement in different solvents are summarized in Table 2.4.3 and 2.4.3a.



Scheme 2.4.3: General proposed pattern and energy profile for naked Amino-Cope Rearrangement.

Solvent	32	TS 33	34	TS 35	36	37	TS 38	39	TS 40	41
Toluene	4.4	16.0	9.0	11.8	-11.5	0.0	15	7.4	13.7	1.0

Table 2.4.3: Relative Gibbs free energies (kcal/mol) of anionic ACR intermediates calculated in toluene.

Solvent	32	TS 33	34	TS 35	36	37	TS 38	39	TS 40	41
THF	4.3	14.0	7.5	9.7	-10.6	0.0	13.2	5.4	10.9	0.5

Table 2.4.3a: Relative Gibbs free energies (kcal/mol) of anionic ACR intermediates calculated in THF.

It is clear from the results that activation barriers in this case (naked ACR) are lower in energy than that of metallated ACR, which can be attributed to the location of the negative charge density on the nitrogen atom. The charge on the nitrogen assists in stabilizing the intermediates and decreasing all the energy barriers in the naked ACR. Similar to the ACR with a metal counterion, the polarity of the solvent can directly affect the activation barriers in naked ACR in which, in a more polar solvent like THF, all the barriers are lower in energy when compared to that in toluene.

2.5 Conclusion

In this study, the possible mechanisms for Amino-Cope Rearrangements and its anionic variants were explored. The findings provided a better understanding of this chemical transformation. Several interesting conclusions from this study have been drawn:

- (1) In the neutral Amino-Cope Rearrangement (Scheme 2.4, **a**), the N-X bond (when X=H) is not polar enough to allow the rearrangement to go through the stepwise mechanism. Thus, the reaction proceeds *via* a concerted mechanism.

- (2) In the neutral ACR (Scheme 2.4.1), it is interesting to note that the less stable substrate **21** forms the more stable product **23**.
- (3) In the metallated ACR (Scheme 2.4, **b**), the N-X bond (X= metal) is sufficiently polar to enable the reaction to go through the stepwise pathway. It is inferred from Tables 2.4.2 and 2.4.2a that, for the case X=K, all the activation barriers are lower than those when X=Li or Na. This is mainly because the N...K interaction is considerably more ionic when compared to N-Li or N-Na.
- (4) In the naked case, since the nitrogen atom is not stabilized by any cationic species and is highly anionic, all the energy barriers of structures are lower in energy compared to the neutral and metallated Amino-Cope Rearrangements.
- (5) In addition, it was found that solvent choice can affect the energy barriers of the intermediates in which more polar solvents such as THF have the ability to stabilize an ionic intermediate with negative charge at the nitrogen atom, resulting in decreased activation barriers for both metal counter ion and naked ACR cases.

2.6 References

- (1) (a) B. S. Furniss, A. J. Hannaford, P. W. G. Smith, A. R. Tatchell, *Vogel's Textbook of Practical Organic Chemistry*, 5th ed., Longman: London, 1989, pp 1227. (b) I. Fleming, *Pericyclic reactions*; Oxford University Press: New York, 1999, pp 1-89. (c) A. P. Marchand, R. E. Lehr, Editors. *Organic Chemistry*, Vol. 35: *Pericyclic Reactions*, Vol. 1; Academic: New York, 1977, pp 286. (d) U. Lindstorm, E. Marcus, *Organic Reactions In Water: Principels, Strategies and Applications*, John Wiley and Sons, 2008. (e) L. M. Harwood, 2006. Sankararaman. *Pericyclic reactions—a textbook: reactions, applications and theory*. Wiley-VCH, 2005, 432pp, ISBN 3-527-31439-3. *Applied Organometallic Chemistry*, 20(6), pp.423-423.
- (2) (a) C. Li, R. Johnson, J. Porco, *J. Am. Chem. Soc.* **2003**, 125, 5095. (b) G. Domínguez, J. P. Castells, *Chem. Soc. Rev.* **2011**, 40, 3430. (c) U. Nubbemeyer, *Synthesis*. **2003**, 7, 961.
- (3) L. E. Overman, M. A. Kakimoto, *J. Am. Chem. Soc.* **1979**, 101, 1310.
- (4) G. S. Hammond, C. D. DeBoer, *J. Am. Chem. Soc.* **1964**, 86, 899.
- (5) W. E. Doering, W. R. Roth, *Tetrahedron*. **1962**, 18, 67.
- (6) W. E. Doering, V. G. Toscano, G. H. Beasley, *Tetrahedron*. **1971**, 27, 5299.
- (7) M. J. S. Dewar, L. E. Wade, *J. Am. Chem. Soc.* **1977**, 99, 4417.
- (8) A. Navarro, M. Prall, P. R. Schreiner, *Org. Lett.* **2004**, 6, 2981.
- (9) S. Blechert, *Synthesis*. **1989**, 2, 71.
- (10) (a) E. L. Stogryn, S. J. Brois, *J. Org. Chem.* **1965**, 30, 88. (b) M. Allin, M. A. C. Button, S. J. Shuttleworth, *Synlett*. **1997**, 17, 725.
- (11) (a) S. M. Allin, M. A. C. Button, *Tetrahedron Lett.* **1999**, 40, 3801. (b) I. Chogii, D. Pradipta, J. S. Fell, K. A. Scott, M. N. Crawford, K. N. Houk, J. T. Njardarson, *J. Am. Chem. Soc.* **2017**, 139, 13141.
- (12) (a) J. A. Berson, M. Jones, *J. Am. Chem. Soc.* **1964**, 86, 5019. (b) M. E. Jung, J. P. Hudspeth, *J. Am. Chem. Soc.* **1978**, 100, 4309.
- (13) D. A. Evans, D. J. Baillargeon, J. V. Nelson, *J. Am. Chem. Soc.* **1978**, 100, 2242.
- (14) T. J. Sprules, J. D. Galpin, D. Macdonald, **1993**, 34, 247.
- (15) H. Y. Yoo, K. N. Houk, *J. Am. Chem. Soc.* **1998**, 120, 206.
- (16) F. Haeffner, K. N. Houk, S. M. Schulze, J. K. Lee, *J. Org. Chem.* **2003**, 68, 2310.
- (17) S. M. Allin, A. C. Button, *Tetrahedron. Lett.* **1998**, 39, 3345.
- (18) M. J. Frisch, G. W. Trucks, H. B. Schlegel, G. E. Scuseria, M. A. Robb, J. R. Cheeseman, G. Scalmani, V. Barone, G. A. Petersson, H. Nakatsuji, X. Li, M. Caricato, A. V. Marenich, J. Bloino, B. G. Janesko, R. Gomperts, B. Mennucci, H. P. Hratchian, J. V. Ortiz, A. F. Izmaylov, J. L. Sonnenberg, D. Williams-Young, F. Ding, F. Lipparini, F. Egidi, J. Goings, B. Peng, A. Petrone, T. Henderson, D.

- Ranasinghe, V. G. Zakrzewski, J. Gao, N. Rega, G. Zheng, W. Liang, M. Hada, M. Ehara, K. Toyota, R. Fukuda, J. Hasegawa, M. Ishida, T. Nakajima, Y. Honda, O. Kitao, H. Nakai, T. Vreven, K. Throssell, J. A. Montgomery, J. E. Peralta, F. Ogliaro, M. J. Bearpark, J. J. Heyd, E. N. Brothers, K. N. Kudin, V. N. Staroverov, T. A. Keith, R. Kobayashi, J. Normand, K. Raghavachari, A. P. Rendell, J. C. Burant, S. S. Iyengar, J. Tomasi, M. Cossi, J. M. Millam, M. Klene, C. Adamo, R. Cammi, J. W. Ochterski, R. L. Martin, K. Morokuma, O. Farkas, J. B. Foresman, D. J. Fox, Gaussian 16, Revision A.03, Gaussian, Inc., Wallingford CT, 2016.
- (19) C. Lee, W. Yang, R. G. Parr, *Phys. Rev. B* **1988**, 37, 785.
- (20) V. Barone, M. Cossi, *J. Phys. Chem. A* **1998**, 102, 1995.
- (21) P. C. Hariharan, J. A. Pople, *Theor. Chim. Acta* **1973**, 28, 213.
- (22) H. K. Dobson, R. LeBlanc, H. Perrier, C. Stephenson, T. R. Welch, D. Macdonald, *Tetrahedron Lett.* **1999**, 40, 3119.
- (23) S. Grimme, W. Hujo, B. Kirchner, *Phys. Chem. Chem. Phys.* **2012**, 14, 4875.

Chapter Three

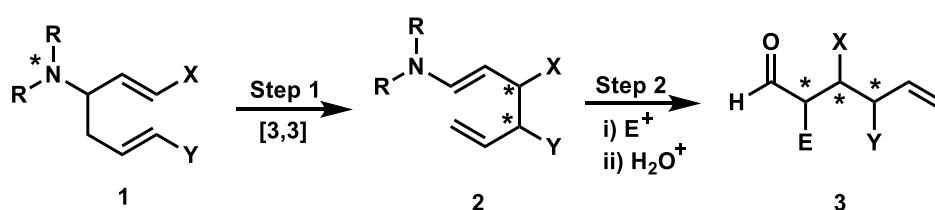
Development of a Novel Synthetic Application of the Anionic Amino-Cope Rearrangement

This chapter outlines the development of an original synthetic method that will provide distinctive access to a range of structurally diverse lycopodium, cylindricine, and lepadiformine alkaloids. Specifically, this is achieved by establishing an unprecedented strategy for the efficient preparation of annulated medium-size N-heterocycles via the novel application of an anionic Amino-Cope Rearrangement (ACR). In addition, by synthesizing the amino-Cope substrate and performing the rearrangement, we were able to probe our computational results in the previous chapter and be the first group to develop a new synthetic application of Amino-Cope Rearrangements with the help of DFT.

3.1 Introduction: The Synthetic Potential of the Amino-Cope Rearrangement

To date, little information has been reported on the synthetic application of the Amino-Cope Rearrangement, and the majority of work done has focused only on the impact of functional groups on reaction rate.¹ However, the [3,3] sigmatropic rearrangement occurs *via* a highly ordered transition structure which allows control of the stereochemistry to obtain the favored product.² The Allin group was the first to explore the Amino-cope Rearrangement of 3-amino-1,5-diene precursors.³ They believed that the Amino-Cope reaction of substituted 3-amino-1,5-diene could be considered as a strong synthetic strategy for the stereoselective formation of highly substituted products in a cascade sequence.

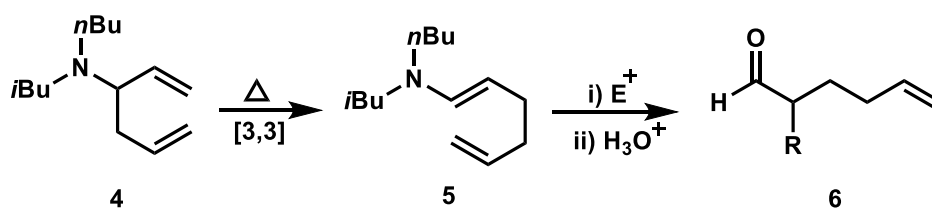
As depicted in Scheme 3.1, a sigmatropic rearrangement of a typical starting material **1** would result in the synthesis of an enamine **2**. During step 1, functionalization at the 1- or 6-position of **1** would lead to the formation of new asymmetric centers in product **2**. High stereoselectivities are induced at chiral positions formed in sigmatropic rearrangements.⁴ If this synthetic route is associated with classic enamine derivatization (step 2), up to three asymmetric centers could be offered in aldehyde **3**. An asymmetric center within the amine part can behave as a chiral multiplier. This would be considered as an important addition to asymmetric synthesis.⁴



Scheme 3.1. Synthetic potential of the Amino-Cope Rearrangement.

3.2 Development of the Amino-Cope Rearrangement

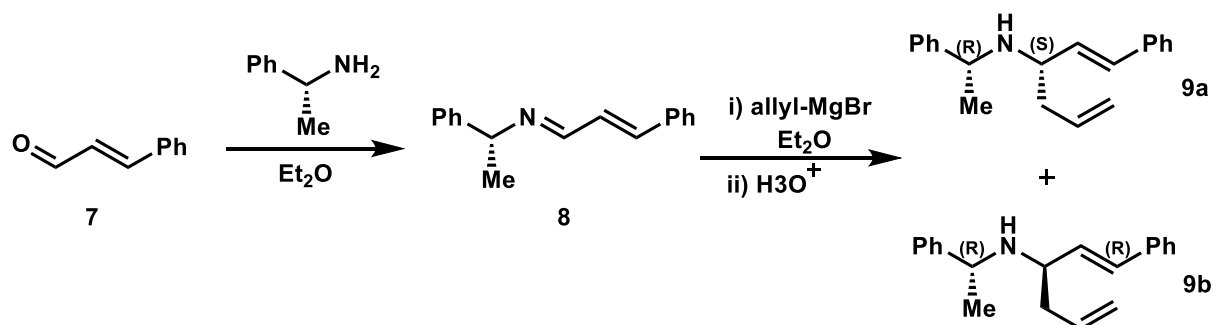
In 1997, Allin and Button⁵ explored Amino-Cope Rearrangement applications and reported the first example of a tandem Amino-Cope Rearrangement/enamine derivatization method, as shown in Scheme 3.2.



Scheme 3.2. Tandem Amino-Cope Rearrangement/enamine derivatization.

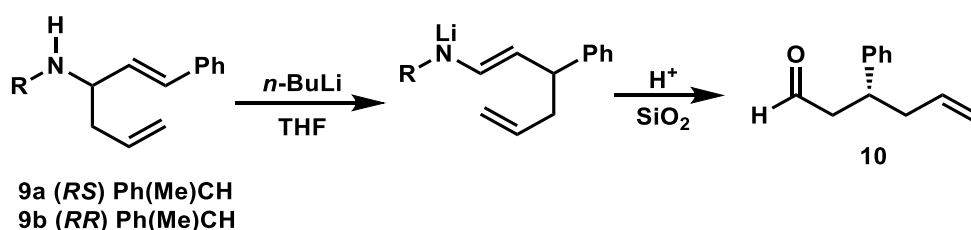
This achievement was followed by addressing asymmetric induction during the anionic Amino-Cope Rearrangement by Allin et al. (Scheme 3.2 a).⁶ This methodology led to formation of pure and non-racemic substrate **9a** and **9b**, that were afforded by addition of allyl bromide

to the related imine **8** obtained from cinnamaldehyde **7** and benzylamine, as shown in Scheme 3.2 a.



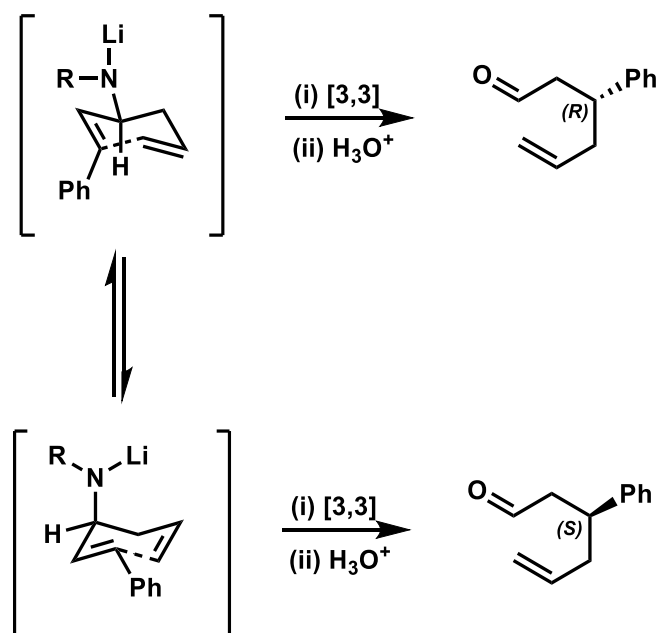
Scheme 3.2 a. Synthesis of secondary amine.

By using *n*-butyllithium as a base, both diastereoisomers performed anionic amino-Cope rearrangements to give the lithiated enamine, which hydrolyzed to afford enantiomerically enriched compound **10** with an enantiomeric excess from 41% to 75% (Scheme 3.2 b).⁶



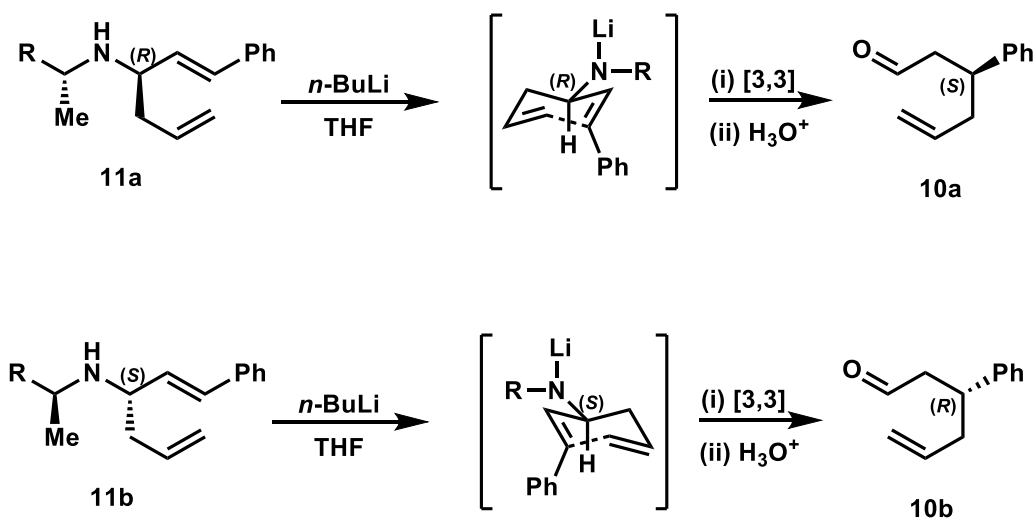
Scheme 3.2 b. Asymmetric anionic Amino-Cope Rearrangement.

The full stereochemistry of the products can be attributed to the simple transition states involved. The main enantiomer is obtained from the chair conformation of the starting material with the amine part in the pseudo-equatorial position, and the minor enantiomer is derived from the amine part occupying the pseudo-axial position, as indicated in Scheme 3.2 c.^{4,5} Allin and co-workers concluded that expanding the bulkiness of the chiral auxiliary^{7,8} would increase the preference of the amine component to occupy the equatorial position in the chair-like transition structure. This would result in the enhancement of enantioselectivity in the asymmetric Amino-Cope Rearrangement.



Scheme 3.2 c. Competing transition state conformations for the Amino-Cope Rearrangement.

The resulting diastereoselectivity during formation of chiral amino-diene precursors is of considerable significance because each diastereomer leads to the opposite enantiomer of the reorganized Amino-Cope Rearrangement product (Scheme 3.2 d).

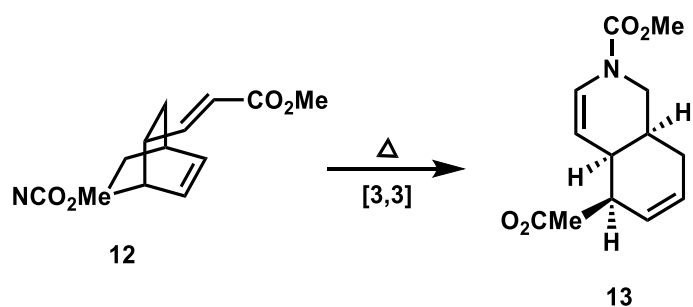


Scheme 3.2 d. Asymmetric induction in the anionic Amino-Cope Rearrangement.

The controlling factor for determining the stereochemistry of the Amino-Cope product is the stereochemistry of the C-3 position of the diene starting material. For example, precursor (*R,S*) has (*S*) chirality at the C-3 position resulting in the (*R*)-aldehyde (Scheme 3.2 d).⁶

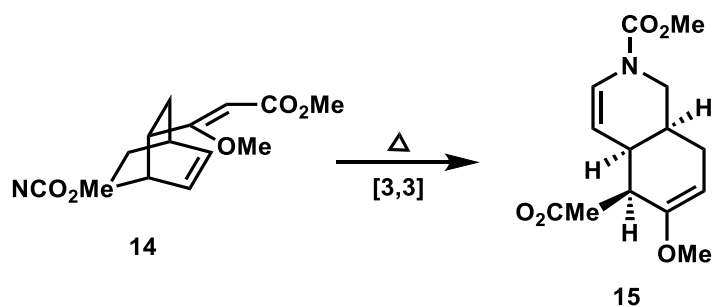
3.3 Synthetic Applications of the Amino-Cope Rearrangement

There have been few examples reported of the synthetic applications of the Amino-Cope Rearrangement in its anionic form. In 1979, the first synthetic utilization of the thermal ACR in tandem with the Diels-Alder cycloaddition was discovered by Wender and co-workers.⁹ The goal was to obtain the *cis*-hydroisoquinoline **13** by pyrolysis of the ester substrate **12** as outlined in Scheme 3.3.



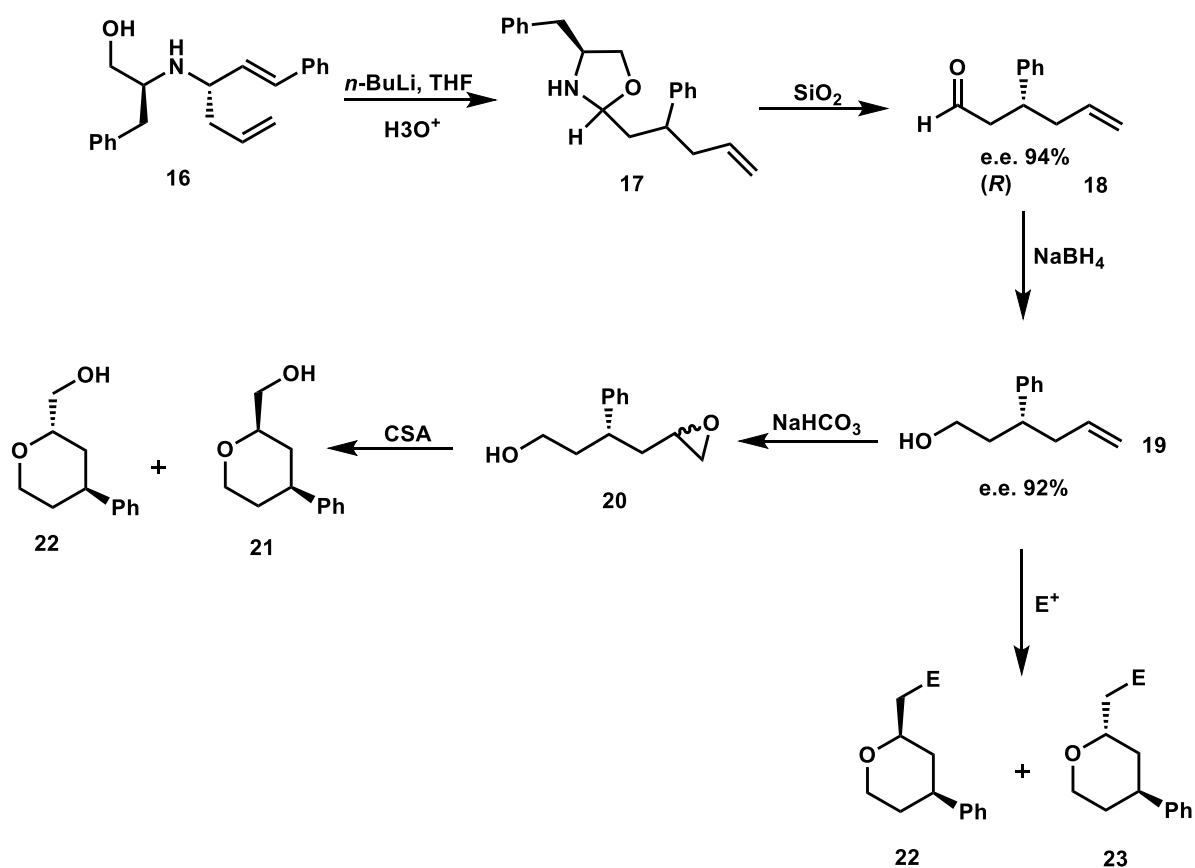
Scheme 3.3. Synthesis of *cis*-hydroisoquinoline *via* the thermal Amino-cope Rearrangement.⁹

After successful formation of the compound **13**, Wender extended his original work and synthesized the C-6 functionalized hydroisoquinoline **15**, which served as a potential substrate to obtain a range of biologically active molecules (Scheme 3.3 a).⁹



Scheme 3.3 a. Synthesis of hydroisoquinoline derivatives.

In 2002, Allin discovered another synthetic application of the ACR.¹⁰ The anionic ACR was utilized for the formation of substituted 2,4-disubstituted tetrahydropyrans in high yields from available substrates. Anionic Amino-Cope Rearrangements have been performed for the diastereomerically pure precursor **16** to afford oxazolidine **17**, which further gives the corresponding aldehyde **18**. Then, the reduction occurred for compound **18** to yield the corresponding alcohol **19** followed by cyclization to form tetrahydropyrans **22** and **23**, or *via* epoxidation of the double bond followed by CSA (Camphorsulfonic acid) treatment to give tetrahydropyran **20** and **21** (Scheme 3.3 b). The products **22** and **23** are potentially applicable chiral blocks for biologically active important molecules.¹¹



Scheme 3.3 b. Enantiomerically enriched tetrahydropyrans *via* the anionic Amino-Cope Rearrangement.

As mentioned above and in chapter one, there have been few examples of ACR reported in the literature (12 reports total). As a result, investigating this interesting transformation and its applications in organic synthesis is highly desirable.

In summary, this chapter aims to: (1) establish a new anionic Amino-Cope Rearrangement that can be used to construct new annulated medium-size *N*-heterocycles **MRKI** (Figure 3.3), (2) utilize these annulated medium-size *N*-heterocycles as key intermediates for the divergent synthesis of a range of structurally diverse and significant natural products and their derivatives (Figure 3.3), (3) performing the Amino-Cope Rearrangement on the substrate **ACRS** in order to probe our computational results in chapter one, and (4) enhance our understanding of the ACR and the properties of medium-size rings and use this knowledge to identify and define new synthetic strategies.

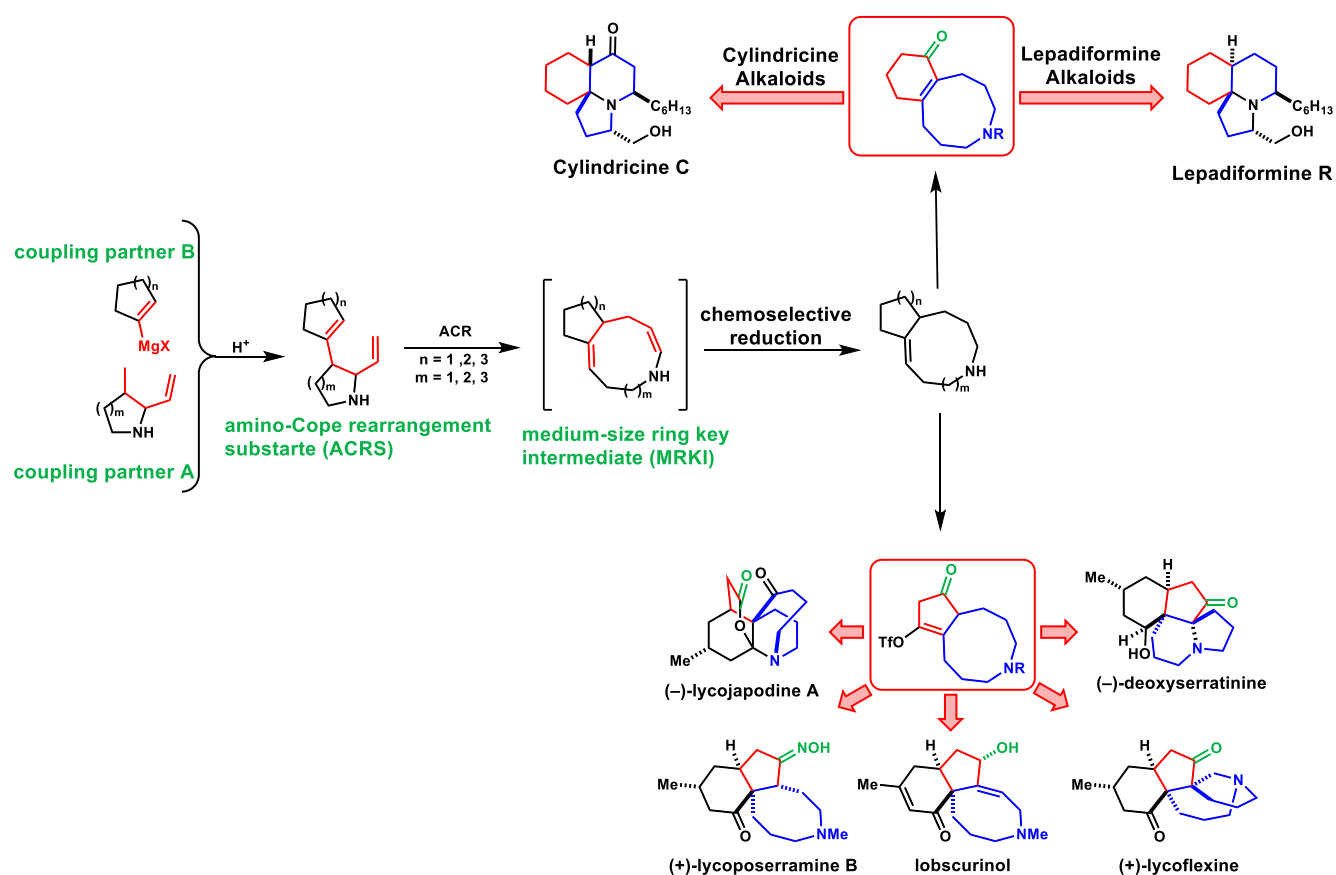
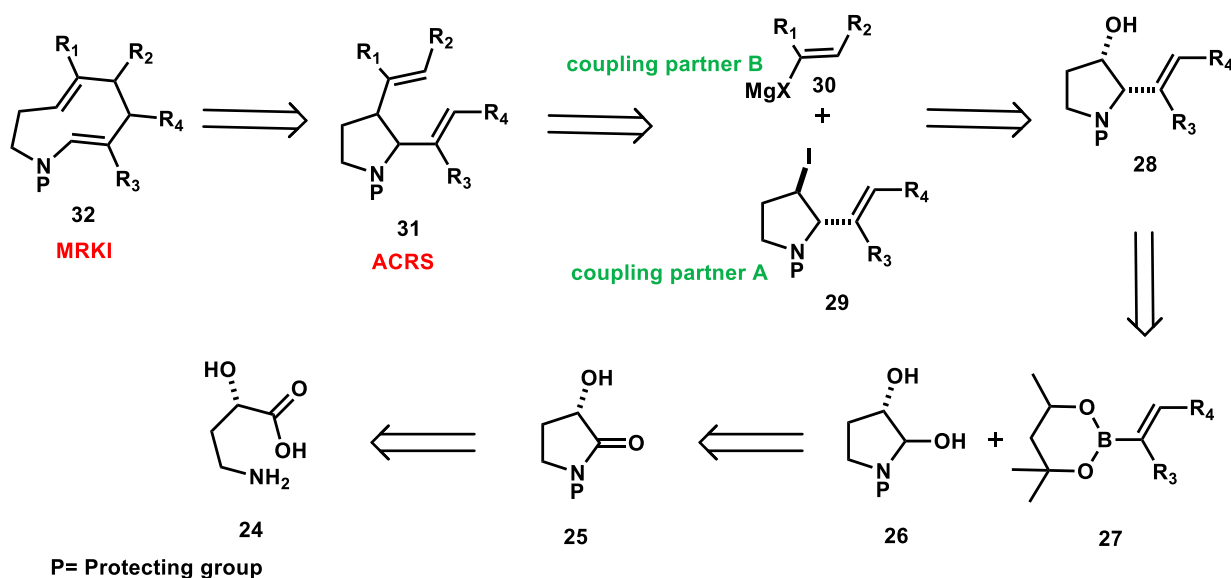


Figure 3.3. Synthesis of biologically active molecules from key medium-size rings derived from ACR substrates.

All the compounds constructed in this chapter have been synthesized, purified, and characterized by the candidate for the first time at University of Tasmania under supervision of Dr. Alex Bissember, except for compound **33** synthesized by Honours student Jonathan Robertson.¹⁵

3.4 Results and Discussion

As discussed in the introduction, this chapter aims to develop a novel application of the Amino-Cope Rearrangement and its derivatives. The formation of natural products provides a great opportunity to examine the application of the Amino-Cope Rearrangement as a new synthetic tool. The main focus of research reported in this chapter was to construct a key substrate that features a nitrogen heterocyclic core applicable for anionic Amino-Cope Rearrangements (**31**). In order to accomplish this goal, a modular synthetic pathway was designed which would provide access to a range of different substituted molecules (Scheme 3.4).



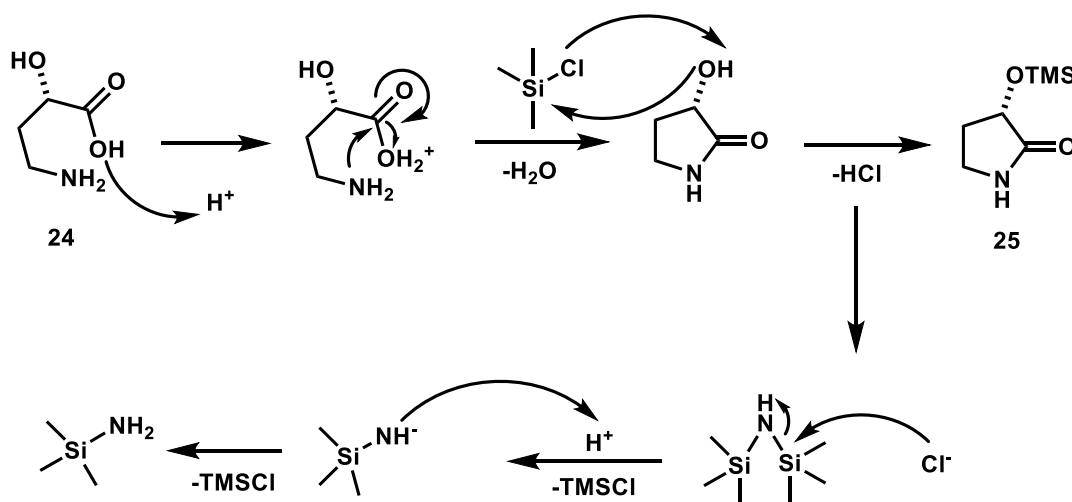
Scheme 3.4. Retrosynthetic analysis for the synthesis of a range of ACR substrates.

For the ACR to take place, the target compound has to consist of both a 1,5-diene and a nitrogen substituent at the 3-position. It was believed that this could be done *via* a transition metal-catalyzed coupling to facilitate reaction between **29** and **30** (Scheme 3.4). It was anticipated that compound **29** could be formed through an S_N2 reaction of iodine and compound **28**. Compound **28** was synthesized *via* a Petasis borono-Mannich coupling with compound **26**.¹² It was envisaged that diol **26** can be formed from the reduction of compound

25 to afford the corresponding alcohol. Finally, compound **25** was constructed through a cyclization reaction from commercially available carboxylic acid **24**. This useful synthetic route will be discussed in this section in more detail.

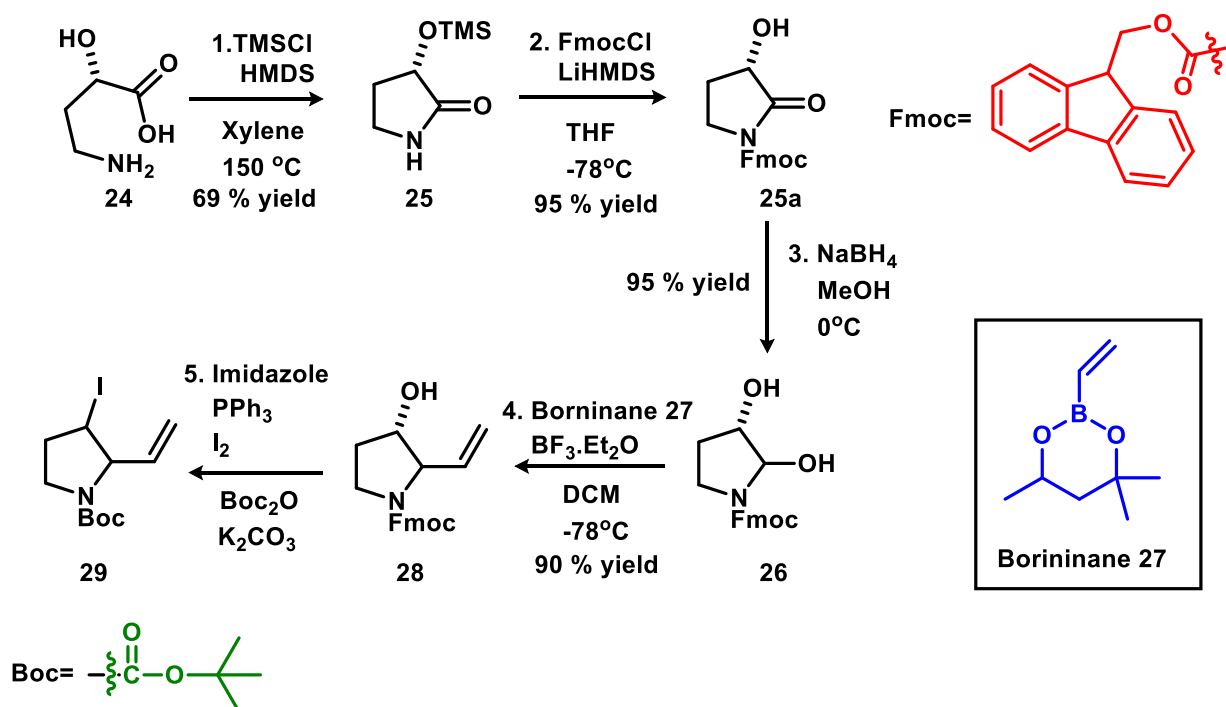
3.4.1 Synthesis of (S)-3-((trimethylsilyl)oxy) pyrrolidin-2-one (**25**)

Pyrrolidinone **25** was constructed through a modified literature method applying the cyclization of (S)-4-amino-2-hydroxybutanoic acid (**24**) (Scheme 3.4.1).¹² The reaction uses 0.05 equivalents of chlorotrimethylsilane (TMSCl) as a catalyst which generates chloride ions and the protected compound **25**. These free ions further react with HMDS (1,1,1,3,3,3-hexamethyldisilazane) to make TMSCl in a catalytic cycle (Scheme 3.4.1). In the ¹H NMR spectrum of compound **25**, a singlet at 0.22 ppm was observed, showing that incorporation of the TMS protecting group was successful.



Scheme 3.4.1. Formation of pyrrolidinone **25**, with the catalytic reformation of TMSCl through chloride attack on HMDS.

The relatively low yield of the reaction (69 %) can be attributed to the generation of the N- and O-TMS derivative of **25**. This affected the following nitrogen protection, as the Fmoc protecting group can not expel the TMS group (Scheme 3.4.1 a).



Scheme 3.4.1 a. Construction of the iodo pyrrolidine **29**.

3.4.2 Synthesis of (S)-(9H-fluoren-9-yl) methyl 3-hydroxy-2-oxopyrrolidine-1-carboxylate (**25a**)

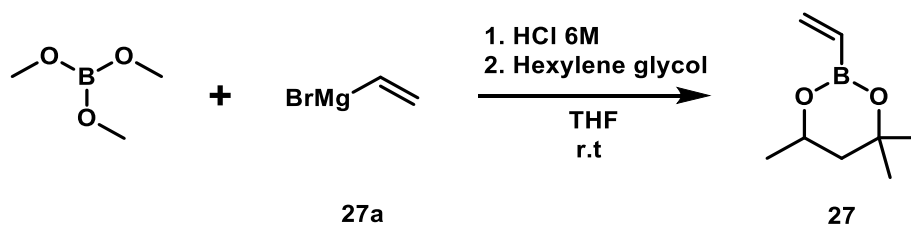
For compound **25**, proton detachment with LiHMDS generated the anionic nitrogen centre which was further attacked by FmocCl to give **25a** (Scheme 3.4.1 a). To isolate the desired product, it was found that **25a** could be purified by recrystallization in which hot hexane was added to a saturated solution in ethyl acetate. The resulting product was obtained in 95% yield on a 10-gram scale. The ¹H NMR of **25a** does not show a singlet at 0.22, which would correspond to the 9 protons of substrate, indicating the loss of TMS protecting group. Furthermore, peaks located at 7.70, 7.66-7.64, 7.34 and 7.26 ppm were detected that integrated for 2 protons each, corresponding to the 8 protons in the Fmoc protecting group. The ¹³C NMR spectrum shows 13 carbon atoms, consistent with the structure **25a**. Peaks detected at 174.2 and 151.4 ppm confirm the presence of both Fmoc and pyrrolidine groups. The IR spectrum of this compound demonstrates a diagnostic -OH stretch at 3300 cm⁻¹ which shows the loss of the TMS group and the presence of a hydroxyl substituent.

3.4.3 Generation of (3S)-(9H-fluoren-9-yl) methyl 2,3-dihydroxypyrrolidine-1-carboxylate (**26**)

The reducing agent sodium borohydride was used to synthesize diol **26** from **25a** in 93% yield on a 10-gram scale (Scheme 3.4.1 a). Sodium borohydride, as a selective and relatively mild reagent for this system, was only able to reduce the carbonyl group and not the Fmoc protecting group which makes it an excellent reducing agent for this system. This reaction was considerably exothermic. As a result, the reaction was performed at 0 °C to avoid having undesired side reactions which would result in low yield. Compound **26** was isolated through a recrystallization process from hot ethyl acetate and hexane. The ¹H NMR spectrum shows a signal at 4.18-4.20 ppm, confirming the formation of diol **26**. In the ¹³C NMR spectrum, there is no peak at 151.4 ppm, showing the absence of amide carbonyl in the substrate. The IR spectrum of **26** does not show a carbonyl peak at 1790 cm⁻¹ and shows a wider and more pronounced -OH stretch, that confirms the conversion of pyrrolidinone into pyrrolidine **26**. The exact mass of 325.37 amu also supports the formation of diol **26**.

3.4.4 Formation of vinyl borinane (**27**)

The next step in the synthetic cycle (Scheme 3.4.1 a) was the Petasis borono-Mannich reaction. Owing to the high cost of the reagent, compound **27** was made in accordance with a reported method.¹³ In this cross-coupling reaction, the coupling partner **27a** was reacted with trimethylborate to give the vinyl boronic acid after workup with HCl. This was further coupled with hexylene glycol through a condensation process to generate **27** as depicted in Scheme 3.4.4.



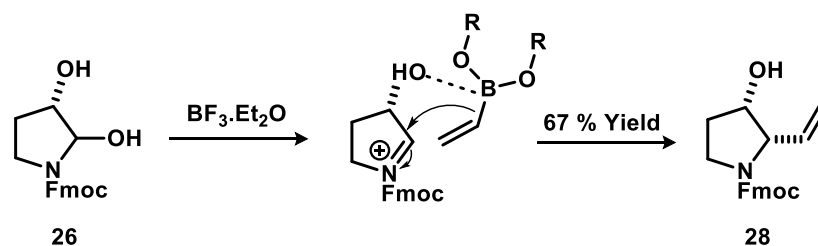
Scheme 3.4.4. Formation of allyl borinane **27**.

The purification of the product was achieved *via* vacuum distillation in 85% yield. The ¹H NMR spectrum of **27** is consistent with the literature,¹³ in which the appearance of a doublet

of doublets and a multiplet peak at 6.07 and 5.91-5.75 ppm confirms the presence of a vinyl group in the product.

3.4.5 Formation of (2*S*,3*S*)-(9*H*-fluoren-9-yl) methyl 3-hydroxy-2-vinylpyrrolidine-1-carboxylate (**28**)

Compound **28** was generated through the Petasis borono-Mannich¹² reaction of diol **26** and borinane **27** as indicated in Scheme 3.4.5. This cross-coupling reaction takes place at the activated diol **26** through an iminium intermediate that emerges *via* the acid promoted dehydration of the 2-hydroxy substituent. The corresponding iminium further underwent nucleophilic attack from borinane **27** that delivers the vinyl group to this active site (Scheme 3.4.5).



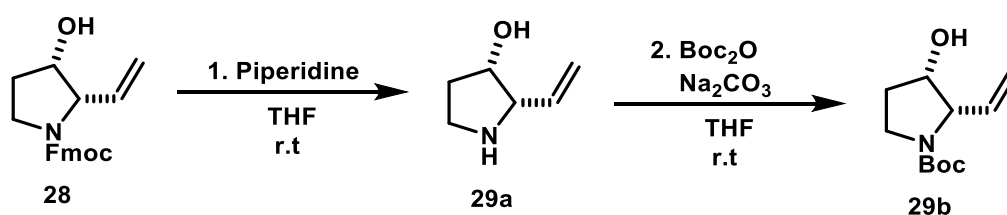
Scheme 3.4.5. Formation of compound **28** from diol **26** and borinane **27**.

The ^1H NMR spectrum depicts peaks at 5.45-5.10 and 5.92-5.73 that belong to 2H and 1H of the vinyl group respectively. The ^{13}C NMR spectrum exhibits signals at 141.4 and 133.6 ppm which confirm the presence of vinyl group in the product **28**.

Since the next step of the synthetic pathway (iodination) did not proceed with the Fmoc group, attributed to the bulkiness of this protecting agent, the Boc group was used as discussed below:

3.4.6 Generation of (2*S*,3*S*)-*tert*-butyl 3-hydroxy-2-vinylpyrrolidine-1-carboxylate (29b)

Compound **29b** with the Boc protection group was formed by the proton detachment of **28** using piperidine to afford the secondary amine **29a**, which was further protected with Boc anhydride to give **29b** (scheme 3.4.6). The resulting product was purified (76% yield) *via* recrystallization using hot hexane and saturated ethyl acetate.

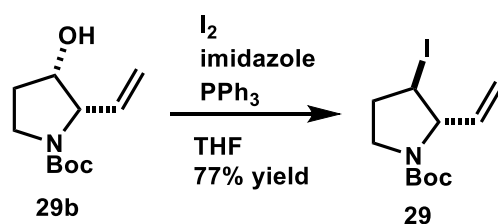


Scheme 3.4.6. Synthesis of the Boc protected pyrrolidine **29b**.

This protecting group exchange was inevitable since the iodination reaction was found to be incompatible with the Fmoc group. The formation of **29b** was confirmed by ¹H NMR spectroscopy in which the loss of 8 protons in the aromatic region shows the successful removal of Fmoc. In addition, a peak at 1.45 ppm belongs to 9 hydrogens of the Boc group which supports the protecting group interchange. Furthermore, the ¹³C NMR spectrum shows a broad signal at 28.4 ppm which again confirms the presence of the Boc substituent.

3.4.7 Formation of (2*S*,3*R*)-*tert*-butyl 3-iodo-2-vinylpyrrolidine-1-carboxylate (29)

The final step of the synthetic pathway which resulted in synthesis of the coupling partner A (figure 3.3) was developed by the iodination reaction of compound **29b**. The corresponding reaction occurred *via* a S_N2 substitution of the hydroxyl group by using iodine, PPh₃, and imidazole under reflux (Scheme 3.4.7). Isolation of the desired product **29** was successful using flash chromatography in 77% yield on a 5-gram scale.



Scheme 3.4.7. Synthesis of iodide **29** through the S_N2 process.

To confirm the successful formation of iodide **29**, the ¹H NMR spectrum of iodide is depicted in Figure 3.4.7. As the NMR spectrum shows, a downfield shifted peak from 4.20-4.05 ppm (**29b**) to a multiplet at 4.75-4.55 ppm (**29**) is seen, which is related to the proton on C-7. Furthermore, peaks of olefin at 5.27-5.16 and 5.75 ppm are consistent with the protons on C-8 and C-9, respectively. The reason that these peaks are broadened can be rationalized by their proximity to the Boc group. The alkyl peaks at 2.32-2.26 and 2.18-2.12 ppm are consistent with the protons on C-5. Also, a total of eighteen hydrogens was seen in the ¹H NMR spectrum which corresponds to the product. Finally, the iodinated carbon was recognized at 4.18-4.20 ppm as shown in Figure 3.4.7.

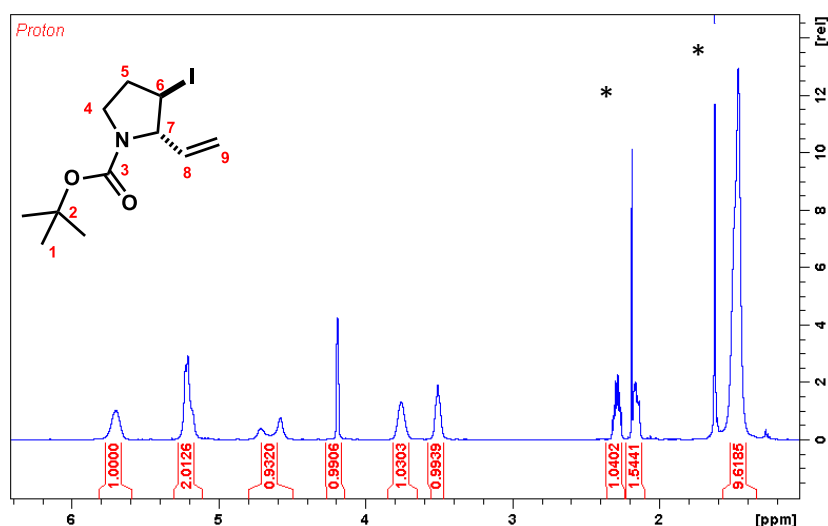


Figure 3.4.7. ¹H NMR spectrum of iodide **29**. * Signals at 2.2 and 1.6, are acetone and water, respectively.

More evidence to show the successful formation of compound **29** can be seen in the ^{13}C NMR spectrum of the iodide **29** (Figure 3.4.7a). Firstly, the loss of a substrate carbon peak at 63.0 ppm shows the elimination of the hydroxyl group and supports the introduction of a different substituent such as iodine. Furthermore, signals at 136.2 (C-9) and 116.1 (C-8) ppm indicate the rotameric impact of the Boc protection group. The exact mass of 323.04 amu also supports the formation of iodide **29**.

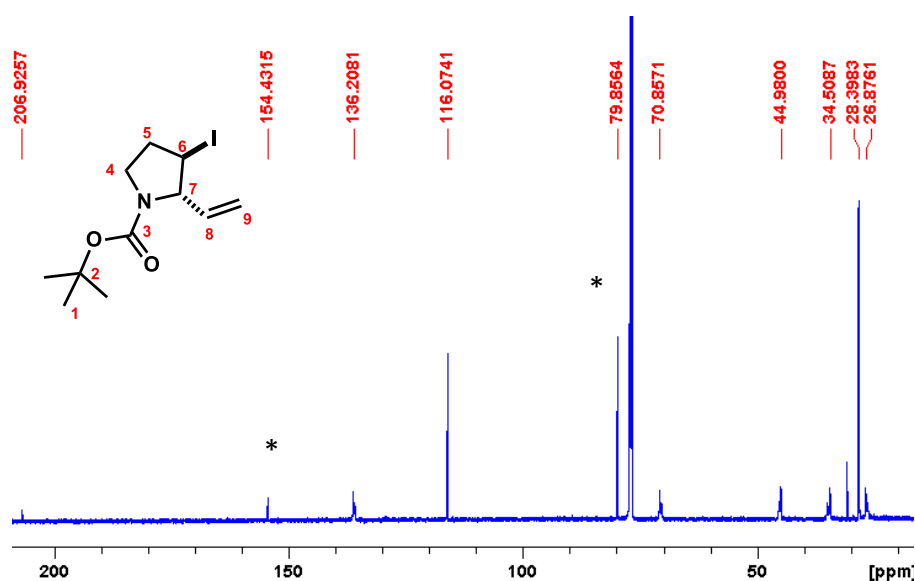


Figure 3.4.7a. ^{13}C NMR spectrum of compound **29** in CDCl₃. * Acetone.

In summary, a useful and scalable synthetic pathway to iodo-functionalized pyrrolidine **29** was provided. This affords the target compound **29** in 59% overall yield through a seven-step sequence. Although just one analogue of **29** was synthesized, more work in future could allow the attainment of a large range of 2-alkenyl-3-iodo-substituted pyrrolidines and piperidines.

Now, with coupling partner A (compound **29**) and coupling partner B which is commercially available (compound **30**) (Scheme 3.4), the cross-coupling reaction between A and B can be attempted to obtain **31**.

3.4.8 Formation of (2*S*,3*R*)-*tert*-butyl 3-iodo-2-vinylpyrrolidine-1-carboxylate (ACRS **31**)

Due to the complexity of the cross-coupling reaction between coupling partners A and B, and also a lack of similar examples of this kind of system in the literature, a comprehensive literature review has been done in this section. In 2014, Knochel and co-workers discovered a new cobalt-catalyzed system by which the cross-coupling reaction of sp^3 -hybridised electrophiles with alkenyl and aryl Grignard nucleophiles is feasible.¹⁴ In one example of this cross-coupling reaction Knochel demonstrated that a range of aryl Grignard reagents can be coupled to iodopyrrolidine with the help of a tetramethylated diamine ligand **33**, as outlined in Scheme 3.4.8.

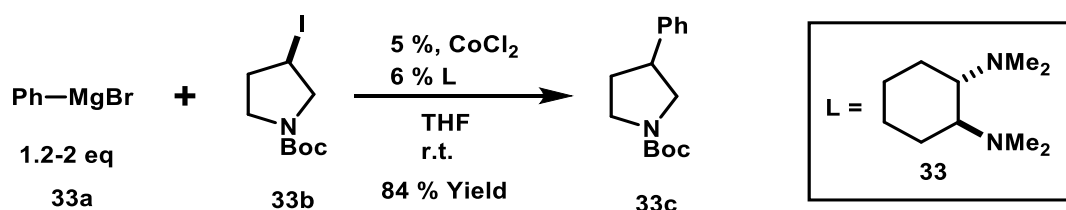


Figure 3.4.8. Cobalt-catalyzed cross-coupling reaction between **33a** and iodide **33b**.

Based on the reaction conditions reported by Knochel, a THF solution of iodide **29** was prepared. To this solution, ligand **33** and cobalt (II) chloride were added following by slow addition of vinyl Grignard **30**, which resulted in an immediate color change from light blue to dark green (Scheme 3.4.8a). In view of the characteristic colour change, this probably provided the proposed product in low yields of 15-10 %. However, it appears that the steric hindrance at the 2-position of iodide, constrained the coordination by the metal.

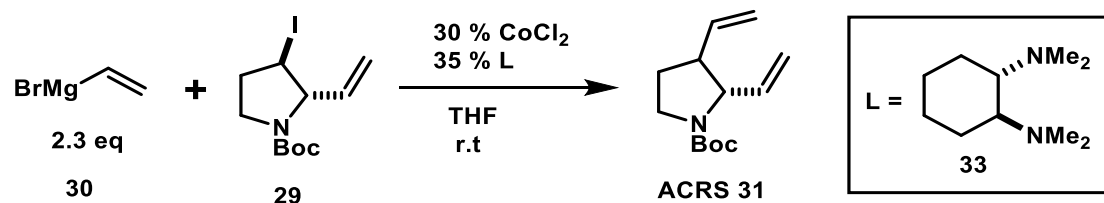


Figure 3.4.8a. Optimized conditions for the formation of ACRS 31. * Ligand **33** was made by an honors student in our group (Jonathan Robertson) in accordance with the literature method.¹⁵

Many different modifications have been performed in order to improve the yield of the reaction including: change in solvent mixtures, the number of equivalents of the Grignard agent, loading of the catalyst, and reaction temperatures. Unfortunately, attempts to optimize the corresponding reaction were not successful which made us to change our focus on the molecule structure itself. It is considered that the presence of the Boc group may be responsible for the low yield and messy NMR spectra owing to its rotamers. As a result, we investigated removal of the Boc group at this stage to determine whether this would lead to further progress in synthesis.

3.4.9 Formation of (2S)-2,3-divinylpyrrolidine (**35**)

The synthesis of **35** was performed through deprotection of compound **31** with the assistance of trifluoroacetic acid (Scheme 3.4.9). The reaction gave the anionic ACR starting material **35**, although the only evidence for this conversion was HRESI. Trifluoroacetic acid addition to **31** caused a rapid color change from orange to strong purple. The purification process for **35** was very challenging since column chromatography was not a viable method owing to the highly volatile nature of **35**. All attempts to purify the desired product failed and resulted in huge product losses due to this volatility issue. Unfortunately, the amount of product was inadequate for ^1H NMR spectroscopy, however mass analysis was consistent with the formation of **35**.

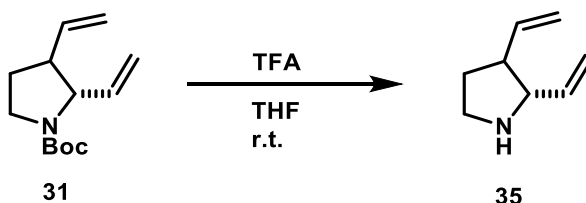


Figure 3.4.9. The formation of divinylpyrrolidine **35**.

In order to solve this issue, we propose in the future changing the structural nature of the coupling partner A as demonstrated in Scheme 3.4.9a. It is believed, using a less volatile alkyl chain substituent in **37**, will decrease the volatility of the desired product. However, owing to the complexity of our synthetic cycle which necessitates many different steps and uncertainty about obtaining a successful result, we decided to abandon the synthetic project at this stage and focus our attention on the computational studies as already discussed in chapter two. Hopefully, this work can be explored in the future in order to complete a comprehensive experimental investigation of the Amino-Cope Rearrangement and its anionic variants.

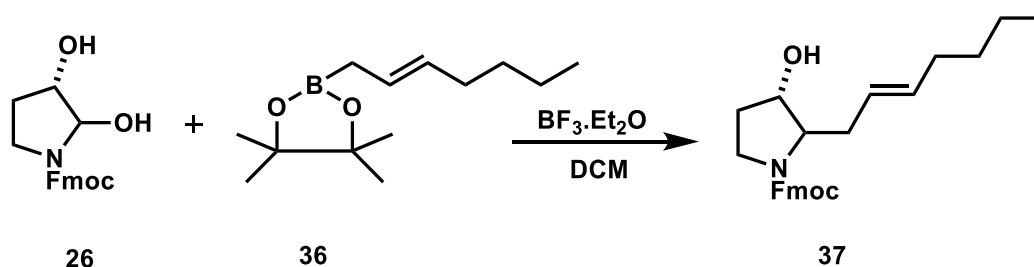


Figure 3.4.9a. The formation of less volatile derivative of diol **26**.

3.5 Conclusion

In summary, this work aimed to develop a novel application of the Amino-Cope Rearrangement to synthesize medium-size *N*-heterocycles under mild conditions, and subsequently have access to a range of biologically important alkaloids as depicted in Figure 3.3. As discussed above, this investigation is one step away from making the **ACRS** which can potentially convert to **MRKI** through the ACR. Aside from exploring a novel application of ACR, by performing the rearrangement of the Amino-Cope substrate employed, probing of the computational results (chapter 2) will finally lead to a comprehensive study of the Amino-Cope Rearrangement and its anionic variant for the first time.

3.6 Experimental Procedures and Data

3.6.1 General experimental considerations

All reactions were carried out under an atmosphere of nitrogen. Solvents are of analytical grade and isolated by standard laboratory methods. Reagents were purchased from Sigma-Aldrich and used as received.

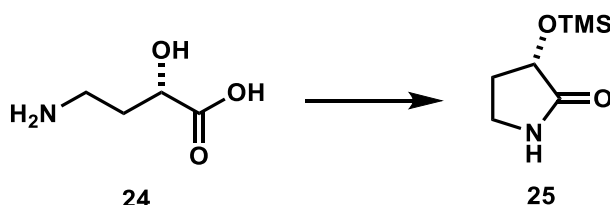
Thin layer chromatography has been done using Merck Silica gel 60-F254 plates, and visualization of the developed chromatogram was carried out by UV absorbance (254 nm); potassium permanganate stain (KMnO_4 , K_2CO_3 , NaOH , H_2O); ninhydrin stain (ninhydrin, AcOH , *n*-butanol) or; cerium molybdate stain ($\text{Ce}(\text{NH}_4)_2(\text{NO}_3)_6$, $(\text{NH}_4)_6\text{Mo}_7\text{O}_{24}\cdot 4\text{H}_2\text{O}$, H_2SO_4 , H_2O), with heating. Flash chromatography was performed using flash grade silica gel (60 μm) with the indicated solvent system in accordance standard techniques.

NMR spectroscopic studies (^1H , ^{13}C) were performed on a Bruker Avance III operating at 400 MHz (^1H) or 100 MHz (^{13}C), or a Bruker Avance III operating at 600 MHz (^1H) or 150 MHz (^{13}C) in CDCl_3 and C_6D_6 as specified. Chemical shifts for NMR spectra are recorded in parts per million (ppm), calibrated to the residual solvent peak (CDCl_3 , δ 7.26 ppm (^1H), 77.0 ppm (^{13}C); and coupling constant (*J*) are recorded in Hz.

Infrared spectroscopy was carried out on a Shimadzu FTIR 8400s spectrometer using thin film technique, with sample deposited by CH_2Cl_2 on NaCl plates.

Mass spectroscopic studies (HREIMS and HRESIMS) were performed by Noel Davies and David Nichols of the Central Science Laboratory (University of Tasmania).

3.6.2 (*S*)-3-((Trimethylsilyl)oxy)pyrrolidine-2-one (25)



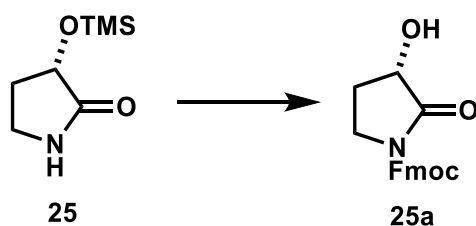
Chlorotrimethylsilane (0.27 mL, 2.1 mmol) was added to a mixture of (*S*)-4-amino-2-hydroxy-butanoic acid (10.0 g, 84.0 mmol) and HMDS (30.7 mL), 147 mmol) in xylene (100

mL) maintained at room temperature. The resulting mixture was heated at reflux for 36 h. After this time, EtOH (150 mL) was added and the ensuing solution was concentrated again. The resulting orange oil was placed under high vacuum to remove residual solvent. The oil, identified as compound **25**, was left to solidify at room temperature overnight, resulting in a brown solid.¹²

¹H NMR (CDCl₃, 400 MHz) δ : 6.08 (1H, s), 4.28 (1H, t, J = 8 Hz), 3.43-3.38 (1H, m), 3.35-3.25 (1H, m), 2.44-2.37 (1H, m), 2.11-2.02 (1H, m), 0.22 (9H, s) ppm.

IR ν_{max} (NaCl): 3422, 3300, 3264, 3188, 3064-2953, 1684, 1615, 1422, 1335, 1105, 1090, 1055, 943 cm⁻¹.

3.6.3 (3S)-(9H-Fluoren-9-yl)methyl 3-hydroxy-2-oxopyrrolidine-1-carboxylate (**25a**)



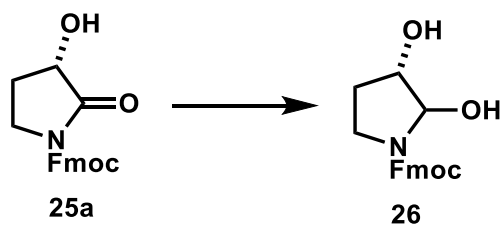
LiHMDS (40 mL of a 1 M solution in THF, 40.0 mmol) was added over 5 min to a solution of pyrrolidine **25** (7.30 g, 42.0 mmol) in THF (100 mL) maintained at -78 °C. After 0.5 h a solution of FmocCl (11.40g, 44.0 mmol) in THF (20 mL) was added dropwise over 0.25 h and the solution was then warmed to room temperature. After 18 h, HCl (20 mL of a 2 M aqueous solution) and brine (15 mL) were added and the layers separated. The aqueous layer was further extracted with CH₂Cl₂ (3 x 20 mL), the combined organic layers were dried (MgSO₄) and concentrated under vacuum to give an orange solid. After recrystallization, compound **25a** was obtained as a clear solid.

¹H NMR (CDCl₃, 400 MHz) δ : 7.70 (2H, d, J = 7 Hz), 7.66-7.64 (2H, m), 7.34 (2H, t, J = 7 Hz), 7.26 (2H, dt, J = 7 Hz), 4.48-4.41 (2H, m), 4.37-4.34 (1H, m), 4.24 (1H, t, J = 7 Hz), 3.80 (1H, t, J = 9 Hz), 3.51-3.46 (1H, m), 3.18 (1H, bs), 2.45-2.40 (1H, m), 1.98-1.90 (1H, m) ppm.

¹³C NMR (CDCl₃, 100 MHz) δ : 174.2, 151.4, 143.3, 141.3, 128.0, 127.3, 127.2, 125.3, 120.0, 70.5, 68.0, 46.6, 42.1, 27.1 ppm.

IR ν_{max} (NaCl): 3600-3100, 3091-2904, 1790, 1712, 1450, 1386, 1301, 970, 759, 740 cm⁻¹.

3.6.4 (3S)-(9H-Fluoren-9-yl)methyl 2,3-dihydroxypyrrolidine-1-carboxylate (**26**)



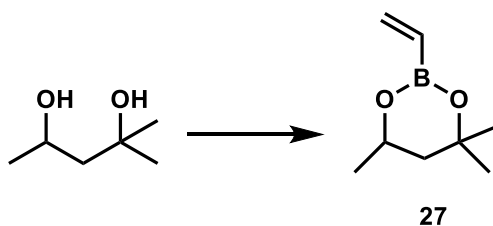
NaBH₄ (2.00 g, 60 mmol) was slowly added to a solution of pyrrolidine **25a** (10.00 g, 30 mmol) in 100 mL of a 10% THF/methanol at 0 °C. The resulting mixture was warmed to room temperature for 2 h, after which it was quenched with H₂O (20 mL) and concentrated under vacuum to remove the methanol. The ensuing mixture was then dissolved in brine (15 mL) and CH₂Cl₂ (50 mL), separated and extracted with CH₂Cl₂ (3 x 20 mL). The organic layers were combined and dried with Na₂SO₄, then concentrated under vacuum to give a solid. After recrystallization, compound **26** was obtained as a clear solid.

¹H NMR (CDCl₃, 400 MHz) δ: 7.70 (2H, d, *J* = 7 Hz), 7.66-7.64 (2H, m), 7.34 (2H, t, *J* = 7 Hz), 7.26 (2H, dt, *J* = 3 Hz, *J* = 7 Hz), 5.81 (1H, m), 5.41-5.07 (2H, m), 4.58-4.14 (4H, m), 3.63-3.48 (2H, m), 2.01-1.81 (1H, bs) ppm.

¹³C NMR (CDCl₃, 100 MHz) δ: 155.2, 144.1, 141.3, 133.6, 127.6, 127.0, 125.0, 119.9, 72.3, 67.0, 47.3, 43.8, 27.8 ppm.

IR ν_{max} (NaCl): 3500-3000, 2980-2891, 1697, 1662, 1597, 1508, 1444, 1417, 1197, 1070, 1039, 898, 736 cm⁻¹.

3.6.5 4,4,6-Trimethyl-2-vinyl-1,3,2-dioxaborinane (**27**)

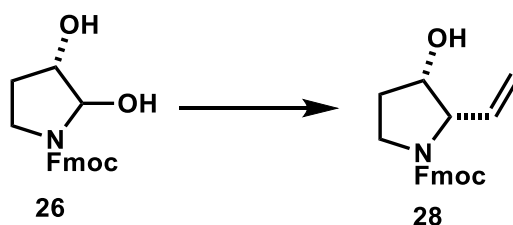


Vinyl magnesium bromide (1 M in THF, 100 mL, 100 mmol) was added to a magnetically stirred solution of trimethyl borate (10.2 mL, 92 mmol) in THF (50 mL) maintained at -78 °C over 10 min. After 1 h, the solution was warmed to room temperature for 5 h. HCl (10 ml of 20% aqueous solution) was added to the solution. This was maintained for 10 min, then 2-methylpentadiol (11.3 mL, 90 mmol) in diethyl ether (9 mL) was added. After 16 h, the resulting mixture was quenched with water and phases separated. The aqueous layer was further extracted with CH₂Cl₂ (3 x 20 mL). The combined organic layers were dried (MgSO₄) and concentrated under vacuum to yield a yellow oil. After distillation using a 1 millibar vacuum (20 °C, 0.1 Torr) the borinane **27** was isolated as a clear oil.¹³

¹H NMR (CDCl₃, 400 MHz) δ: 6.07 (1 H, dd, *J* = 24 Hz, *J* = 8 Hz), 5.91-5.75 (2H, m), 4.25 (1 H, m), 1.81 (1 H, dd, *J* = 20 Hz, *J* = 4 Hz), 1.57-1.49 (1 H, m), 1.33 (6 H, s), 1.29 (3 H, d, *J* = 8 Hz) ppm.

IR ν_{\max} (NaCl): 3064-2872, 1747, 1614, 1448, 1417, 1390, 1298, 1263, 966 cm⁻¹.

3.6.6 (2*S*,3*S*)-(9*H*-Fluoren-9-yl)methyl 3-hydroxy-2-vinylpyrrolidine-1-carboxylate (**28**)



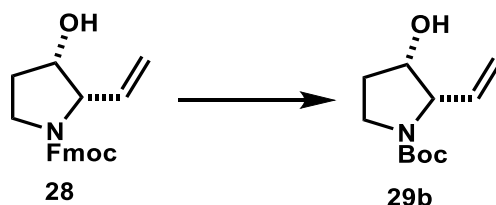
Borinane **27** (5.00 g, 32 mmol) was added to a solution of diol **26** (4.80 g, 15 mmol) in CH₂Cl₂ (150 mmol) and cooled to -78 °C. Boron trifluoride diethyl etherate (15 mL, 120 mmol) was slowly added over 0.25 h. The solution was slowly warmed to room temperature. After 16 h, the resulting mixture was quenched with saturated NaHCO₃ and separated. The aqueous layer was then extracted with CH₂Cl₂ (3x 20 mL) and the organic layers were combined, dried with MgSO₄ and concentrated under vacuum to give a pale brown oil. The desired product was isolated through recrystallization to afford compound **28** as a viscous yellow oil.

¹H NMR (CDCl₃, 400 MHz) δ: 7.82 (2H, d, *J* = 4 Hz), 7.65 (2H, d, *J* = 4 Hz), 7.45-7.30 (4H, m), 5.93-5.76 (1H, m), 5.45-5.05 (2H, m), 4.58-4.18 (4H, m) 3.70-3.45 (2H, m), 2.00-1.85 (1H, m) ppm.

^{13}C NMR (CDCl_3 , 100 MHz) δ : 171.3, 141.4, 133.6, 127.7, 127.0, 125.0, 120.0, 67.0, 60.4, 47.4, 43.8, 31.6, 22.7, 21.1, 14.0 ppm.

IR ν_{max} (NaCl): 3600-3200, 3066-2893, 1670, 1452, 1417, 1356, 1248, 1113, 995, 920, 758 cm^{-1} .

3.6.7 (2S,3S)-tert-Butyl 3-hydroxy-2-vinylpyrrolidine-1-carboxylate (29b)



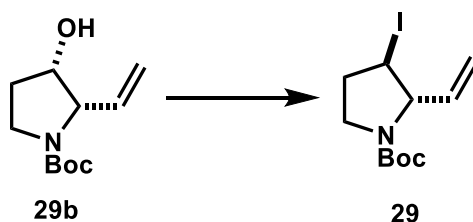
Piperidine (0.70 mL, 7.2 mmol) was added to a solution of the compound **28** (0.80 g, 2.6 mmol) in THF (20 mL) at room temperature. After 2 h, the solvent was removed *in vacuo* to give a yellow salt, which was triturated with ether to remove the solid, to provide a yellow oil. To the solution of the resulting oil in THF (30 mL), Boc_2O (1.25 g, 5.1 mmol) and sodium carbonate (0.60 g, 5.6 mmol) were added slowly at room temperature. After 16 h the ensuing mixture was then quenched with brine (10 mL) and the phases separated. The aqueous layer was then extracted with CH_2Cl_2 (3 x 15 mL). The combined organic phases were then dried and concentrated through vacuum to give a yellowish oil. Compound **29b** was purified *via* flash chromatography, as a pale-yellow oil.

^1H NMR (CDCl_3 , 400 MHz) δ : 5.73-5.52 (1H, m), 5.18-5.05 (2H, m), 4.27-4.10 (2H, m), 3.4-3.2 (2H, m), 1.94-1.87 (1H, m), 1.72-1.64 (1H, m), 1.45 (9H, s) ppm.

^{13}C NMR (CDCl_3 , 100 MHz) δ : 207.0, 134.4, 118.0, 72.5, 63.0, 44.0, 43.4, 30.9, 28.4, 27.4 ppm.

IR ν_{max} (NaCl): 3650-3100, 2978, 2933, 2893, 1670, 1477, 1406, 1367, 1253, 1167, 1114, 1064, 918, 896, 771, 736 cm^{-1} .

3.6.8 (2R,3S)-tert-Butyl 3-iodo-2-vinylpyrrolidine-1-carboxylate (29)



Iodine (1.57 g, 1.2 mmol) and imidazole (1.2 g, 1.5 mmol) were added to a stirred solution of pyrrolidine **29b** (0.85 g, 1 mmol) and triphenylphosphine (1.50 g, 1.3 mmol) in THF (25 mL) maintained at 0 °C. After 1 h, the resulting mixture was warmed to room temperature and stirred for 16 h. The reaction mixture was further quenched with brine (10 mL) and extracted with CH₂Cl₂ (3 x 15 mL). The combined organic fractions were dried and concentrated under vacuum to afford a yellow oil. The oil was isolated through flash chromatography to give the iodide **29** as a yellow oil.¹⁵

¹H NMR (CDCl₃, 400 MHz) δ: 5.74 (1H, bs), 5.27-5.16 (2H, m), 4.75-4.55 (1H, m), 4.20-4.18 (1H, m), 3.76 (1H, bs), 3.51 (1H, bs), 2.32-2.26 (1H, m), 2.18-2.12 (1H, m), 1.47 (9H, s) ppm.

¹³C NMR (CDCl₃, 100 MHz) δ: 206.9, 136.2, 116.1, 70.9, 45.0, 34.5, 30.9, 28.4, 26.9 ppm.

IR ν_{max} (NaCl): 2976, 2931, 2889, 1697, 1447, 1390, 1365, 1257, 1167, 1113, 1060, 912, 769 cm⁻¹.

3.7 References

- (1) (a) R. W. Jemison, W. D. Ollis, I. O. Sutherland, J. Tannock, *J. Chem. Soc. Perkin Trans. 1*. **1980**, 1462. (b) M. Dollinger, W. Henning, W. Kirmse, *Chem Ber.* **1982**, 115, 2309. (c) T. J. Sprules, J. D. Galpin, D. Macdonald, *Tetrahedron Lett.* **1993**, 34, 247. (d) J. P. Hagen, K. D. Lewis, S. W. Lovell, P. Rossi, A. Z. Tezcan, *J. Org. Chem.* **1995**, 60, 7471.
- (2) (a) E. J. Corey, D. H. Lee, *J. Am. Chem. Soc.* **1991**, 113, 4026. (b) S. Ito, T. Tsunoda, J. Chin, *Chem. Soc.* **1992**, 39, 205. (c) T. Tsunoda, S. Tatsuki, Y. Shiraishi, M. Akasaka, S. Ito, *Tetrahedron Lett.* **1993**, 34, 3297. (d) T. Tsunoda, S. Tatsuki, K. Kataoka, S. Ito, *Chem. Lett.* **1994**, 543. (e) D. Enders, M. Knopp, R. Schiffers, *Tetrahedron asymm.* **1996**, 7, 1847. (f) M. Kobayashi, K. Masumoto, E. Nakai, T. Nakai, *Tetrahedron Lett.* **1996**, 37, 3005. (g) A. Krebs, U. Kazmaier, *Tetrahedron Lett.* **1996**, 37, 7495.
- (3) S. M. Allin, M. A. C. Button, *Tetrahedron Lett.* **1999**, 40, 3801.
- (4) E. J. Corey, S. G. Pyne, W. Su, *Tetrahedron Lett.* **1980**, 21, 3175.
- (5) S. M. Allin, M. A. C. Button, S. J. Shuttleworth, *Synlett.* **1997**, 725.
- (6) S. M. Allin, M. A. C. Button, *Tetrahedron Lett.* **1998**, 39, 3345.
- (7) R. D. Baird, PhD Thesis, Loughborough University, **2001**.
- (8) S. M. Allin, M. A. C. Button, R. D. Baird, *Synlett.* **1998**, 1117.

- (9) P. A. Wender, J. M. Schause, D. C. Torney, *Tetrahedron Lett.* **1979**, 27, 2485.
- (10) S. M. Allin, R. D. Baird, R. J. Lins, *Tetrahedron Lett.* **2002**, 43, 4195.
- (11) I. E. Marko, J. M. Plancher, *Tetrahedron Lett.* **1999**, 40, 5259.
- (12) K. E. Miller, A. J. Wright, M. K. Olesen, M. T. Hovey, J. R. Scheerer, *J. Org. Chem.* **2015**, 80, 1569.
- (13) A. P. Lightfoot, S. J. R. Twiddle, A. Whiting, *Org. Biomol. Chem.* **2005**, 3, 3167.
- (14) J. M. Hammann, A. K. Steib, P. Knochel, *Org. Lett.* **2014**, 16, 6500.
- (15) J. Robertson, PhD Thesis, University of Tasmania, **2016**.

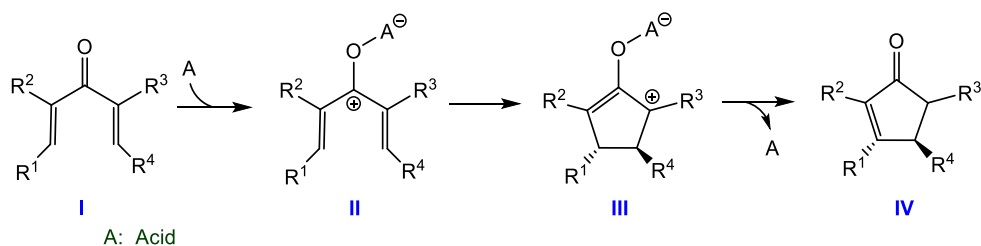
Chapter Four

Nazarov Cyclisations Initiated by DDQ-Oxidised Pentadienyl Ether: A Mechanistic Investigation from the DFT Perspective

*Density functional theory (DFT) has been utilised to study the mechanism of Nazarov cyclisations initiated by oxidation of pentadienyl ethers by a benzoquinone derivative (DDQ), as recently reported by West et al. (Angew. Chem. Int. Ed., **2017**, 56, 6335). It was determined that the reaction is most likely initiated by a hydride transfer from the pentadienyl ether to an oxygen of DDQ through a concerted pathway and not a single electron transfer mechanism. Interestingly, an excellent correlation between the hydride transfer activation energy and the gap between the ether HOMO and the benzoquinone LUMO ($R^2=0.99$) was also found. Based on this correlation, a formula for predicting the activation energy of the oxidation process mediated by DDQ is also provided.*

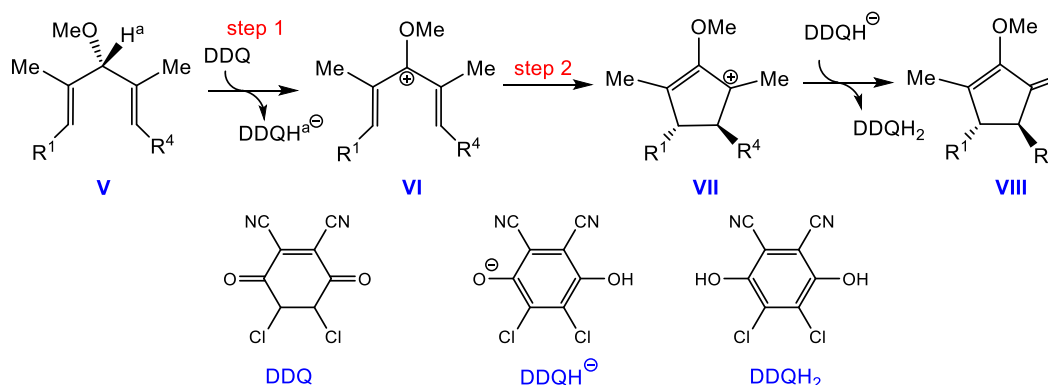
4.1 Introduction

Nazarov cyclisations are an extremely useful tool in the organic synthesis of cyclopentenones from dienones in the presence of Brønsted or Lewis acids (Scheme 4.1).¹ Indeed, the addition of an acid to acyclic divinyl ketone **I** generates crucial cationic intermediate **II** from which access to the process of 4π -electron conrotatory ring closure becomes feasible.² The reaction proceeds so reliably that it can be used to synthesise five-membered rings with multiple functional group substituents (yields of up to 90% can be achieved).³ It is notable that Nazarov cyclisation is also reachable by numerous promoters, e.g. UV radiation, and transition metal catalysis.³



Scheme 4.1. Nazarov electrocycloisatlon reaction passing through key carbocation **II** leading to a cyclopentenone.

The formation of pentadienyl carbocation **II** is a prerequisite for the electrocycloisatlon to occur. Interestingly, West et al. recently introduced a new strategy for formation of the key carbocation intermediate, accessed through oxidation of bis(allylic) ether **V** by DDQ (2,3-dichloro-5,6-dicyano-1,4-benzoquinone, Scheme 4.1a).⁴ The first step of the reaction is assumed to be formation of **VI** *via* oxidative abstraction of H^a by DDQ. Subsequent to the formation of the carbocation, the electrocycloisatlon takes place to give **VII**. Finally, DDQH[•] deprotonates carbocation **VII** to afford the dienol ether product **VIII**.

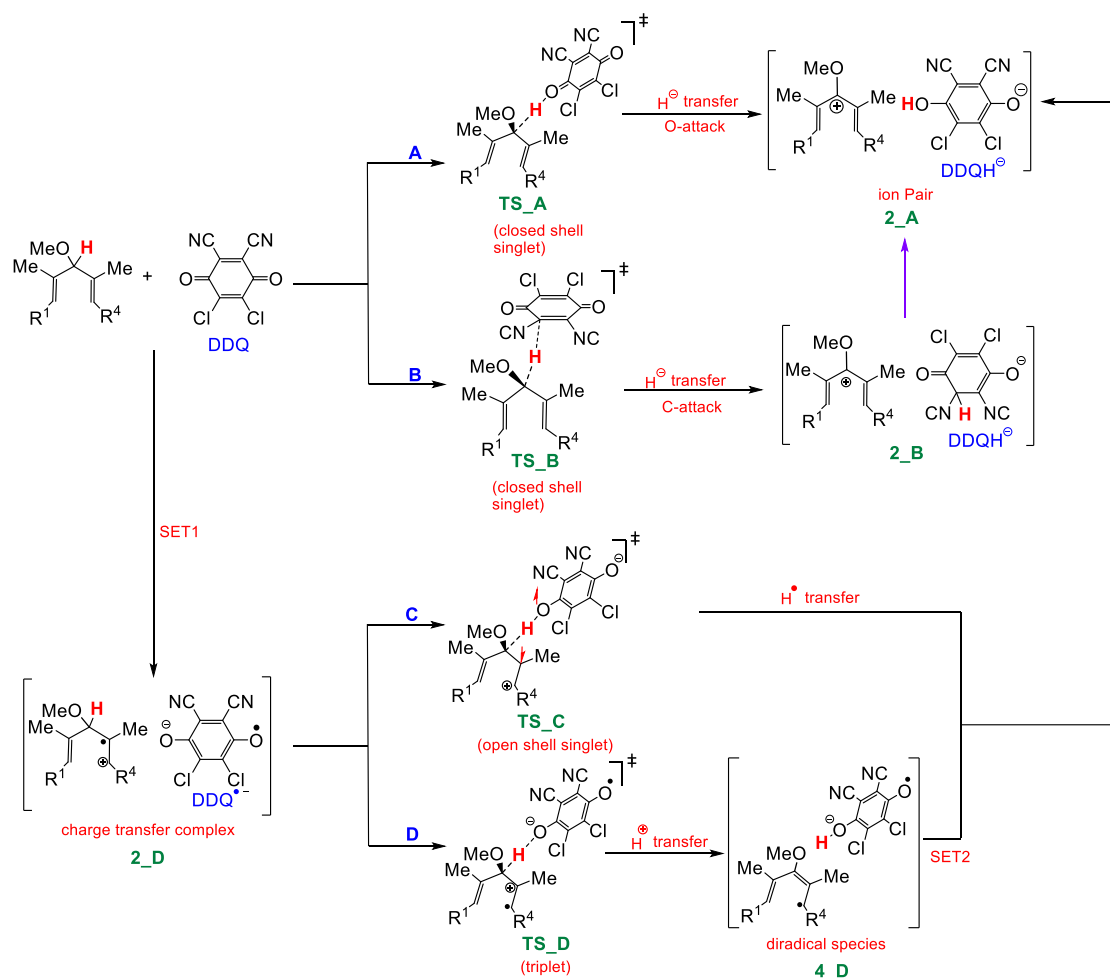


Scheme 4.1a. DDQ-initiated Nazarov reaction starting from pentadienyl ether **V**, yielding cyclopentadienyl ether **VIII** as the product.

Four closely related mechanisms have been reported in the literature for DDQ-mediated C-H bond cleavage reactions.⁵ These mechanisms (pathways **A** to **D**) are distinct in how the hydrogen abstraction occurs, as detailed in Scheme 4.1b. Pathways **A** and **B** feature direct hydride (H[•]) transfer; pathway **C** features hydrogen radical (H[•]) transfer and pathway **D** features a proton (H⁺) transfer. There are two pathways for H[•] transfer; O-attack and C-attack. In the O-attack case, a one-step H[•] transfer to a DDQ oxygen can directly generate ion

pair complex **2_A** whereas, in the C-attack case, the hydride transfer to a carbon atom attached to a cyano group on DDQ forms ion pair **2_B**. This intermediate can then undergo a hydrogen transfer to give the more stable isomer **2_A**.

The single electron transfer (SET) from bis(allylic) ether to DDQ creates charge transfer complex **2_D** from which two pathways (**C** or **D**) may be accessed. The rationale for this branching point stems from the fact that DDQ^{•-} has two active sites on its oxygen centres. The radical oxygen of DDQ can abstract H[•] *via* transition structure **TS_C** on an open shell singlet surface to give ion pair complex **2_A** (pathway **C**). This ion pair is also accessible if the anionic oxygen site of DDQ^{•-} abstracts a proton *via* transition structure **TS_D** on a triplet surface, followed by a second SET from biradical species **4_D** (pathway **D**).



Scheme 4.1b. Four different mechanisms considered for DDQ-mediated formation of ion pair **2_A**.⁵

West and co-workers proposed the SET mechanism *via* pathway **C** for generation of the key carbocation intermediate. The hypothesis for a SET mechanism may have originated from the observation of an instantaneous colour change from clear to deep purple, upon addition of DDQ to **V** (Scheme 4.1a).⁴

It is worth noting that the mechanisms of this transformation and many analogous processes involving DDQ as an oxidant have been under debate in recent computational and experimental reports. In 2017, Todd et al. explored the mechanism of DDQ-mediated cross-dehydrogenative coupling (CDC) reactions and suggested that a SET mechanism is likely to occur.⁶ Similarly, Xu and co-workers reported an oxidative C-C bond formation by treatment of benzyl ethers with DDQ.⁷ For this process, an immediate colour change was observed. The

authors attributed this colour change to formation of an ion pair analogues to **2_A** and not a charge transfer complex.

In a series of experimental studies, Jackman et al. demonstrated that the oxidation of hydrocarbons by DDQ normally takes place by formation of a crucial carbocation through a rate-determining direct hydride transfer,⁸ a statement supported by the DFT studies of Yamabe et al. and Heesing et al.⁹ In contrast, in an experimental investigation, Ruchardt and co-workers inferred the intermediacy of radicals from spin trapping experiments in the quinone dehydrogenation of hydroaromatics and assigned a SET mechanism for the process.⁵ⁱ In a DFT study Chan and Radom determined that the trapping of radicals was not conclusive evidence of a radical pathway.¹⁰ They found that a radical mechanism operates if the reaction is conducted in the gas phase or in a non-polar solvent such as heptane. In 2012, Batista and co-workers explored the oxidative functionalisation of benzylic C-H bonds by DDQ theoretically and indicated that direct hydride abstraction is about 10 kcal/mol more favourable than a SET mechanism.¹¹ Mayr et al. explored computationally and experimentally the kinetics of hydride abstraction by DDQ from numerous boranes (B-H), stannanes (Sn-H) dienes and dihydropyridines (C-H).^{5d} They demonstrated that the C-attack pathway is observed for the B-H and Sn-H hydride donors, whereas the O-attack is the preferred pathway for C-H hydride donors. Recently, a detailed experimental and computational study by Liu and Floreancig et al. came to the conclusion that the C- and O-attack pathways are very competitive for C-H bond functionalisation of benzylic, allylic, and alkenyl ether substrates mediated by DDQ.¹²

Due to these ambiguities regarding the mechanism of C-H bond functionalization by DDQ, this chapter aimed to clarify the Nazarov cyclisation initiated by the DDQ reduction (developed by West et al., Scheme 4.1a) using DFT calculations. For this class of reactions, all four possible pathways (Scheme 4.1b) were explored, and indicated that direct hydride transfer to a DDQ oxygen is most likely to operate. The correlations between the ease of C-H bond oxidative cleavage and the nature of substituents on the bis(allylic) ether and benzoquinones was also established. In agreement with experimental reports, it is inferred from the results that electron donating groups on the ether substrate accelerate the hydride transfer process.⁴ In contrast, the same substituents on benzoquinones are suggested to retard

it. Remarkably, we were able to provide an equation by which one may predict H⁺ transfer activation barriers based upon electronic parameters.

All the calculations performed in this work have been done by the candidate in the CCL group at UTAS under supervision of Assoc. Prof. Alireza Ariaferd and Prof. Brian F. Yates.

4.2 Computational Study

Gaussian 16¹³ was used to fully optimize all the structures involved in this study at the B3LYP level of density functional theory (DFT)¹⁴ in CH₂Cl₂ using the CPCM solvation model.¹⁵ The 6-31G(d) basis set was used for all atoms.¹⁶ Frequency analyses were performed at the same level of theory to ensure that a minimum or transition structure was achieved. To further refine the energies obtained from the B3LYP/6-31G(d) calculations, single-point energy calculations for all of the structures with 6-311+G(2d,p) basis set in CH₂Cl₂ using the SMD solvation model at the M06-2X level was carried out. The Gibbs free energies obtained from the M062X/6-311+G(2d,p)//B3LYP/6-31G(d) calculations in CH₂Cl₂ was used throughout the chapter. Minimum energy crossing point (MECP) between closed shell singlet and triplet states were located using the code of Harvey et al.¹⁷

4.3 Results and Discussion

The investigation was commenced by calculating all four possible pathways discussed in Scheme 4.1b using bis(allylic) ether **sub_1** as the model substrate (Figure 4.3). Direct hydride transfer to an oxygen of DDQ from **sub_1** (pathway A) is computed to be the most favourable pathway with an activation barrier of 21.7 kcal/mol. Pathway B in which the hydride directly transfers to a CN-substituted carbon of DDQ is about 6.8 kcal/mol higher in energy than pathway A. The higher activation energy of pathway B with respect to pathway A may be attributed to the adjacency of two highly π -conjugated styrenyl moieties to the transferring hydride. The SET pathways are required to pass through charge transfer complex **2_D** lying 5.4 kcal/mol above transition structure **TS_A**. This result suggests that the SET mechanisms are unlikely to operate. Our calculations at different levels of theory (M06-2X-D3 and B3LYP-D3) validate this claim and confirm unfavourability of the SET mechanism. Despite the unlikeliness of the SET mechanism, pathway D was included in this investigation for the sake of completeness. The favourability of pathway A compared to pathway C is further supported by the fact that many attempts to locate a transition structure on an open shell singlet surface (**TS_C**) always collapsed to the closed-shell transition structure **TS_A**, demonstrating that the redox process *via* pathway C is not feasible. The key transition structure for pathway D was computed to be 33.7 kcal/mol which further supports the SET mechanism being not feasible. To understand how easily structure **1_D** on a singlet surface connects with **2_D** on a triplet surface, the minimum energy crossing point (MECP) for this process was calculated. Notably, the energy of the MECP is calculated to be very close to the energy of **2_D**, suggesting that conversion of **1_D** to **2_D** should occur without any significant reaction barrier. In short, although West et al. proposed a SET mechanism for the hydride transfer process,⁴ our calculations at different levels of theory support direct hydride transfer *via* pathway A.

At this juncture, attention was turned to the Nazarov cyclisation step starting from the pentadienyl cation **5**. It was found that the 4π -electrocyclisation occurs with an activation barrier of 8.7 kcal/mol through transition structure **TS₅₋₆** to give alkoxy cyclopentadienyl cation **6** (Figure 4.3a 1). The structure **6** can be a branching point for two competitive routes (Figure 4.3a 2). In one of them (route I), the anionic oxygen of **5** can react with carbocation **6**

via **TS**₈₋₁₀ to give ether **10**. In the other one (route II), the anionic oxygen site of DDQH⁻ can abstract a proton from **6** by passing through **TS**₇₋₉ to afford final product **9**. The energy of **TS**₇₋₉ and **TS**₈₋₁₀ are computed to be comparable, implying that both products **9** and **10** should form simultaneously. However, it is interesting to note that **10** is about 7.1 kcal/mol less stable than **9** and reaction **8**→**10** is reversible due to the fact that **TS**₈₋₁₀ lies only 16.2 kcal/mol above **10**. In such a case, **10** is expected to surmount an activation barrier of 16.5 kcal/mol and transform into the more stable product **9**. This result is in accord with the experimental observation that only product **9** was characterized.⁴

It is inferred from the calculations that the reaction **sub_1** + DDQ → **9** + DDQH₂ proceeds through three major steps: (i) direct hydride transfer to DDQ *via* pathway A, (ii) 4π-electrocyclisation and (iii) deprotonation. The activation barrier for these three steps is calculated to be 21.7, 8.7, and 16.5 kcal/mol, respectively. This demonstrates that the rate determining step for this process is most likely the first step, a result which is entirely consistent with the interpretation of West et al.⁴

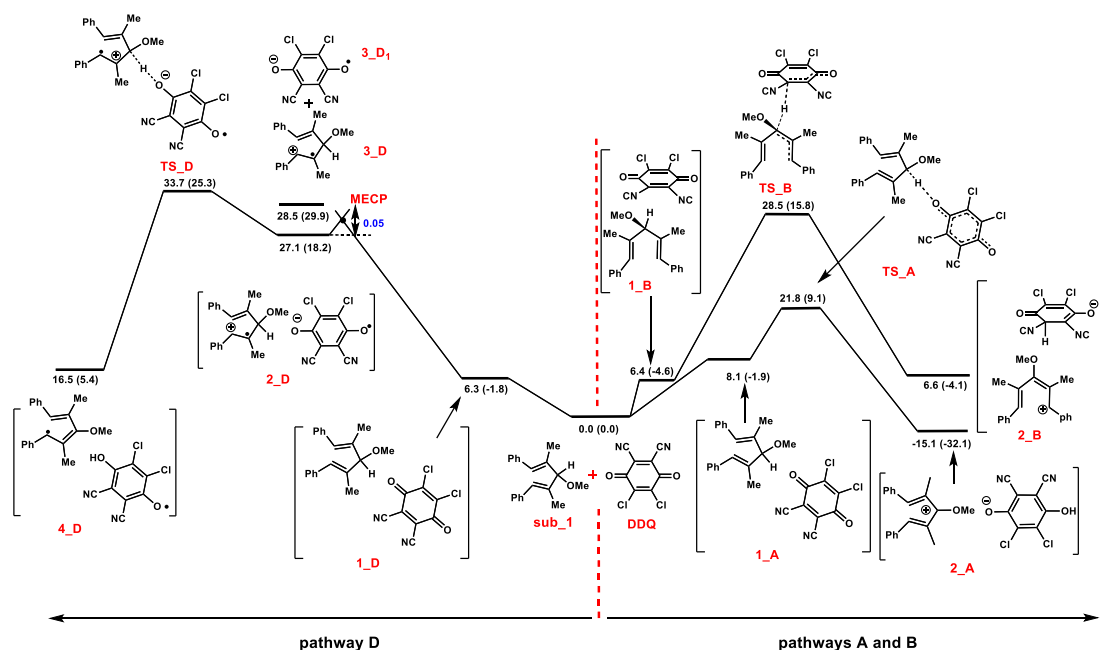


Figure 4.3. Energy profile for the reaction between pentadienyl ether (**sub_1**) and DDQ through pathways A, B, and D. The relative Gibbs and potential energies (in parentheses) obtained from M06-2X/6-311+G(2d,p)//B3LYP/6-31G(d) calculations are given in kcal/mol.

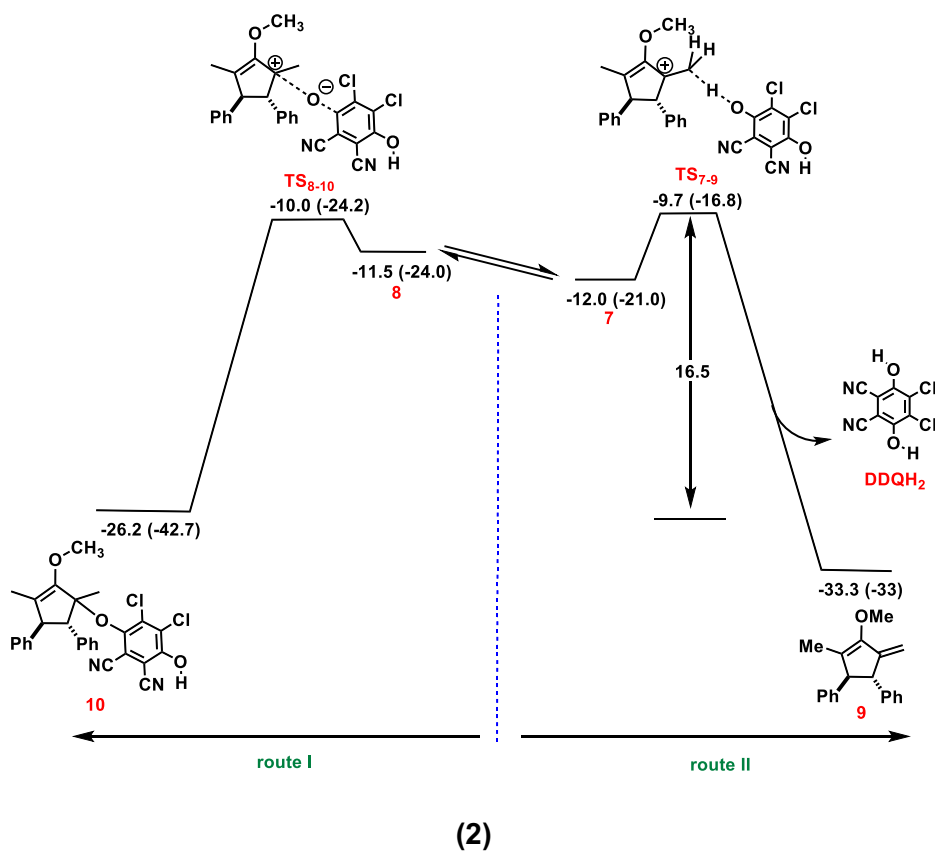
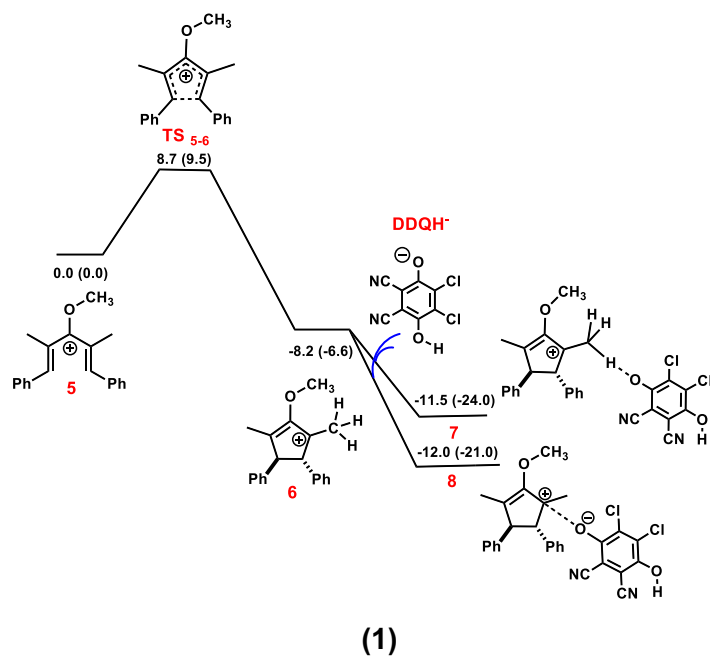


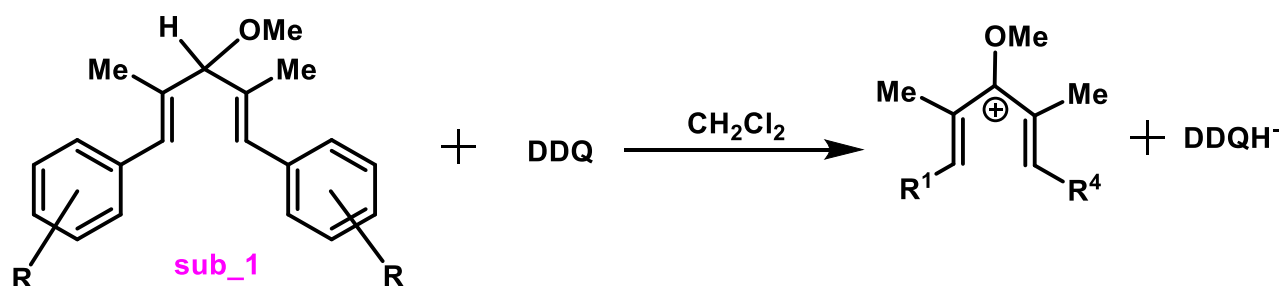
Figure 4.3a. Energy profiles for (1) the 4π electrocyclicalisation step starting from **5** and (2) trapping of carbocation **6** via two different routes I and II. The relative Gibbs and potential energies (in parentheses) obtained from M06-2X/6-311+G(2d,p)//B3LYP/6-31G(d) calculations are given in kcal/mol.

4.3.1 Substitution effects of the dienes substrate on the ease of the C-H bond cleavage

West et al. found that if the phenyls on the diene **sub_1** are substituted by electron donating groups, then the reaction accelerates.⁴ On that basis, they suggested that the H⁺ transfer from diene to DDQ should be the rate determining step. To evaluate this claim, the energy of transition structures **TS_A**, **TS_B**, **TS_D**, charge transfer complex **2_D** and intermediate **2_A** were calculated for different substituents (Table 4.3.1). As established for **sub_1** with R = H (Table 4.3.1), it was impossible to locate transition structure **TS_C** for any of these assays and all attempts to do so collapsed to **TS_A**. Several points are inferred from Table 4.3.1. First, for all **sub_1**, pathway A was found to be most favourable, implying that regardless of the diene nature, DDQ always abstracts H⁺ from the diene in a concerted fashion. Second, in line with the findings of West et al., aryl rings with electron donating substituents such as Me, OMe and NH₂ have a lower activation energy than those with electron withdrawing substituents such as CN and Cl. Third, charge transfer complex **2_D** is stabilised when the aryl ring is substituted by electron donating groups. Fourth, formation of **2_D** is always an endergonic process which implies that detection of such an intermediate should be unlikely. Fifth, in contrast to the energy of **TS_A** and **2_D** which showed a strong dependence on the electronic nature of the ether substituents, the stability of **2_A** is less sensitive to such substituents; the energy of **2_A** only spans a narrow range from -13.5 to -17.4 kcal/mol.

Interestingly, it was found that the HOMO of **sub_1** plays an important role in controlling the activation energy of pathway A. Electron donating groups raise the energy of the HOMO, facilitating the H⁺ transfer process. An excellent correlation between the energy of **TS_A** and the **sub_1** HOMO ($R^2=0.97$) lends support to the claim (Figure 4.3.1). The HOMO energy also affects the energy of charge transfer complex **2_D**. The higher the destabilised HOMO the lower the energy of **2_D**; an excellent correlation was obtained between these two parameters (Figure 4.3.1a). At this point, it was noteworthy that the energy of **2_D** spans a wider range (from 9.2 to 39.9 kcal/mol) compared to that of **TS_A** which spans a narrower range (from 16.2 to 29.2 kcal/mol). This implies that the energy of the charge transfer complex **2_D** is more sensitive to the HOMO than that of **TS_A**.

Table 4.3.1. Relative Gibbs free energy (kcal/mol) of transition structures **TS_A**, **TS_B**, and **TS_D** and intermediates **2_D** and **2_A** calculated for cases where the pentadienyl ether is substituted by a variety of R groups.



Entry	R-Ph	ΔG (kcal/mol)					HOMO (ev)
		(TS_A)	(TS_B)	(TS_D)	(2_D)	(2_A)	
1	para-CN-Ph	26.3	31.7	37.0	35.1	-14.2	-7.86
2	para-Cl-Ph	23.7	29.5	34.5	29.2	-15.1	-7.56
3	Ph	21.7	28.5	33.7	27.1	-15.2	-7.52
4	para-Me-Ph	21.2	27.7	31.8	25.4	-15.3	-7.33
5	para-OMe-Ph	19.1	26.1	30.3	19.5	-15.6	-7.08
6	para-NH ₂ -Ph	16.2	24.3	27.8	11.0	-16.1	-6.74
7	para-NMe ₂ -Ph	13.8	22.7	24.5	9.2	-17.4	-6.37
8	meta-CN-Ph	29.2	35.7	40.0	39.9	-13.5	-8.21
9	meta-OMe-Ph	22.7	29.4	34.0	26.6	-14.7	-7.38
10	meta-Me-Ph	20.8	27.3	32.8	27.0	-15.8	-7.40

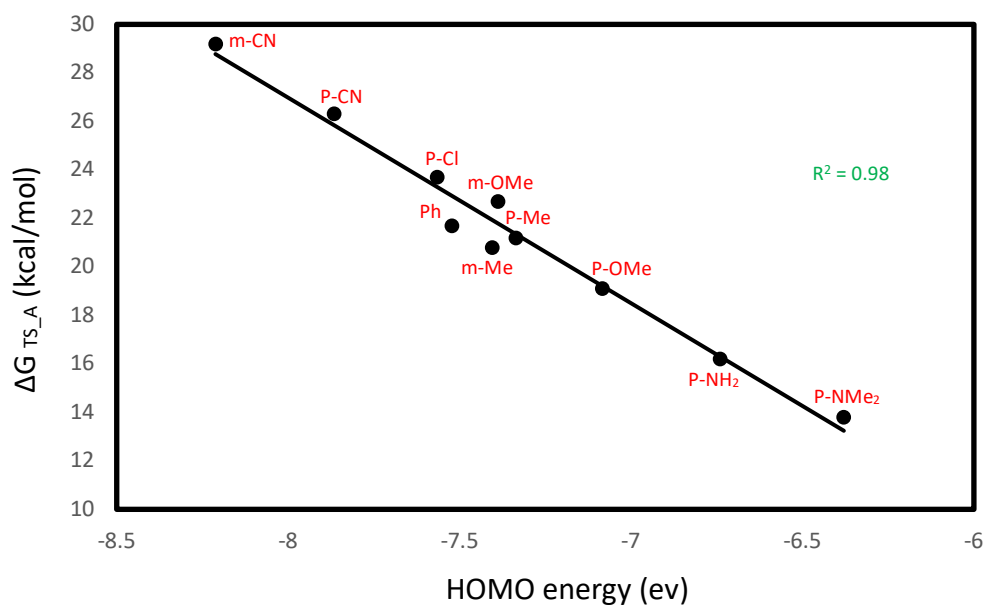


Figure 4.3.1. A plot of correlation between ΔG_{TS_A} and HOMO energy of different **sub_1** derivatives.

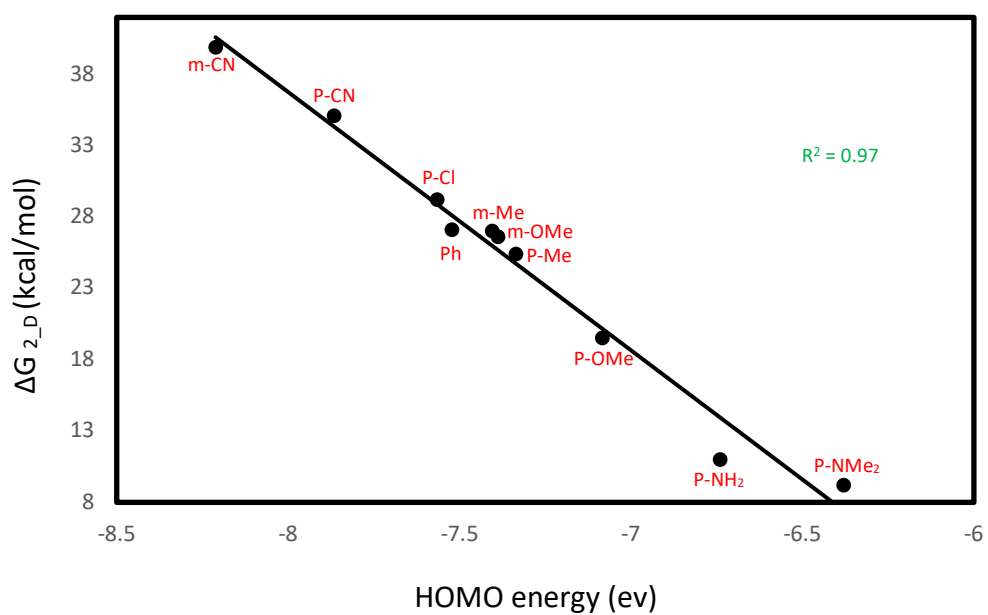


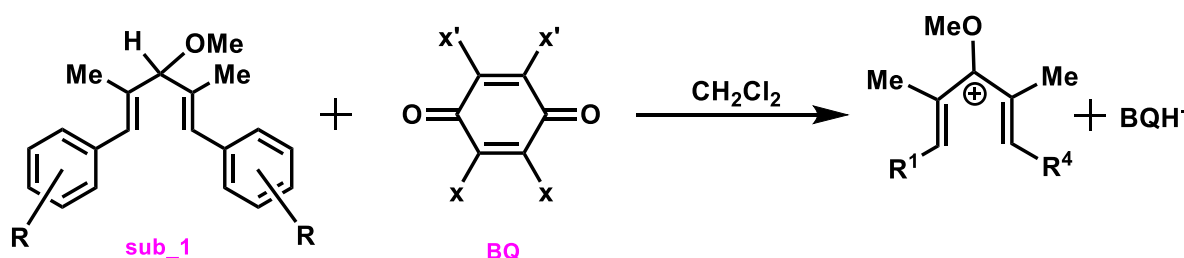
Figure 4.3.1a. A plot of correlation between ΔG_{2_D} and HOMO energy of different **sub_1** derivatives.

4.3.2 Substitution effects of benzoquinone on the hydride transfer mechanism

As aforementioned, the HOMO of **sub_1** was shown to modulate the ease of reaction between DDQ and **sub_1**. A question arises here about whether the LUMO of a benzoquinone (**BQ**) can have a similar effect. In this case, it was expected that a benzoquinone with a more stabilised LUMO would be a better hydride acceptor. To demonstrate this claim, we investigated different benzoquinones with a variety of substituents as depicted in Table 4.3.2. Clear inferences to be drawn from our findings are listed as follows. First, regardless of the **BQ** nature, pathway A is favoured over the others. Second, the energy of **2_D** and **TS_A** is affected by the LUMO energy of the **BQ**: the more stabilised the LUMO, the lower the energy for both stationary points **2_D** and **TS_A**. Third, a lower activation barrier invariably results in a more exergonic hydride transfer.

The excellent correlations between the **BQ** LUMO energy and the **TS_A** energy ($R^2=0.98$) as well as those between the **BQ** LUMO energy and the **2_D** energy ($R^2=0.97$) corroborates some of the points mentioned above (Figure 4.3.2 and 4.3.2a). From Table 4.3.2 it is apparent that only **BQ** oxidants having electron withdrawing groups adequately facilitate the hydride transfer process. As such, the corresponding Nazarov reaction is predicted not to proceed under mild conditions if an unsubstituted **BQ** (i.e. quinone) is used as the oxidant.

Table 4.3.2. Relative Gibbs free energy (kcal/mol) of transition structures **TS_A**, **TS_B**, and **TS_D** and intermediates **2_D** and **2_A** calculated for different benzoquinones with a variety of X and X' groups.



Entry	X	X'	ΔG (kcal/mol)					LUMO (ev)
			(TS_A)	(TS_B)	(TS_D)	(2_D)	(2_A)	
1	H	H	35.0	42.4	54.1	55.4	-6.5	-2.80
2	Cl	Cl	28.1	41.0	43.1	40.0	-5.2	-3.42
3	CN	H	26.0	31.1	35.7	34.7	-12.6	-3.86
4	CN	Cl	21.7	28.5	33.7	27.1	-15.2	-4.12
5	CN	CN	17.3	25.8	26.6	18.2	-22.1	-4.62

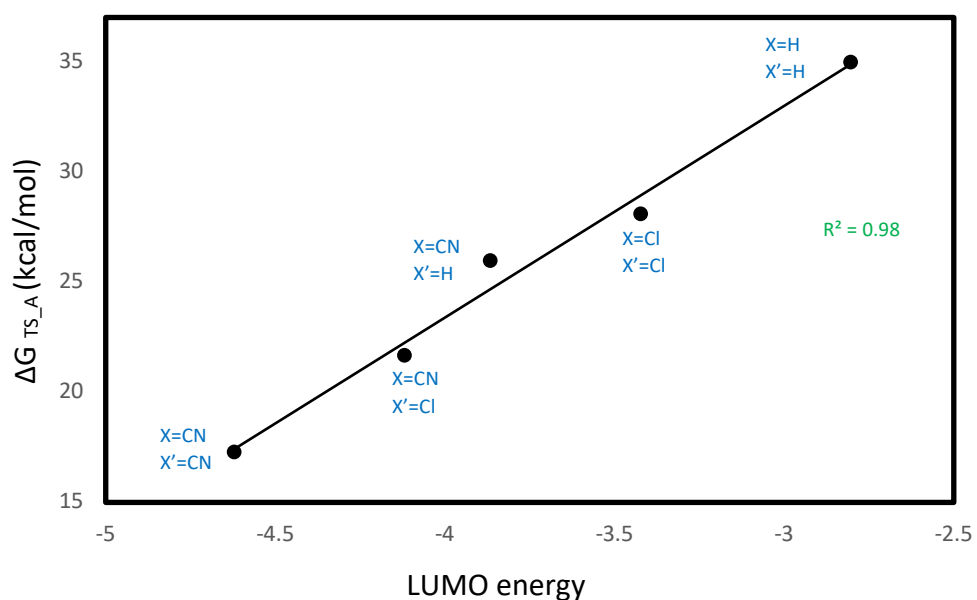


Figure 4.3.2. A plot of correlation between ΔG_{TS_A} and LUMO energy of different **BQ** derivatives.

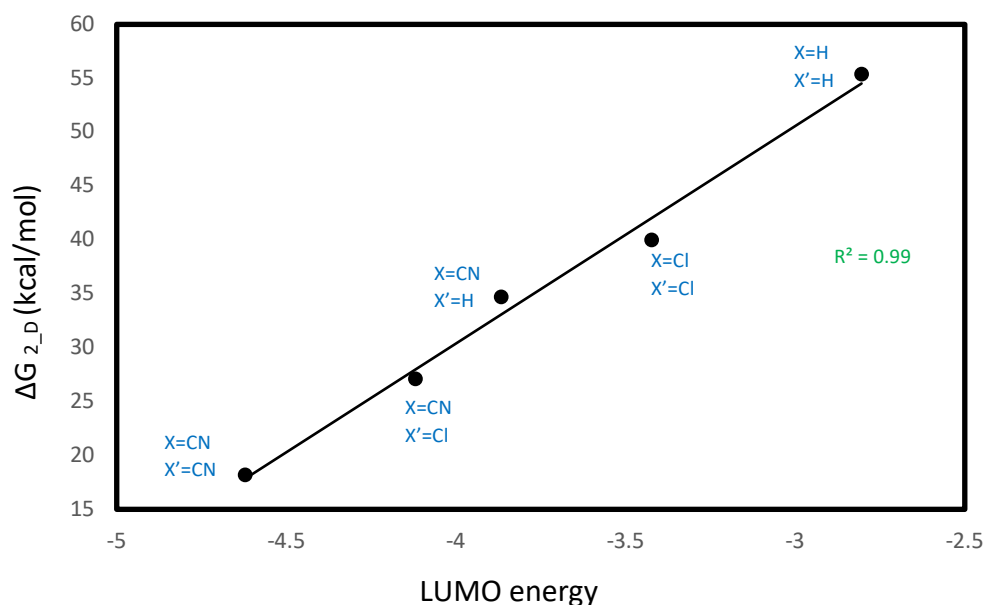


Figure 4.3.2a. A plot of correlation between ΔG_{2-D} and LUMO energy of different **BQ** derivatives.

4.3.3 A predictive formula for the reactivity of C-H bond cleavage mediated by DDQ

Recently Liu and Floreancig et al. proposed a predictive model designed in terms of the stability of the key carbocation intermediate and the extent of electron transfer in the transition structure for hydride transfer between DDQ and the ether substrate.¹² In this study, a new formula that can be expressed based only upon the energy of the reductant HOMO and the oxidant LUMO was defined. It was found that the reactivity of these substrates toward hydride transfer is determined by the gap between the reductant HOMO and the oxidant LUMO: the smaller the gap, the faster the reaction. The plot given in Figure 4.3.3 lends support to the above claim as there is an excellent correlation ($R^2=0.98$) between the HOMO-LUMO gap and the **TS_A** Gibbs energy. The predictive formula for oxidative C-H bond functionalisation is also presented in Figure 4.3.3. In terms of this formulation, one can estimate the activation energy required for the hydride transfer process, regardless of the identity of the redox partners.

This HOMO-LUMO gap also enables us to predict the stability of charge transfer complex **2_D**. As the HOMO-LUMO gap decreases, the stability of **2_D** increases. The predictive formula for the stability of this charge transfer complex is presented in Figure 4.3.3a.

A comparison between the formulas given in Figure 4.3.3 and Figure 4.3.3a indicates that the slope of the latter (19.01) is almost twice as large as that of the former (8.78), implying that ΔG_{2_D} is more sensitive to the HOMO-LUMO gap than ΔG_{TS_A} . This statement gains strong support from the fact that ΔG_{2_D} spans a wider range (9.2 – 55.4 kcal/mol) while ΔG_{TS_A} spans a narrower range (13.8 – 35.0 kcal/mol).

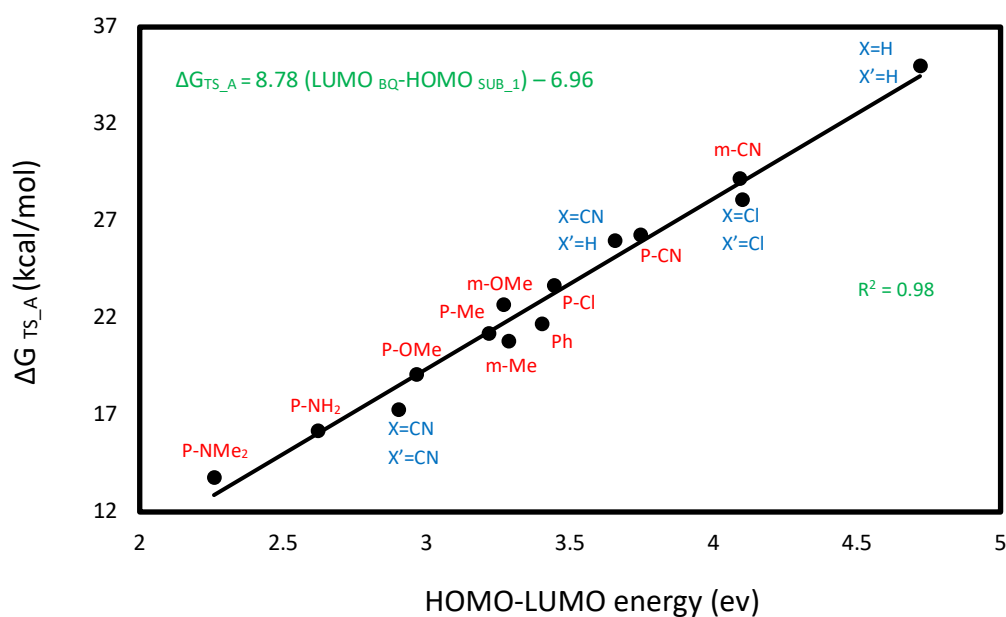


Figure 4.3.3. A plot of correlation between ΔG_{TS_A} and the gap energy between the **sub_1** HOMO and the **BQ** LUMO.

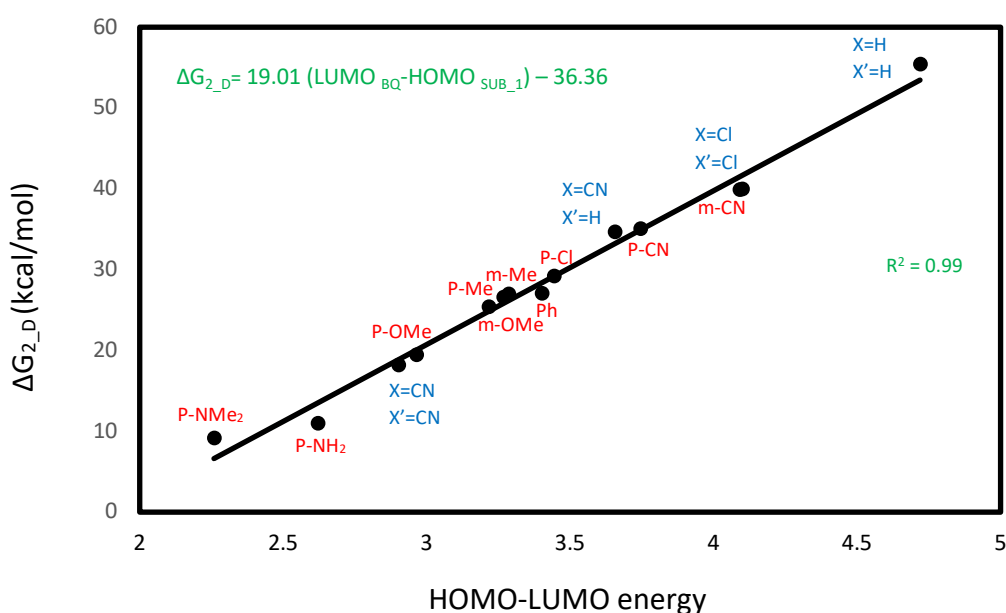
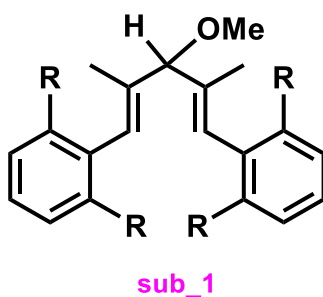


Figure 4.3.3a. A plot of correlation between ΔG_{2_D} and the gap energy between the **sub_1** HOMO and the **BQ** LUMO.

4.3.4 Application of predictive formula for substrates with *ortho*-substituted aryl rings

The predictive formula given in Figure 4.3.3 was obtained for the pentadienyl ether substrates with aryl rings substituted at the *meta* and *para* positions. Surprisingly, it was found that this formula does not effectively predict the hydride transfer activation energy for the substrates bearing *ortho* substituents on their aryl rings. For the *ortho* substituted substrates, the calculated activation barriers are higher than those predicted using the formula (Table 4.3.4). *Ortho* substituents create steric congestion which significantly distorts transition structure **TS_A** in a way that the C¹-C² π bond completely projects out of the plane defined by C², C³ and C⁴. This reduces the stability afforded by π -conjugation in the system, elevating the energy of **TS_A** and thereby making hydride abstraction from a substrate with *ortho* substituents an extremely strenuous process. This statement gains support from the large dihedral angle found for C⁴-C³-C²-C¹ in **TS_A** with CN substituted in the *ortho* positions (Figure 4.3.4). In contrast, the relevant dihedral angle is considerably smaller in **TS_A** when the aryl rings of the ether are substituted at the *para* position (Figure 4.3.4).

Table 4.3.4. Summary of activation energies for different *ortho* substituted aryl rings of the pentadienyl ether substrate; the calculated and predicted Gibbs free energies are given in kcal/mol.



Entry	R-Ph	ΔG (TS_A)	2A	HOMO (ev)	Predicted
1	ortho-CN-Ph	37.0	-14.3	-8.49	31.4
2	ortho-Cl-Ph	38.2	-14.7	-8.18	28.7
3	ortho-Me-Ph	34.3	-13.1	-7.75	25.0
4	ortho-NH ₂ -Ph	29.0	-15.3	-6.90	17.5

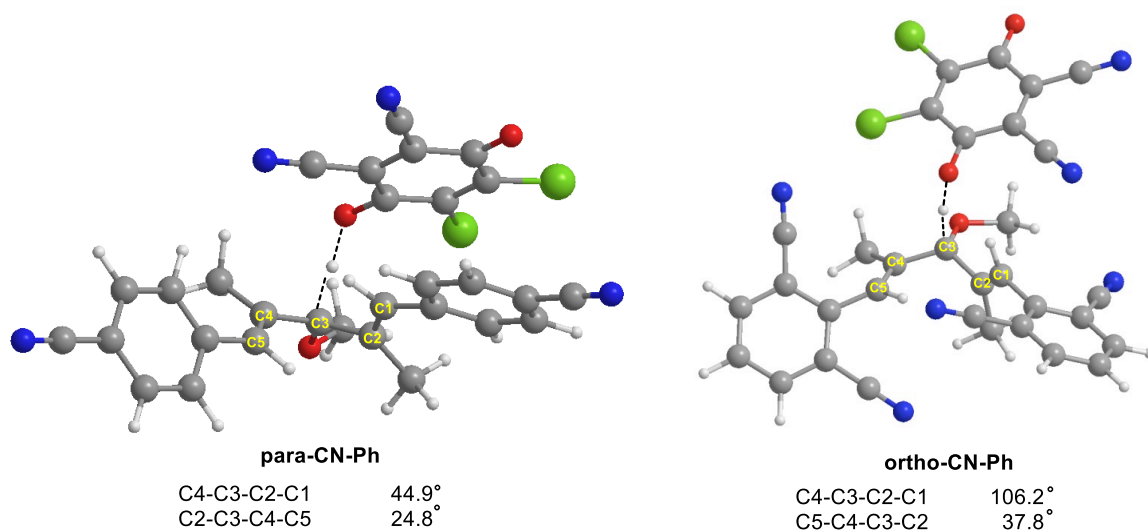


Figure 4.3.4. Optimized structures of TS_A for **para-CN-Ph** and **ortho-CN-Ph**.

4.4 Conclusion

In this study, the possible mechanisms for DDQ-initiated Nazarov cyclisations of 1,4-pentadienyl ethers were explored. These findings provide a better understanding of this chemical reaction. This work enabled several important conclusions to be drawn:

- (1) This reaction is composed of three primary steps: (i) hydride transfer to DDQ giving a pentadienyl cation and DDQH⁻; (ii) 4 π -electrocyclisation yielding a 2-alkoxycyclopentadienyl cation, and (iii) deprotonation of the ensuing cation by DDQH⁻ affording the final product. Consistent with the experimental results, calculations have shown that the first step is rate determining.
- (2) The first step of this reaction was computed to occur through direct hydrogen transfer from the pentadienyl ether substrate to an oxygen of DDQ, and not through a SET mechanism.
- (3) Interestingly, the HOMO energy of the pentadienyl ether and the LUMO energy of the benzoquinone were found to control the ease of the hydride abstraction step and determine the stability of the charge transfer complex.

- (4) Substrates bearing aryl rings with electron donating substituents undergo faster hydride transfer to DDQ due to having a higher lying HOMO.
- (5) Benzoquinones with electron withdrawing substituents act as good hydride abstractors owing to the presence of a lower lying LUMO.
- (6) The reactivity of substrates for losing a hydride in the presence of a benzoquinone shows a strong correlation with the energy gap between the substrate HOMO and the benzoquinone LUMO with a formulation of $\Delta G_{TS_A} = 8.78 (\text{LUMO BQ-HOMO SUB_1}) - 6.96 \text{ kcal/mol}$.
- (7) The aforementioned formula is not applicable for the case when the aryl rings of the substrate are substituted at the ortho position. The calculated activation barrier for hydride transfer in those cases is higher than the ones estimated using the formula. This can be attributed to the steric congestion inherent to an ortho substituent.

4.5 References

- (1) (a) A. J. Frontier, C. Collison, *Tetrahedron*. **2005**, *61*, 7577. (b) K. L. Habermas, S. E. Denmark, T. K. Jones, *Org. React.* **1994**, *45*, 1. (c) H. Pellissier, *Tetrahedron*. **2005**, *61*, 6517. (d) M. A. Tius, *Eur. J. Org. Chem.* **2005**, *11*, 2206.
- (2) For some selective studies aimed at elucidating the Nazarov mechanism see (a) D. A. Smith, C. W. Ulmer II, *Tetrahedron Lett.* **1991**, *32*, 725. (b) D. A. Smith, C. W. Ulmer II, *J. Org. Chem.* **1991**, *56*, 4444. (c) A. Cavalli, M. Masetti, M. Recanatini, C. Prandi, A. Guarna, E. G. Occhiato, *Chem. Eur. J.* **2006**, *12*, 2836. (d) T. Vaidya; R. Eisenberg; A. J. Frontier, *ChemCatChem*. **2011**, *3*, 1531.
- (3) (a) S. Cai, Z. Xiao; Y. Shi, S. Gao, *Chem. Eur. J.* **2014**, *20*, 8681. (b) J. Huang, D. Leboeuf, A. J. Frontier, *J. Am. Chem. Soc.* **2011**, *133*, 6317. (c) D. Leboeuf, J. Huang, V. Gandon, A. J. Frontier, *Angew. Chem. Int. Ed.* **2011**, *50*, 10981. (d) G. Liang; S. N. Gradl, D. Trauner, *Org. Lett.* **2003**, *5*, 4931. (e) S. Pusch, D. Schollmeyer, T. Opatz, *Org. Lett.* **2016**, *18*, 3043. (f) X. Shi, D. J. Gorin, F. D. Toste, *J. Am. Chem. Soc.* **2005**, *127*, 5802. (g) V. Z. Shirinian,

- A. G. Lvov, A. M. Yanina, V. V. Kachala, M. Krayushkin, *Chem. Heterocycl. Compd.* **2015**, 51, 234. (h) L. Zhang, S. Wang, *J. Am. Chem. Soc.* **2006**, 128, 1442.
- (4) R. J. Fradette, M. Kang, F. G. West, *Angew. Chem. Int. Ed.* **2017**, 56, 6335.
- (5) (a) E. A. Braude, L. M. Jackman, R. P. Linstead, *J. Chem. Soc.* **1954**, 3548. (b) E. A. Braude, L. M. Jackman, R. P. Linstead, *J. Chem. Soc.* **1954**, 3564. (c) H. Roth; N. Romero, D. Nicewicz, *Synlett.* **2016**, 27, 714. (d) X. Guo, H. Zipse, H. Mayr, *J. Am. Chem. Soc.* **2014**, 136, 13863. (e) C. Hofler, C. Rüchardt, *Liebigs Ann.* **1996**, 2, 183. (f) R. M. Scribner, *J. Org. Chem.* **1966**, 31, 3671. (g) H. H. Jung, P. E. Floreancig, *Tetrahedron.* **2009**, 65, 10830. (h) D. A. Pratt, J. S. Wright, K. U. Ingold, *J. Am. Chem. Soc.* **1999**, 121, 4877. (i) C. Rüchardt, M. Gerst, J. Ebenhoch, *Angew. Chem. Int. Ed.* **1997**, 36, 1406. (j) F. Wurche, W. Sicking, R. Sustmann, F. G. Klärner, C. Rüchardt, *Chem. Eur. J.* **2004**, 10, 2707. (k) X. Li, Y. Wang, Y. Wang, M. Tangm, L. Qu, Z. Li, D. Wei, *J. Org. Chem.* **2018**, 83, 8543.
- (6) A. S. K. Tsang, A. S. K. Hashmi, P. Comba, M. Kerscher, B. Chan, M. H. Todd, *Chem. Eur. J.* **2017**, 23, 9313.
- (7) B. P. Ying, B. G. Trogden, D. T. Kohlman, S. X. Liang, Y. C. Xu, *Org. Lett.* **2004**, 6, 1523.
- (8) (a) E. A. Braude, R. P. Linstead, K. R. Wooldridge, *J. Chem. Soc.* **1956**, 3070. (b) J. R. Barnard, L. M. Jackman, *J. Chem. Soc.* **1960**, 3110. (c) E. A. Braude, L. M. Jackman, R. P. Linstead, J. S. Shannon, *J. Chem. Soc.* **1960**, 3116. (d) E. A. Braude, L. M. Jackman, R. P. Linstead, G. Lowe, *J. Chem. Soc.* **1960**, 3123. (e) E. A. Braude, L. M. Jackman, R. P. Linstead, G. Lowe, *J. Chem. Soc.* **1960**, 3133.
- (9) (a) M. Brock, H. Hintze, A. Heesing, *Chem. Ber.* **1986**, 119, 3727. (b) R. Paukstat, M. Brock, A. Heesing, *Chem. Ber.* **1985**, 118, 2579 (c) S. Yamabe, S. Yamazaki, S. Sakaki, *Int. J. Quantum Chem.* **2015**, 115, 1533.
- (10) B. Chan, L. Radom, *J. Phys. Chem. A.* **2007**, 111, 6456.
- (11) V. S. Batista, R. H. Crabtree, S. J. Konezny, O. R. Luca, J. M. Praetorius, *New J. Chem.* **2012**, 36, 1141.
- (12) C. A. Morales-Rivera, P. E. Floreancig, P. Liu, *J. Am. Chem. Soc.* **2017**, 139, 17935.
- (13) Gaussian 16, Revision A.03, M. J. Frisch, G. W. Trucks, H. B. Schlegel, G. E. Scuseria, M. A. Robb, J. R. Cheeseman, G. Scalmani, V. Barone, G. A. Petersson, H. Nakatsuji, X. Li, M. Caricato, A. V. Marenich, J. Bloino, B. G. Janesko, R. Gomperts, B. Mennucci, H. P. Hratchian, J. V. Ortiz, A. F. Izmaylov, J. L. Sonnenberg, D. Williams-Young, F. Ding,

F. Lipparini, F. Egidi, J. Goings, B. Peng, A. Petrone, T. Henderson, D. Ranasinghe, V. G. Zakrzewski, J. Gao, N. Rega, G. Zheng, W. Liang, M. Hada, M. Ehara, K. Toyota, R. Fukuda, J. Hasegawa, M. Ishida, T. Nakajima, Y. Honda, O. Kitao, H. Nakai, T. Vreven, K. Throssell, J. A. Montgomery, J. E. Peralta, F. Ogliaro, M. J. Bearpark, J. J. Heyd, E. N. Brothers, K. N. Kudin, V. N. Staroverov, T. A. Keith, R. Kobayashi, J. Normand, K. Raghavachari, A. P. Rendell, J. C. Burant, S. S. Iyengar, J. Tomasi, M. Cossi, J. M. Millam, M. Klene, C. Adamo, R. Cammi, J. W. Ochterski, R. L. Martin, K. Morokuma, O. Farkas, J. B. Foresman and D. J. Fox, Gaussian, Inc., Wallingford CT, **2016**.

(14) C. Lee, W. Yang, R. G. Parr, *Phys. Rev. B.*, **1988**, 37, 785.

(15) V. Barone, M. Cossi, *J. Phys. Chem. A.*, **1998**, 102, 1995.

(16) P. C. Hariharan, J. A. Pople, *Theor. Chim. Acta.*, **1973**, 28, 213.

(17) J. N. Harvey, M. Aschi, H. Schwarz, W. Koch, *Theor. Chem. Acc.*, **1998**, 99, 95.

Mechanistic Investigation of Chiral Brønsted Acid Catalyzed Enantioselective Dehydrative Nazarov-type Electrocyclization (DNE) of Aryl and 2-Thienyl Vinyl Alcohols

An efficient chiral Brønsted acid-catalyzed enantioselective dehydrative Nazarov-type electrocyclization (DNE) of electron-rich aryl- and 2-thienyl- β -amino-2-en-1-ols is described. The 4π conrotatory electrocyclization reaction affords access to a wide variety of the corresponding 1H-indenes and 4H-cyclopenta[b]thiophenes in excellent yields of up to 99% and enantiomeric excess (ee) values of up to 99%. Computational studies based on a proposed intimate contact ion-pair species that is further assisted by hydrogen bonding between the amino group of the substrate cation and chiral catalyst anion provide insight into the observed product enantioselectivities.

5.1 Introduction: Synthetic Scope of the Nazarov Cyclization

Electrocyclic processes in organic chemistry are considered as versatile transformations, being able to generate new carbon-carbon bonds stereospecifically.¹ One of the most useful examples of this series is Nazarov cyclization, which is a 4π -electron reaction involving divinyl ketones **a** conversion to cyclopentenones **e**, triggered by a Lewis acid (Figure 5.1).² Figure 5.1 indicates the generally accepted mechanism of Nazarov cyclization in which a divinyl ketone **a** interacts with a Lewis acid to afford a pentadienyl cation **b**; cyclization creates

an oxyallyl cation **c**; a proton elimination gives a Lewis-acid-enolate adduct **d**; finally, enolate protonation takes place to afford a cyclopentenone product **e**.²

It is important to note that cyclization of pentadienyl cation **b** should occur with orbital symmetry conservation, dictating conrotatory ring closure to yield **e** with an *anti*-relationship between R₁ and R₂ (**c**, Figure 5.1). As the disrotatory closure is prohibited, stereospecificity is provided for the formation of the new bond. Therefore, the Nazarov reaction is potent for transforming an achiral compound into a single stereoisomeric product.²

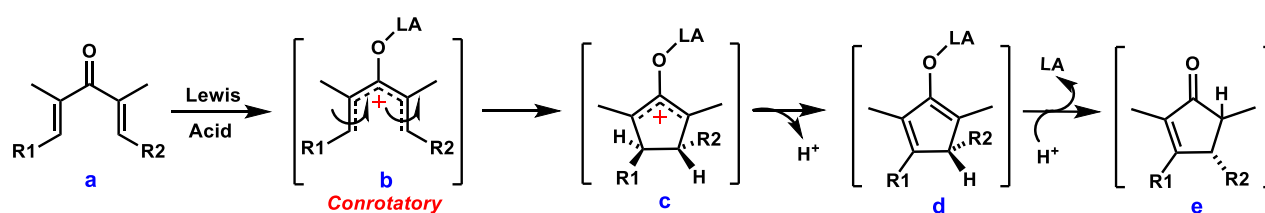
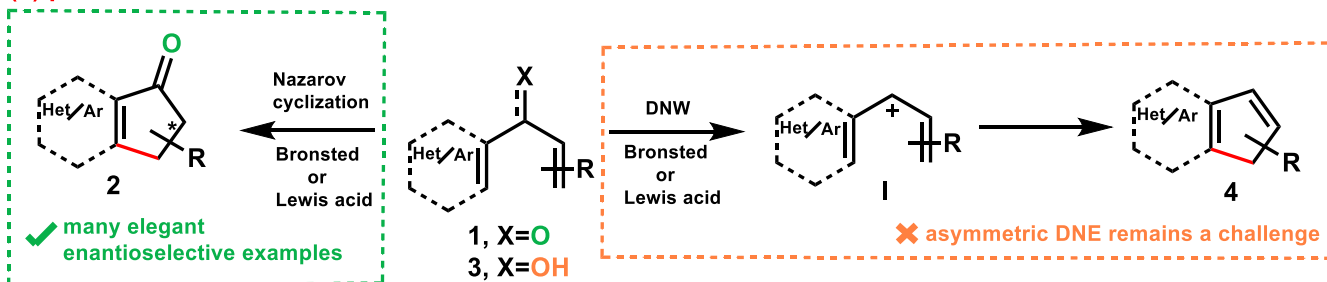


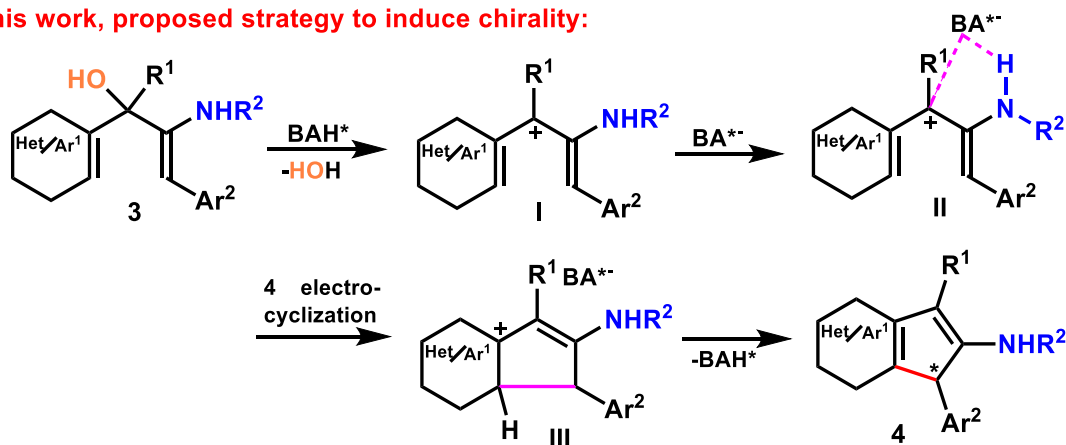
Figure 5.1. Widely accepted mechanism for Nazarov cyclization.

The Nazarov cyclization of divinyl and (hetero)aryl vinyl ketones mediated by a Brønsted or Lewis acid is among one of the most powerful and efficient methods for the synthesis of cyclopentenone derivatives (Scheme 5.1).³⁻⁸ A reflection of this is its frequent use in synthetic strategies for natural and synthetic compounds of current biological and materials interest containing the structural motif, or as a building block (Figure 5.1a).^{4,5} This functional group transformation has also inspired the development of new 4π electrocyclization processes that have included the Dehydrative Nazarov-type Electrocyclization (DNE) of electron-rich divinyl and (hetero)aryl vinyl alcohols to cyclopenta-1,3-dienes (Scheme 5.1a).⁶⁻⁸

(a) previous works:



(b) this work, proposed strategy to induce chirality:



Scheme 5.1. Nazarov cyclization and DNE of divinyl and (Hetero)aryl vinyl ketones and alcohols.

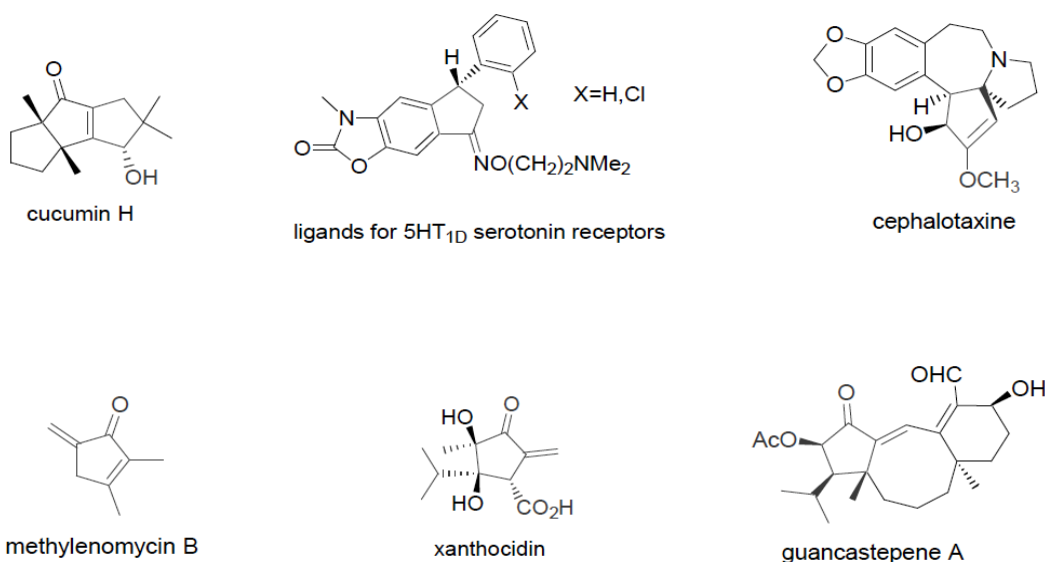


Figure 5.1a. Examples of molecules with biological activities containing five membered rings.

5.2 Enantioselective Dehydrative Nazarov-type Electrocyclization (DNE)

In contrast to Nazarov cyclization, an asymmetric variant of the DNE reaction, either by using a chiral auxiliary or catalyst, has not been widely explored so far and still remains a challenge (Scheme 5.1a).¹¹ This is mainly because typical substrates for Nazarov reactions are limited, and thus applying strong Brønsted acids or Lewis acids in most reactions is inevitable.⁹ Aggarwal and Belfield, in 2003, reported the first example of highly enantioselective Nazarov cyclization in which chiral copper bisoxazoline (BOX) and pyBOX complexes have been used as stoichiometric and substoichiometric catalysts (Figure 5.2)¹⁰.

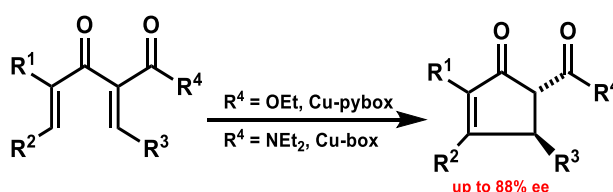


Figure 5.2. First example of asymmetric Nazarov cyclization by Aggarwal and Benfield.¹⁰

In 2009, France and co-workers have reported another example of catalysis for the DNE reaction, as illustrated in Figure 5.2a.^{11a} The product was directly formed from calcium-catalyzed, dehydrative, Nazarov-type electrocyclization of alkenyl thienyl carbinols in up to 82% yield. They synthesized different indene derivatives in order to explore the substituent effect and concluded that the electrocyclization was selective for the thermodynamic isomer of alkene.^{11a}

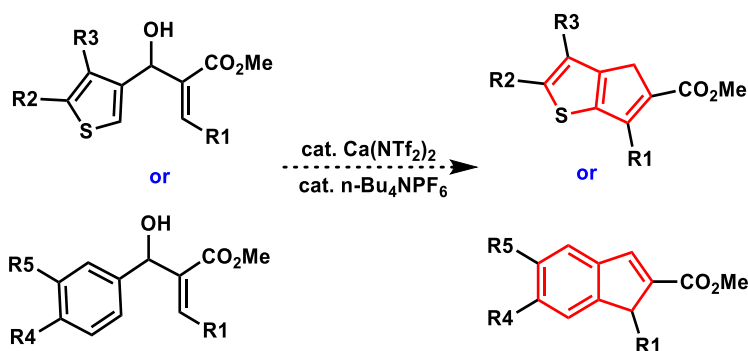


Figure 5.2a. Calcium-catalyzed, dehydrative cyclizations of cyclopropyl or alkenyl (hetero)aryl carbinols.^{11a}

Since there are not too many examples of DNE cyclization in the literature, investigation of this Nazarov-type cyclization and its mechanistic features would be of interest, and is examined in this chapter.

From a mechanistic viewpoint, the Brønsted acid-mediated DNE reaction is thought to involve initial protonation of the alcohol motif in the electron-rich substrate by the catalyst (Scheme 5.1). This is followed by elimination of a molecule of water to give the substrate cation, with one or more of the remaining pendant electron-rich (hetero)aryl or vinyl groups facilitating the dehydration step by stabilizing the putative carbocationic species. Subsequent 4π conrotatory electrocyclization would then deliver the cyclopenta-1,3-dienyl ring system with product enantioselectivity believed to be determined by this latter step. However, this has often been thought to be challenging due to the limited stereoelectronic interactions creating a poorly defined stereochemical environment in the proposed acyclic precursor **I** shown in Scheme 5.1a.¹²

In this context, the work reported in this chapter aimed to investigate the potential enantioselective DNE chemistry for this compound class with a pendant amino group catalyzed by a chiral Brønsted acid (BAH, Scheme 5.1b).^{3,8} It was anticipated that this would provide the corresponding intimate ion-pair species **II** in which the amino group of the associated cation of the substrate and anion of the chiral catalyst can additionally participate in hydrogen bonding interactions. With the chiral Brønsted acid anion now occupying one face of the substrate cation as a result, this might then allow asymmetric induction in the ensuing pericyclic reaction step to be accomplished to give the pentacyclic product in an enantioselective manner. The results of this study offer an expedient route to these two potentially useful members of the 1H-indene and 4H-cyclopenta[b]thiophene compound family in excellent yields and enantioselectivities.

Experimental studies in this project have been undertaken by Chan et al. at Monash University.

In order to complete a comprehensive study, the results of density functional theory (DFT) calculations on the origin of the observed product enantioselectivities is presented here.

Some important parts of the experimental results of Chan et al. are also presented here, as they provide insight into the mechanism and assisted the DFT investigation.

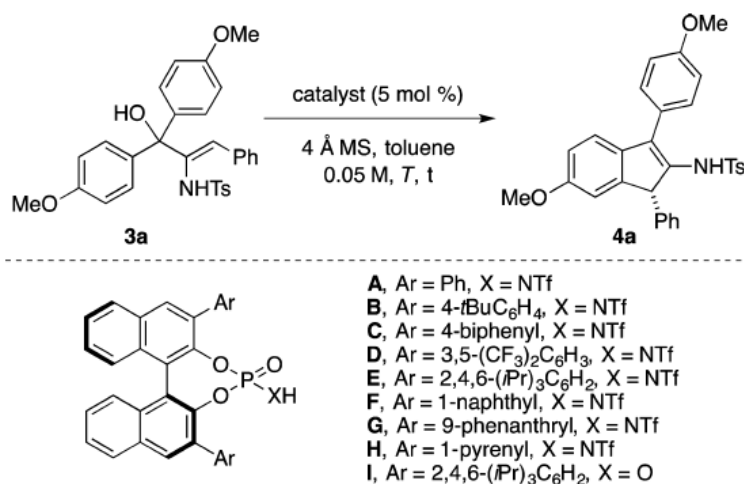
5.3 Computational Study

Gaussian 09¹³ was used to fully optimize all the structures reported at the B3LYP level of density functional theory (DFT).¹⁴ The 6-31G(d) basis set was chosen to describe all atoms. The proposed mechanism in this chapter involves hydride transfer which depends on the proportion of Fock exchange, the use of diffuse function for H atoms and dispersion. Frequency calculations were carried out at the same level of theory as those for the structural optimization. Transition structures were located using the Berny algorithm. Intrinsic reaction coordinate (IRC) calculations were used to confirm the connectivity between transition structures and minima.¹⁵ To further refine the energies obtained from the B3LYP/6-31G(d) calculations, single-point energy calculations for all the structures with the larger basis set 6-31+G (d, p) in toluene using the CPCM solvation model at the M06 level of theory were carried out.^{16,17} All thermodynamic data were calculated at the standard state (298.15 K and 1 atm). To estimate the corresponding Gibbs free energies in toluene, entropy corrections were calculated at the B3LYP/6-31G(d) level and added to the single point potential energies.

5.4 Results and Discussion

The experimental studies in this work began by examining the chiral Brønsted acid-mediated enantioselective DNE of **3a** to establish the optimum reaction conditions (Table 5.4). This initially required subjecting the substrate to 5 mol % of chiral *N*-triflyl phosphoramidate (*S*)-**A**, and 4 Å molecular sieves (MS) in toluene at 25 °C for 1 h to give **4a** in 95% yield and an ee value of 63% (entry 1). The structure and absolute stereochemistry of the carbocyclic adduct were determined by NMR measurements and X-ray crystallographic analysis of two closely related products.

Table 5.4. Optimization of the Reaction Conditions for the Chiral Brønsted Acid-Mediated enantioselective DNE of **3a**^a.



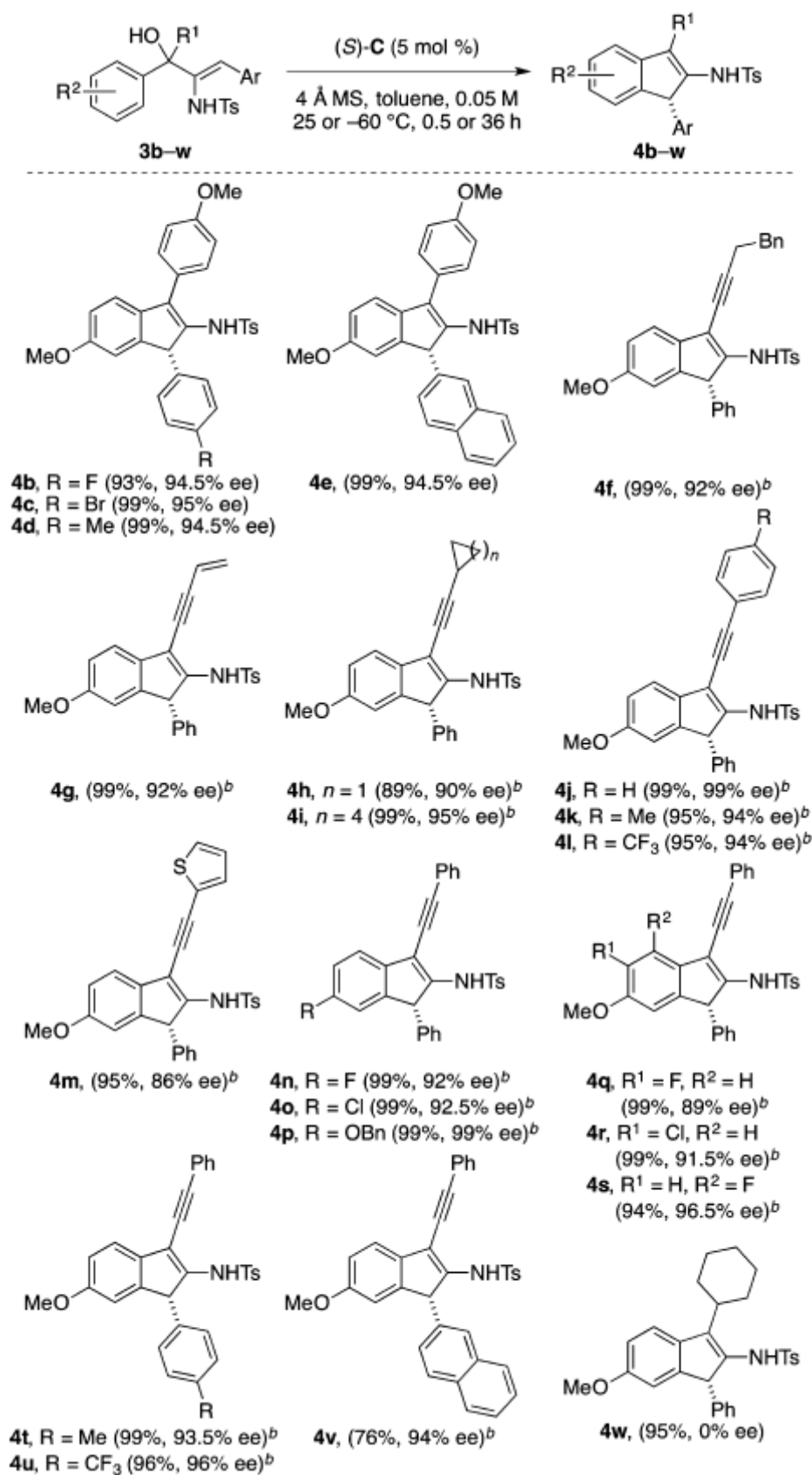
entry	catalyst	<i>T</i> (°C)	<i>t</i> (h)	yield (%) ^a	ee (%) ^c
1	(<i>S</i>)- A	25	1	95	63
2	(<i>S</i>)- B	25	1	95	35
3	(<i>S</i>)- C	25	1	99	73
4 ^d	(<i>S</i>)- C	25	1	92	40
5 ^e	(<i>S</i>)- C	25	1	94	45
6	(<i>S</i>)- C	−40	24	94	91
7	(<i>S</i>)- C	−60	24	95	95
8	(<i>S</i>)- C	−78	48	82	82
9	(<i>S</i>)- D	25	1	93	30

10	(<i>S</i>)- E	25	12	97	58
11	(<i>S</i>)- F	25	1	74	66
12	(<i>S</i>)- G	25	1	99	60
13	(<i>S</i>)- H	25	1	97	54
14	(<i>S</i>)- I	25	24	— ^f	—

^aAll reactions were performed at the 0.1 mmol scale with 5 mol % of catalyst, 4 Å MS (100 mg) in toluene (2 mL) at given temperature and time. ^bIsolated yield. ^cEe values were determined using an AD-H chiral column with *n*hexane:*i*PrOH (9:1) as the eluent. ^dReaction conducted with CH₂Cl₂ as the solvent. ^eReaction conducted with (CH₂Cl)₂ as the solvent. ^fNo reaction detected by TLC analysis and ¹H NMR measurement with recovery of **3a** in 99% yield.

With the reaction conditions established, the next step involved evaluating the generality of the present procedure using a series of electron-rich aryl-β-amino-2-en-1-ols **3b–w** (Table 5.4a). Overall, the (*S*)-**C**-catalyzed reaction conditions were shown to be broad, providing a family of 1*H*-indenes **4b–w** containing a variety of substitution patterns in excellent yields and ee values from the corresponding substrates.

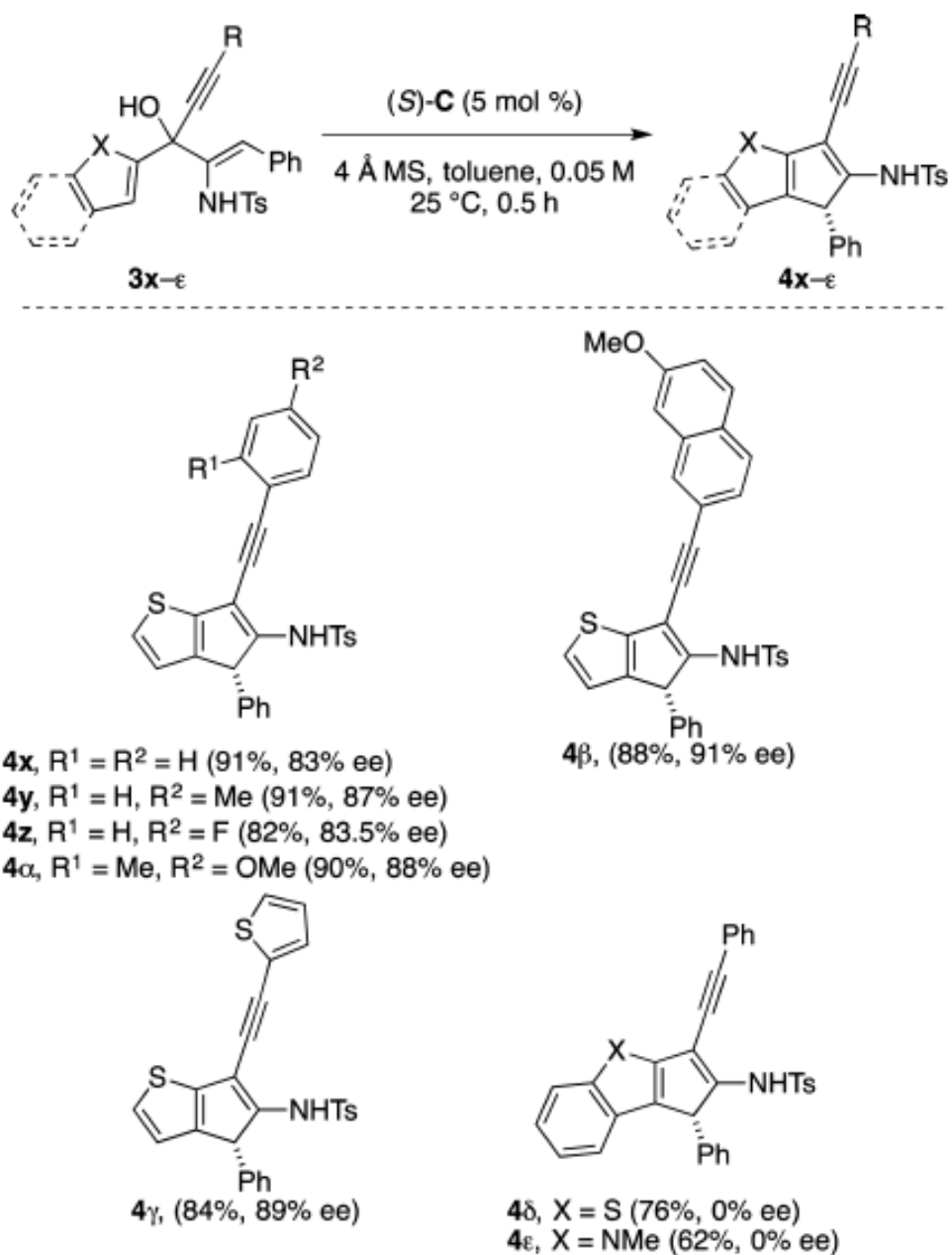
Table 5.4a. Enantioselective DNE of Aryl- β -amino-2-en-1-ols **3b–w** Catalyzed by (S)-**C**^a.



^aAll reactions were performed at the 0.1 mmol scale with 5 mol % of (S)-**C**, 4 Å MS (100 mg) in toluene (2 mL) at -60 °C for 36 h. Values in parentheses denote isolated product yields and ee values determined using an AD-H chiral column (eluent: *n*-hexane:*i*PrOH = 9:1). ^bReaction conducted at 25 °C for 0.5 h.

Having established the generality of the reaction conditions that gave 1*H*-indenes, the scope of the methodology for the enantioselective synthesis of 4*H*-cyclopenta[*b*]-fused heterocycles was explored at this stage (Table 5.4b). With this in mind, the (S)-**C**-mediated enantioselective DNE of electron-rich 2-thienyl-substituted 1,4-enynols **3x-α** in which the alkyne motif contained an aryl group were first examined. It was found that, the corresponding *S*-heterocycles **4x-α** could be furnished in 82–91% yield and 83–88% ee.

Table 5.4b. Enantioselective DNE of 2-Heteroaryl- β -amino-2-en-1-ols **3x– ϵ** Catalyzed by (S)-**C**^a.



^aAll reactions were performed at the 0.1 mmol scale with 5 mol % of (S)-**C**, 4 Å MS (100 mg) in toluene (2 mL) at 25 °C for 36 h. Values in parentheses denote isolated product yields and ee values, determined using an AD-H chiral column (eluent: *n*-hexane:*i*PrOH = 9:1).

A tentative mechanistic rationale for the origin of the product enantioselectivities obtained in the present chiral Brønsted acid-catalyzed asymmetric DNE reactions was proposed by Chan and is presented in Figure 5.4. Using **3j** as a representative example, this might initially involve protonation of the substrate by the chiral Brønsted acid to give the carbocationic species **Ij** and **Ij'** and the catalyst anion (*S*)-**C'** on release of a molecule of water. Building on the premise put forward in Scheme 5.1 b that chiral induction might then be achieved in the ion-pair species forming step, this would give the four possible conformers **IIj_a**, **IIj_b**, **IIj'_a** and **IIj'_b**. In all four cases, it was surmised that the amino motif hydrogen atom in the ion-pair species acts as a directing group through its ability to hydrogen bond with the catalyst anion, thereby determining whether it sits on the *re* or *si* face of the substrate cation. For **IIj_a**, clockwise 4π conrotatory electrocyclization of the ion-pair species would lead to **IIIj_a** being formed with the resulting acidic aryl proton (labeled red in Figure 5.4a) and chiral Brønsted acid anion positioned on the same face of the cyclic adduct. This is important, as it is anticipated to permit the facile deprotonation and rearomatization of the Wheland-type intermediate **IIIj_a** by the chiral Brønsted acid anion to deliver the product (*R*)-**4j**.¹⁸ Conversely, the counterclockwise pericyclic reaction of **IIj_b** would give **IIIj_b** whereby the acidic aryl proton and chiral Brønsted acid anion are now situated on the opposite faces of the carbocyclic cation. As a consequence, this might prevent the deprotonation step from occurring and the formation of this cyclic carbocation is anticipated to lead to a dead end unless it undergoes the reverse reaction. A second possibility is that intermediate **IIIj_b** could be deprotonated if water serves as a base, the ability of which is dependent on the size of the water cluster (H₂O)_{*n*} involved in the process. However, this was thought to be less likely based on Chan's experience predicting such deprotonations to require an activation energy of ca. 17 kcal/mol, which is higher than that required for the conversion of **IIj_a** → **IIIj_a** vide infra. As illustrated in Figure 5.4b for the pathways involving **IIj'_a** and **IIj'_b**, a similar rationale would account for the preferential outcome of the enantiomer (*S*)-**4j**. In this regard, Chan's hypothesis predicts that product formation can only come from pathways involving the ion-pair species **IIIj_a** and **IIIj'_b** with the dominant ion-pair species in solution being the former in view of a product ee value of 99%. It was also implied that the catalyst anion may not preferentially occupy one face of the substrate cation in an ion-pair species containing a tertiary amino substituent. In the absence of the directing group, this might

subsequently allow both the clockwise and counterclockwise pericyclic reaction pathways to be operative in equal measure and give the product as a racemate. Consistent with this are findings in a control reaction with the *N,N*-disubstituted substrate **3ζ** under the (*S*)-**C**-catalyzed conditions described in Scheme 5.4, which gave **4ζ** in 99% yield and 0% ee. The proposed involvement of the ion-pair species **II** by Chan would explain the marked differences in product ee values obtained for the reactions of **3a** in toluene, dichloromethane and 1,2-dichloroethane detailed in Table 5.4, entries 3–5. It might be expected that an increase in interactions between the substrate cation and catalyst anion with the reaction medium might occur as the solvent dielectric constant (ϵ) increases on going from toluene (ϵ = 2.4, 290 K) to dichloromethane (ϵ = 9.2, 288 K) and 1,2-dichloroethane (ϵ = 11.0, 288 K).¹⁹ As a consequence, this may disrupt the ability of the substrate cation and catalyst anion to form a tight ion-pair species, resulting in a decrease in product ee values. A similar rationale could be in play in the reactions of **3w**, **3δ** and **3ε** that lead to the corresponding products being obtained as a racemate. The presence of a bulky cyclohexyl or benzofused ring in these substrates might provide sufficient unfavourable steric interactions to prevent the substrate cation and catalyst anion forming the requisite intimate ion-pair species **II**.

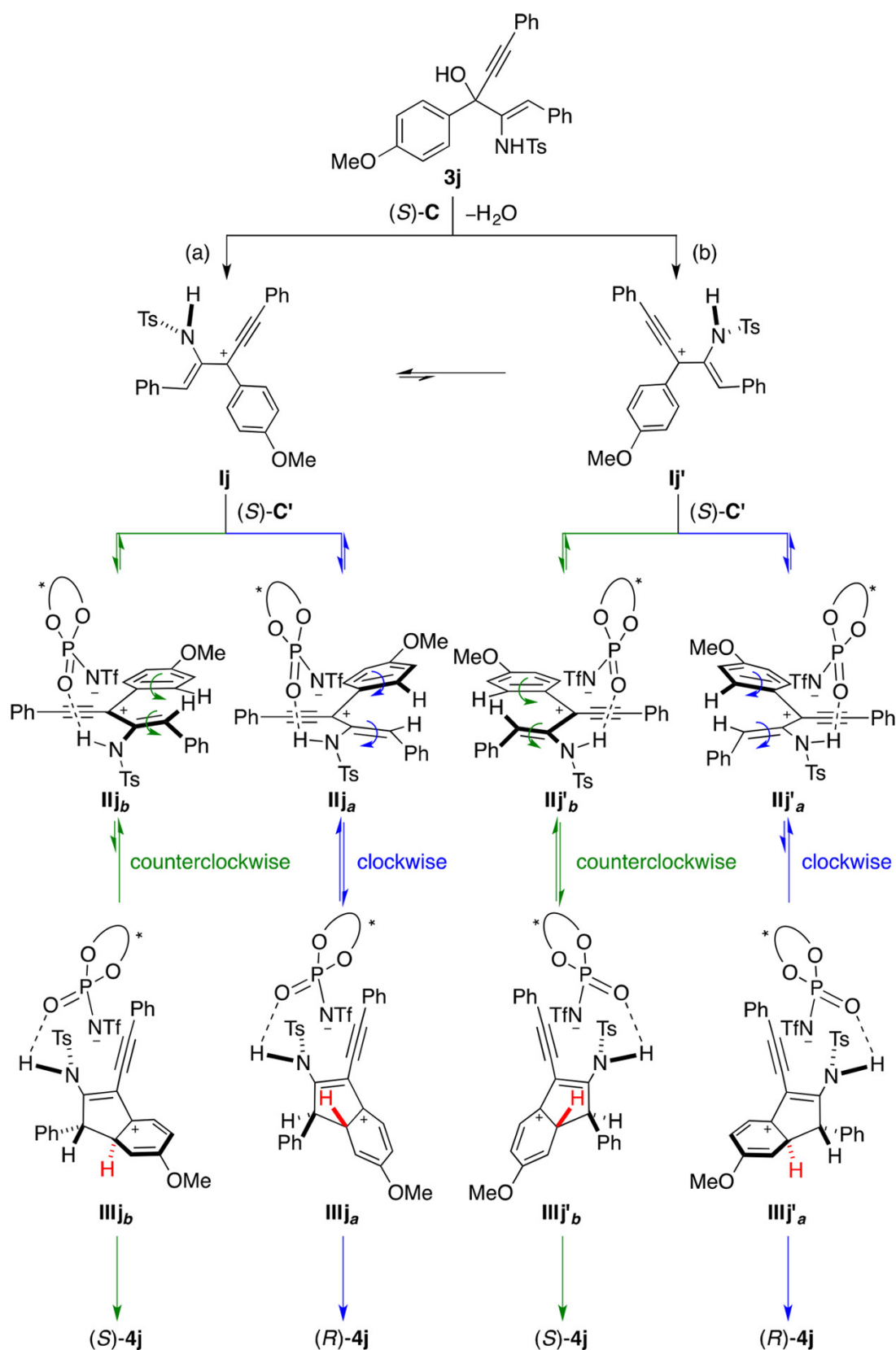
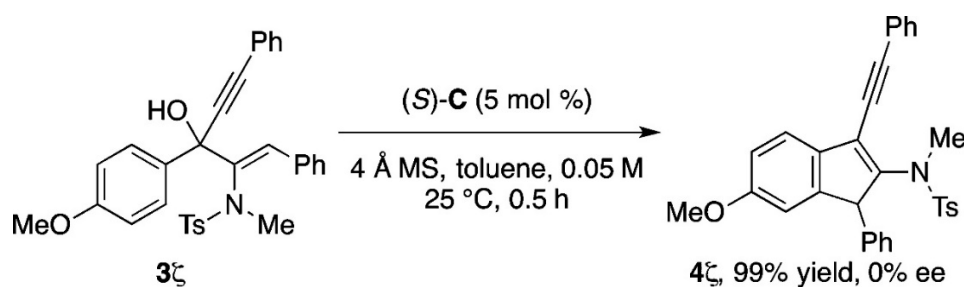


Figure 5.4. Proposed mechanistic rationale for the product enantioselectivities obtained for the (S)-C-catalyzed asymmetric DNE of electron-rich aryl- and 2-thienyl- β -amino-2-en-1-ols represented by **3j**.



Scheme 5.4. Control Experiment with **3ζ**.

To examine the proposed mechanistic rationale for the observed product enantioselectivities outlined in Figure 5.4, a series of DFT calculations was performed. As summarized in Figure 5.4a, a number of transition structures and intermediates were produced in the two possible reaction pathways *a* and *b* from **Ij** and **Ij'** to the corresponding (*R*) and (*S*) enantiomers of **4j**. On the basis of these calculations, pathway *a* was revealed to be favoured with rotation from **Ij** to **Ij'** shown to be endergonic by 2.6 kcal/mol. Accordingly, the latter conformer was found to be sparsely populated, which is in good agreement with the experimental findings showing (*R*)-**4j** being afforded in 99% ee. This was followed by the interaction of the substrate cation with (*S*)-**C'**, which lowers the energy of the carbocationic species by >26 kcal/mol. As such, the ensuing ion-pair species **IIj_a** functioned as a thermodynamic sink that prevented interconversion between the two substrate cation conformers. In the ion-pair species, the chiral Brønsted acid anion was found to be located on the *re* face of the substrate cation due to hydrogen bonding interactions between the former and the latter, as evidenced by a P=O⋯HN bond distance of 1.751 Å. The ion-pair species **IVj_a** depicted in Figure 5.4b, the most stable among other possible interactions, was also considered. However, this latter hydrogen bonded ion-pair species was thought to be less likely as it was found to be 5.4 kcal/mol less stable and had a slightly longer S=O⋯HN bond distance of 1.807 Å. The calculations further suggested clockwise 4π conrotatory electrocyclization of **IIj_a** to **IIIj_a** occurred through **TS_{IIj_a-IIIj_a}** with an energy barrier of 11.3 kcal/mol. For the reaction steps after the formation of the Wheland-type intermediate **IIIj_a**, the Brønsted acid anion was found to play a crucial role in the deprotonation of the adduct. By accepting the aryl proton sitting on the same face of the catalyst anion, this provided the product (*R*)-**4j** and (*S*)-**C''** via **TS_{IIIj_a-(R)-4j}** with an energy barrier of 3.0 kcal/mol. This implied that the rearomatization process was more facile than the preceding carbocyclic ring forming

step. Regeneration of the chiral Brønsted acid catalyst was readily achieved through tautomerization of (*S*)-**C''**, which was found to be exergonic by 3.2 kcal/mol.

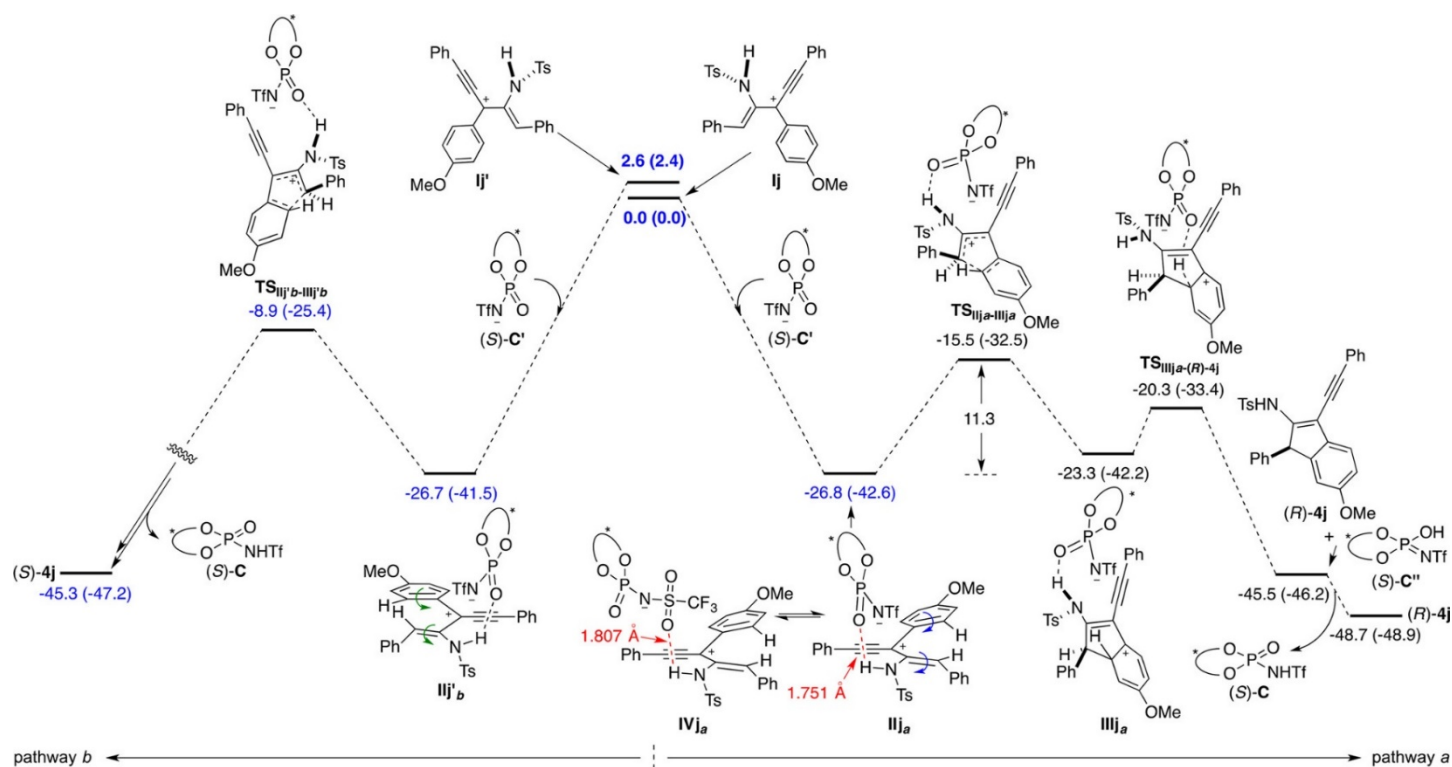


Figure 5.4a. Energy profile of pathways *a* and *b* for the (*S*)-**C**-catalyzed enantioselective DNE of **3j** to (*R*)-**4j** and (*S*)-**4j**, respectively. Structures **IIj** and **IVj** show short P=O \cdots HN and S=O \cdots HN interactions (1.751, 1.807 Å) that indicate hydrogen bonding. The relative Gibbs and potential energies (in parentheses) obtained from M06-CPCM/6-31+G(d,p)//B3LYP-CPCM/6-31G(d) calculations are given in kcal/mol and bond lengths in Å.

In a second set of calculations in the absence of (*S*)-**C**, the activation energy required for the 4 π electrocyclozation step was demonstrated to increase by 6.1 kcal/mol, as shown in Figure 5.4b (a). This suggested that the interaction between the cation of the substrate and the anion of the catalyst in **TS_{IIIj-a-IIIj'a}** was stronger than that in **IIj_a**. Repeating these calculations for **3a** in the absence of the Brønsted acid revealed the pericyclic reaction step required an activation energy of 13.7 kcal/mol (Figure 5.4a (b)). This implied that **3a** was intrinsically more reactive than **3j** toward carbocyclic ring formation and is in good agreement with the need for lower experimental temperatures of -60 °C to achieve chiral induction in such diaryl-substituted substrates. The source of this greater reactivity was attributed to the steric demand of the aryl ring limiting its ability to stabilize the cationic charge by π -conjugation in **Ia**, as

corroborated by the much longer C1–C2 bond distance in the carbocation species than in **Ij** (cf. Figures 5.4b (a) and 4.4b (b)). As with **3j**, the experimentally observed product enantioselectivity obtained from **3a** was found to be a result of conformer **Ia** being 2.4 kcal/mol more stable than that of conformer **Ia'**.

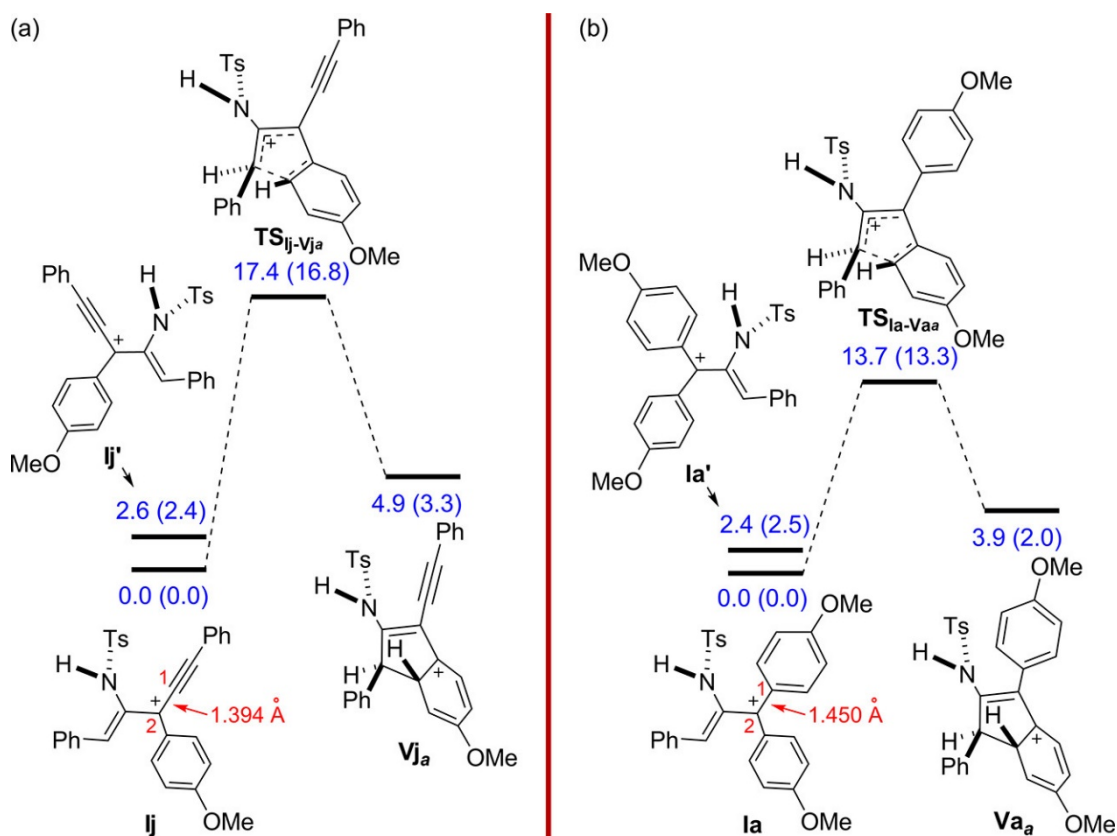
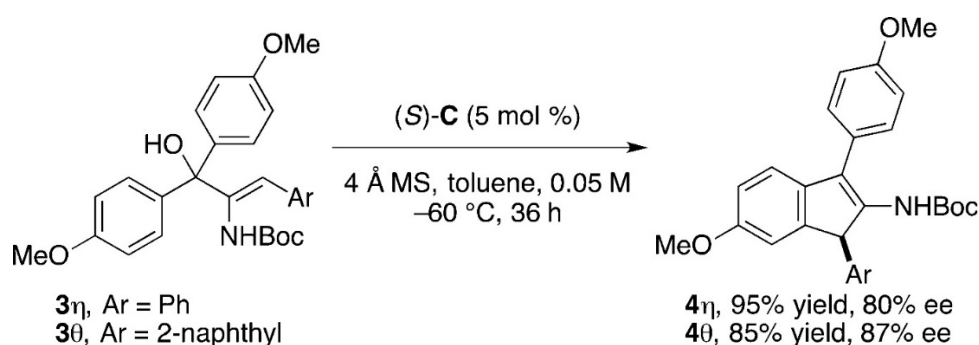


Figure 5.4b. Energy profiles for the 4π conrotatory electrocyclization step of (a) **3j** and (b) **3a** in the absence of (*S*)-**C**. The relative Gibbs and potential energies (in parentheses) obtained from M06-CPCM/6-31+G(d,p)//B3LYP-CPCM/6-31G(d) calculations are given in kcal/mol and bond lengths in Å.

In a final set of calculations, the Gibbs energy on forming **IVj_a** from **Ij** and (*S*)-**C'** was determined to be –13.3 and –30.8 kcal/mol at the B3LYP-CPCM/6-31+G(d,p)//B3LYP-CPCM/6-31G(d) and B3LYP-D3-CPCM/6-31+G(d,p)//B3LYP-CPCM/6-31G(d) level, respectively. While the analogous calculations could not be accomplished for the formation of **IIj_a**, these findings nonetheless indicated that the dispersive interactions implied in Scheme 5.1b are operative and play a key role in the stability of the ion-pair species.

Interestingly, the DFT studies also revealed that if the stereoelectronic nature of the amino substituent in the substrate was changed by replacing the *N*-Ts motif with a *N*-Boc group, as in **3η** shown in Scheme 5.4a, a switch in the stereochemical outcome of the reaction should be observed. Calculations for the substrate in the absence of (*S*)-**C** at the M06-CPCM/6-31+G(d,p)//B3LYP-CPCM/6-31G(d) and B3LYP-CPCM/6-311+G(d,p)//B3LYP-CPCM/6-31G(d) level found **1η'** to be more stable than **1η** by 0.5 and 1.9 kcal/mol, respectively, which implied the (*S*)-enantiomer would be afforded as the major product. Pleasingly, this was supported by subsequent findings in experiments by Chan with **3η** and its 2-naphthyl substituted analogue **3θ** catalyzed by (*S*)-**C** under the conditions described in Scheme 5.4a. In these test reactions, the corresponding 1*H*-indene adducts **4η** and **4θ** were furnished in respective yields of 95 and 85% and ee values of 80 and 87% with the (8*S*) absolute configuration of the former ascertained by X-ray crystallography.



Scheme 5.4a. (*S*)-**C**-Catalyzed Asymmetric DNE of **3η** and **3θ**.

5.5 Conclusion

In summary, a chiral Brønsted acid-catalyzed method for the asymmetric synthesis of 1*H*-indenes and 4*H*-cyclopenta[*b*]thiophenes from the respective electron-rich aryl- and 2-thienyl-β-amino-2-en-1-ols was developed by Chan and analysed by computational chemistry. DFT studies suggest the origin of the observed product enantioselectivity was initially due to the more stable conformation of the substrate cation. The ensuing ion-pair species then acted as a thermodynamic sink to prevent interconversion between these two conformers. Also instrumental was the role of the amino group in the substrate cation in directing the chiral

catalyst anion to preferentially sit on one face of the adduct and the ability of the latter to efficiently facilitate rearomatization to give the product. It was envisioned that the present synthetic method will encourage the further development of asymmetric strategies in reactions where there is such intrinsic low directionality through the installation of a directing group.

5.6 References

- (1) (a) W. R. Dolbier, H. Koroniak, K. N. Houk, C. Sheu, *Acc. Chem. Res.* **1996**, 29, 471.
(b) M. J. S. Dewar, *Tetrahedron*. **1966**, 22, 75.
- (2) A. J. Frontier, C. Collison, *Tetrahedron*. **2005**, 61, 7577.
- (3) (a) S. P. Simeonov, J. P. M. Nunes, K. Guerram, V. B. Kurteva, C. A. M. Afonso, *Chem. Rev.* **2016**, 116, 5744. (b) M. Di Grandi, *Org. Biomol. Chem.* **2014**, 12, 5331. (c) M. A. Tius, *Chem. Soc. Rev.* **2014**, 43, 2979. (d) W. T. Spencer, T. Vaidya, A. J. Frontier, *Eur. J. Org. Chem.* **2013**, 2013, 3621. (e) S. Naoyuki, S. Craig, M. A. Tius, *Tetrahedron*. **2011**, 67, 5851. (f) S. Thompson, A. G. Coyne, P. C. Knipe, M. D. Smith, *Chem. Soc. Rev.* **2011**, 40, 4217. (g) T. Vaidya, R. Eisenberg, A. J. Frontier, *ChemCatChem*. **2011**, 3, 1531. (h) T. N. Grant, C. J. Rieder, F. G. West, *Chem. Commun.* **2009**, 5676. (i) W. Nakanish, F. G. West, *Curr. Opin. Drug Discovery Devel.* **2009**, 12, 732. (j) K. L. Habermas, S. E. Denmark, T. K. Jones, *Organic Reactions*. L. A. Paquette Ed., John Wiley & Sons: New York, **1994**, Vol. 45, pp 1–158.
- (4) (a) J. Krieger, T. Smeilus, O. Schackow, A. Giannis, *Chem. - Eur. J.* **2017**, 23, 5000. (b) M. L. Tang, P. Peng, Z. Y. Liu, J. Zhang, J. M. Yu, X. Sun, *Chem. - Eur. J.* **2016**, 22, 14535. (c) W. Rao, J. W. Boyle, P. W. H. Chan, *Chem. - Eur. J.* **2016**, 22, 6532. (d) X. Chen, D. P. Day, W. T. Teo, P. W. H. Chan, *Org. Lett.* **2016**, 18, 5936. (e) A. S. Marques, V. Coeffard, I. Chataigner, G. Vincent, X. Moreau, *Org. Lett.* **2016**, 18, 5296. (f) Y. W. Huang, A. J. Frontier, *Org. Lett.* **2016**, 18, 4896. (g) A. H. Asari, Y. H. Lam, M. A. Tius, K. N. Houk, *J. Am. Chem. Soc.* **2015**, 137, 13191. (h) D. Susanti, L.-J. Liu, W. Rao, S. Lin, D.-L. Ma, C.-H. Leung, P. W. H. Chan, *Chem. - Eur. J.* **2015**, 21, 9111. (i) W. Rao, D. Susanti, B. J. Ayers, P. W. H. Chan, *J. Am. Chem.*

- Soc.* **2015**, *137*, 6350. (j) Y. K. Wu, C. R. Dunbar, R. McDonald, M. J. Ferguson, F. G. West, *J. Am. Chem. Soc.* **2014**, *136*, 14903. (k) T. Vaidya, R. Cheng, P. N. Carlsen, A. J. Frontier, R. Eisenberg, *Org. Lett.* **2014**, *16*, 800. (l) W. Rao, M. J. Koh, D. Li, H. Hirao, P. W. H. Chan, *J. Am. Chem. Soc.* **2013**, *135*, 7926.
- (5) (a) C.-S. Wang, J.-L. Wu, C. Li, L.-Z. Li, G.-J. Mei, F. Shi, *Adv. Synth. Catal.* **2018**, *360*, 846. (b) G.-P. Wang, M.-O. Chen, S.-F. Zhu, Q.-L. Zhou, *Chem. Sci.* **2017**, *8*, 7197. (c) B.-M. Yang, P.-J. Cai, Y.-Q. Tu, Z.-X. Yu, Z.-M. Chen, S.-H. Wang, S.-H. Wang, F.-M. Zhang, *J. Am. Chem. Soc.* **2015**, *137*, 8344. (d) K. Kitamura, N. Shimada, C. Stewart, A. C. Atesin, T. A. Atesin, M. A. Tius, *Angew. Chem. Int. Ed.* **2015**, *54*, 6288. (e) T. Takeda, S. Harada, A. Nishida, *Org. Lett.* **2015**, *17*, 5184. (f) W. Zi, H. Wu, F. D. Toste, *J. Am. Chem. Soc.* **2015**, *137*, 3225. (g) S. Raja, M. Nakajima, M. Rueping, *Angew. Chem., Int. Ed.* **2015**, *54*, 2762. (h) R. William, S. Wang, F. Ding, E. N. Arviana, X.-W. Liu, *Angew. Chem., Int. Ed.* **2014**, *54*, 10742. (i) A. Jolit, P. M. Walleser, G. P. A. Yap, M. A. Tius, *Angew. Chem., Int. Ed.* **2014**, *53*, 6180. (j) B. L. Flynn, N. Manchala, E. H. Krenske, *J. Am. Chem. Soc.* **2013**, *135*, 9156. (k) G. E. Hutson, Y. E. Turkmen, V. H. Rawal, *J. Am. Chem. Soc.* **2013**, *135*, 4988. (l) A. K. Basak, N. Shimada, W. F. Bow, D. A. Vicic, M. A. Tius, *J. Am. Chem. Soc.* **2010**, *132*, 8266. (m) J. Huang, A. J. Frontier, *J. Am. Chem. Soc.* **2007**, *129*, 8060. (n) F. Dhoro, T. E. Kristensen, V. Stockmann, G. P. A. Yap, M. A. Tius, *J. Am. Chem. Soc.* **2007**, *129*, 7256. (o) M. Rueping, W. Ieawsuwan, A. P. Antonchick, B. J. Nachtsheim, *Angew. Chem., Int. Ed.* **2007**, *46*, 2097. (p) G. Liang, D. Trauner, *J. Am. Chem. Soc.* **2004**, *126*, 9544. (q) V. K. Aggarwal, A. J. Belfield, *Org. Lett.* **2003**, *5*, 5075.
- (6) (a) M. C. Martin, M. J. Sandridge, C. W. Williams, Z. A. Francis, S. France, *Tetrahedron.* **2017**, *73*, 4093. (b) Z. Wang, X. Xu, Z. Gu, W. Feng, H. Qian, Z. Li, X. Sun, O. Kwon, *Chem. Commun.* **2016**, *52*, 2811. (c) L. Lempenauer, E. Dunach, G. Lemiére, *Org. Lett.* **2016**, *18*, 1326. (d) D. Seema, S. S. V. Ramasastry, *Org. Lett.* **2015**, *17*, 5116. (e) M. J. Riveira, M. P. Mischne, *Chem. - Eur. J.* **2012**, *18*, 2382. (f) D. L. Usanov, M. Naodovic, M. Brasholz, H. Yamamoto, *Helv. Chim. Acta.* **2012**, *95*, 1773. (g) C. J. Hastings, M. P. Backlund, R. G. Bergman, K. N. Raymond, *Angew. Chem., Int. Ed.* **2011**, *50*, 10570. (h) C. J. Rieder, K. L. Winberg, F.

- G. West, *J. Org. Chem.* **2011**, 76, 50. (i) C. J. Hastings, M. D. Pluth, R. G. Bergman, K. N. Raymond, *J. Am. Chem. Soc.* **2010**, 132, 693. (j) P. Cordier, C. Aubert, M. Malacria, E. Lacote, V. Gandon, *Angew. Chem., Int. Ed.* **2009**, 48, 8757.
- (7) (a) H. Li, R. Tong, J. Sun, *Angew. Chem., Int. Ed.* **2016**, 55, 15125. (b) Y. Cai, Y. Tang, I. Atodiressei, M. Rueping, *Angew. Chem., Int. Ed.* **2016**, 55, 14126. (c) F.-L. Sun, M. Zeng, Q. Gu, S.-L. You, *Chem. - Eur. J.* **2009**, 15, 8709.
- (8) (a) J. Merad, C. Lalli, G. Bernadat, J. Maury, G. Masson, *Chem. - Eur. J.* **2018**, 24, 3925. (b) T. James, M. van Gemmeren, B. List, *Chem. Rev.* **2015**, 115, 9388. (c) T. Akiyama, K. Mori, *Chem. Rev.* **2015**, 115, 9277. (d) C. Zhu, K. Saito, M. Yamanaka, T. Akiyama, *Acc. Chem. Res.* **2015**, 48, 388. (e) D. Parmar, E. Sugiono, S. Raja, M. Rueping, *Chem. Rev.* **2014**, 114, 9047. (f) M. Mahlau, B. List, *Angew. Chem., Int. Ed.* **2013**, 52, 518. (g) C. H. Cheon, H. Yamamoto, *Chem. Commun.* **2011**, 47, 3043. (h) M. Terada, *Synthesis*. **2010**, 2010, 1929. (i) M. Terada, *Chem. Commun.* **2008**, 4097.
- (9) N. Shimada, C. Stewart, M. A. Tius, *Tetrahedron*. **2011**, 67, 5851.
- (10) V. K. Aggarwal, A. J. Belfield, *Org. Lett.* **2003**, 5, 5075.
- (11) (a) M. C. Martin, M. J. Sandridge, C. W. Williams, Z. A. Francis, S. France, *Tetrahedron*. **2009**, 73, 4093. (b) A. H. Asari, Y. Lam, M. Tius, K. N. Houk, *J. Am. Chem. Soc.* **2015**, 137, 13191. (c) J. Jin, Y. Zhao, E. M. L. Sze, P. Kothandaraman, P. W. H. Chan, *Adv. Synth. Catal.* **2018**, 360, 4744. (d) M. Rueping, W. Ieawsuwan, *Chem. Comm.* **2011**, 47, 11450. (e) T. Vaidya, R. Eisenberg, A. Frontier, *Chemcatchem*. **2011**, 3, 1531.
- (12) C. D. Smith, G. Rosocha, L. Mui, R. A. Batey, *J. Org. Chem.* **2010**, 75, 4716.
- (13) M. J. Frisch, G. W. Trucks, H. B. Schlegel, G. E. Scuseria, M. A. Robb, J. R. Cheeseman, G. Scalmani, V. Barone, B. Mennucci, G. A. Petersson, H. Nakatsuji, M. Caricato, X. Li, H. P. Hratchian, A. F. Izmaylov, J. Bloino, G. Zheng, J. L. Sonnenberg, M. Hada, M. Ehara, K. Toyota, R. Fukuda, J. Hasegawa, M. Ishida, T. Nakajima, Y. Honda, O. Kitao, H. Nakai, T. Vreven, J. A. Montgomery, J. E. Peralta, F. Ogliaro, M. Bearpark, J. J. Heyd, E. Brothers, K. N. Kudin, V. N. Staroverov, R. Kobayashi, J. Normand, K. Raghavachari, A. Rendell, J. C. Burant, S. S. Iyengar, J. Tomasi, M. Cossi, N. Rega, J. M. Millam, M. Klene, J. E. Knox, J. B. Cross, V. Bakken,

- C. Adamo, J. Jaramillo, R. Gomperts, R. E. Stratmann, O. Yazyev, A. J. Austin, R. Cammi, C. Pomelli, J. W. Ochterski, R. L. Martin, K. Morokuma, V. G. Zakrzewski, G. A. Voth, P. Salvador, J. J. Dannenberg, S. Dapprich, A. D. Daniels, O. Farkas, J. B. Foresman, J. V. Ortiz, J. Cioslowski, D. J. Fox, Gaussian, Revision D.; Gaussian, Inc.: Wallingford, CT, 2009.
- (14) (a) C. T. Lee, W. T. Yang, R. G. Parr, *Phys. Rev. B.* **1988**, 37, 785. (b) B. Miehlich, A. Savin, H. Stoll, H. Preuss, *Chem. Phys. Lett.* **1989**, 157, 200. (c) A. D. Becke, *J. Chem. Phys.* **1993**, 98, 5648.
- (15) (a) K. Fukui, *J. Phys. Chem.* **1970**, 74, 4161. (b) K. Fukui, *Acc. Chem. Res.* **1981**, 14, 363.
- (16) V. Barone, M. Cossi, *J. Phys. Chem. A.* **1998**, 102, 1995.
- (17) Y. Zhao, D. G. Truhlar, *Acc. Chem. Res.* **2008**, 41, 157.
- (18) G. W. Wheland, *J. Am. Chem. Soc.* **1942**, 64, 900.
- (19) C. Wohlfarth, In *Supplement to IV/6. Landolt-Börnstein-Group IV Physical Chemistry (Numerical Data and Functional Relationships in Science and Technology)*; M. Lechner, Ed.; Springer: Berlin, Heidelberg, **2008**; Vol. 17.

Chapter Six

A Computational Mechanistic Investigation into Reduction of Gold(III) Complexes by the Amino Acid Glycine: A New Variant for Amine Oxidation

This chapter provides a mechanistic exploration of the reduction of gold (III) complexes by the amino acid glycine. Interestingly, when the nitrogen atom of glycine coordinates to the gold (III) centre, its C α -hydrogen atom becomes so acidic that it can be easily deprotonated. This deprotonation, assisted by a mild base, converts the amino acid into a potent reductant by which gold (III) is reduced to gold(I) with a moderate activation energy. To our knowledge, this is the first contribution suggesting that primary amines are oxidized to imines via direct α -carbon deprotonation. This work also provides a rationalization behind why gold (III) complexes with amine-based polydentate ligands are reluctant to undergo a redox process.

6.1 Introduction

Despite enormous efforts to develop and improve anticancer treatment, the spectrum of accessible potent drugs is relatively limited. Thus, there is a noticeable demand for the development of novel drugs. Organometallic compounds, which are described as metal complexes containing at least one direct covalent metal-carbon interaction, have been recently discovered to be excellent anticancer drug alternatives.¹ These compounds, with a huge structural variety ranging from linear to octahedral, offer more diverse stereochemistry in

comparison with organic molecules. In addition, the organometallic M-C bonds are normally kinetically stable, uncharged and lipophilic with a metal atom which is in a low oxidation state.¹ Due to these basic differences compared to “classical coordination complexes”, organometallics suggest great opportunities in the design of new classes of biologically active molecules. Although there are numerous examples of the application of classical organometallic compounds as catalysis or biosensing in the literature, their application in medicinal chemistry, especially in cancer treatment, is becoming more prevalent in recent years (Figure 6.1).¹

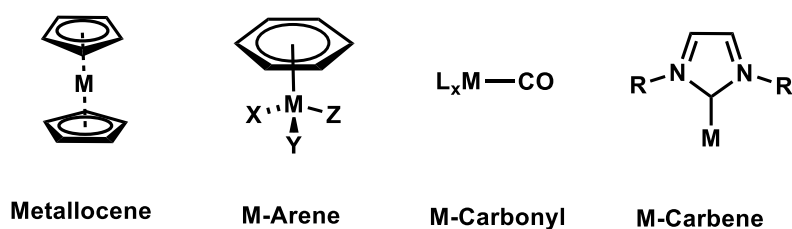


Figure 6.1. Typical classes of organometallics used in the drug industry.

Platinum (II) compounds, such as cisplatin (*cis*-PtCl₂(NH₃)₂), are used in 50% of the treatments for people who suffer from cancer.² Despite the tremendous success of cisplatin towards different cancers, finding alternative safer drugs is highly desirable. This is mainly because the use of cisplatin in cancer therapy is usually associated with severe side effects, including normal tissue toxicity, apoptosis (normal cell death) and treatment resistance.² Gold complexes have gained increased attention recently as promising anticancer drugs.³

6.1.1 The origin of gold therapy

The application of gold in the drug industry goes back as far as 2500 BC, with the first use of gold as a therapeutic agent in China.⁴ The current interest in the medicinal use of gold complexes arises from the discovery by Robert Koch in 1890 that gold cyanide constrains the growth of *tubercle bacillus*.⁵ Following this, it was found that gold therapy can remarkably decrease the joint pain for non-tubercular patients, leading to more investigation by physician

Jacques Forestier⁶. Forestier discovered that gold drugs have a beneficial impact in treatment of rheumatoid arthritis. Some gold thiolate compounds, which were introduced to the market in the 1920s and still medically used, are capable of reducing the disease progression (Figure 6.1.1). Following this, in the 1970s, Sutton et al. discovered an oral gold phosphine complex, auranofin (Figure 6.1.1), for the treatment of rheumatoid arthritis, which shows promising effects.⁷

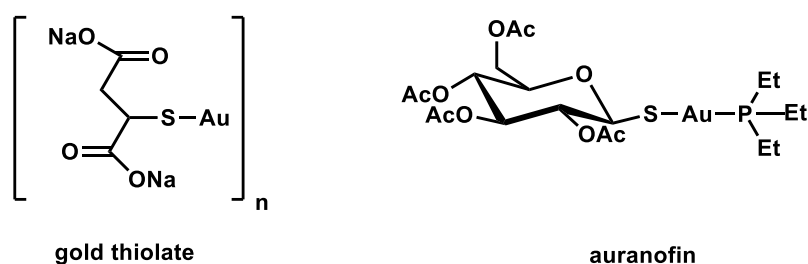


Figure 6.1.1. Examples of gold drugs for rheumatoid arthritis treatment.

6.1.2 Gold(III) anticancer complexes

In the 1980s, Au(III) compounds were first explored as potential anticancer candidates, owing to their square planar geometry with d^8 electron configuration, which is isoelectronic with Pt(II).⁵ It was proposed that Au(III) complexes may be able to mimic the activity of cisplatin without causing the harmful side effects in body cells. Normally, gold(III) compounds are relatively unstable in physiological environments due to their high reduction potential. However, recently, a handful of strategies have been presented to stabilize the gold(III) oxidation state, and a large number of gold(III) complexes have indicated cytotoxicity against cancerous cells *in vitro*.⁸ However, not many Au(III) complexes have been known to show anticancer activity *in vivo*. There are three different classes of gold (III) compounds that demonstrate antitumor effects *in vivo* (Figure 6.1.2): the first one is Au(III) dithiocarbamate compounds discovered by Fregona in 2005. The compounds $[\text{Au}(\text{DMDT})\text{X}_2]$ and $[\text{Au}(\text{ESDT})\text{X}_2]$ (DMDT = N,N-dimethylthiocarbamate, ESDT = ethylsarcosinedithiocarbamate; $\text{X} = \text{Cl}, \text{Br}$) show more toxicity *in vitro* compared to cisplatin, and to human cancerous cell lines naturally resistant to cisplatin.⁹ A well-known example of this series, $[\text{Au}(\text{DMDT})\text{Br}_2]$ (Figure

6.1.2), was indicated to remarkably inhibit the expansion of MDA-MB-231 breast cancer xenografts in mice.¹⁰ The second class is Au(III) porphyrins explored by Che et.al,¹¹ which show promising impact *in vivo* as antitumor treatments in a range of different cancer cells, with selectivity for sick cells over healthy ones. An example that has been studied most widely is the prototypical complex [Au(III)(TPP)]Cl (Figure 6.1.2), showing auspicious *in vivo* activity over many tumour models in animals.¹² The porphyrinato ligand considerably stabilizes the gold(III) ion against reduction by reducing agents in body such as glutathione (GSH) and ascorbic acid. Recently, Che and co-workers have discovered that a cyclometallated gold (III) NHC (N-heterocyclic carbene) compound ([Au(CNC)(NHC)]⁺, Figure 6.1.2) abolishes tumour expansion in a mice model.¹³

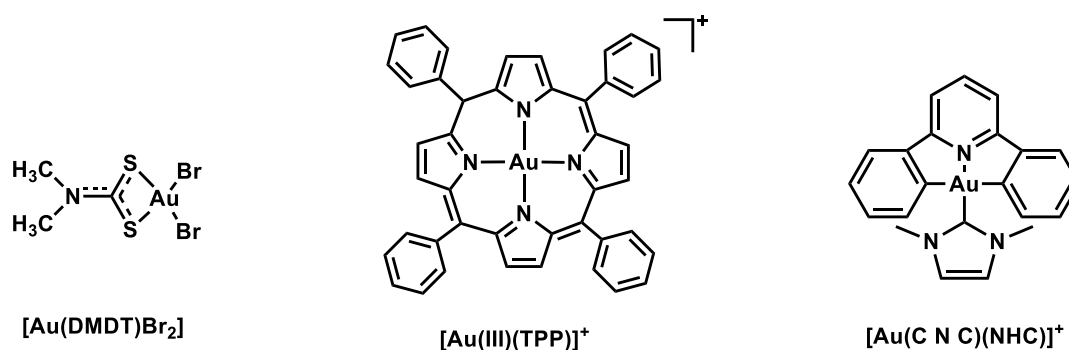
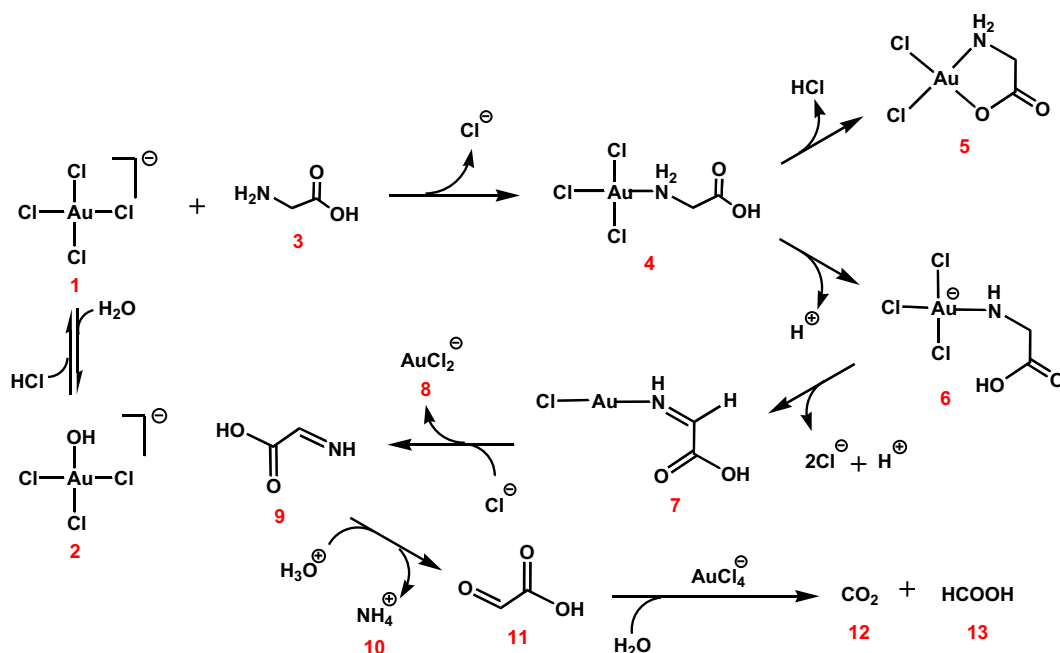


Figure 6.1.2. Examples of Au(III) complexes that have shown anticancer activity *in vivo*.

6.1.3 Au(III) reducing agents in the human body

As mentioned above, there is a strong relation between platinum(II) and gold(III) in fields such as organometallic chemistry and catalysis since they have the same isoelectronic configuration (d⁸). For Au(III) compounds to be isostructural with platinum(II) complexes and consequently show similar medicinal properties, it is imperative that the oxidation state of gold(III) remains intact.¹⁴ This constraint is complicated by the high cathodic reduction potential of Au(III), enabling biological reductants to easily reduce it.¹⁵ In this context, reducing agents such as GSH, Ascorbic acid and most importantly amino acids, which exist in body cell environments, have been reported to reduce Au(III) to Au(I).¹⁶ For instance, Sadler

et al. found that glycine (Gly) (**3**) is capable of reducing gold(III) under acidic, neutral, and physiological conditions at room temperature to give glyoxylic acid (GA) (**11**) as the primary product (Scheme 6.1.3).¹⁷ Sadler has proposed a mechanism for the reduction, which remains generally accepted (Scheme 6.1.3). According to this mechanism, coordination of the amine group to the Au(III) centre gives **4**, while **1** and **2** are in equilibrium with $[1] \gg [2]$. Two alternative pathways are then suggested: either **4** undergoes a substitution-type reaction to terminate at **5**, or a redox reaction to afford the gold(I)-imine intermediate **7**, followed by its subsequent hydrolysis to **11**. In the latter pathway, intermediate **6** obtained from the deprotonation of **4** is proposed to drive the reduction thermodynamically. Finally, GA (**11**) in the presence of an additional gold(III) complex undergoes oxidative decarboxylation and affords **13**.¹⁷



Scheme 6.1.3. Mechanism for reduction of gold (III) by Gly proposed by Sadler.¹⁷ The mechanism considers only the reaction of **1** with **3** due to the predominant concentration of **1** over **2**.

As part of a series of ongoing studies related to the reduction of transition metal complexes by biological reductants¹⁸, a comprehensive density functional theory (DFT) investigation into the mechanism of this remarkable reaction was conducted. This contribution seeks to offer new insights into how amines are oxidized in the presence of a centre with high cathodic reduction potential. These new findings also provide an explanation as to why the chelate complex **5** is not reactive toward the redox process, and sheds light on

the process of gold(III)-mediated GA oxidative decarboxylation by suggesting a novel mechanism.

Computational calculations in this work have been done by the candidate in the CCL laboratory at UTAS under supervision of Assoc. Prof. Alireza Ariafard and Prof. Brian. F. Yates.

6.2 Computational Details

Gaussian 09¹⁹ was used to fully optimize all the structures reported in this chapter at the B3LYP level of theory.²⁰ For all the calculations, solvent effects were considered using the CPCM solvation model with water as the solvent.²¹ The effective core potential of Hay and Wadt with a double- ξ valence basis set (LANL2DZ) was chosen to describe Au.²² The 6-31G(d) basis set was used for other atoms.²³ A polarization function was also added for Au ($\xi_f = 1.050$).²⁴ This basis set combination will be referred to as BS1. Frequency calculations were carried out at the same level of theory as those for the structural optimization. Transition structures were located using the Berny algorithm. Intrinsic reaction coordinate (IRC) calculations were used to confirm the connectivity between transition structures and minima.²⁵ To further refine the energies obtained from the B3LYP-CPCM/BS1 calculations and to consider dispersive interactions,²⁶ single-point energy calculations using the B3LYP-D3 functional method for all of the structures with a larger basis set (BS2) and the SMD²⁷ solvation model were carried out. BS2 utilizes the def2-TZVP basis set²⁸ on all atoms. Effective core potentials including scalar relativistic effects were used for the gold atom. Tight convergence criterion and ultrafine grids were also employed to increase the accuracy of the calculations. The benchmark calculations show that B3LYP-D3-SMD/BS2//B3LYP-CPCM/BS1 yields results in closer agreement with the experimental data and thus we used the results obtained from this functional set for interpreting our findings. Natural bond orbital (NBO) analysis was carried out using NBO6 software²⁹ integrated into Gaussian09.

Given that the solvation free energy³⁰ and gas phase free energy of a proton are reported as -264.0 and -6.3 kcal/mol, respectively, a number of -270.3 kcal/mol was used as the free energy of H^+ in the calculations.

In this work, the free energy for each species in solution was calculated using Equation (1):

$$G = E(\text{BS2}) + G(\text{BS1}) - E(\text{BS1}) + \Delta G^{\text{1atm} \rightarrow \text{1M}} \quad (1)$$

Where $\Delta G^{\text{1atm} \rightarrow \text{1M}} = 1.89$ kcal/mol is the free-energy change for compression of 1 mol of an ideal gas from 1 atm to the 1 M solution phase standard state³¹ and $E(\text{BS2})$ is the potential energy obtained by basis set BS2 for structural optimization by BS1.

An additional correction to Gibbs free energies was made to consider solvent (water) concentration where a water cluster $(\text{H}_2\text{O})_n$ is directly involved in transformations. In such a case, the free energy of $(\text{H}_2\text{O})_n$ is described by Equation (2):

$$G = E(\text{BS2}) + G(\text{BS1}) - E(\text{BS1}) + \Delta G^{\text{1atm} \rightarrow \text{1M}} + RT \ln(55.34/n) \quad (2)$$

The last term corresponds to the free energy required to change the standard state of $(\text{H}_2\text{O})_n$ from 55.34/ n M to 1 M.³²

Benchmark calculations.

The reaction given in eq **S1** was reported by Bekker and Robb to have a Gibbs free energy of +0.8 kcal/mol.³² To test how accurate our calculations are, the Gibbs free energy for this transformation was calculated at different levels of theory. In our calculations, the Gibbs free energy for a solvated proton was considered to be -270.3 kcal/mol. As listed in Table 6.2, both M06 and B3LYP levels with CPCM solvation model give a value of ~ -6 kcal/mol for proton loss from $\text{AuCl}_3(\text{H}_2\text{O})$ which is not in agreement with the experimental data (+0.8 kcal/mol). This suggests that the CPCM solvation model is inadequate for study of a proton loss from similar gold(III) complexes. In contrast, when the CPCM is replaced by the SMD, the calculation results become much more consistent with the experimental data. Thus, to obtain more reliable results, the solvation energies are required to be approximated using the SMD solvation model.

entry	method for optimization	method for single points	$\Delta G(\text{kcal/mol})$
1	B3LYP-CPCM/BS1	B3LYP-D3-CPCM/BS2	-6.1
2	B3LYP-CPCM/BS1	M06-CPCM/BS2	-6.0
3	B3LYP-CPCM/BS1	M06-D3-CPCM/BS2	-5.9
4	B3LYP-CPCM/BS1	B3LYP-D3-SMD/BS2	-0.3
5	B3LYP-CPCM/BS1	M06-SMD/BS2	-0.2
6	B3LYP-CPCM/BS1	M06-D3-SMD/BS2	-0.3

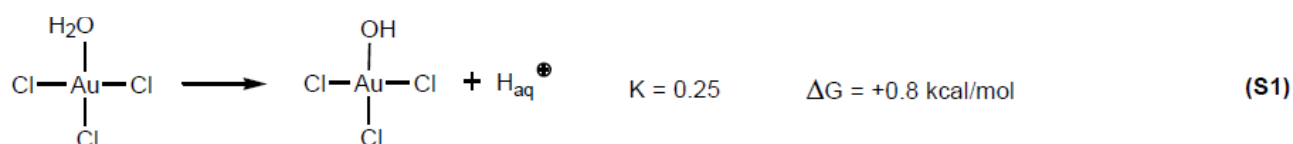


Table 6.2. Gibbs reaction energy for the reaction given in eq **S1** calculated at different levels of theory.

To find out which method gives more accurate results relating to the redox process, single point calculations were carried out at the different levels of theory using SMD solvation models for the transformation given in eq **S2**. For this reaction, ΔG^\ddagger and ΔH^\ddagger are reported by Pal et al to be ~ 18.4 and ~ 5.2 kcal/mol, respectively.³² It is inferred from Table 6.2a that B3LYP-D3 functional gives activation energies in closer agreement with the experimental data than the other methods. To this end, all the energies discussed in the text are from the B3LYP-D3-SMD/BS2//B3LYP-CPCM/BS1 calculations.

entry	method for optimization	method for single points	ΔG^\ddagger (kcal/mol)	ΔH^\ddagger (kcal/mol)
1	B3LYP-CPCM/BS1	B3LYP-D3-SMD/BS2	18.4	8.2
2	B3LYP-CPCM/BS1	M06-SMD/BS2	20.5	10.4
3	B3LYP-CPCM/BS1	B97D-SMD/BS2	13.1	2.9
4	B3LYP-CPCM/BS1	M06-2X-SMD/BS2	23.3	13.2
5	B3LYP-CPCM/BS3 ^a	B3LYP-D3-SMD/BS2	18.1	7.5
6	M06-CPCM/BS2	B3LYP-D3-SMD/BS2	21.4	8.9

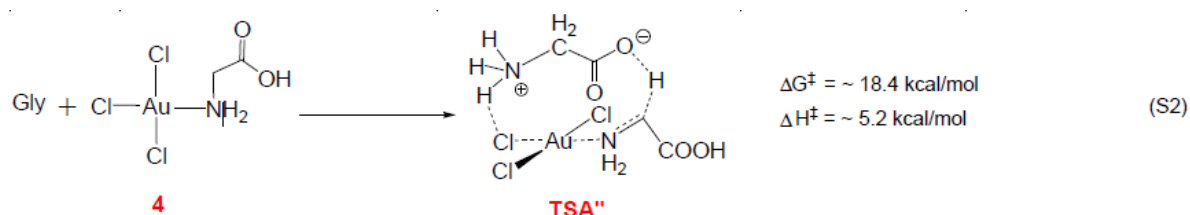


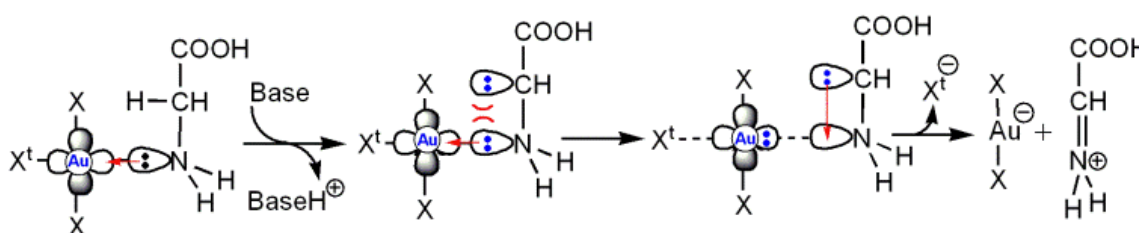
Table 6.2a. Gibbs reaction energy for the reaction given in eq **S2** calculated at different levels of theory.

We also found that the replacement of 6-31G(d) with 6-31G(d,p) and B3LYP with M06 for geometry optimization insignificantly affected the activation energies (entries 5 and 6 in Table 6.2a). This indicates that, although B3LYP-CPCM/BS1, B3LYP-CPCM/BS3, and M06-CPCM/BS1 predict slightly different structures, the activation energy for the following transformation shows an insignificant dependence on the method employed for optimization.

a) BS3: LANL2DZ(f) basis set/LANL2DZ ECP for gold and 6-31G(d,p) for other atoms

6.3 Results and Discussion

Based on our calculations, it was found that, the coordination of amino acid to gold(III) *via* its nitrogen centre makes its α -carbon (C^α) hydrogen very acidic (Scheme 6.3). The C^α position deprotonation of glycine zwitterion is calculated to be extremely endergonic at $\Delta G=42.9 \text{ kcal mol}^{-1}$, a result which is in reasonable agreement with $pK_a=29$ ($\Delta G=39 \text{ kcal mol}^{-1}$) for the same process reported by Richard et al.³³ This result emphasizes that in the absence of the gold centre, the C^α hydrogen is not acidic at all.



Scheme 6.3. Molecular orbital representation of how the C^α deprotonation drives the reduction of gold(III) and formation of protonated imine.

During the deprotonation by an appropriate base, the amino acid is rendered a strong reductant owing to the nitrogen lone pair suffering a repulsive interaction with the lone pair being generated at the C^α centre. This forces the nitrogen lone pair onto the gold(III) centre, which distributes into its $d_{x^2-y^2}$ orbital, culminating in the concerted formation of a protonated imine, *trans*-ligand (X^t) ejection and reduction of gold(III) to gold(I). Direct formation of the protonated imine is completely in agreement with the fact that Sadler et al. could not identify the imines **7** and **9** (Scheme 6.1.3).¹⁷

Three different candidates for the base by which the C^α is deprotonated were considered: i) a *cis*-ligand, ii) a water cluster (solvent), and iii) a free amino acid and it was concluded that the free amino acid (zwitterion form of Gly) creates lower energy transition structures than the neutral one. Figure 6.3 demonstrates the critical transition structures of the deprotonation step. Considering that compound **4** was identified by NMR analysis,¹⁷ we set it as the reference point for our calculations.

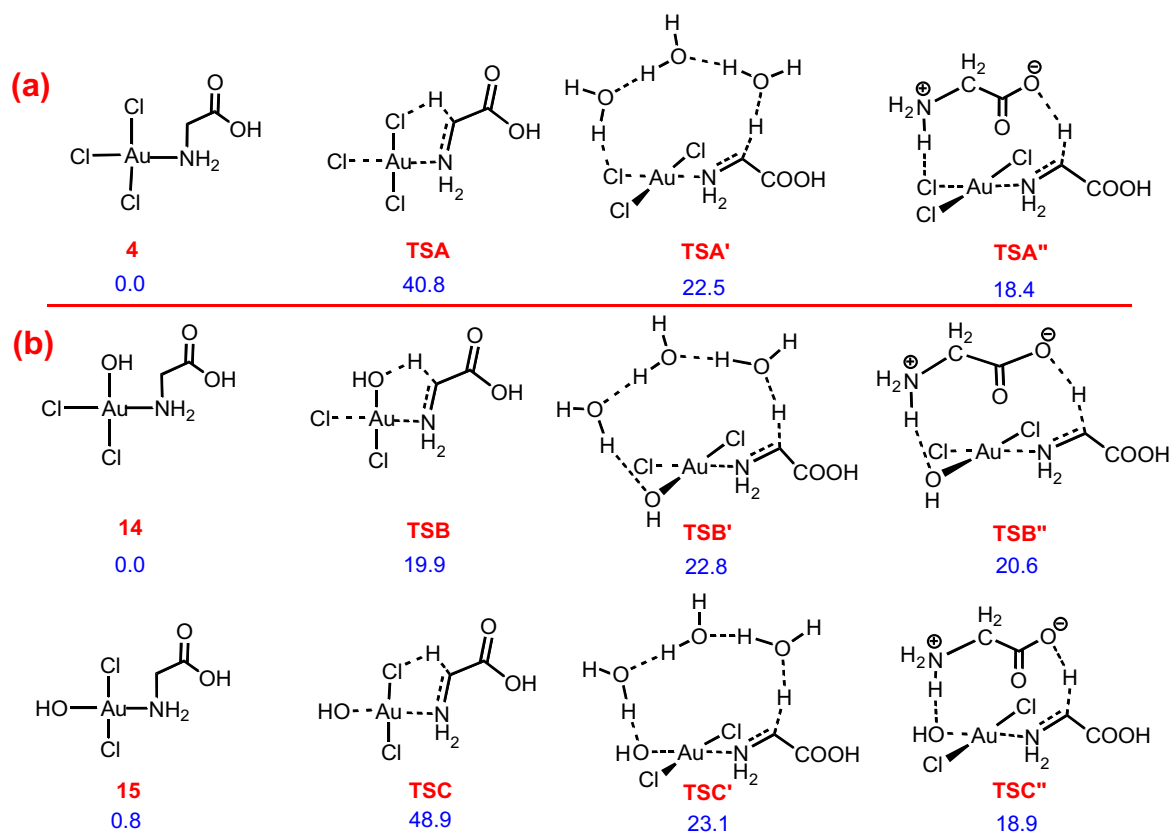


Figure 6.3. Calculated critical transition structures for deprotonation of C $^{\alpha}$ position by Cl and OH ligands, (H₂O)₃ and a free Gly from a) AuCl₃(Gly) and b) AuCl₂(OH)(Gly). Free energies are given in kcal mol⁻¹.

As depicted in Figure 6.3, the transition structure of [AuCl₃(Gly)] **TSA''** is 4.1 kcal mol⁻¹ lower in energy than **TSA'**; **TSA'** is 18.3 kcal mol⁻¹ lower in energy than **TSA**. These results suggest that the preferred base in this example is a free glycine and, in its absence, water is most likely to act as the deprotonating agent. For [AuCl₂(Gly)(OH)], two isomers **14** and **15**, which differ in the relative position of the OH and Gly ligands are anticipated to be in equilibrium. For this set, the energy of **TSB** is found to be comparable to **TSB''** and **TSC''**, implying that the deprotonation may also occur by the *cis*-hydroxide ligand of **14**. This comparison shows that while the OH ligand can deprotonate the C $^{\alpha}$ -H, the Cl ligand cannot. This can be explained by the higher basicity of hydroxide compared to the chloride ion. In addition, water (solvent) or a free amino acid can both serve as the base and trigger the gold(III) reduction by the C $^{\alpha}$ deprotonation of the coordinated Gly. As determined by NBO analysis, the gold metal centre is reduced only to a small extent in the transition structures (Figure 6.3a). According to Figure 6.3a, upon going from **4'** to **TSA'**, the Au-N and Au-Cl bonds are elongated only by 0.076 Å and 0.083 Å, respectively. This result suggests that the gold metal

centre is reduced only to a small extent in the transition structure **TSA'**. The NBO analysis also corroborates this assertion; the $d_{x^2-y^2}$ population in **TSA'** (1.449 \AA) is only 0.105 higher than that in **4'** (1.344) and the second order perturbation energy (E2) for interaction of the lone pair being created on α -carbon and $\sigma^*\text{Au-N}$ in **TSA'** is calculated to be only 10.3 kcal/mol. The NBO analysis also shows that the water cluster, $(\text{H}_2\text{O})_3$, is more positively charged in **TSA'** (+0.266) than in **4'** (+0.012) and AuCl_3 moiety more negatively charged in **TSA'** (-0.704) than in **4'** (-0.352). All these results lend support to the idea that the water serves as a base and by abstracting a proton from the coordinated glycine results in AuCl_3 acting as a charge receiver. The energy profiles of three different base candidates are shown in Figure 6.3b.

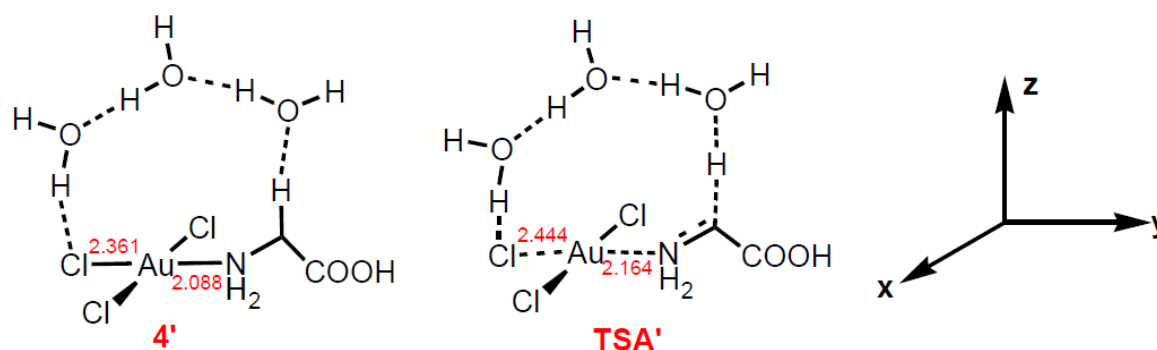


Figure 6.3a. Selective bond distances (Å) for optimized structures **4'** and **TSA'**.

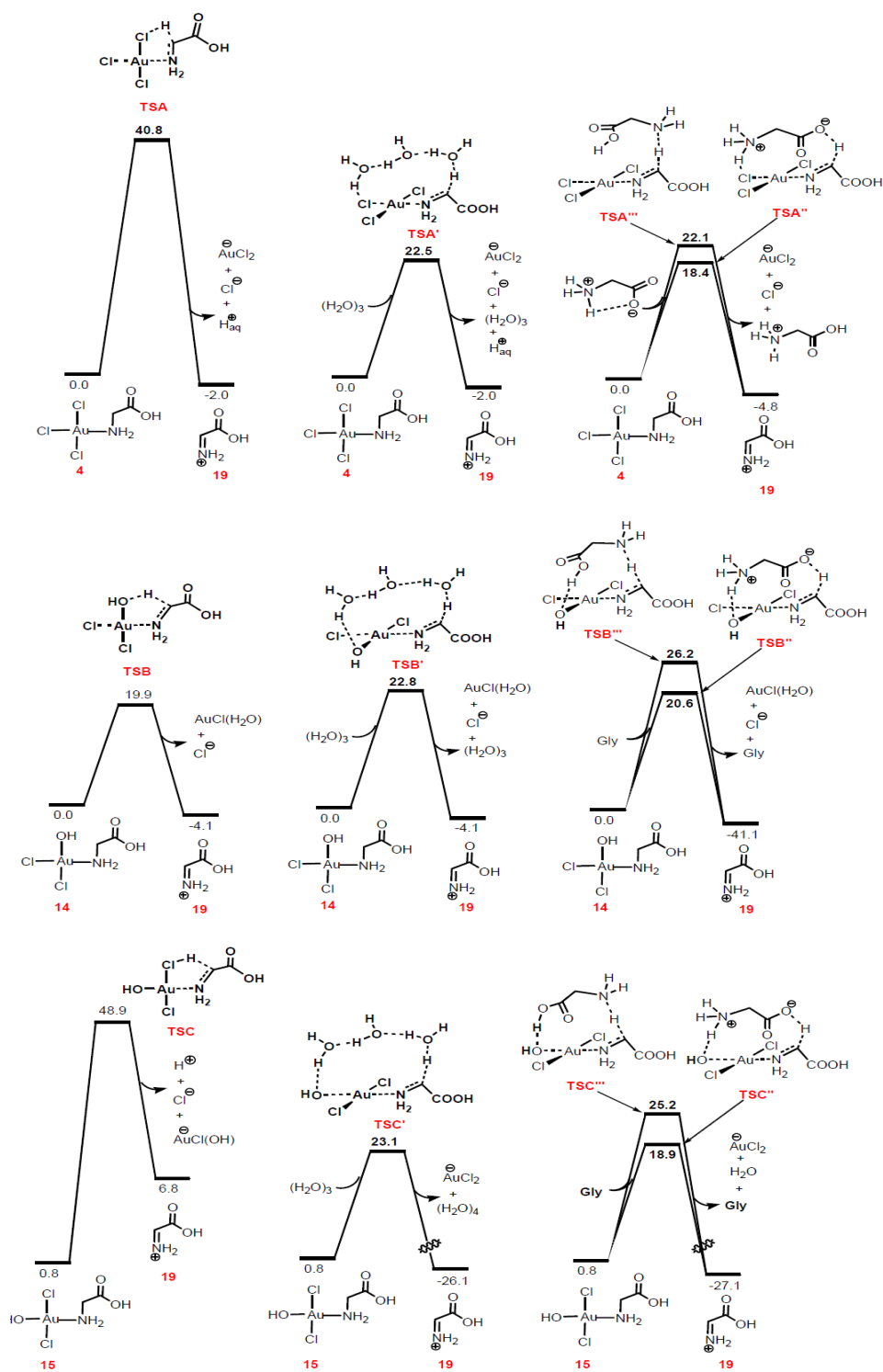


Figure 6.3b. Gibbs free energy profiles for deprotonation of C α hydrogen by OH and Cl ligands, $(\text{H}_2\text{O})_3$, and a free Gly from $\text{AuCl}_2(\text{OH})(\text{Gly})$. Free energies are given in kcal/mol.

In this work, $(\text{H}_2\text{O})_3$ was considered as the water cluster (Scheme 6.3c).³⁴ Activation free energies for C^α deprotonation of **4** by H_2O , $(\text{H}_2\text{O})_2$, $(\text{H}_2\text{O})_3$, and $(\text{H}_2\text{O})_4$ were calculated to be 34.1, 27.6, 22.5, and 24.2 kcal mol⁻¹, respectively, indicating that water in the trimeric form serves as the most efficient base. Figure 6.3c shows why water clusters in this case are more basic than a single water molecule.

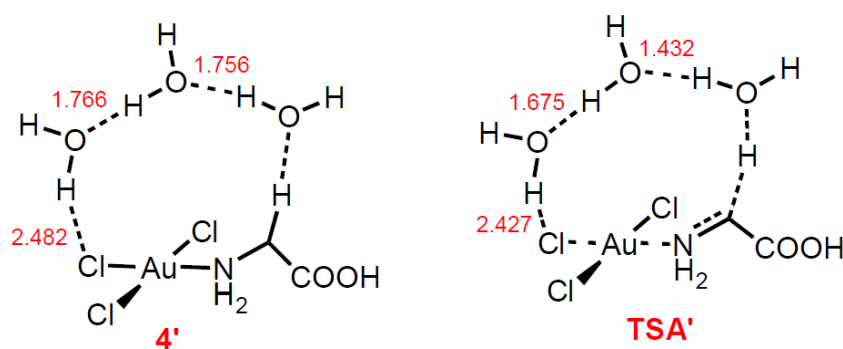


Figure 6.3c. Selective bond distances (Å) for optimized structures **4'** and **TSA'**.

As indicated, H-O and H-Cl distances are shorter in **TSA'** than in **4'**, suggesting that the hydrogen bond interactions are stronger in transition structure **TSA'**. The strengthening of the hydrogen bonds in **TSA'** as compared to that in **4'** provides an extra stability to the system, facilitating the C^α deprotonation. This explains why a single water molecule with an activation barrier of 34.1 kcal/mol is not basic enough to act as a deprotonating agent.³⁵

6.3.1 Can the redox reaction proceed through intermediate **6**?

As demonstrated in scheme 6.1.3, gold(III) reduction was suggested to proceed *via* intermediate **6**. This may have originated from the widely accepted mechanism³⁶ⁱ for transition metal-mediated amine oxidation in which deprotonation of the coordinated NH_2 group is proposed to be essential for the reaction to start.³⁶ Calculations indicate that an amine proton abstraction from **4** by water is substantially endergonic (15.0 kcal mol⁻¹). In this case, the pivotal transition structures in which the C^α position of **6** is deprotonated have high energies; 38.3 kcal mol⁻¹ for the case where $(\text{H}_2\text{O})_3$ is considered as the deprotonating agent and 32.9 kcal mol⁻¹ for Gly (Figure 6.3.1).

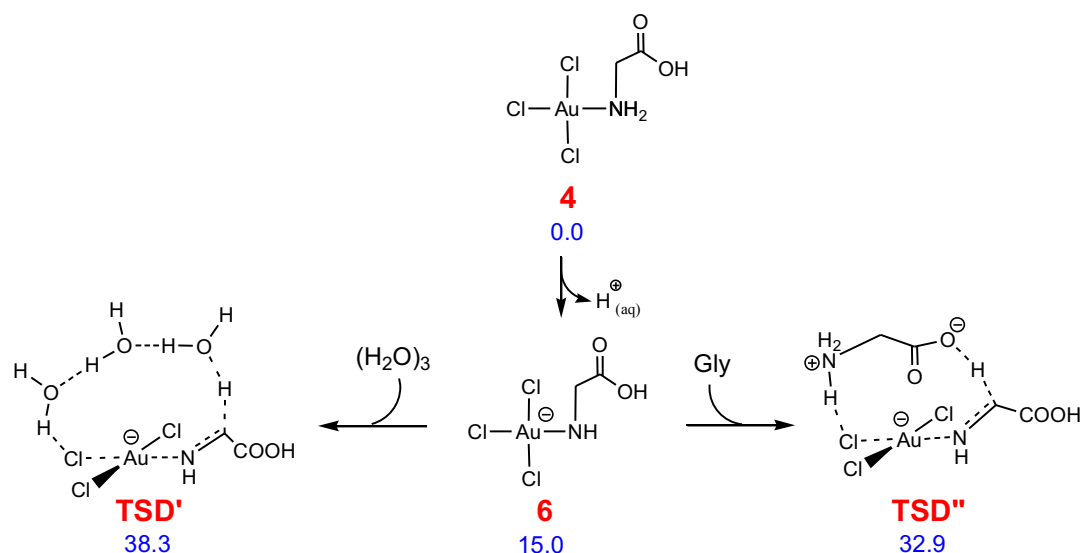


Figure 6.3.1. Calculated mechanism of reduction of gold(III) by Gly where intermediate **6** is formed during the redox process (conventional mechanism). Free energies are given in kcal mol⁻¹.

Potential energy surface (PES) scans for elongation of N-H bond in **4''** and C^α-H bond in **4'** calculated at the B3LYP-CPCM/BS1 level are shown in Figure 6.3.1a. This Figure shows that although a water cluster deprotonates the NH with a similar activation energy to the C^α-H, the former is calculated to be extremely endothermic. This endothermicity is the main reason the conventional mechanism, in which deprotonation of the N-H occurs first, is unlikely to operate.

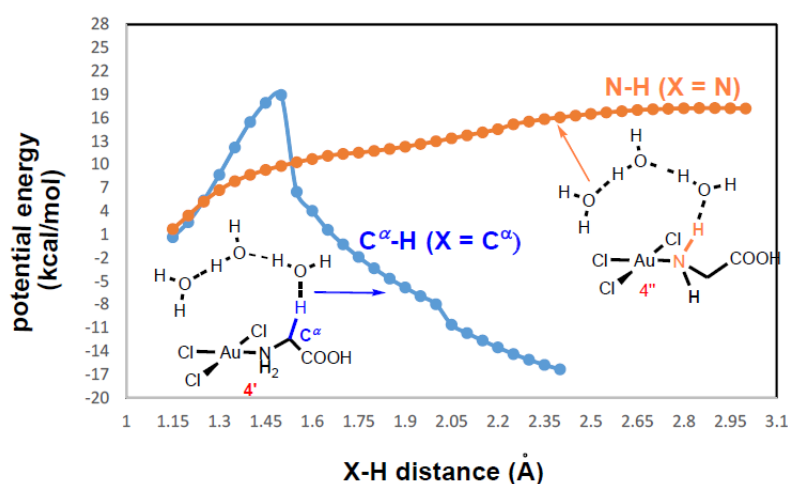


Figure 6.3.1a. PES scan for elongation of N-H bond in **4''** and C^α-H bond in **4'**.

Complex **14** is also predicted to be unreactive towards a redox process *via* deprotonation of the Gly NH₂ group (Figure 6.3.1b). The proton transfer from the NH₂ group to the OH ligand in **14** is an endergonic process with $\Delta G=13.9$ kcal mol⁻¹, indicating that the protons of NH₂ in **14** are much less acidic when compared to those of the water ligand in **14'**. The higher acidity of a proton of water ligand in **14'** is also evident from low endergonicity of transformation **14'**→**6'**+H⁺_{aq} ($\Delta G=3.8$ kcal mol⁻¹). The Gly oxidation *via* this variant requires an overall activation Gibbs energy of 34.8 kcal mol⁻¹. In short, this investigation demonstrates that, due to the absence of a strong base in neutral or acidic media, the amine is oxidized by direct deprotonation of a glycine C^α hydrogen, and not through intermediates **6** or **6'** (conventional mechanism). The result is a new insight into the mechanism of metal mediated amine oxidation wherein amine protons remain intact during the course of the redox process.

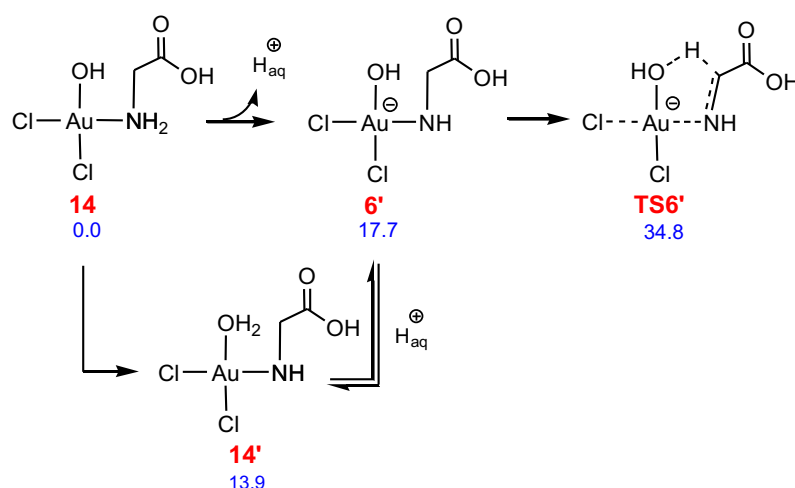


Figure 6.3.1b. Calculated mechanism of reduction of gold(III) by Gly where intermediate **6** is formed during the redox process (conventional mechanism). Free energies are given in kcal mol⁻¹.

6.3.2 Chelate effect

In this section, the lack of reactivity of the chelate complex **5** toward redox processes, reported by Sadler et al, is explored computationally (Scheme 6.1.3).¹⁷ Results show that chelation causes a large increase in the activation barrier of the redox reaction. As illustrated in Figure 6.3 a, water-assisted deprotonation of **4** (TSA') requires an activation energy of 22.5 kcal mol⁻¹, whereas the same process for **5** is computed to occur with an activation Gibbs

energy as high as 33.5 kcal mol⁻¹ (Figure 6.3.2). This large difference in energy provides a clue as to why the chelate complex **5** is not reactive at all. It is inferred from the structures in Figure 6.3.2a that planarity of the Au, N, C^α and H¹ atoms is needed for deprotonation to take place with a minimal activation energy. The planarity maximizes the reductant capability of the Gly ligand by allowing its C^α *p*-orbital to find the best alignment for interacting with the nitrogen *p*-orbital in the transition structure of the deprotonation step. Chelation prevents the molecule from adopting this optimal configuration, elevating the activation energy by 11.0 kcal mol⁻¹. A comparison of the optimised geometries for **TSA'** and **TSE'** lends support for the above argument. As indicated in Figure 6.3.2a, the Au, N, C^α and H¹ atoms in **TSE'** are not in the same plane with a dihedral angle of 66.7°, while those atoms are nearly coplanar in **TSA'**. In addition, the longer C^α-H¹ bond distance in **TSE'** shows that deprotonation from the chelate complex take place *via* a later transition structure, elucidating the lower reactivity of the chelated gold(III) complexes toward reduction.

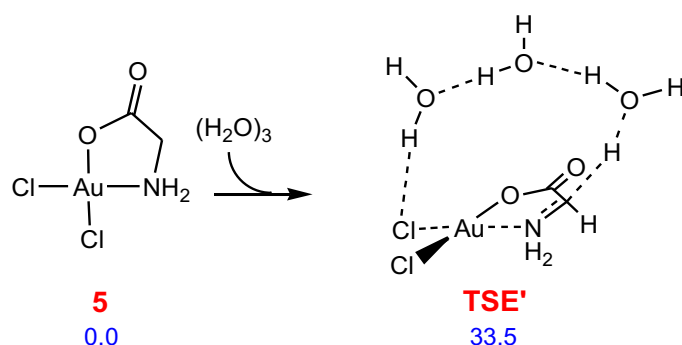


Figure 6.3.2. Calculated transition structure for deprotonation of C^α position of chelated complex **5** by water. Free energies are given in kcal mol⁻¹.

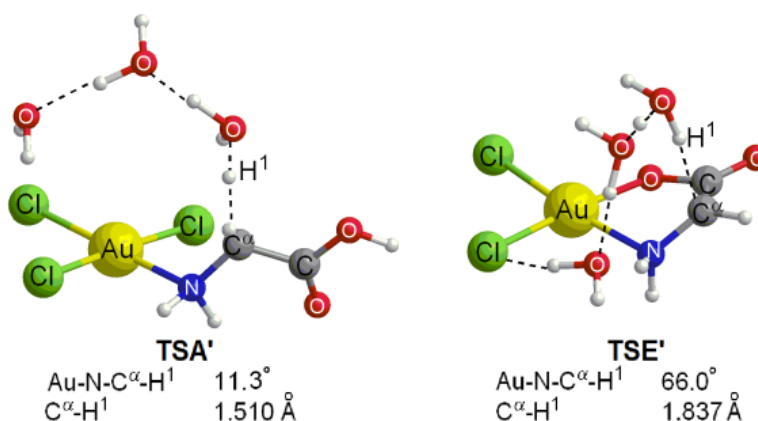
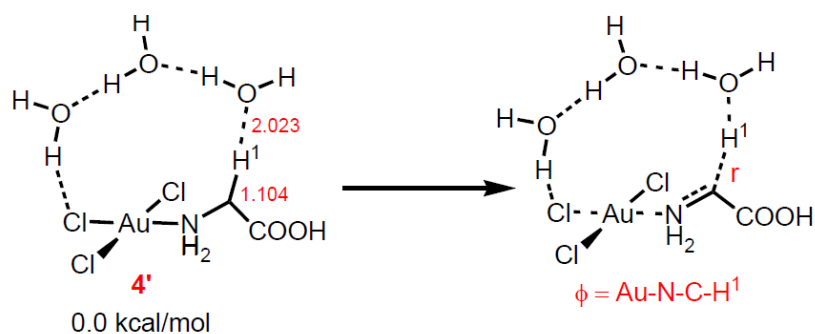


Figure 6.3.2a. Optimized structures of **TSA'** and **TSE'**.

To address how dependent the activation energy of gold (III) reduction is on the Au-N-C-H¹ dihedral angle, we scanned PES by optimizing geometry of **4'** at various fixed values of the C-H¹ distance (r) with frozen dihedral angle Au-N-Ca-H¹. The calculations show that as the dihedral angle increases, the activation energy increases (Table 6.3.2).



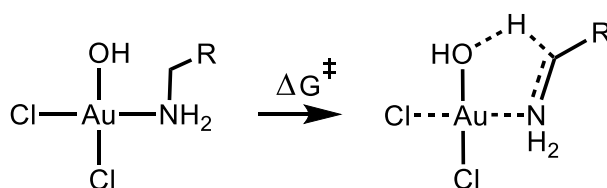
$r(\text{\AA}) \backslash \phi(^{\circ})$	0	40	70
1.150	1.6	1.7	1.8
1.200	3.6	3.7	3.9
1.250	6.3	6.4	6.8
1.300	9.6	9.7	10.3
1.350	13.0	13.1	14.1
1.400	16.2	16.5	17.7
1.450	18.5	19.4	21.2
1.500	19.2	21.1	24.0
1.550	6.8	21.7	26.1
1.600	4.4	3.3	27.2
1.650	2.3	1.1	3.4

Table 6.3.2. Calculation results for PES scan by optimizing geometry of **4'** at various fixed values of the C-H¹ distance (r) with frozen dihedral angle Au-N-C^a-H¹ (ϕ) at 0, 40, and 70°.

6.3.3 Impact of carboxylic acid functional group on the redox activation energy

In order to find out the impact of the carboxylic acid functional group on the ease of the deprotonation step, the activation Gibbs free energies of the transformation for a range of R substituents were calculated as illustrated in Table 6.3.3. The data suggests that while R=COCH₃ shows the lowest activation energy, R=H gives the highest. It follows that the stronger the π -accepting ability of the R group, the lower the activation barrier (a less marked effect is shown for the σ -interacting functional group (CF₃, CH₃, H)). The π -accepting

functional groups are capable of accepting electron density from the developing anion on C $^{\alpha}$, stabilizing the corresponding transition structure more efficiently. This finding demonstrates that the carboxylic acid group is not inert in the redox processes and contributes to lower the activation energy of the critical transition structures shown in Figure 6.3. These results indicate that many amines can be oxidized by gold(III) through a mechanism in which the C $^{\alpha}$ position is directly deprotonated to afford a protonated imine.³⁷



R	COCH ₃	COH	COOH	p-NO ₂ -Ph	Ph	CF ₃	CH ₃	H
ΔG^{\ddagger}	16.0	17.0	19.9	21.9	24.2	25.0	27.6	28.4

Table 6.3.3. Calculated activation energy for transformation **14**→**TSB** with various R groups. Free energies are given in kcal mol⁻¹.

6.3.4 An alternative mechanism for amino acid oxidation via decarboxylation

As illustrated in Scheme 6.1.3, amino acids are oxidized by two equivalents of a gold(III) complex to afford formic acid and carbon dioxide. In this regard, Pal et al.³⁵ suggested an alternative mechanism in which CO₂ evolution take place by just one equivalent of gold(III). In this pathway, the redox reaction is originated from coordination of the amino acid zwitterion, and not the neutral form. This alternative can be formulated by our DFT calculations as depicted in Figure 6.3.4.

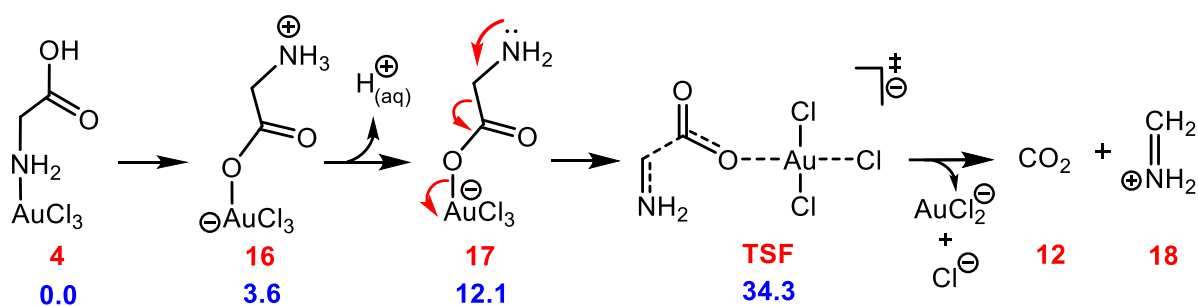


Figure 6.3.4. Calculated mechanism of reduction of gold(III) from zwitterion complex **16** leading to loss of CO₂. Free energies are given in kcal mol⁻¹.

Based on this reaction, GA is never generated during the reaction. This is not in agreement with empirical findings reported by Sadler.¹⁷ This analysis also discounts the pathway suggested by Pal. It is inferred from the results that zwitterion complex **16** is less stable in comparison with complex **4** due to the presence of gold centre by 3.6 kcal mol⁻¹, which is supported by NMR data provided by Sadler et al., indicating coordination of the neutral Gly form to the Au(III) centre.¹⁷ For the Gly to behave as a reductant in this variant, the amine moiety of **16** needs to be protonated first in order to generate anionic intermediate **17**. Once **17** is formed, its nitrogen lone pair promotes the reaction *via* the electron flow mechanism by passing through the transition structure **TSF** as depicted in Figure 6.3.4. In this reaction, nitrogen lone pair interaction with the C^α-C^β σ* orbital initiates the redox process *via* the heterolytic cleavage of the C^α-C^β bond. The computational results show that the gold reduction mechanism in this case is relatively energy demanding with an activation Gibbs energy of 32.4 kcal mol⁻¹, confirming that the redox process is unlikely to occur from compound **16** (Figure 6.3.4a). It is obvious from this picture that decarboxylation of **16** in the presence of a water cluster as the base *via* **TSF'** is more energy consuming than that in the absence of the base (**TSF**). This result shows the importance of the nitrogen lone pair in triggering the decarboxylation process. Indeed, in **TSF**, the nitrogen lone pair is stabilized by (H₂O)₂(H₃O)⁺ and therefore is less available for interaction with the C^α-C^β σ* orbital.

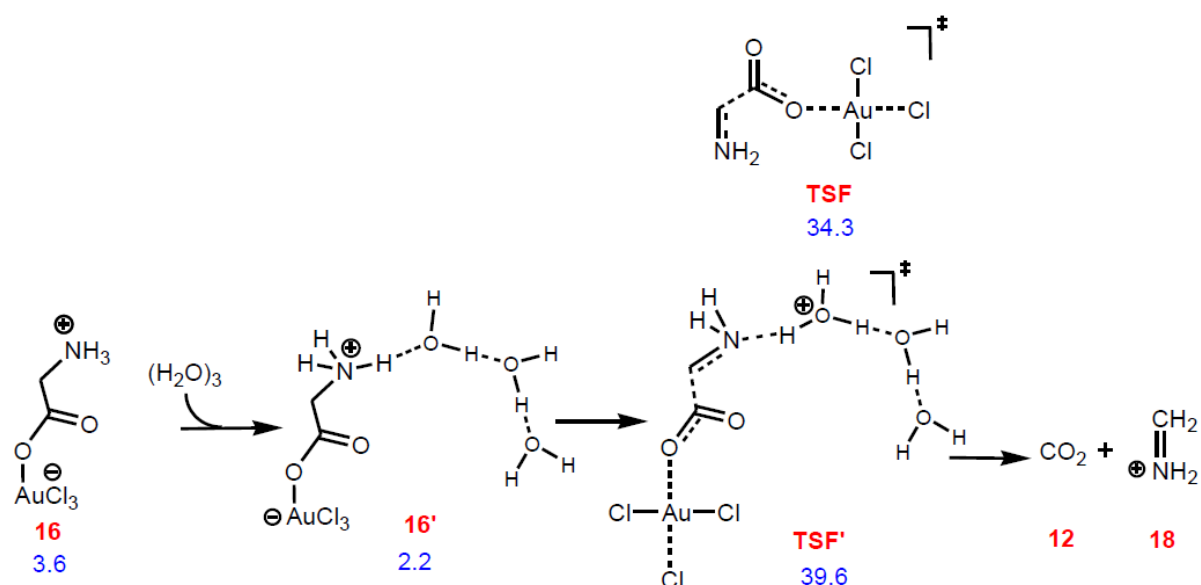


Figure 6.3.4a. Calculated mechanism of reduction of gold(III) from zwitterion complex **16** assisted by a water cluster as the base. Free energies are given in kcal/mol.

6.3.5 Hydrolysis of protonated imine³⁸

According to the proposed mechanism, gold(III) is reduced to gold(I) with concomitant formation of the protonated imine **19** (Scheme 6.3.5). Once **19** is formed, water can attack the C $^{\alpha}$ centre to give **20**, followed by a proton transfer to nitrogen to generate **21**. Formation of compound **11** (GA) *via* transition structure **TSG''** is then facilitated by a new water cluster. The deamination was found considerably endergonic unless water helps to deprotonate the alcohol OH group from **21**. It is interesting to note that deamination and deprotonation of the OH group should occur in one step *via* the transition structure **TSG''**. The above hydrolysis is calculated to be exergonic by -9.9 kcal mol⁻¹ and needs an overall activation Gibbs free energy of 16.8 kcal mol⁻¹ as depicted in Figure 6.3.5. The comparison of the activation barriers for the hydrolysis step and redox step (C $^{\alpha}$ deprotonation) shows that the latter is the rate determining step for formulation of **11** (GA) (**TSB''** or **TSC''** in Figure 6.3).³⁹

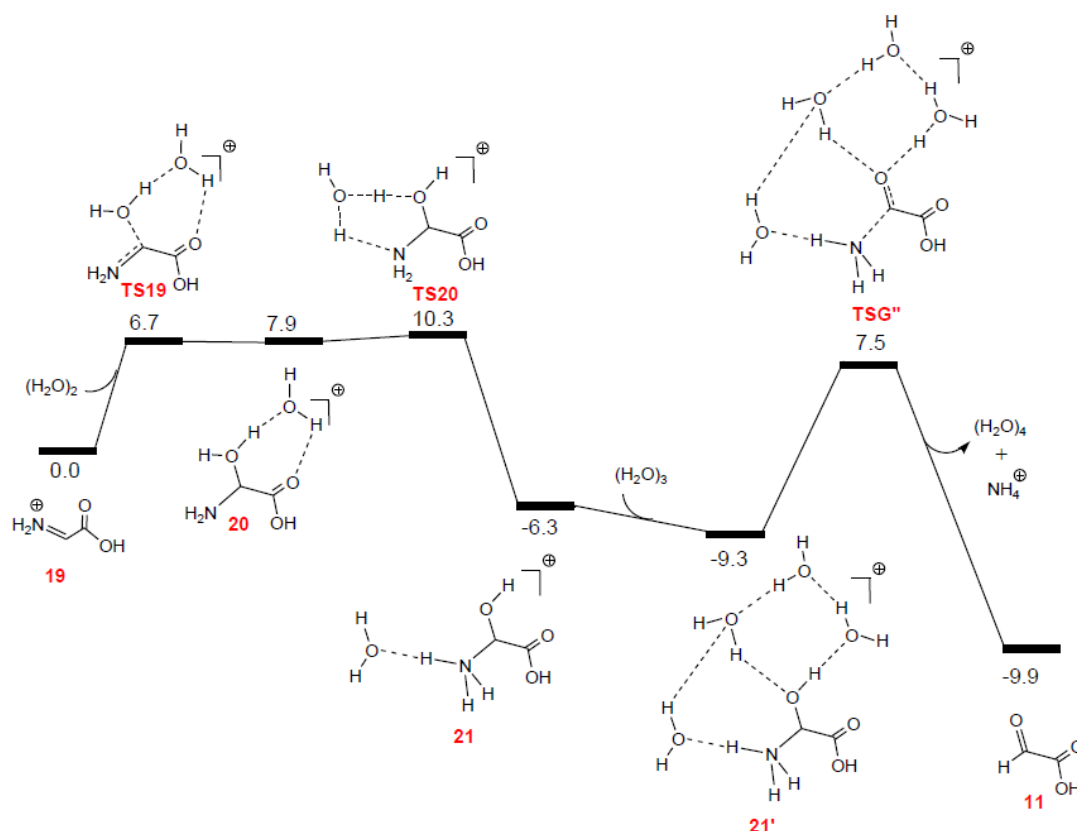
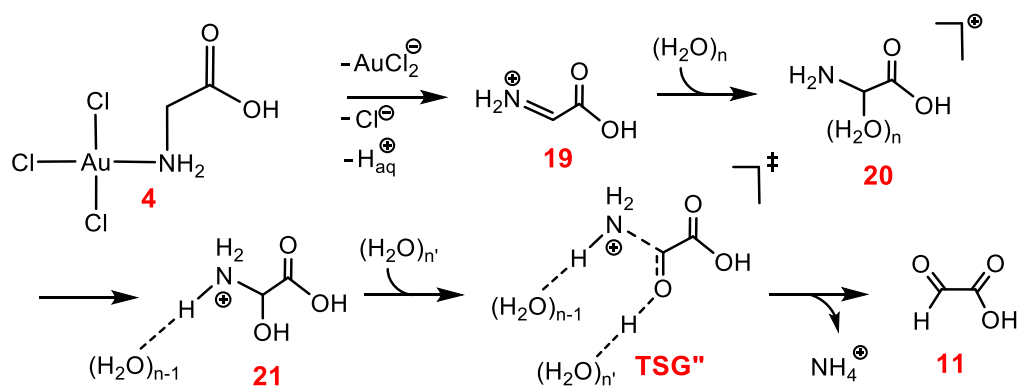


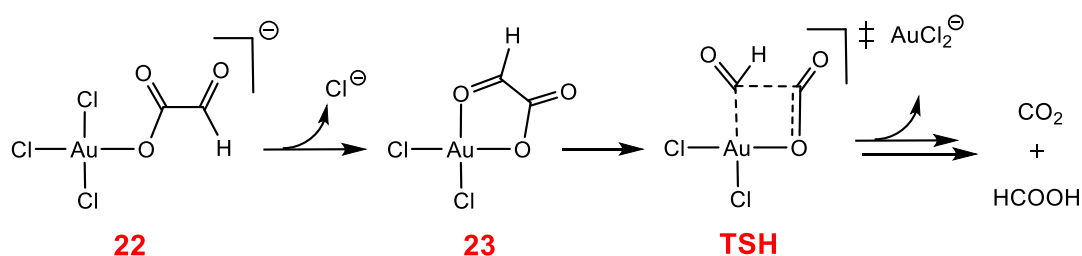
Figure 6.3.5. Gibbs free energy profile for hydrolysis of protonated imine **19**. Free energies are given in kcal/mol.



Scheme 6.3.5. Mechanism for hydrolysis of the protonated imine **19**.

6.3.6 Oxidative decarboxylation of glyoxylic acid

Finally, work reported in this chapter aimed to clarify the mechanism by which GA (**13**) undergoes oxidative decarboxylation, as observed by Sadler et al. (Scheme 6.1.1).¹⁷ We anticipated that the decarboxylation should proceed *via* the conventional mechanism in which the transition metal is directly involved in cleaving the C-C bond *via* β-R-elimination (Scheme 6.3.6).⁴⁰



Scheme 6.3.6. Decarboxylation of intermediate **18** through the conventional mechanism in which transition structure **TSH** is expected to be formed.

Based on this proposal, the reaction is expected to pass through the key transition structure **TSH**. This possibility was evaluated and found to be highly energy consuming, confirming that decarboxylation should not occur through the classical mechanism (36.0 and 64.6 kcal mol⁻¹ starting from [Au-Cl₂(OH)(GA)] and [AuCl₃(GA)], respectively). This prompted us to consider an alternative mechanism by which the oxidation decarboxylation might occur with a lower activation barrier (Figure 6.3.6).

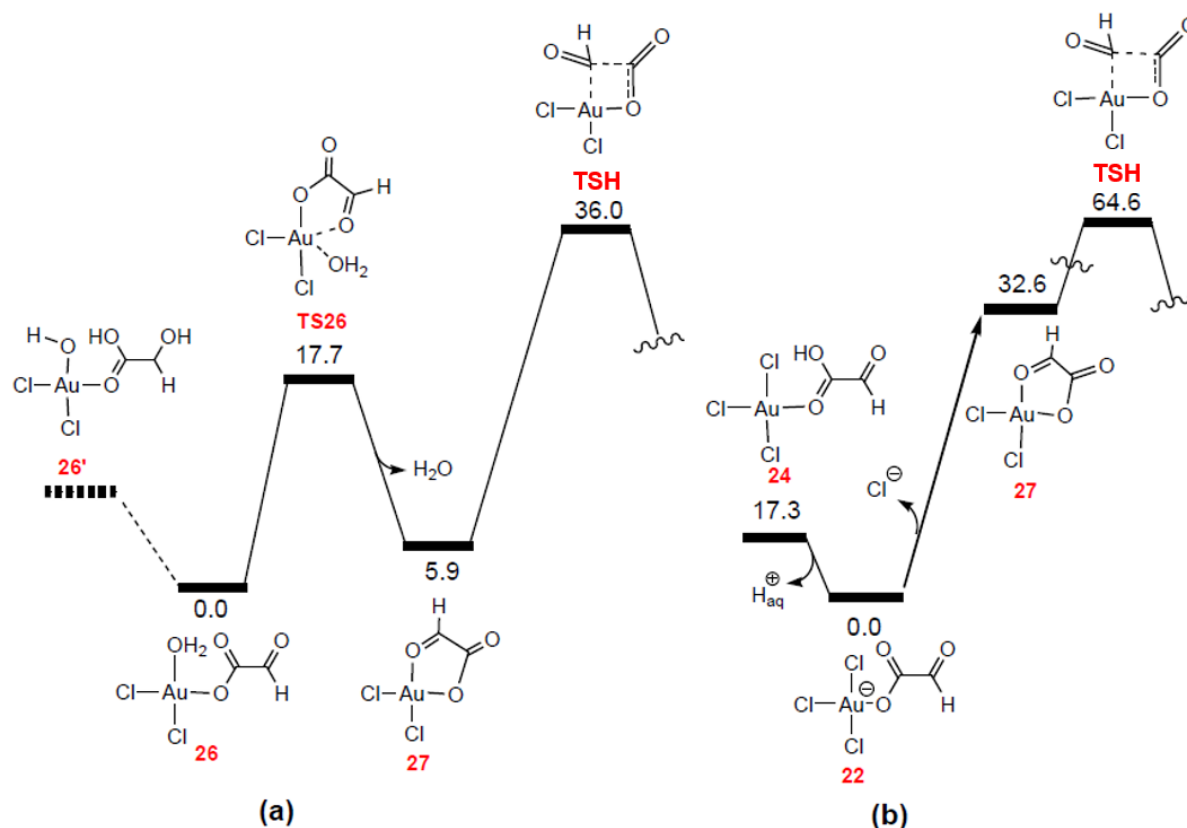


Figure 6.3.6. Gibbs free energy profiles associated with decarboxylation of glyoxylic acid *via* the conventional mechanism starting from a) *cis*-[AuCl₂(OH)(GA)] and b) [AuCl₃(GA)]. Structure **26'** is not a local minimum and collapses to **26**. Free energies are given in kcal/mol.

Following this, a novel mechanism for this fundamentally important reaction was proposed as shown in Figure 6.3.6a. As is well-documented, an aldehyde in aqueous solution will react with water to produce a geminal diol.⁴¹ Interestingly, the geminal diol was found to drive the oxidative decarboxylation process as detailed below.

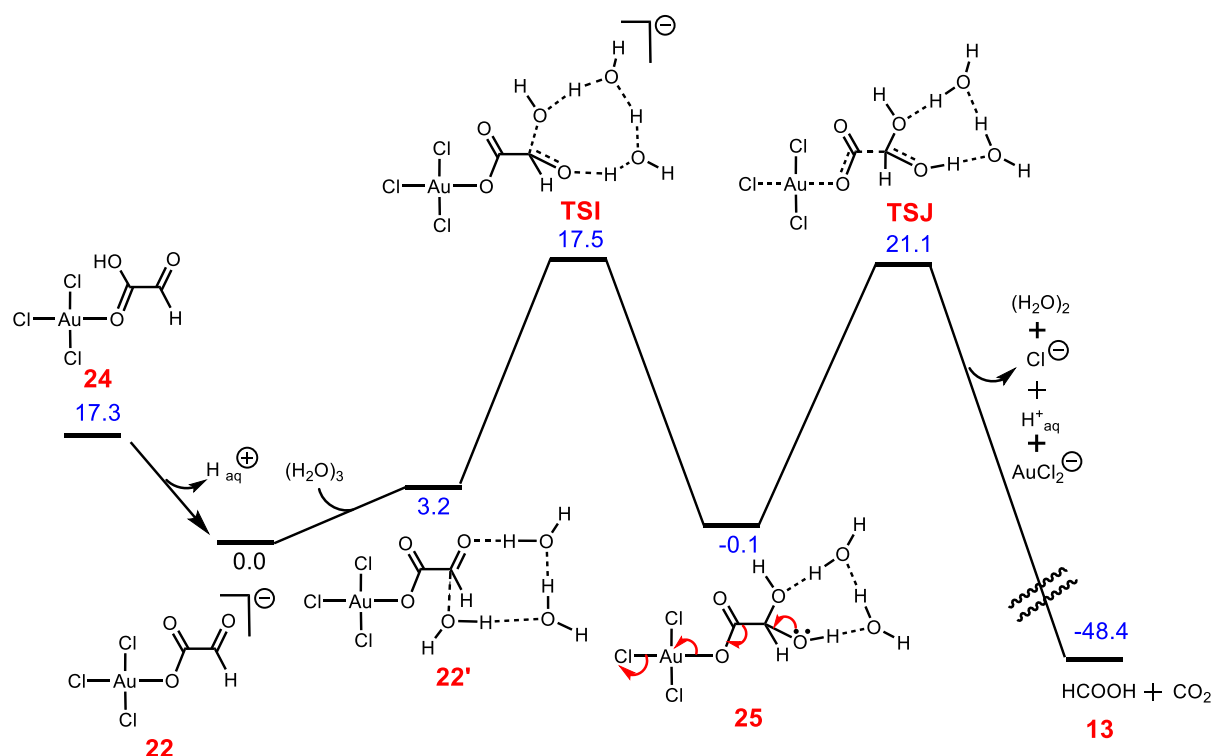


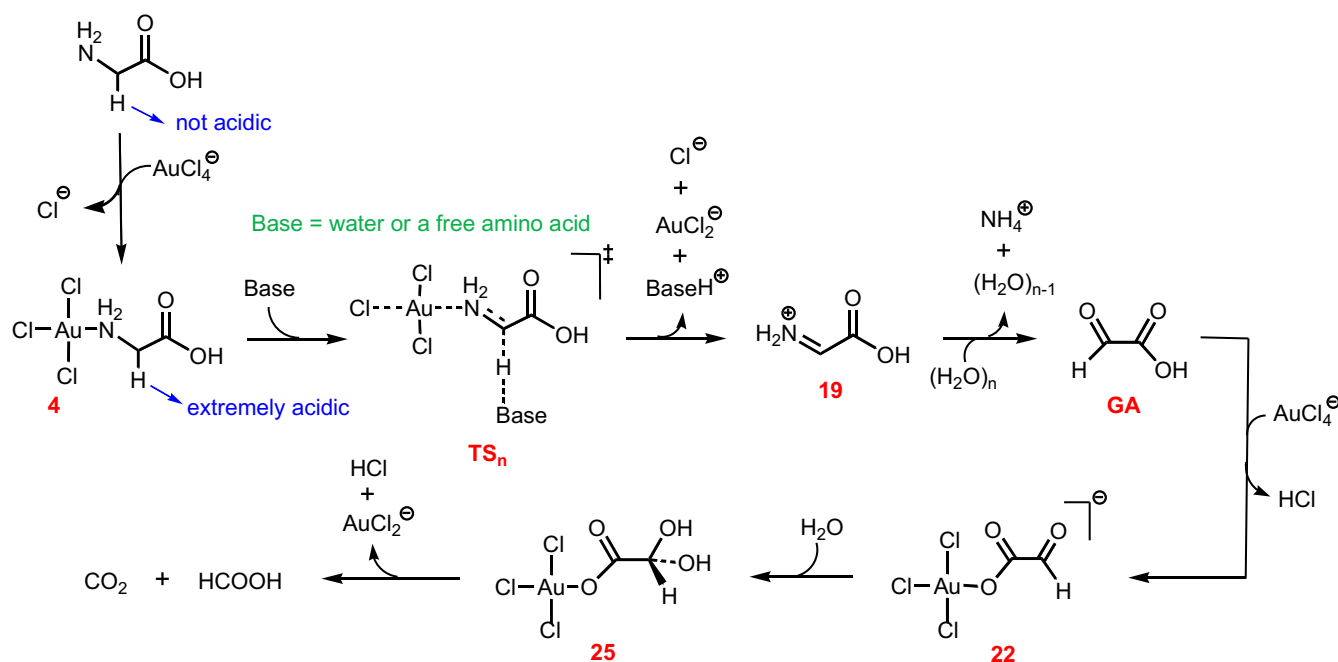
Figure 6.3.6a. Gibbs free energy profile for the oxidative decarboxylation of glyoxylic acid mediated by gold(III). Free energies are given in kcal mol⁻¹.

The profile shows the reaction starting from **24** where GA is coordinated to the metal *via* its carboxylic acid functional group. This interaction makes the carboxylic acid proton become intensely acidic, undergoing a facile dissociation to afford compound **22**. The geminal diol complex **25** is then formed *via* reaction of $(\text{H}_2\text{O})_3$ with **22**. As expected, structure **25** has a similar energy to compound **22'**, confirming that the geminal diol is in equilibrium with the aldehyde. Subsequently, the gold(III) reduction is boosted by the electron flow mechanism to yield CO₂ and HCOOH *via* transition structure **TSJ** lying 21.1 kcal mol⁻¹ above the reactant **22**.

That the intermediacy of the geminal diol complex **25** is a prerequisite for the decarboxylation to occur with a low activation energy finds some support from the experimental observations. Sadler et al. found that although GA in the presence of a gold(III) complex was reactive toward the CO₂ loss, formic acid was not.¹⁷

6.3.7 Summary of the novel proposed mechanism for reduction of Au(III)

This work presents for the first time an intriguing mechanism for gold(III) reduction by an amino acid, which may be applicable for oxidation of many amines where a centre of high cathodic reduction potential is used as the oxidant as depicted in Scheme 6.3.7. The high cathodic reduction potential of gold(III) in complex **4** renders the C $^{\alpha}$ -hydrogen acidic enough to be deprotonated by a mild base. This deprotonation facilitates the nitrogen lone-pair of the amino acid to transfer to the gold(III) metal centre, culminating in reduction of gold(III) and formation of protonated imine **19**. Subsequently, hydrolysis of the protonated imine gives glyoxylic acid. The latter in the presence of a second gold(III) complex undergoes an oxidative decarboxylation process *via* passing through geminal diol intermediates **25** to afford CO₂ and HCOOH.



Scheme 6.3.7. Our proposed mechanism for the gold(III)-mediated oxidation of glycine in acidic or neutral media.

6.4 Conclusion

In summary, in this chapter, a new mechanism for reduction of gold(III) by the amino acid glycine is presented. Based on this mechanism, the amino acid coordination to gold(III) strongly acidifies the C $^{\alpha}$ -hydrogen atom.³³ In such a case, the C $^{\alpha}$ position can be deprotonated

by a mild base like water or another amino acid, thereby enabling the amino acid to act as a strong reductant to give directly a protonated imine and a gold(I) complex. For the amino acid ligand to become a potent reductant, the prerequisite is the planarity of the H, C α , N and Au atoms. The chelated amino acid complexes which are not able to provide this necessity are therefore much less reactive toward redox. This accounts for the inertness of chelated complex 5 toward reduction and explains why gold(III) complexes with amine-based polydentate ligands are sufficiently stable to perform well as anticancer drugs.⁴² To our knowledge, the mechanism by which amines are directly oxidised to protonated imines has not been reported and should be considered as a new possibility in future studies. This mechanism is predicted to be feasible when an amine is coordinated to a centre of high cathodic reduction potential like gold(III).^{39,43} The reduction commencing from [AuCl₂(OH)(Gly)] does not need an external base, as it can occur *via* the OH ligand. The ensuing protonated imine in reaction with water can readily undergo hydrolysis to produce glyoxylic acid (GA). Finally, this acid is oxidatively decarboxylated and reduces another gold(III) complex to gold(I) *via* a geminal diol intermediate formed by reaction of water with the aldehyde functional group of the coordinated GA.

6.5 References

- (1) (a) A. Alama, B. Tasso, F. Novelli, F. Sparatore, *Organometallic compounds in oncology: implications of novel organotin as antitumor agents. Drug discovery today*, 14(9-10), 2009, pp.500-508. (b) A. L. Noffke, A. Habtemariam, A. M. Pizarro, P. J. Sadler, *Designing organometallic compounds for catalysis and therapy. Chemical Communications*, 48(43), 2012, pp.5219-5246. (c) M. Frezza, S. Hindo, D. Chen, A. Davenport, S. Schmitt, D. Tomco, Q. Ping Dou. *Novel metals and metal complexes as platforms for cancer therapy. Current pharmaceutical design*, 16(16), 2010, pp.1813-1825. (d) A. M. Pizarro, A. Habtemariam, P. J. Sadler. *Activation mechanisms for organometallic anticancer complexes. In Medicinal organometallic chemistry*, 2010, (pp. 21-56). Springer, Berlin, Heidelberg.
- (2) D. Wang, S. J. Lippard. *Cellular processing of platinum anticancer drugs. Nature reviews Drug discovery*, 4(4), 2005, pp.307.
- (3) S. J. Berners-Price, A. Filipovska, *Gold compounds as therapeutic agents for human diseases. Metallomics*, 3(9), 2011, pp.863-873.
- (4) H. Zhao, Y. Ning, *Gold Bull.* **2001**, 34, 24.
- (5) T. G. Benedek, J. Hist, *Med. All. Sci.* **2004**, 59, 50.
- (6) W. F. Kean, F. Forestier, Y. Kassam, W. W. Buchanan, P. J. Rooney, *Semin. Arthritis Rheum.* **1985**, 14, 180.
- (7) B. M. Sutton, E. McGusty, D. T. Walz, M. J. DiMartino, *J. Med. Chem.* **1972**, 15, 1095.
- (8) (a) L. Messori, G. Marcon, *Met. Ions Biol. Syst.* **2004**, 42, 385. (b) C. Gabbiani, A. Casini, L. Messori, *Gold Bull.* **2007**, 40, 73. (c) I. Ott, *Coord. Chem. Rev.* **2009**, 253, 1670.
- (9) S. Nobili, E. Mini, I. Landini, C. Gabbiani, A. Casini, L. Messori, *Med. Res. Rev.* **2010**, 30, 550.
- (10) V. Milacic, D. Chen, L. Ronconi, K. R. Landis-Piwowar, D. Fregona, Q. P. Dou, *Cancer Res.* **2006**, 66, 10478.
- (11) C.-M. Che, R. W.-Y. Sun, W.-Y. Yu, C.-B. Ko, N. Zhu, H. Sun, *Chem. Commun.* **2003**, 14, 1718.
- (12) R. W.-Y. Sun, C.-M. Che, *Coord. Chem. Rev.* **2009**, 253, 1682.
- (13) J. J. Yan, A. L.-F. Chowm, C.-H. Leung, R. W.-Y. Sun, D.-L. Ma, C.-M. Che, *Chem. Commun.* **2010**, 46, 3893.

- (14) (a) C. F. Shaw, *Chem. Rev.* **1999**, 99, 2589. (b) Z. Guo, P. J. Sadler, *Angew. Chem. Int. Ed.* **1999**, 38, 1512.
- (15) B. D. Glis̃ić, U. Rychlewska, M. I. Djuran, *Dalton Trans.* **2012**, 41, 6887.
- (16) G. Natile, E. Bordignon, L. Cattalini, *Inorg. Chem.* **1976**, 15, 246.
- (17) J. Zou, Z. Guo, J. A. Parkinson, P. J. Sadler, *Chem. Commun.* **1999**, 15, 1359.
- (18) A. Ariafard, E. S. Tabatabaie, S. Aghmasheh, S. Najaflo, B. F. Yates, *Inorg. Chem.* **2012**, 51, 8002.
- (19) Gaussian 09, Revision D.01, M. J. Frisch, G. W. Trucks, H. B. Schlegel, G. E. Scuseria, M. A. Robb, J. R. Cheeseman, G. Scalmani, V. Barone, B. Mennucci, G. A. Petersson, H. Nakatsuji, M. Caricato, X. Li, H. P. Hratchian, A. F. Izmaylov, J. Bloino, G. Zheng, J. L. Sonnenberg, M. Hada, M. Ehara, K. Toyota, R. Fukuda, J. Hasegawa, M. Ishida, T. Nakajima, Y. Honda, O. Kitao, H. Nakai, T. Vreven, J. A. Montgomery, J. E. Peralta, F. Ogliaro, M. Bearpark, J. J. Heyd, E. Brothers, K. N. Kudin, V. N. Staroverov, R. Kobayashi, J. Normand, K. Raghavachari, A. Rendell, J. C. Burant, S. S. Iyengar, J. Tomasi, M. Cossi, N. Rega, J. M. Millam, M. Klene, J. E. Knox, J. B. Cross, V. Bakken, C. Adamo, J. Jaramillo, R. Gomperts, R. E. Stratmann, O. Yazyev, A. J. Austin, R. Cammi, C. Pomelli, J. W. Ochterski, R. L. Martin, K. Morokuma, V. G. Zakrzewski, G. A. Voth, P. Salvador, J. J. Dannenberg, S. Dapprich, A. D. Daniels, A. Farkas, J. B. Foresman, J. V. Ortiz, J. Cioslowski, D. J. Fox, Gaussian, Inc., Wallingford CT, 2009.
- (20) (a) C. T. Lee, W. T. Yang, R. G. Parr, *Phys. Rev. B.* **1988**, 37, 785. (b) B. Miehlich, A. Savin, H. Stoll, H. Preuss, *Chem. Phys. Lett.* **1989**, 157, 200. (c) A. D. Becke, *J. Chem. Phys.* **1993**, 98, 5648.
- (21) (a) V. Barone, M. Cossi, *J. Phys. Chem. A.* **1998**, 102, 1995. (b) M. Cossi, N. Rega, G. Scalmani, V. Barone, *J. Comput. Chem.* **2003**, 24, 669.
- (22) (a) P. J. Hay, W. R. Wadt, *J. Chem. Phys.* **1985**, 82, 270. (b) W. R. Wadt, P. J. Hay, *J. Chem. Phys.* **1985**, 82, 284.
- (23) P. C. Hariharan, J. A. Pople, *Theor. Chim. Acta.* **1973**, 28, 213.
- (24) A. W. Ehlers, M. B̃chme, S. Dapprich, A. Gobbi, A. H̃llwarth, V. Jonas, K. F. K̃hler, R. Stegmann, A. Veldkamp, G. Frenking, *Chem. Phys. Lett.* **1993**, 208, 111.
- (25) (a) K. Fukui, *J. Phys. Chem.* **1970**, 74, 4161. (b) K. Fukui, *Acc. Chem. Res.* **1981**, 14, 363.

- (26) S. Grimme, J. Antony, S. Ehrlich, H. Krieg, *J. Chem. Phys.* **2010**, *132*, 154104.
- (27) A. V. Marenich, C. J. Cramer, D. G. Truhlar, *J. Phys. Chem. B* **2009**, *113*, 6378.
- (28) F. Weigend, F. Furche, R. Ahlrichs, *J. Chem. Phys.* **2003**, *119*, 12753.
- (29) E. D. Glendening, J. K. Badenhoop, A. E. Reed, J. E. Carpenter, J. A. Bohmann, C. M. Morales, C. R. Landis, F. Weinhold, Natural Bond Order 6.0, Theoretical Chemistry Institute, University of Wisconsin, Madison, WI (USA), 2013, <http://nbo6.chem.wisc.edu>.
- (30) M. D. Tissandier, K. A. Cowen, W. Y. Feng, E. Gundlach, M. H. Cohen, A. Earhart, J. V. Coe, T. R. Tuttle, *J. Phys. Chem. A* **1998**, *102*, 7787.
- (31) J. Ochterski, Thermochemistry, Gaussian, Gaussian, Inc., Wallingford, CT, 2000, pp. 1–19.
- (32) (a) V. S. Bryantsev, M. S. Diallo, W. A. Goddard, *J. Phys. Chem. B* **2008**, *112*, 9709. (b) J. A. Keith, E. A. Carter, *J. Chem. Theory Comput.* **2012**, *8*, 3187. (c) P. Bekker, Z. Van, W. Robb, *Inorg. Nucl. Chem. Lett.* **1972**, *8*, 849. (d) P. K. Sen, N. Gani, J. K. Midya, B. Pal, *Transition Met. Chem.* **2008**, *33*, 229.
- (33) A. Rios, T. L. Amyes, J. P. Richard, *J. Am. Chem. Soc.* **2000**, *122*, 9373.
- (34) For the concept of water clusters serving as efficient proton shuttles in gold catalysis see C. M. Krauter, A. S. K. Hashmi, M. Pernpointner, *ChemCatChem*. **2010**, *2*, 1226.
- (35) P. K. Sen, N. Gani, J. K. Midya, B. Pal, *Transition Met. Chem.* **2008**, *33*, 229.
- (36) (a) S. E. Diamond, G. M. Tom, H. Taube, *J. Am. Chem. Soc.* **1975**, *97*, 2661. (b) M. J. Ridd, F. R. Keene, *J. Am. Chem. Soc.* **1981**, *103*, 5733. (c) F. R. Keene, M. J. Ridd, M. R. Snow, *J. Am. Chem. Soc.* **1983**, *105*, 7075. (d) F. Richard Keene, *Coord. Chem. Rev.* **1999**, *187*, 121. (e) J. P. Saucedo-Vzquez, V. M. Ugalde-Salvador, A. R. Toscano, P. M. H. Kroneck, M. E. Sosa-Torres, *Inorg. Chem.* **2009**, *48*, 1214. (f) G. J. Christian, A. Arbuse, X. Fontrodona, M. A. Martinez, A. Llobet, F. Maseras, *Dalton Trans.* **2009**, 6013. (g) G. J. Christian, A. Llobet, F. Maseras, *Inorg. Chem.* **2010**, *49*, 5977. (h) J. P. Saucedo-Vzquez, P. M. H. Kroneck, M. E. Sosa-Torres, *Dalton Trans.* **2015**, *44*, 5510. (i) Z. Tang, C. Tejel, M. M. de S. Buchaca, M. Lutz, J. I. van der Vlugt, B. de Bruin, *Eur. J. Inorg. Chem.* **2016**, 963. (j) H. Yu; Y. Zhai, G. Dai, S. Ru, S. Han, Y. Wei, *Chem. Eur. J.* **2017**, *23*, 13883. (k) R.

- Ray, S. Chandra, V. Yadav, P. Mondal, D. Maiti, G. K. Lahiri, *Chem. Commun.* **2017**, 53, 4006. (l) S. Saranya, R. Ramesh, J. G. Malecki, *Eur. J. Org. Chem.* **2017**, 6726.
- (37) For amine oxidation by gold(III) complexes see: (a) Y. Zhang, H. Peng, M. Zhang, Y. Cheng, C. Zhu, *Chem. Commun.* **2011**, 47, 2354. (b) J. Xie, H. Li, J. Zhou, Y. Cheng, C. Zhu, *Angew. Chem. Int. Ed.* **2012**, 51, 1252. (c) W. Yang, L. Wei, F. Yi, M. Cai, *Tetrahedron* **2016**, 72, 4059. (d) M. Ni, Y. Zhang, T. Gong, B. Feng, *Adv. Synth. Catal.* **2017**, 359, 824.
- (38) For imine hydrolysis investigated computationally see: (a) C. Flinn, R. A. Poirier, W. A. Sokalski, *J. Phys. Chem. A* **2003**, 107, 11174. (b) H. Si, C. Zhang, X. Luo, R. Chen, G. Liang, *Theor. Chem. Acc.* **2016**, 135, 80.
- (39) K. Sreenath, Z. Yuan, M. Macias-Contreras, V. Ramachandran, R. J. Clark, L. Zhu, *Eur. J. Inorg. Chem.* **2016**, 3728.
- (40) (a) L. Xue, W. Su, Z. Lin, *Dalton Trans.* **2011**, 40, 11926. (b) R. A. J. O'Hair, N. J. Rijs, *Acc. Chem. Res.* **2015**, 48, 329.
- (41) P. Greenzaid, Z. Luz, D. Samuel, *J. Am. Chem. Soc.* **1967**, 89, 749.
- (42) (a) R. V. Parish, B. P. Howe, J. P. Wright, J. Mack, R. G. Pritchard, R. G. Buckley, A. M. Elsome, S. P. Fricker, *Inorg. Chem.* **1996**, 35, 1659. (b) R. G. Buckley, A. M. Elsome, S. P. Fricker, G. R. Henderson, B. R. C. Theobald, R. V. Parish, B. P. Howe, L. R. Kelland, *J. Med. Chem.* **1996**, 39, 5208.
- (43) K. C. Nicolaou, C. J. N. Mathison, T. Montagnon, *J. Am. Chem. Soc.* **2004**, 126, 5192.

Appendices

1. **A. Gouranourimi**; A. Chipman; R. Babaahmadi; A. Olding; B. F. Yates; A. Ariafield, *Nazarov Cyclisation Initiated by DDQ-Oxidized Pentadienyl Ether: A Mechanistic Investigation from the DFT Perspective*, *Org. Biomol. Chem.* **2018**, 16, 9021-9029. (**Hot Paper, Chapter 4**)
2. J. Jin; Y. Zhao; **A. Gouranourimi**; A. Ariafield; P. W. H. Chan, *Mechanistic Investigation of Chiral Brønsted Acid Catalyzed Enantioselective Dehydrative Nazarov-type Electrocyclization (DNE) of Aryl and 2-Thienyl Vinyl Alcohols*, *J. Am. Chem. Soc.* **2018**, 140, 5834-5841. (**Chapter 5**)
3. A. Chipman; **A. Gouranourimi**; K. Farshadfar; A. Olding; B. F. Yates; A. Ariafield, *A Computational Mechanistic Investigation into Reduction of Gold(III) Complexes by Amino Acid Glycine: A New Variant for Amine Oxidation*, *Chem. Eur. J.* **2018**, 24, 8361-8368. (**Hot Paper, Chapter 6**)

Appendix 3 has been removed for copyright or proprietary reasons.



Cite this: *Org. Biomol. Chem.*, 2018, **16**, 9021

Nazarov cyclisations initiated by DDQ-oxidised pentadienyl ether: a mechanistic investigation from the DFT perspective†

Ali Gouranourimi, Antony Chipman, Rasool Babaahmadi, , Angus Olding, Brian F. Yates* and Alireza Ariaferd *

The Nazarov cyclisation is an important and reliable reaction for the synthesis of cyclopentenones. Density functional theory (DFT) has been utilised to study the mechanism of Nazarov cyclisations initiated by oxidation of pentadienyl ethers by a benzoquinone derivative (DDQ), as recently reported by West *et al.* (*Angew. Chem., Int. Ed.*, 2017, **56**, 6335). We determined that the reaction is most likely initiated by a hydride transfer from the pentadienyl ether to an oxygen of DDQ through a concerted pathway and not a single electron transfer mechanism. This oxidation by hydride abstraction leads to the formation of a pentadienyl cation from which the 4π electrocyclisation occurs, giving an alkoxy-cyclopentenyl cation. The ensuing cation is subsequently deprotonated by the reduced DDQ to afford an enol ether product. Consistent with experimental results, the hydride transfer is calculated to be the rate determining step and it can be accelerated by using electron donating substituents on the pentadienyl ether substrate. Indeed, the electron donating substituents increase the HOMO energy of the ether, making it more reactive toward oxidation. It is predicted that an unsubstituted benzoquinone, due to having a higher lying LUMO, shows much less reactivity than DDQ. Interestingly, we found an excellent correlation between the hydride transfer activation energy and the gap between the ether HOMO and the benzoquinone LUMO. From this correlation, we propose a predictive formula for reactivity of different types of substrates in the corresponding reaction.

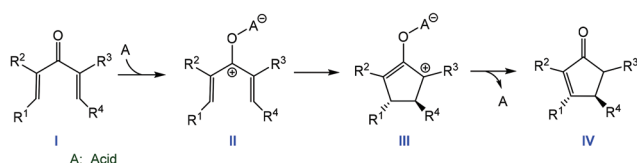
Received 19th October 2018,
Accepted 7th November 2018

DOI: 10.1039/c8ob02590h

rsc.li/obc

Introduction

Nazarov cyclisations are an extremely useful tool in the organic synthesis of cyclopentenones from dienones in the presence of Brønsted or Lewis acids (Scheme 1).¹ Indeed, the addition of an acid to acyclic divinyl ketone **I** generates crucial cationic intermediate **II** from which access to the process of 4π -electron conrotatory ring closure becomes feasible.² The reaction pro-



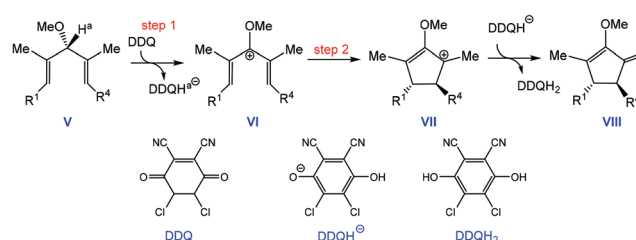
Scheme 1 Nazarov electrocycloaddition reaction passing through key carbocation **II** leading to a cyclopentenone.

School of Natural Sciences-Chemistry, University of Tasmania, Hobart, Tasmania 7001, Australia. E-mail: Brian.Yates@utas.edu.au, Alireza.Ariaferd@utas.edu.au

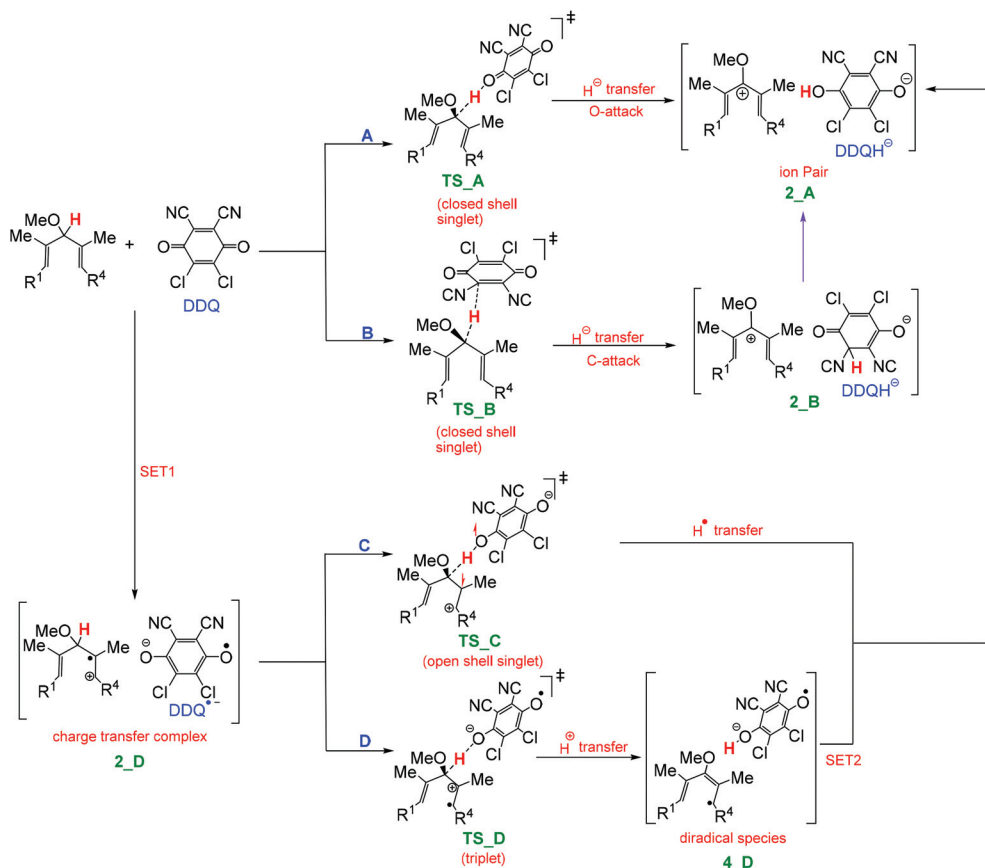
†Electronic supplementary information (ESI) available. See DOI: 10.1039/c8ob02590h

ceeds so reliably that it can be used to synthesise five-membered rings with multiple functional group substituents (yields of up to 90% can be achieved).³ It is notable that Nazarov cyclisation is also accessible by numerous promoters, *e.g.* UV radiation, and transition metal catalysis.³

The formation of pentadienyl carbocation **II** is a prerequisite for the electrocycloaddition to occur. Interestingly, West *et al.* recently introduced a new strategy for formation of the key carbocation intermediate, accessed through oxidation of bis(allylic) ether **V** by DDQ (2,3-dichloro-5,6-dicyano-1,4-benzoquinone, Scheme 2).⁴ The first step of the reaction is assumed



Scheme 2 DDQ-initiated Nazarov reaction starting from pentadienyl ether **V**, yielding cyclopentenyl ether **VIII** as the product.



Scheme 3 Four different mechanisms considered for DDQ-mediated formation of ion pair **2_A**.

to be formation of **VI** via oxidative abstraction of H^a by DDQ. Subsequent to the formation of the carbocation, the electrocyclisation takes place to give **VII**. Finally, $DDQH^-$ deprotonates carbocation **VII** to afford the dienol ether product **VIII**.

Four closely related mechanisms have been reported in the literature for DDQ-mediated C–H bond cleavage reactions.⁵ These mechanisms (pathways **A** to **D**) are distinct in how the hydrogen abstraction occurs, as detailed in Scheme 3. Pathways **A** and **B** feature direct hydride (H^-) transfer; pathway **C** features hydrogen radical (H^\bullet) transfer and pathway **D** features a proton (H^+) transfer. There are two pathways for H^- transfer; O-attack and C-attack. In the O-attack case, a one-step H^- transfer to a DDQ oxygen can directly generate ion pair complex **2_A** whereas, in the C-attack case, the hydride transfer to a carbon atom attached to a cyano group on DDQ forms ion pair **2_B**. This intermediate can then undergo a hydrogen transfer to give more stable isomer **2_A**.

The single electron transfer (SET) from bis(allylic) ether to DDQ creates charge transfer complex **2_D** from which two pathways (**C** or **D**) may be accessed. The rationale for this branching point stems from the fact that $DDQ^{\bullet-}$ has two active sites on its oxygen centres. The radical oxygen of DDQ can abstract H^\bullet via transition structure **TS_C** on an open shell singlet surface to give ion pair complex **2_A** (pathway **C**). This ion pair is also accessible if the anionic oxygen site of $DDQ^{\bullet-}$

abstracts a proton via transition structure **TS_D** on a triplet surface, followed by a second SET from biradical species **4_D** (pathway **D**).

West and co-workers proposed the SET mechanism via pathway **C** for generation of the key carbocation intermediate. The hypothesis for a SET mechanism may have originated from the observation of an instantaneous colour change from clear to deep purple, upon addition of DDQ to **V** (Scheme 2).⁴

It is worth noting that the mechanisms of this transformation and many analogous processes involving DDQ as an oxidant have been under debate in recent computational and experimental reports. In 2017, Todd *et al.* explored the mechanism of DDQ-mediated cross-dehydrogenative coupling (CDC) reactions and suggested that a SET mechanism is likely to occur.⁶ Similarly, Xu and co-workers reported an oxidative C–C bond formation by treatment of benzyl ethers with DDQ.⁷ For this process, an immediate colour change was observed. The authors attributed this colour change to formation of an ion pair analogues to **2_A** and not a charge transfer complex.

In a series of several studies, Jackman *et al.* demonstrated that the oxidation of hydrocarbons by DDQ normally takes place by formation of a crucial carbocation through a rate-determining direct hydride transfer,⁸ a statement supported by the studies of Yamabe *et al.* and Heesing *et al.*⁹ In contrast, Ruchardt and co-workers inferred the intermediacy of radicals

from spin trapping experiments in the quinone dehydrogenation of hydroaromatics and assigned a SET mechanism for the process.⁵ⁱ In a DFT study Chan and Radom determined that the trapping of radicals was not conclusive evidence of a radical pathway.¹⁰ They found that a radical mechanism operates if the reaction is conducted in the gas phase or in a non-polar solvent such as heptane. In 2012, Batista and co-workers explored the oxidative functionalisation of benzylic C–H bonds by DDQ and indicated that direct hydride abstraction is about 10 kcal mol^{−1} more favourable than a SET mechanism.¹¹ Mayr *et al.* explored computationally and experimentally the kinetics of hydride abstraction by DDQ from numerous boranes (B–H), stannanes (Sn–H) dienes and dihydropyridines (C–H).^{5d} They demonstrated that the C-attack pathway is observed for the B–H and Sn–H hydride donors, whereas the O-attack is the preferred pathway for C–H hydride donors. Recently, a detailed study by Liu and Floreancig *et al.* came to the conclusion that the C- and O-attack pathways are very competitive for C–H bond functionalisation of benzylic, allylic, and alkenyl ether substrates mediated by DDQ.¹²

Due to these conflicting reports regarding the mechanism of C–H bond functionalization by DDQ, we have attempted to clarify the Nazarov cyclisation initiated by the DDQ reduction (developed by West *et al.*, Scheme 2) using DFT calculations. For this class of reactions, we investigated all possible pathways and found that direct hydride transfer to a DDQ oxygen is most likely to operate. We also established correlations

between the ease of C–H bond oxidative cleavage and the nature of substituents on the bis(allylic) ether and benzoquinones. In agreement with experimental reports, our results showed that electron donating groups on the ether substrate accelerate the hydride transfer process.⁴ In contrast, the same substituents on benzoquinones are suggested to retard it. Remarkably, we were able to provide an equation by which one may predict H[−] transfer activation barriers based upon electronic parameters.

Results and discussion

We commenced our investigation by calculating all four possible pathways discussed in Scheme 3 using bis(allylic) ether **sub_1** as the model substrate (Fig. 1). Direct hydride transfer to an oxygen of DDQ from **sub_1** (pathway A) is computed to be the most favourable pathway with an activation barrier of 21.8 kcal mol^{−1}. Pathway B in which the hydride directly transfers to a CN-substituted carbon of DDQ is about 6.7 kcal mol^{−1} higher in energy than pathway A. The higher activation energy of pathway B with respect to pathway A may be attributed to the adjacency of two highly π -conjugated styrenyl moieties to the transferring hydride.¹³ The SET pathways are required to pass through charge transfer complex **2_D** lying 5.3 kcal mol^{−1} above transition structure **TS_A**. This result suggests that the SET mechanisms are unlikely to operate. Our calculations at

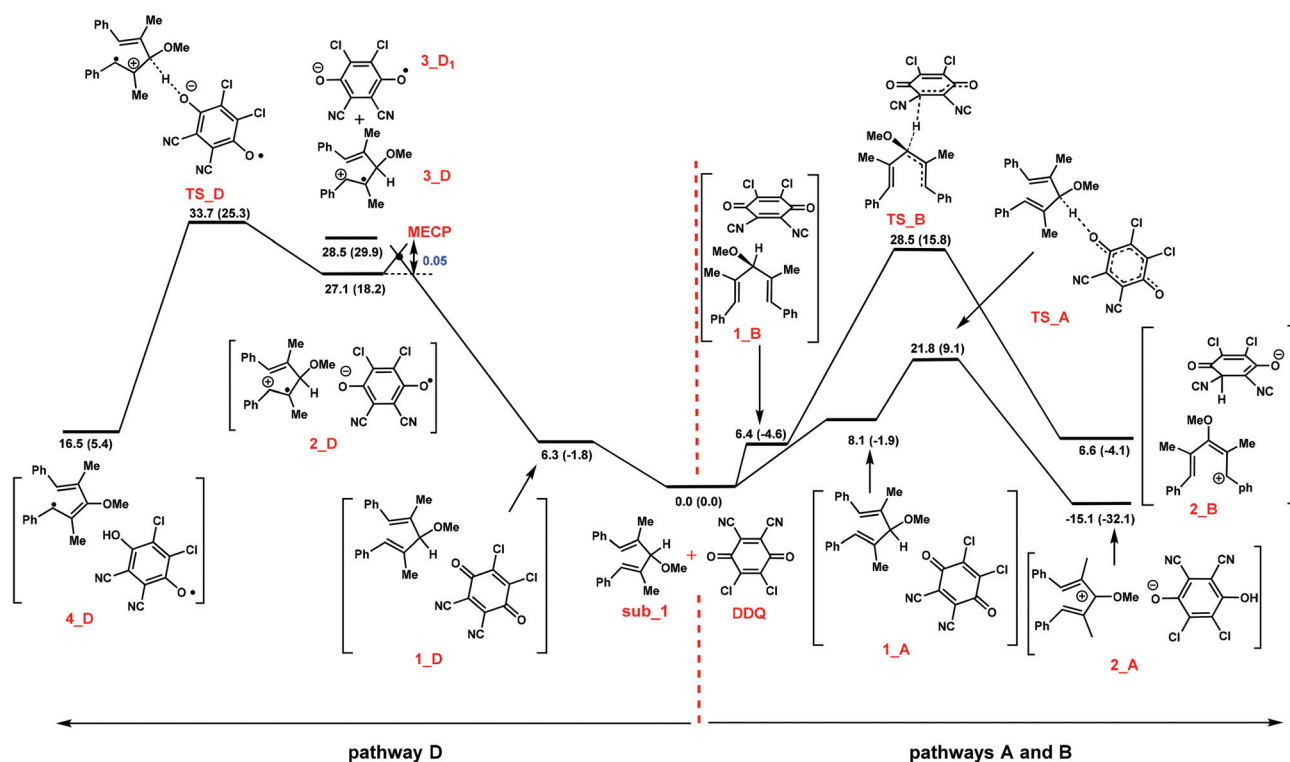


Fig. 1 Energy profile for the reaction between pentadienyl ether (**sub_1**) and DDQ through pathways A, B, and D. The relative Gibbs and potential energies (in parentheses) obtained from M06-2X/6-311+G(2d,p)//B3LYP/6-31G(d) calculations are given in kcal mol^{−1}.

different levels of theory (M06-2X-D3 and B3LYP-D3) validate this claim and confirm unfavourability of the SET mechanism (see Tables S1a and S1b in the ESI†). Despite the unlikelihood of the SET mechanism, we included pathway D in our investigation for the sake of completeness. The favourability of pathway A compared to pathway C is further supported by the fact that many attempts to locate a transition structure on an open shell singlet surface (TS_C) always collapsed to the closed-shell transition structure TS_A, demonstrating that the redox process *via* pathway C is not feasible. The key transition structure for pathway D was computed to be 33.7 kcal mol⁻¹ which further supports the SET mechanism being infeasible. To understand how easily structure 1_D on a singlet surface connects with 2_D on a triplet surface, the minimum energy crossing point (MECP) for this process was calculated. Notably, the energy of the MECP is calculated to be very close to the energy of 2_D, suggesting that conversion of 1_D to 2_D should occur without any significant reaction barrier. In short, although West *et al.* proposed a SET mechanism for the hydride transfer process,⁴ our calculations at different levels of theory support direct hydride transfer *via* pathway A.

At this juncture, we turned our attention to the Nazarov cyclisation step starting from the pentadienyl cation 5. We found that the 4 π -electrocyclisation occurs with an activation barrier of 8.7 kcal mol⁻¹ through transition structure TS₅₋₆ to give alkoxy cyclopentadienyl cation 6 (Fig. 2a). The structure 6 can be a branching point for two competitive routes (Fig. 2b). In one of them (route I), the anionic oxygen of 5 can react with carbocation 6 *via* TS₈₋₁₀ to give ether 10. In the other one (route II), the anionic oxygen site of DDQH⁻ can abstract a proton from 6 by passing through TS₇₋₉ to afford final product 9. The energy of TS₇₋₉ and TS₈₋₁₀ are computed to be comparable, implying that both products 9 and 10 should form simultaneously. However, we have to note that 10 is about 7.1 kcal mol⁻¹ less stable than 9 and reaction 8 \rightarrow 10 is reversible due to the fact that TS₈₋₁₀ lies only 16.2 kcal mol⁻¹ above 10. In such a case, 10 is expected to surmount an activation barrier of 16.5 kcal mol⁻¹ and transform into the more stable product 9. This result is in accord with the experimental observation that only product 9 was characterized.⁴

It is inferred from our calculations that the reaction **sub_1** + DDQ \rightarrow 9 + DDQH₂ proceeds through three major steps: (i) direct hydride transfer to DDQ *via* pathway A, (ii) 4 π -electrocyclisation and (iii) deprotonation. The activation barrier for these three steps is calculated to be 21.8, 8.7, and 16.5 kcal mol⁻¹, respectively. This demonstrates that the rate determining step for this process is most likely the first step, a result which is entirely consistent with the interpretation of West *et al.*⁴

Substitution effects of the diene substrate on the ease of the C–H bond cleavage

West *et al.* found that if the phenyls on the diene **sub_1** are substituted by electron donating groups, then the reaction accelerates.⁴ On that basis, they suggested that the H⁻ transfer from diene to DDQ should be the rate determining step. To

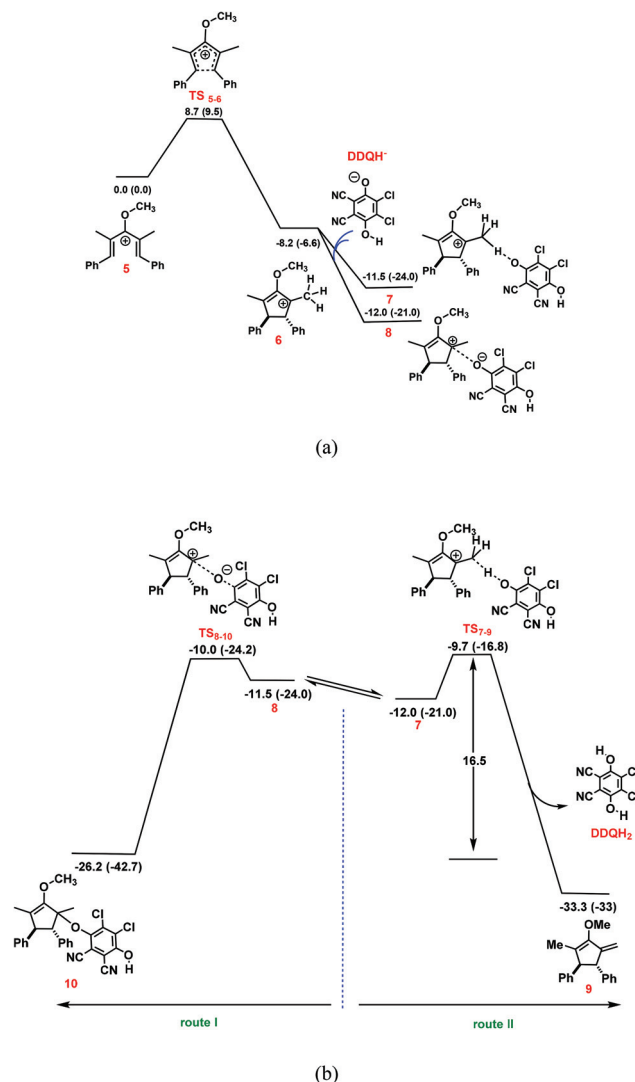


Fig. 2 Energy profiles for (a) the 4 π electrocyclisation step starting from 5 and (b) trapping of carbocation 6 via two different routes I and II. The relative Gibbs and potential energies (in parentheses) obtained from M06-2X/6-311+G(2d,p)//B3LYP/6-31G(d) calculations are given in kcal mol⁻¹.

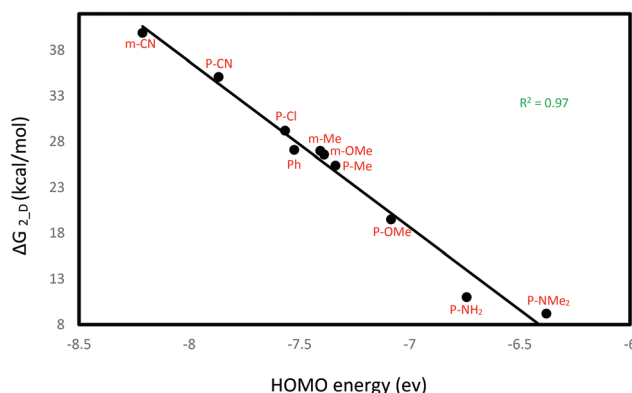
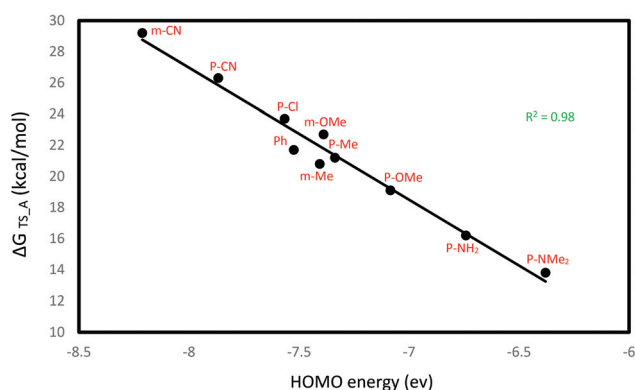
evaluate this claim, we calculated the energy of transition structures TS_A, TS_B, TS_D, charge transfer complex 2_D and intermediate 2_A for different substituents (Table 1). As established for **sub_1** with R = H (Fig. 1), we were unable to locate transition structure TS_C for any of these assays and all attempts to do so collapsed to TS_A. Several points are inferred from Table 1. First, for all **sub_1**, pathway A was found to be most favourable, implying that regardless of the diene nature, DDQ always abstracts H⁻ from the diene in a concerted fashion. Second, in line with the findings of West *et al.*, aryl rings with electron donating substituents such as Me, OMe and NH₂ have a lower activation energy than those with electron withdrawing substituents such as CN and Cl. Third, charge transfer complex 2_D is stabilised when the aryl ring is substituted by electron donating groups. Fourth, formation of

Table 1 Relative Gibbs free energy (kcal mol⁻¹) of transition structures TS_A, TS_B, and TS_D and intermediates 2_D and 2_A calculated for cases where the pentadienyl ether is substituted by a variety of R groups

Entry	R-Ph	ΔG (kcal mol ⁻¹)					HOMO (eV)
		(TS_A)	(TS_B)	(TS_D)	(2_D)	(2_A)	
1	<i>para</i> -CN-Ph	26.3	31.7	37.0	35.1	-14.2	-7.86
2	<i>para</i> -Cl-Ph	23.7	29.5	34.5	29.2	-15.1	-7.56
3	Ph	21.7	28.5	33.7	27.1	-15.2	-7.52
4	<i>para</i> -Me-Ph	21.2	27.7	31.8	25.4	-15.3	-7.33
5	<i>para</i> -OMe-Ph	19.1	26.1	30.3	19.5	-15.6	-7.08
6	<i>para</i> -NH ₂ -Ph	16.2	24.3	27.8	11.0	-16.1	-6.74
7	<i>para</i> -NMe ₂ -Ph	13.8	22.7	24.5	9.2	-17.4	-6.37
8	<i>meta</i> -CN-Ph	29.2	35.7	40.0	39.9	-13.5	-8.21
9	<i>meta</i> -OMe-Ph	22.7	29.4	34.0	26.6	-14.7	-7.38
10	<i>meta</i> -Me-Ph	20.8	27.3	32.8	27.0	-15.8	-7.40

2_D is always an endergonic process which implies that detection of such an intermediate should be unlikely. Fifth, in contrast to the energy of TS_A and 2_D which showed a strong dependence on the electronic nature of the ether substituents, the stability of 2_A is less sensitive to such substituents; the energy of 2_A only spans a narrow range from -13.5 to -17.4 kcal mol⁻¹.

Interestingly, we found that the HOMO of **sub_1** plays an important role in controlling the activation energy of pathway A. Electron donating groups raise the energy of the HOMO, facilitating the H⁻ transfer process. An excellent correlation between the energy of TS_A and the **sub_1** HOMO ($R^2 = 0.97$) lends support to the claim (Fig. 3). The HOMO energy also effects the energy of charge transfer complex 2_D. The higher the destabilised HOMO, the lower the energy of 2_D; an excellent correlation was obtained between these two parameters (Fig. 4). At this point, we have to note that the energy of 2_D spans a wider range (from 9.2 to 39.9 kcal mol⁻¹) compared to that of TS_A which spans a narrower range (from 16.2 to

**Fig. 4** A plot of correlation between ΔG_{2_D} and HOMO energy of different **sub_1** derivatives.**Fig. 3** A plot of correlation between ΔG_{TS_A} and HOMO energy of different **sub_1** derivatives.

29.2 kcal mol⁻¹). This implies that the energy of the charge transfer complex 2_D is more sensitive to the HOMO than that of TS_A.

Substitution effect of benzoquinone on the hydride transfer mechanism

As aforementioned, the HOMO of **sub_1** was shown to modulate the ease of reaction between DDQ and **sub_1**. A question arises here about whether the LUMO of a benzoquinone (BQ) can have a similar effect. In this case, we expect that a benzoquinone with a more stabilised LUMO is a better hydride acceptor. To demonstrate this claim, we investigated different benzoquinones with a variety of substituents as depicted in Table 2. Clear inferences to be drawn from our findings are listed as follows. First, regardless of the BQ nature, pathway A is favoured over the others. Second, the energy of 2_D and TS_A is affected by the LUMO energy of the BQ; the more stabilised the LUMO, the lower

Table 2 Relative Gibbs free energy (kcal mol⁻¹) of transition structures TS_A, TS_B, and TS_D and intermediates 2_D and 2_A calculated for different benzoquinones with a variety of X and X' groups

Entry	X	X'	ΔG (kcal mol ⁻¹)					LUMO (eV)
			(TS_A)	(TS_B)	(TS_D)	(2_D)	(2_A)	
1	H	H	35.0	42.4	54.1	55.4	-6.5	-2.80
2	Cl	Cl	28.1	41.0	43.1	40.0	-5.2	-3.42
3	CN	H	26.0	31.1	35.7	34.7	-12.6	-3.86
4	CN	Cl	21.7	28.5	33.7	27.1	-15.2	-4.12
5	CN	CN	17.3	25.8	26.6	18.2	-22.1	-4.62

the energy for both stationary points 2_D and TS_A. Third, a lower activation barrier invariably results in a more exergonic hydride transfer (Table 2).

The excellent correlations between the BQ LUMO energy and the TS_A energy ($R^2 = 0.98$) as well as those between the BQ LUMO energy and the 2_D energy ($R^2 = 0.97$) corroborates

some of the points mentioned above (Fig. 5 and 6). From Table 2 it is apparent that only BQ oxidants having electron withdrawing groups adequately facilitate the hydride transfer process. As such, the corresponding Nazarov reaction is predicted not to proceed under mild conditions if an unsubstituted BQ (*i.e.* quinone) is used as the oxidant.

A predictive formula for the reactivity of C-H bond cleavage mediated by DDQ

Recently Liu and Floreancig *et al.* proposed a predictive model designed in terms of the stability of the key carbocation intermediate and the extent of electron transfer in the transition structure for hydride transfer between DDQ and the ether substrate.¹² In this study, we define a new formula that can be expressed based only upon the energy of the reductant HOMO and the oxidant LUMO. We found that the reactivity of these substrates toward hydride transfer is determined by the gap between the reductant HOMO and the oxidant LUMO; the smaller the gap, the faster the reaction. The plot given in Fig. 7 lends support to the above claim as there is an excellent correlation ($R^2 = 0.98$) between the HOMO-LUMO gap and the TS_A Gibbs energy. Our predictive formula for oxidative C-H bond

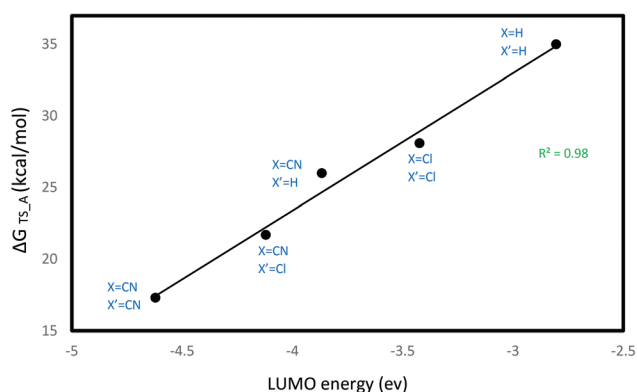


Fig. 5 A plot of correlation between ΔG_{TS_A} and LUMO energy of different BQ derivatives.

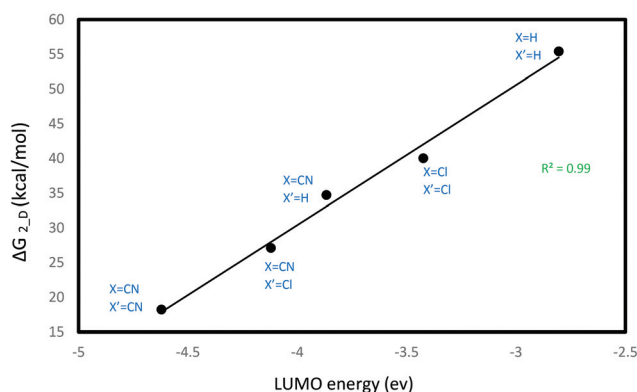


Fig. 6 A plot of correlation between ΔG_{2_D} and LUMO energy of different BQ derivatives.

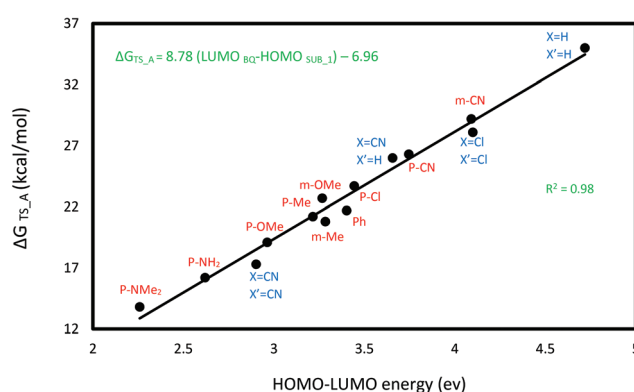


Fig. 7 A plot of correlation between ΔG_{TS_A} and the gap energy between the sub_1 HOMO and the BQ LUMO.

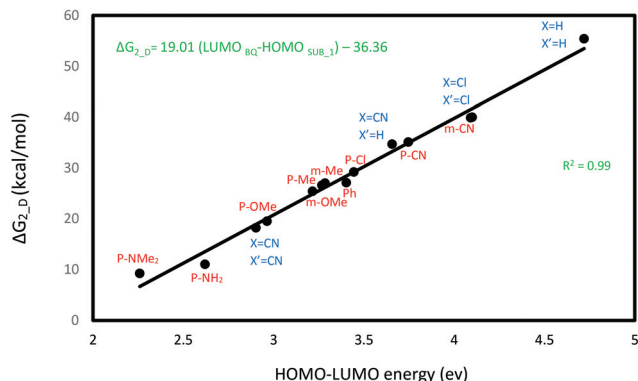


Fig. 8 A plot of correlation between ΔG_{2_D} and the gap energy between the sub_1 HOMO and the BQ LUMO.

functionalisation is also presented in Fig. 7. In terms of this formulation, one can estimate the activation energy required for the hydride transfer process, regardless of the identity of the redox partners.

Table 3 Summary of activation energies for different *ortho* substituted aryl rings of the pentadienyl ether substrate; the calculated and predicted Gibbs free energies are given in kcal mol⁻¹

sub_1

Entry	R-Ph	ΔG (TS_A)	2A	HOMO (eV)	Predicted
1	<i>ortho</i> -CN-Ph	37.0	-14.3	-8.49	31.4
2	<i>ortho</i> -Cl-Ph	38.2	-14.7	-8.18	28.7
3	<i>ortho</i> -Me-Ph	34.3	-13.1	-7.75	25.0
4	<i>ortho</i> -NH ₂ -Ph	29.0	-15.3	-6.90	17.5

This HOMO-LUMO gap also enables us to predict the stability of charge transfer complex **2_D**. As the HOMO-LUMO gap decreases, the stability of **2_D** increases. The predictive formula for the stability of this charge transfer complex is presented in Fig. 8.

A comparison between the formulas given in Fig. 7 and 8 indicates that the slope of the latter (19.01) is almost twice as large as that of the former (8.78), implying that ΔG_{2_D} is more sensitive to the HOMO-LUMO gap than ΔG_{TS_A} . This statement gains strong support from the fact that the ΔG_{2_D} spans a wider range (9.2–55.4 kcal mol⁻¹) while ΔG_{TS_A} spans a narrower range (13.8–35.0 kcal mol⁻¹).

Application of predictive formula for substrates with *ortho*-substituted aryl rings

The predictive formula given in Fig. 7 was obtained for the pentadienyl ether substrates with aryl rings substituted at the *meta* and *para* positions. Surprisingly, we found that this formula does not effectively predict the hydride transfer activation energy for the substrates bearing *ortho* substituents on their aryl rings. For the *ortho* substituted substrates, the calculated activation barriers are higher than those predicted using our formula (Table 3). *Ortho* substituents create steric congestion which significantly distorts transition structure **TS_A** in a way that the C¹-C² π bond completely projects out of the plane defined by C², C³ and C⁴. This reduces the stability afforded by π -conjugation in the system, elevating the energy **TS_A** and thereby making hydride abstraction from a substrate with *ortho* substituents an extremely strenuous process. This statement gains support from the large dihedral angle found for C⁴-C³-C²-C¹ in **TS_A** with CN substituted in the *ortho* positions (Fig. 9). In contrast, the relevant dihedral angle is considerably smaller in **TS_A** when the Aryl rings of the ether are substituted at *para* position (Fig. 9).

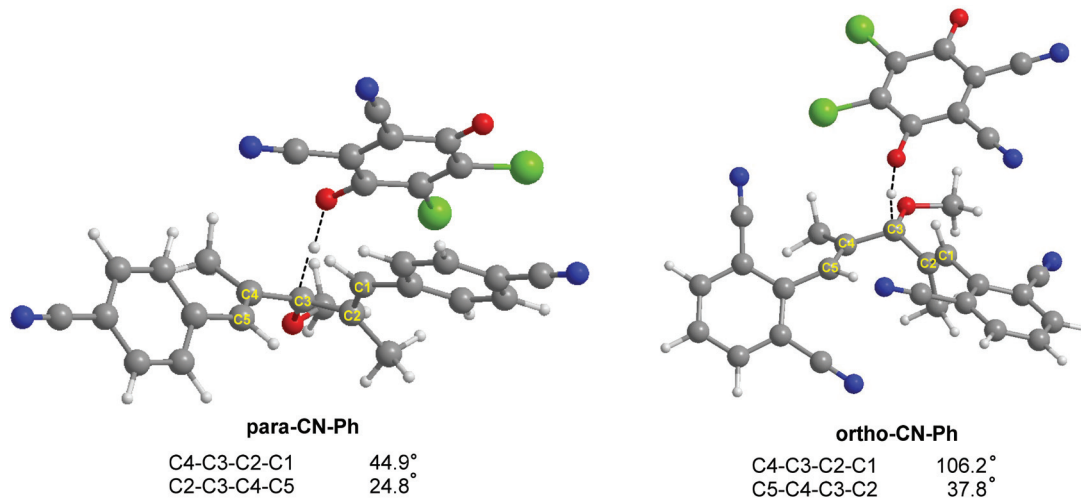


Fig. 9 Optimized structures of TS_A for *para*-CN-Ph and *ortho*-CN-Ph.

Conclusion

In this study, we explored the possible mechanisms for DDQ-initiated Nazarov cyclisations of 1,4-pentadienyl ethers. Our findings provide a better understanding of this chemical reaction. We have been able to draw several important conclusions from this study:

(1) This reaction is composed of three primary steps: (i) hydride transfer to DDQ giving a pentadienyl cation and DDQH[−], (ii) 4 π -electrocyclisation yielding a 2-alkoxycyclopentadienyl cation, and (iii) deprotonation of the ensuing cation by DDQH[−] affording the final product. Consistent with the experimental results, our calculations have shown that the first step is rate determining.

(2) The first step of this reaction was computed to occur through direct hydrogen transfer from the pentadienyl ether substrate to an oxygen of DDQ, and not through a SET mechanism.

(3) Interestingly, the HOMO energy of the pentadienyl ether and the LUMO energy of the benzoquinone were found to control the ease of the hydride abstraction step and determine the stability of the charge transfer complex.

(4) The substrates bearing aryl rings with electron donating substituents undergo faster hydride transfer to DDQ due to having a higher lying HOMO.

(5) Benzoquinones with electron withdrawing substituents act as good hydride abstractors owing to having a lower lying LUMO.

(6) The reactivity of substrates for losing a hydride in the presence of a benzoquinone shows a strong correlation with the energy gap between the substrate HOMO and the benzoquinone LUMO with a formulation of $\Delta G_{TS_A} = 8.78 (\text{LUMO}_{BQ} - \text{HOMO}_{SUB_1}) - 6.96 \text{ kcal mol}^{-1}$.

(7) The aforementioned formula is not applicable for the case when the aryl rings of the substrate are substituted at the *ortho* position. Indeed, the calculated activation barrier for hydride transfer in those cases is higher than the ones estimated using the formula. This inconsistency can be attributed to the steric congestion inherent to an *ortho* substituent.

Computational study

Gaussian 16¹⁴ was used to fully optimize all the structures involved in this study at the B3LYP level of density functional theory (DFT)¹⁵ in CH₂Cl₂ using the CPCM solvation model.¹⁶ The 6-31G(d) basis set was used for all atoms.¹⁷ Frequency analyses were performed at the same level of theory to ensure that a minimum or transition state was achieved. To further refine the energies obtained from the B3LYP/6-31G(d) calculations, we carried out single-point energy calculations for all of the structures with 6-311+G(2d,p) basis set in CH₂Cl₂ using the SMD solvation model at the M06-2X level. We have used the Gibbs free energies obtained from the M062X/6-311+G(2d,p)//B3LYP/6-31G(d) calculations in CH₂Cl₂ throughout the paper. Minimum energy crossing point (MECP) between closed shell singlet and triplet states were located using the code of Harvey *et al.*¹⁸

Conflicts of interest

There are no conflicts to declare.

Acknowledgements

We thank the Australian Research Council for financial support (project number DP180100904) and the Australian National Computational Infrastructure and the University of Tasmania for computing resources.

References

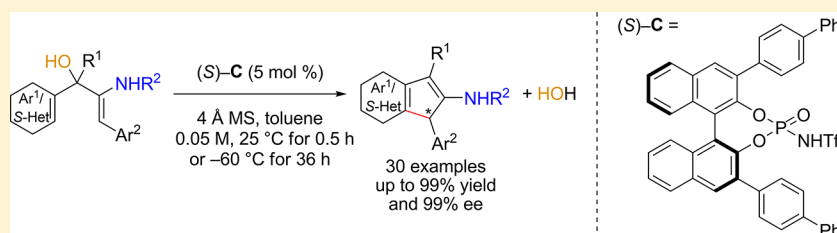
- (a) A. J. Frontier and C. Collison, *Tetrahedron*, 2005, **61**, 7577; (b) K. L. Habermas, S. E. Denmark and T. K. Jones, *Org. React.*, 1994, **45**, 1; (c) H. Pellissier, *Tetrahedron*, 2005, **61**, 6517; (d) M. A. Tius, *Eur. J. Org. Chem.*, 2005, 2206.
- For some selective studies aimed at elucidating the Nazarov mechanism see: (a) D. A. Smith and C. W. Ulmer II, *Tetrahedron Lett.*, 1991, **32**, 725; (b) D. A. Smith and C. W. Ulmer II, *J. Org. Chem.*, 1991, **56**, 4444; (c) A. Cavalli, M. Masetti, M. Recanatini, C. Prandi, A. Guarna and E. G. Occhiato, *Chem. – Eur. J.*, 2006, **12**, 2836; (d) T. Vaidya, R. Eisenberg and A. J. Frontier, *ChemCatChem*, 2011, **3**, 1531.
- (a) S. Cai, Z. Xiao, Y. Shi and S. Gao, *Chem. – Eur. J.*, 2014, **20**, 8681; (b) J. Huang, D. Leboeuf and A. J. Frontier, *J. Am. Chem. Soc.*, 2011, **133**, 6317; (c) D. Leboeuf, J. Huang, V. Gandon and A. J. Frontier, *Angew. Chem., Int. Ed.*, 2011, **50**, 10981; (d) G. Liang, S. N. Gradl and D. Trauner, *Org. Lett.*, 2003, **5**, 4931; (e) S. Pusch, D. Schollmeyer and T. Opatz, *Org. Lett.*, 2016, **18**, 3043; (f) X. Shi, D. J. Gorin and F. D. Toste, *J. Am. Chem. Soc.*, 2005, **127**, 5802; (g) V. Z. Shirinian, A. G. Lvov, A. M. Yanina, V. V. Kachala and M. Krayushkin, *Chem. Heterocycl. Compd.*, 2015, **51**, 234; (h) L. Zhang and S. Wang, *J. Am. Chem. Soc.*, 2006, **128**, 1442.
- R. J. Fradette, M. Kang and F. G. West, *Angew. Chem., Int. Ed.*, 2017, **56**, 6335.
- (a) E. A. Braude, L. M. Jackman and R. P. Linstead, *J. Chem. Soc.*, 1954, 3548; (b) E. A. Braude, L. M. Jackman and R. P. Linstead, *J. Chem. Soc.*, 1954, 3564; (c) H. Roth, N. Romero and D. Nicewicz, *Synlett*, 2016, **27**, 714; (d) X. Guo, H. Zipse and H. Mayr, *J. Am. Chem. Soc.*, 2014, **136**, 13863; (e) C. Hofler and C. Ruchardt, *Liebigs Ann.*, 1996, **2**, 183; (f) R. M. Scribner, *J. Org. Chem.*, 1966, **31**, 3671; (g) H. H. Jung and P. E. Floreancig, *Tetrahedron*, 2009, **65**, 10830; (h) D. A. Pratt, J. S. Wright and K. U. Ingold, *J. Am. Chem. Soc.*, 1999, **121**, 4877; (i) C. Ruchardt, M. Gerst and J. Ebenhoch, *Angew. Chem., Int. Ed. Engl.*, 1997, **36**, 1406; (j) F. Wurche, W. Sicking, R. Sustmann, F. G. Klärner and C. Ruchardt, *Chem. – Eur. J.*, 2004, **10**, 2707; (k) X. Li, Y. Wang, Y. Wang, M. Tang, L. Qu, Z. Li and D. Wei, *J. Org. Chem.*, 2018, **83**, 8543.

- 6 A. S. K. Tsang, A. S. K. Hashmi, P. Comba, M. Kerscher, B. Chan and M. H. Todd, *Chem. – Eur. J.*, 2017, **23**, 9313.
- 7 B. P. Ying, B. G. Trogden, D. T. Kohlman, S. X. Liang and Y. C. Xu, *Org. Lett.*, 2004, **6**, 1523.
- 8 (a) E. A. Braude, R. P. Linstead and K. R. Wooldridge, *J. Chem. Soc.*, 1956, 3070; (b) J. R. Barnard and L. M. Jackman, *J. Chem. Soc.*, 1960, 3110; (c) E. A. Braude, L. M. Jackman, R. P. Linstead and J. S. Shannon, *J. Chem. Soc.*, 1960, 3116; (d) E. A. Braude, L. M. Jackman, R. P. Linstead and G. Lowe, *J. Chem. Soc.*, 1960, 3123; (e) E. A. Braude, L. M. Jackman, R. P. Linstead and G. Lowe, *J. Chem. Soc.*, 1960, 3133.
- 9 (a) M. Brock, H. Hintze and A. Heesing, *Chem. Ber.*, 1986, **119**, 3727; (b) R. Paukstat, M. Brock and A. Heesing, *Chem. Ber.*, 1985, **118**, 2579; (c) S. Yamabe, S. Yamazaki and S. Sakaki, *Int. J. Quantum Chem.*, 2015, **115**, 1533.
- 10 B. Chan and L. Radom, *J. Phys. Chem. A*, 2007, **111**, 6456.
- 11 V. S. Batista, R. H. Crabtree, S. J. Konezny, O. R. Luca and J. M. Praetorius, *New J. Chem.*, 2012, **36**, 1141.
- 12 C. A. Morales-Rivera, P. E. Floreancig and P. Liu, *J. Am. Chem. Soc.*, 2017, **139**, 17935.
- 13 When the aryl ring of the ether substrate is replaced by a Me group, pathway B becomes favoured over pathway A by 1.5 kcal mol^{−1} which supports our assertion that the high level of π -conjugation in the styrenyl affects the favourability of pathway A (for details see Scheme ESI1†).
- 14 M. J. Frisch, G. W. Trucks, H. B. Schlegel, G. E. Scuseria, M. A. Robb, J. R. Cheeseman, G. Scalmani, V. Barone, G. A. Petersson, H. Nakatsuji, X. Li, M. Caricato, A. V. Marenich, J. Bloino, B. G. Janesko, R. Gomperts, B. Mennucci, H. P. Hratchian, J. V. Ortiz, A. F. Izmaylov, J. L. Sonnenberg, D. Williams-Young, F. Ding, F. Lipparini, F. Egidi, J. Goings, B. Peng, A. Petrone, T. Henderson, D. Ranasinghe, V. G. Zakrzewski, J. Gao, N. Rega, G. Zheng, W. Liang, M. Hada, M. Ehara, K. Toyota, R. Fukuda, J. Hasegawa, M. Ishida, T. Nakajima, Y. Honda, O. Kitao, H. Nakai, T. Vreven, K. Throssell, J. A. Montgomery, J. E. Peralta, F. Ogliaro, M. J. Bearpark, J. J. Heyd, E. N. Brothers, K. N. Kudin, V. N. Staroverov, T. A. Keith, R. Kobayashi, J. Normand, K. Raghavachari, A. P. Rendell, J. C. Burant, S. S. Iyengar, J. Tomasi, M. Cossi, J. M. Millam, M. Klene, C. Adamo, R. Cammi, J. W. Ochterski, R. L. Martin, K. Morokuma, O. Farkas, J. B. Foresman and D. J. Fox, *Gaussian 16, Revision A.03*, Gaussian, Inc., Wallingford CT, 2016.
- 15 C. Lee, W. Yang and R. G. Parr, *Phys. Rev. B: Condens. Matter Mater. Phys.*, 1988, **37**, 785.
- 16 V. Barone and M. Cossi, *J. Phys. Chem. A*, 1998, **102**, 1995.
- 17 P. C. Hariharan and J. A. Pople, *Theor. Chim. Acta*, 1973, **28**, 213.
- 18 J. N. Harvey, M. Aschi, H. Schwarz and W. Koch, *Theor. Chem. Acc.*, 1998, **99**, 95.

Chiral Brønsted Acid Catalyzed Enantioselective Dehydrative Nazarov-Type Electrocyclization of Aryl and 2-Thienyl Vinyl Alcohols

Jianwen Jin,[†] Yichao Zhao,[†] Ali Gouranourimi,[§] Alireza Ariafard,^{*,§} and Philip Wai Hong Chan^{*,†,‡,§}[†]School of Chemistry, Monash University, Clayton, Victoria 3800, Australia[‡]Department of Chemistry, University of Warwick, Coventry, CV4 7AL, United Kingdom[§]School of Physical Sciences–Chemistry, University of Tasmania, Hobart, Tasmania 7001, Australia

Supporting Information



ABSTRACT: An efficient chiral Brønsted acid-catalyzed enantioselective dehydrative Nazarov-type electrocyclic cyclization (DNE) of electron-rich aryl- and 2-thienyl- β -amino-2-en-1-ols is described. The 4π conrotatory electrocyclic cyclization reaction affords access to a wide variety of the corresponding 1*H*-indenes and 4*H*-cyclopenta[*b*]thiophenes in excellent yields of up to 99% and enantiomeric excess (ee) values of up to 99%. Experimental and computational studies based on a proposed intimate contact ion-pair species that is further assisted by hydrogen bonding between the amino group of the substrate cation and chiral catalyst anion provide insight into the observed product enantioselectivities.

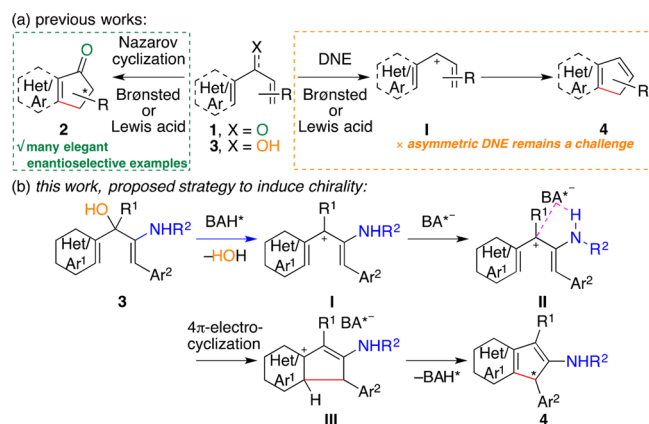
INTRODUCTION

The Nazarov cyclization of divinyl and (hetero)aryl vinyl ketones mediated by a Brønsted or Lewis acid is among one of the most powerful and efficient methods for the synthesis of cyclopentenone derivatives (Scheme 1).^{1–6} A reflection of this is its frequent use in synthetic strategies to natural and synthetic compounds of current biological and materials interest containing the structural motif or as a building block.^{2,3} This functional group transformation has also inspired the development of new 4π electrocyclic cyclization processes that has included

the DNE of electron-rich divinyl and (hetero)aryl vinyl alcohols to cyclopenta-1,3-dienes (Scheme 1a).^{4–6} Unlike the Nazarov cyclization, an asymmetric variant of the DNE reaction, either by using a chiral auxiliary or catalyst, by contrast, has so far remained a challenge (Scheme 1a).^{3,5}

From a mechanistic viewpoint, the Brønsted acid-mediated DNE reaction is thought to involve initial protonation of the alcohol motif in the electron-rich substrate by the catalyst (Scheme 1a). This is followed by elimination of a molecule of water to give the substrate cation, with one or more of the remaining pendant electron-rich (hetero)aryl or vinyl groups facilitating the dehydration step by stabilizing the putative carbocationic species. Subsequent 4π conrotatory electrocyclic cyclization would then deliver the cyclopenta-1,3-dienyl ring system with product enantioselectivity believed to be determined by this latter step. However, this has often been thought to be challenging due to the limited stereoelectronic interactions creating a poorly defined stereochemical environment in the proposed acyclic precursor I shown in Scheme 1a.⁴ⁱ In this context, we were drawn to the potential enantioselective DNE chemistry of this compound class with a pendant amino group catalyzed by a chiral Brønsted acid (BAH*, Scheme 1b).^{1,6} We reasoned this would provide the corresponding intimate ion-pair species II in which the amino group of the associated cation of the substrate and anion of the chiral

Scheme 1. Nazarov Cyclization and DNE of Divinyl and (Hetero)aryl Vinyl Ketones and Alcohols



Received: February 28, 2018

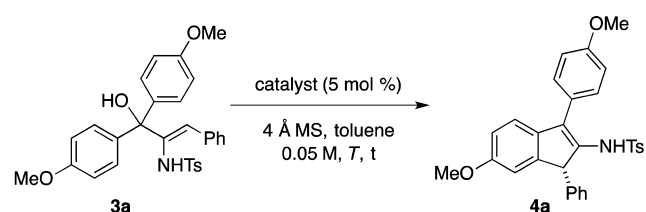
Published: April 9, 2018

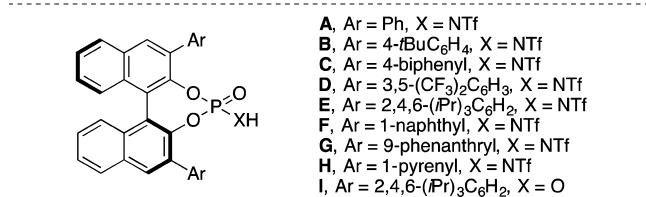
catalyst can additionally participate in hydrogen bonding interactions. With the chiral Brønsted acid anion now occupying one face of the substrate cation as a result, this might then allow asymmetric induction in the ensuing pericyclic reaction step to be accomplished to give the pentacyclic product in an enantioselective manner. Herein, we report the details of this study that offers an expedient route to these two potentially useful members of the 1*H*-indene and 4*H*-cyclopenta[*b*]thiophene compound family in excellent yields and enantioselectivities.⁷ A density functional theory (DFT) calculation on the origin of the observed product enantioselectivities is also presented.

RESULTS AND DISCUSSION

We began our studies by examining the chiral Brønsted acid-mediated enantioselective DNE of **3a** to establish the optimum reaction conditions (Table 1). This initially revealed subjecting the substrate to 5 mol % of chiral *N*-triflyl phosphoramidate (**S**)-**A**, 4 Å molecular sieves (MS) in toluene at 25 °C for 1 h gave **4a** in 95% yield and an ee value of 63% (entry 1). The structure and absolute stereochemistry of the carbocyclic adduct was determined by NMR measurements and X-ray crystallographic

Table 1. Optimization of the Reaction Conditions for the Chiral Brønsted Acid-Mediated Asymmetric DNE of **3a**^a





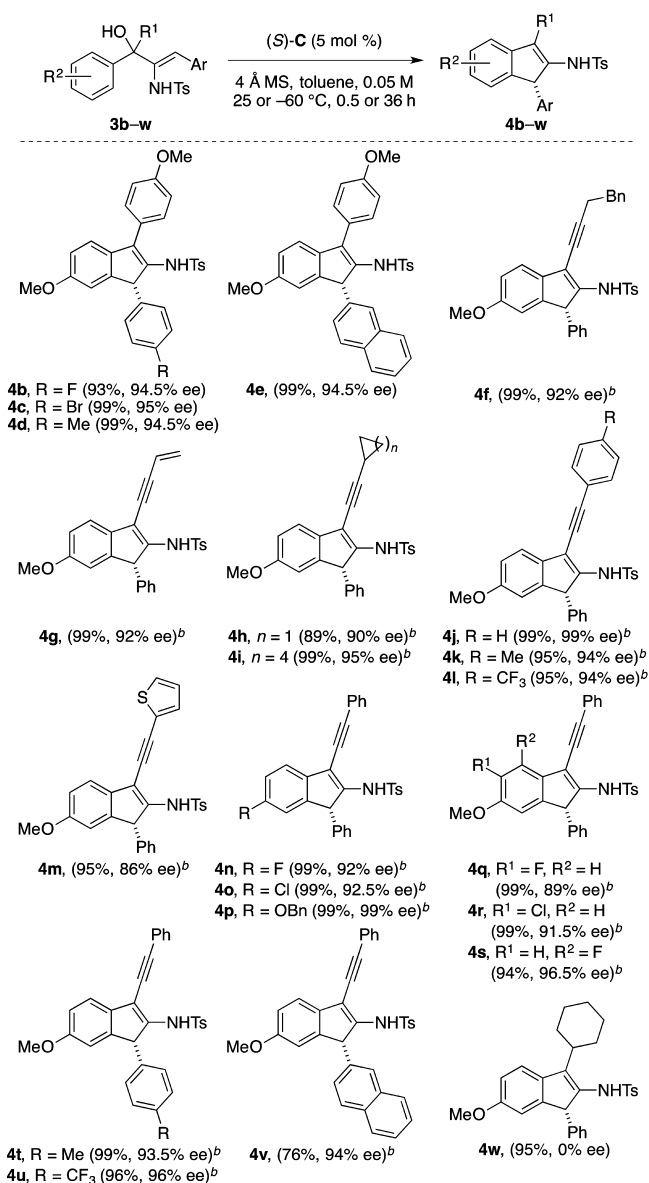
entry	catalyst	T (°C)	t (h)	yield (%) ^b	ee (%) ^c
1	(<i>S</i>)- A	25	1	95	63
2	(<i>S</i>)- B	25	1	95	35
3	(<i>S</i>)- C	25	1	99	73
4 ^d	(<i>S</i>)- C	25	1	92	40
5 ^e	(<i>S</i>)- C	25	1	94	45
6	(<i>S</i>)- C	−40	24	94	91
7	(<i>S</i>)- C	−60	36	95	95
8	(<i>S</i>)- C	−78	48	82	82
9	(<i>S</i>)- D	25	1	93	30
10	(<i>S</i>)- E	25	12	97	58
11	(<i>S</i>)- F	25	1	74	66
12	(<i>S</i>)- G	25	1	99	60
13	(<i>S</i>)- H	25	1	97	54
14	(<i>S</i>)- I	25	24	— ^f	—

^aAll reactions were performed at the 0.1 mmol scale with 5 mol % of catalyst, 4 Å MS (100 mg) in toluene (2 mL) at given temperature and time. ^bIsolated yield. ^cee values were determined using an AD-H chiral column (eluent: *n*-hexane:*i*-PrOH = 9:1). ^dReaction conducted with CH₂Cl₂ as the solvent. ^eReaction conducted with (CH₂Cl)₂ as the solvent. ^fNo reaction detected by TLC analysis and ¹H NMR measurements with recovery of **3a** in 99% yield.

analysis of two closely related products *vide infra*.⁸ An examination of other chiral Brønsted acid catalysts showed the performance of (*S*)-**B**, (*S*)-**C**, (*S*)-**D**, (*S*)-**E**, (*S*)-**F**, (*S*)-**G** and (*S*)-**H** for 1–12 h gave product yields of 74–99% along with ee values of 30–73% (entries 2, 3, and 9–13). Likewise, the analogous control reactions mediated by (*S*)-**C** in which toluene was replaced by dichloromethane or 1,2-dichloroethane as the solvent were found to give product yields of 92 and 94% along with ee values of 40 and 45%, respectively (entries 4 and 5). Our subsequent studies found that repeating the (*S*)-**C**-catalyzed reaction in toluene as the solvent at −60 °C for 36 h gave the best result, providing the 1*H*-indene product in 95% yield and 95% ee (entry 7). However, increasing the reaction temperature to −40 °C for 24 h or decreasing it to −78 °C for 48 h was found to lead to slightly lower product yields of 94 and 82% and ee values of 91 and 82%, respectively (entries 6 and 8). In a final control experiment with the less acidic chiral phosphoric acid (*S*)-**I** as the catalyst, no reaction was detected and the substrate was recovered in near quantitative yield (entry 14).

With the reaction conditions established, we next sought to evaluate the generality of the present procedure using a series of electron-rich aryl-β-amino-2-en-1-ols **3b–w** (Table 2). Overall, the (*S*)-**C**-catalyzed reaction conditions were shown to be broad, providing a family of 1*H*-indenes **4b–w** containing a variety of substitution patterns in excellent yields and ee values from the corresponding substrates. Reactions of starting materials with a pendant *para*-substituted electron-withdrawing phenyl (**3b,c**), *p*-tolyl (**3d**), or 2-naphthyl (**3e**) group at the alkenyl carbon center were found to react well, giving **4b–e** in 93–99% yield and 94.5–95% ee. Likewise, electron-rich substrates containing an acetylenic motif with a phenethyl (**3f**), vinyl (**3g**), cycloalkyl (**3h,i**), aryl (**3j–l**), or 2-thienyl (**3m**) substituent in place of a *p*-anisyl group were found to have minimal influence on the outcome of the reaction. In these experiments, which could be conducted at 25 °C, the corresponding 1*H*-indene products **4f–m** were afforded in 89–99% yield and 86–99% ee with the (8*R*) absolute configuration of **4j** established by X-ray crystallography.⁸ Added to this, starting 1,4-enynols containing an aryl motif with electron-donating and/or -withdrawing substituent at various positions of the ring at the carbinol or alkynyl carbon center, as in **3n–v**, gave the corresponding carbocycles **4n–v** in 76–99% yield and 89–99% ee. The reaction of **3w** containing a cyclohexyl motif at the carbinol carbon center was the only instance to give the corresponding 1*H*-indene adduct **4w** as a racemate in 95% yield.

Having established the generality of the reaction conditions that gave 1*H*-indenes, we next examined the scope of the methodology for the enantioselective synthesis of 4*H*-cyclopenta[*b*] fused heterocycles (Table 3). With this in mind, the (*S*)-**C**-mediated enantioselective DNE of electron-rich 2-thienyl-substituted 1,4-enynols **3x–α** in which the alkyne motif contained an aryl group were first examined. This led us to find that the corresponding *S*-heterocycles **4x–α** could be furnished in 82–91% yield and 83–88% ee. Under similar conditions, the reaction of substrates with a pendant 7-methoxy-2-naphthyl (**3β**) or 2-thienyl (**3γ**) on the acetylenic carbon center gave **4β** and **4γ** in respective yields of 88 and 84% and ee values of 91 and 89%. The reactions of substrates containing a 2-benzothienyl (**3δ**) or *N*-methyl indolyl (**3ε**) group in place of the 2-thienyl moiety at the carbinol carbon center were observed to be the only exception. In these

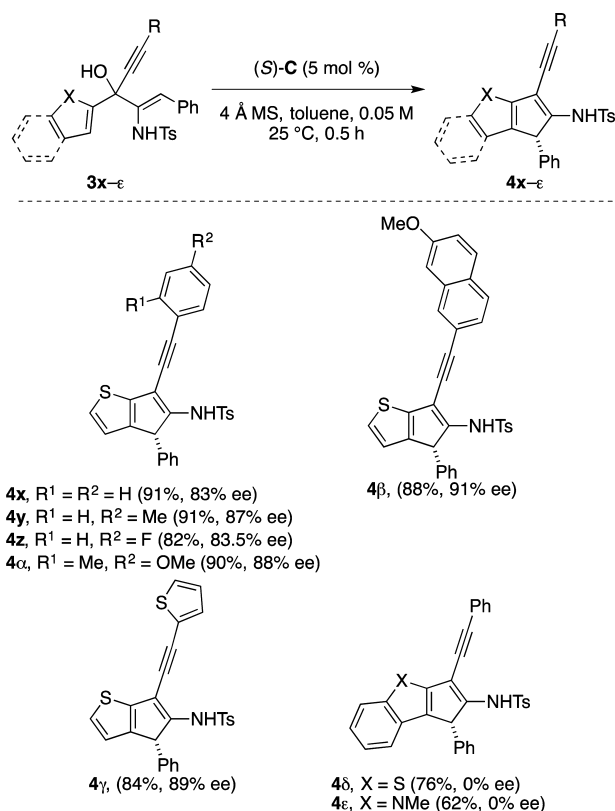
Table 2. Enantioselective DNE of Aryl- β -amino-2-en-1-ols 3b-w Catalyzed by (S)-C^a

^aAll reactions were performed at the 0.1 mmol scale with 5 mol % of (S)-C, 4 Å MS (100 mg) in toluene (2 mL) at -60 °C for 36 h. Values in parentheses denote isolated product yields and ee values determined using an AD-H chiral column (eluent: *n*-hexane:*i*PrOH = 9:1).

^bReaction conducted at 25 °C for 0.5 h.

experiments, the corresponding tricyclic adducts **4d** and **4e** were afforded as a racemate in respective yields of 76 and 62%. On the other hand, in all the above experiments, no other cyclic adducts that could be formed from competitive arylation of the aryl vinyl group of the substrate or product isomerization was detected by ¹H NMR analysis of the crude mixtures.

A tentative mechanistic rationale for the origin of the product enantioselectivities obtained in the present chiral Brønsted acid-catalyzed asymmetric DNE reactions is presented in Figure 1. Using **3j** as a representative example, this might initially involve protonation of the substrate by the chiral Brønsted acid to give the carbocationic species **Ij** and **Ij'** and the catalyst anion (S)-C' on release of a molecule of water. Building on the premise put forward in Scheme 1b that chiral induction might then be

Table 3. Enantioselective DNE of 2-Heteroaryl- β -amino-2-en-1-ols 3x-ε Catalyzed by (S)-C^a

^aAll reactions were performed at the 0.1 mmol scale with 5 mol % of (S)-C, 4 Å MS (100 mg) in toluene (2 mL) at 25 °C for 36 h. Values in parentheses denote isolated product yields and ee values, determined using an AD-H chiral column (eluent: *n*-hexane:*i*PrOH = 9:1).

achieved in the ion-pair species forming step, this would give the four possible conformers **IIj_a**, **IIj_b**, **IIj'_a** and **IIj'_b**. In all four cases, we surmise that the amino motif hydrogen atom in the ion-pair species acts as a directing group through its ability to hydrogen bond with the catalyst anion, thereby determining whether it sits on the *re* or *si* face of the substrate cation. For **IIj_a**, clockwise 4 π conrotatory electrocyclization of the ion-pair species would lead to **IIIj_a** being formed with the resulting acidic aryl proton (labeled red in Figure 1a) and chiral Brønsted acid anion positioned on the same face of the cyclic adduct. This is important as we reason it would permit the facile deprotonation and rearomatization of the Wheland-type intermediate **IIIj_a** by the chiral Brønsted acid anion to deliver the product (R)-**4j**.⁹ Conversely, the counterclockwise pericyclic reaction of **IIj_b** would give **IIIj_b**, whereby the acidic aryl proton and chiral Brønsted acid anion are now situated on the opposite faces of the carbocyclic cation. As a consequence, this might prevent the deprotonation step from occurring and the formation of this cyclic carbocation is anticipated to lead to a dead end unless it undergoes the reverse reaction. A second possibility is that intermediate **IIIj_b** could be deprotonated if water serves as a base, the ability of which is dependent on the size of the water cluster (H₂O)_n involved in the process. However, this was thought to be less likely based on our experience predicting such deprotonations to require an activation energy of ca. 17 kcal/mol, which is higher than that required for the conversion of **IIj_a** → **IIIj_a** vide infra. As

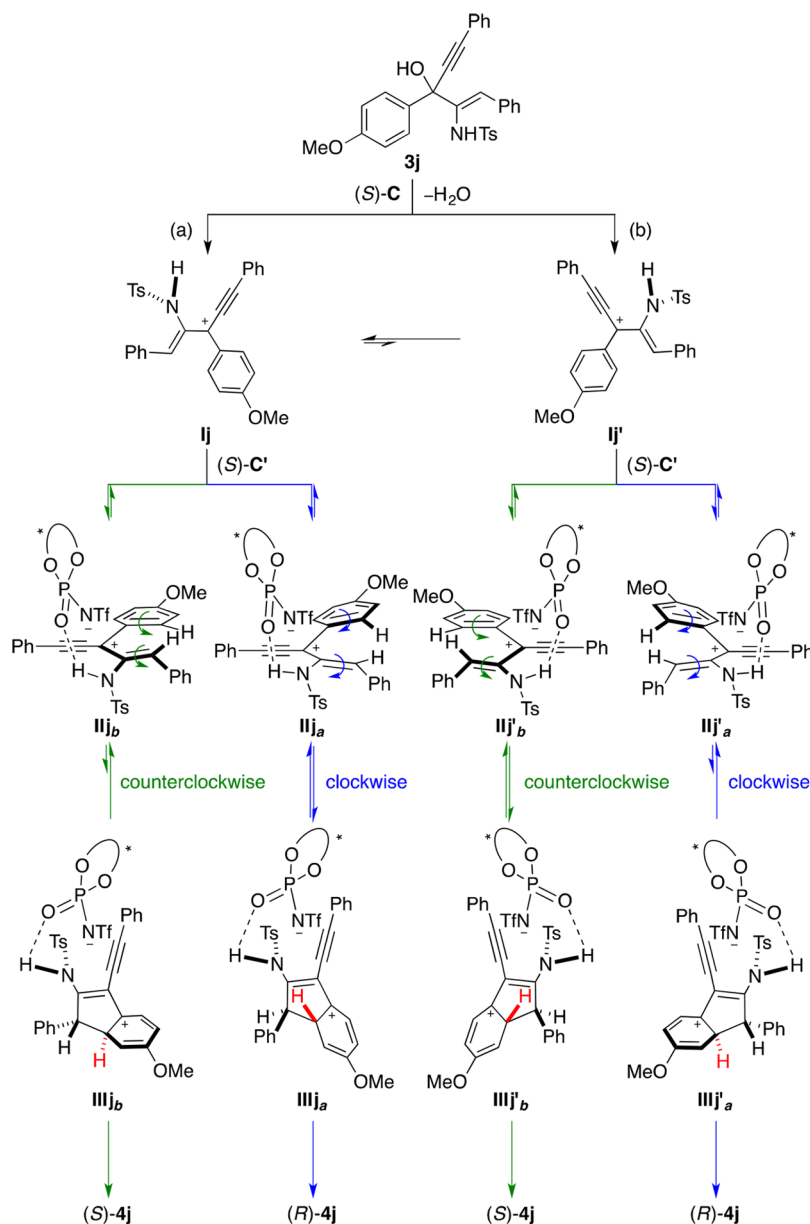
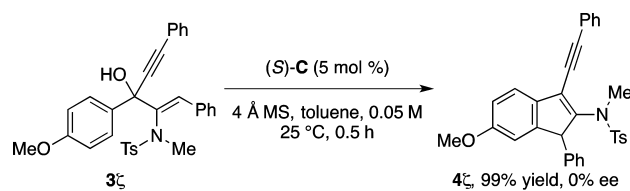


Figure 1. Proposed mechanistic rationale for the product enantioselectivities obtained for the (S)-C-catalyzed asymmetric DNE of electron-rich aryl- and 2-thienyl- β -amino-2-en-1-ols represented by **3j**.

illustrated in Figure 1b for the pathways involving **IIj'_a** and **IIj'_b**, a similar rationale would account for the preferential outcome of the enantiomer (S)-**4j**. In this regard, our hypothesis predicts that product formation can only come from pathways involving the ion-pair species **IIIj_a** and **IIIj'_b**, with the dominant ion-pair species in solution being the former in view of a product ee value of 99%. It also implies that the catalyst anion may not preferentially occupy one face of the substrate cation in an ion-pair species containing a tertiary amino substituent. In the absence of the directing group, this might subsequently allow both the clockwise and counter-clockwise pericyclic reaction pathways to be operative in equal measure and give the product as a racemate. Consistent with this are our findings in a control reaction with the *N,N*-disubstituted substrate **3ζ** under the (S)-C-catalyzed conditions described in Scheme 2, which gave **4ζ** in 99% yield and 0% ee. The posited involvement of the ion-pair species **II** would explain the marked differences in product ee values obtained for

Scheme 2. Control Experiment with **3ζ**



the reactions of **3a** in toluene, dichloromethane and 1,2-dichloroethane detailed in Table 1, entries 3–5. It might be expected that is an increase in interactions between the substrate cation and catalyst anion with the reaction medium as the solvent dielectric constant (ϵ) increases on going from toluene ($\epsilon = 2.4$, 290 K) to dichloromethane ($\epsilon = 9.2$, 288 K) and 1,2-dichloroethane ($\epsilon = 11.0$, 288 K).¹⁰ As a consequence, this may disrupt the ability of the substrate cation and catalyst anion to form a tight ion-pair species, resulting in a decrease in

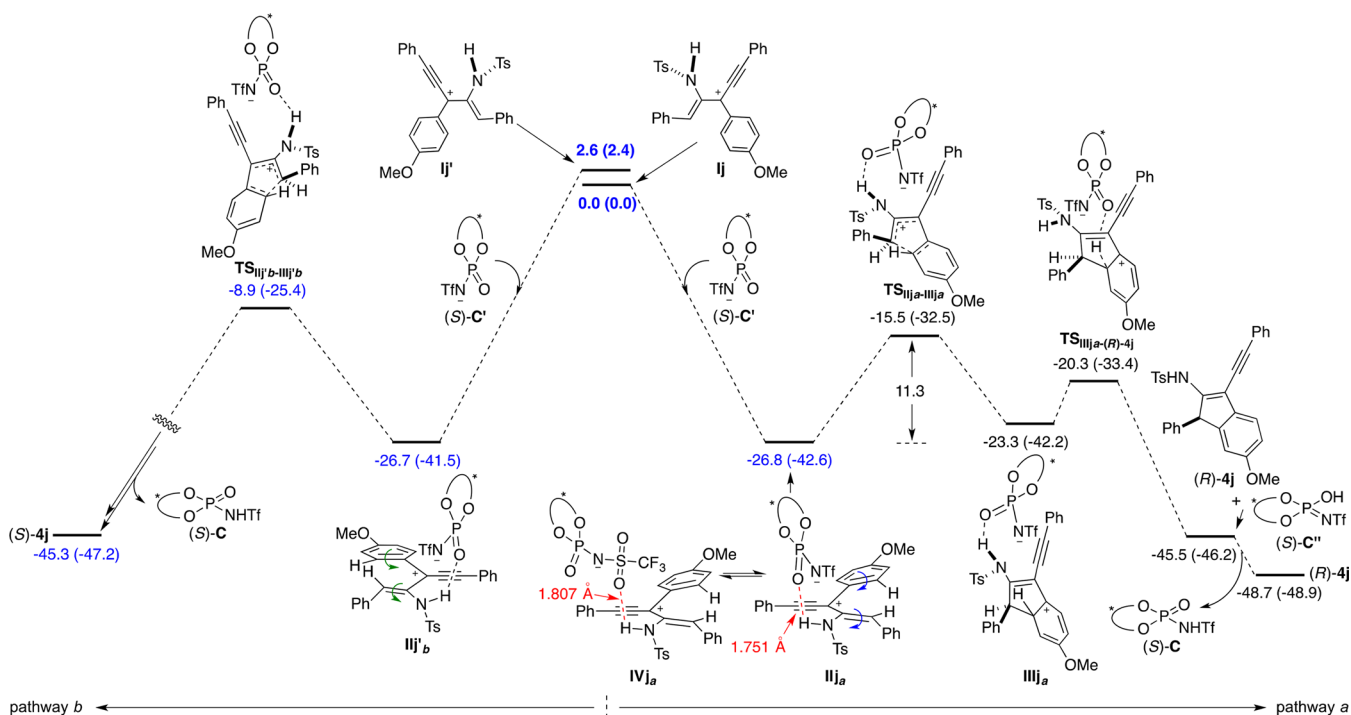


Figure 2. Energy profile of pathways *a* and *b* for the (*S*)-*C*-catalyzed enantioselective DNE of **3j** to (*R*)-**4j** and (*S*)-**4j**, respectively. Structures **IIj** and **IVj** show short $\text{P}=\text{O} \cdots \text{HN}$ and $\text{S}=\text{O} \cdots \text{HN}$ interactions (1.751, 1.807 Å) that indicate hydrogen bonding. The relative Gibbs and potential energies (in parentheses) obtained from M06-CPCM/6-31+G(d,p)//B3LYP-CPCM/6-31G(d) calculations are given in kcal/mol and bond lengths in Å.

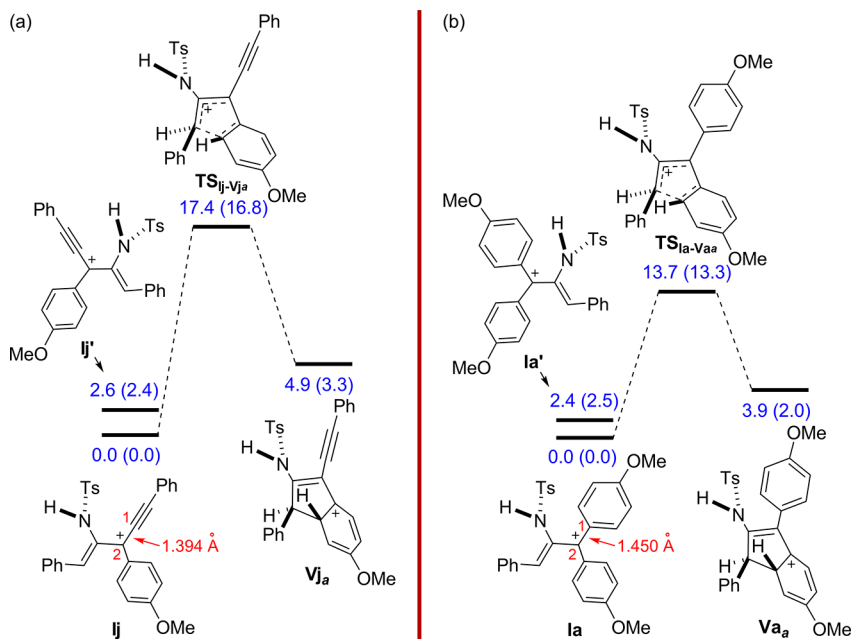


Figure 3. Energy profiles for the 4π conrotatory electrocyclicization step of (a) **3j** and (b) **3a** in the absence of (*S*)-*C*. The relative Gibbs and potential energies (in parentheses) obtained from M06-CPCM/6-31+G(d,p)//B3LYP-CPCM/6-31G(d) calculations are given in kcal/mol and bond lengths in Å.

product ee values. We reason a similar rationale could be in play in the reactions of **3w**, **3d** and **3e** that led to the corresponding products being obtained as a racemate. The presence of a bulky cyclohexyl or benzofused ring in these substrates might provide sufficient unfavorable steric interactions to prevent the substrate cation and catalyst anion forming the requisite intimate ion-pair species **II**.

To verify the proposed mechanistic rationale for the observed product enantioselectivities outlined in Figure 1, we performed a series of DFT calculations. As summarized in Figure 2, a number of transition states and intermediates were produced in the two possible reaction pathways *a* and *b* from **Ij** and **Ij'** to the corresponding (*R*) and (*S*) enantiomers of **4j**. On the basis of these calculations, pathway *a* was revealed to be favored with rotation from **Ij** to **Ij'** shown to be endergonic by

2.6 kcal/mol. Accordingly, the latter conformer was found to be sparsely populated, which is in good agreement with our experimental findings showing (*R*)-**4j** being afforded in 99% ee. This was followed by the interaction of the substrate cation with (*S*)-**C'**, which lowers the energy of the carbocationic species by >26 kcal/mol. As such, the ensuing ion-pair species **IIj_a** functioned as a thermodynamic sink that prevented interconversion between the two substrate cation conformers. In the ion-pair species, the chiral Brønsted acid anion was found to be located on the *re* face of the substrate cation due to hydrogen bonding interactions between the former and the latter, as evidenced by a P=O...HN bond distance of 1.751 Å. The ion-pair species **IVj_a** depicted in Figure 2, the most stable among other possible interactions, was also considered. However, this latter hydrogen bonded ion-pair species was thought to be less likely as it was found to be 5.4 kcal/mol less stable and had a slightly longer S=O...HN bond distance of 1.807 Å. Our calculations further suggested clockwise 4 π conrotatory electrocyclization of **IIj_a** to **IIIj_a** occurred through **TS_{IIj_a-IIIj_a}** with an energy barrier of 11.3 kcal/mol. For the reaction steps after the formation of the Wheland-type intermediate **IIIj_w**, the Brønsted acid anion was found to play a crucial role in the deprotonation of the adduct. By accepting the aryl proton sitting on the same face of the catalyst anion, this provided the product (*R*)-**4j** and (*S*)-**C''** via **TS_{IIIj_a-(R)-4j}** with an energy barrier of 3.0 kcal/mol. This implied that the rearomatization process was more facile than the preceding carbocyclic ring forming step. Regeneration of the chiral Brønsted acid catalyst was readily achieved through tautomerization of (*S*)-**C''**, which was found to be exergonic by 3.2 kcal/mol.

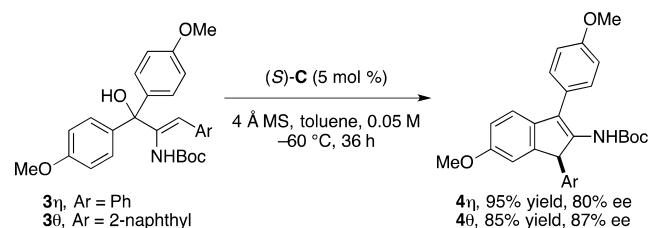
In a second set of calculations in the absence of (*S*)-**C**, the activation energy required for the 4 π electrocyclization step was demonstrated to increase by 6.1 kcal/mol, as shown in Figure 3a. This suggested that the interaction between the cation of the substrate and the anion of the catalyst in **TS_{IIj_a-IIIj_a}** was stronger than that in **IIj_a**. Repeating these calculations for **3a** in the absence of the Brønsted acid revealed the pericyclic reaction step required an activation energy of 13.7 kcal/mol (Figure 3b). This implied that **3a** was intrinsically more reactive than **3j** toward carbocyclic ring formation and is in good agreement with the need for lower experimental temperatures of -60 °C to achieve chiral induction in such diaryl-substituted substrates. The source of this greater reactivity was attributed to the steric demand of the aryl ring limiting its ability to stabilize the cationic charge by π -conjugation in **1a**, as corroborated by the much longer C1–C2 bond distance in the carbocation species than in **1j** (cf. Figures 3a and 3b). As with **3j**, the experimentally observed product enantioselectivity obtained from **3a** was found to be a result of conformer **1a** being 2.4 kcal/mol more stable than that of conformer **1a'**.

In a final set of calculations, the Gibbs energy on forming **IVj_a** from **Ij** and (*S*)-**C'** was determined to be -13.3 and -30.8 kcal/mol at the B3LYP-CPCM/6-31+G(d,p)//B3LYP-CPCM/6-31G(d) and B3LYP-D3-CPCM/6-31+G(d,p)//B3LYP-CPCM/6-31G(d) level, respectively. While the analogous calculations could not be accomplished for the formation of **IIj_w**, these findings nonetheless indicated that the dispersive interactions implied in Scheme 1b are operative and play a key role in the stability of the ion-pair species.

Interestingly, our DFT studies also revealed that if the stereoelectronic nature of the amino substituent in the substrate was changed by replacing the *N*-Ts motif with a *N*-Boc group,

as in **3η** shown in Scheme 3 and Figure S1 in the Supporting Information (SI), a switch in the stereochemical outcome of the

Scheme 3. (*S*)-**C**-Catalyzed Asymmetric DNE of **3η** and **3θ**



reaction should be observed. Calculations for the substrate in the absence of (*S*)-**C** at the M06-CPCM/6-31+G(d,p)//B3LYP-CPCM/6-31G(d) and B3LYP-CPCM/6-311+G(d,p)//B3LYP-CPCM/6-31G(d) level found **1η'** to be more stable than **1η** by 0.5 and 1.9 kcal/mol, respectively, which implied the (*S*)-enantiomer would be afforded as the major product. Pleasingly, this was supported by our subsequent findings in experiments with **3η** and its 2-naphthyl substituted analogue **3θ** catalyzed by (*S*)-**C** under the conditions described in Scheme 3. In these test reactions, the corresponding 1*H*-indene adducts **4η** and **4θ** were furnished in respective yields of 95 and 85% and ee values of 80 and 87% with the (*S*)-absolute configuration of the former ascertained by X-ray crystallography.⁸

CONCLUSIONS

In summary, we have developed a chiral Brønsted acid-catalyzed method for the asymmetric synthesis of 1*H*-indenes and 4*H*-cyclopenta[*b*]thiophenes from the respective electron-rich aryl- and 2-thienyl- β -amino-2-en-1-ols. The excellent product ee values were achieved by realizing the first example of an enantioselective DNE from a posited chiral ion-pair species to asymmetrically assemble the bicyclic ring system. Our studies suggest the origin of the observed product enantioselectivity was initially due to the more stable conformation of the substrate cation. The ensuing ion-pair species then acted as a thermodynamic sink to prevent interconversion between these two conformers. Also instrumental was the role of the amino group in the substrate cation in directing the chiral catalyst anion to preferentially sit on one face of the adduct and the ability of the latter to efficiently facilitate rearomatization to give the product. We envision that the present synthetic method will encourage the further development of asymmetric strategies in reactions where there is such intrinsic low directionality through the installation of a directing group.

EXPERIMENTAL SECTION

General Considerations. All reactions were performed in oven-dried glassware under a nitrogen atmosphere. Unless specified, all reagents and starting materials were purchased from commercial sources and used as received. The chalcones used in the synthesis of substrates **3** and chiral Brønsted acids **A–I** were prepared following literature procedures.^{11,12} Toluene was freshly distilled from sodium/benzophenone. Analytical thin layer chromatography (TLC) was performed using precoated silica gel plate. Visualization was achieved by UV light (254 nm). Flash chromatography was performed using silica gel and gradient solvent system (*n*-hexane:EtOAc as the eluent). ¹H and ¹³C NMR spectra were recorded on 300 and 400 MHz spectrometers. Chemical shifts (ppm) were recorded with tetrame-

thylsilane (TMS) as the internal reference standard. Multiplicities are given as s (singlet), br s (broad singlet), d (doublet), t (triplet), dd (doublet of doublets) or m (multiplet). The number of protons (*n*) for a given resonance is indicated by *n*H and coupling constants are reported as a *J* value in Hz. Infrared spectra were taken on a IR spectrometer. High resolution mass spectra (HRMS) were obtained on a LC/HRMS TOF spectrometer using simultaneous electrospray (ESI). Ee values were determined by high performance liquid chromatography (HPLC) analysis using a AD-H column. Optical rotations were measured in CHCl₃ on a polarimeter with a sodium vapor lamp at 589 nm and 10 cm cell (*c* given in g/100 mL).

General Procedure for (S)-C-Catalyzed Asymmetric DNE of Aryl Vinyl Alcohols 3a–3e, 3*η*, 3*θ* and 3*ω*. To a round-bottom flask was charged the substrate (0.1 mmol), chiral Brønsted acid (S)-C (3.9 mg, 0.005 mmol, 5 mol %) and 4 Å MS (100 mg) followed by the addition of toluene (2 mL) at –60 °C. The reaction mixture was stirred at this temperature for 36 h. On completion, the reaction mixture was quenched with NaHCO₃ (8.4 mg, 0.1 mmol). After warming to room temperature, the reaction mixture was directly passed through a silica gel column (eluent: *n*-hexane/EtOAc = 8:1) to give the title compound.

General Procedure for (S)-C-Catalyzed Asymmetric DNE of Aryl Vinyl Alcohols 3*f*–3*v* and 3*x*–3*z*. To a round-bottom flask was charged the substrate (0.1 mmol), chiral Brønsted acid (S)-C (3.9 mg, 0.005 mmol, 5 mol %) and 4 Å MS (100 mg) followed by the addition of toluene (2 mL) at 25 °C. The reaction mixture was allowed to stir at room temperature for 30 min. Upon completion, the reaction mixture was directly passed through a silica gel column (eluent: *n*-hexane/EtOAc = 8:1) to give the title compound.

■ ASSOCIATED CONTENT

■ Supporting Information

The Supporting Information is available free of charge on the ACS Publications website at DOI: 10.1021/jacs.8b02339.

Crystal data for 4*j* (CIF)

Crystal data for 4*η* (CIF)

Detailed experimental procedures, characterization data and ¹H and ¹³C NMR spectra for all starting materials and products, raw DFT data, XYZ coordinates (PDF)

■ AUTHOR INFORMATION

Corresponding Authors

*alireza.ariafard@utas.edu.au

*phil.chan@monash.edu; p.w.h.chan@warwick.ac.uk

ORCID

Philip Wai Hong Chan: 0000-0002-8786-6143

Notes

The authors declare no competing financial interest.

■ ACKNOWLEDGMENTS

This work was supported by a Discovery Project Grant (DP160101682) from the Australian Research Council.

■ REFERENCES

(1) Selected reviews on Nazarov and Nazarov-type cyclizations: (a) Simeonov, S. P.; Nunes, J. P. M.; Guerra, K.; Kurteva, V. B.; Afonso, C. A. M. *Chem. Rev.* **2016**, *116*, 5744. (b) Di Grandi, M. *Org. Biomol. Chem.* **2014**, *12*, 5331. (c) Tius, M. A. *Chem. Soc. Rev.* **2014**, *43*, 2979. (d) Spencer, W. T.; Vaidya, T.; Frontier, A. J. *Eur. J. Org. Chem.* **2013**, *2013*, 3621. (e) Naoyuki, S.; Craig, S.; Tius, M. A. *Tetrahedron* **2011**, *67*, 5851. (f) Thompson, S.; Coyne, A. G.; Knipe, P. C.; Smith, M. D. *Chem. Soc. Rev.* **2011**, *40*, 4217. (g) Vaidya, T.; Eisenberg, R.; Frontier, A. J. *ChemCatChem* **2011**, *3*, 1531. (h) Grant, T. N.; Rieder, C. J.; West, F. G. *Chem. Commun.* **2009**, 5676. (i) Nakanishi, W.; West, F. G. *Curr. Opin. Drug Discovery Devel.* **2009**,

12, 732. (j) Frontier, A. J.; Collison, C. *Tetrahedron* **2005**, *61*, 7577. (k) Habermas, K. L.; Denmark, S. E.; Jones, T. K. In *Organic Reactions*; Paquette, L. A., Ed.; John Wiley & Sons: New York, 1994, Vol. 45, pp 1–158.

(2) Selected recent examples: (a) Krieger, J.; Smeilus, T.; Schackow, O.; Giannis, A. *Chem. - Eur. J.* **2017**, *23*, 5000. (b) Tang, M. L.; Peng, P.; Liu, Z. Y.; Zhang, J.; Yu, J. M.; Sun, X. *Chem. - Eur. J.* **2016**, *22*, 14535. (c) Rao, W.; Boyle, J. W.; Chan, P. W. H. *Chem. - Eur. J.* **2016**, *22*, 6532. (d) Chen, X.; Day, D. P.; Teo, W. T.; Chan, P. W. H. *Org. Lett.* **2016**, *18*, 5936. (e) Marques, A. S.; Coeffard, V.; Chataigner, I.; Vincent, G.; Moreau, X. *Org. Lett.* **2016**, *18*, 5296. (f) Huang, Y. W.; Frontier, A. J. *Org. Lett.* **2016**, *18*, 4896. (g) Asari, A. H.; Lam, Y. H.; Tius, M. A.; Houk, K. N. *J. Am. Chem. Soc.* **2015**, *137*, 13191. (h) Susanti, D.; Liu, L.-J.; Rao, W.; Lin, S.; Ma, D.-L.; Leung, C.-H.; Chan, P. W. H. *Chem. - Eur. J.* **2015**, *21*, 9111. (i) Rao, W.; Susanti, D.; Ayers, B. J.; Chan, P. W. H. *J. Am. Chem. Soc.* **2015**, *137*, 6350. (j) Wu, Y. K.; Dunbar, C. R.; McDonald, R.; Ferguson, M. J.; West, F. G. *J. Am. Chem. Soc.* **2014**, *136*, 14903. (k) Vaidya, T.; Cheng, R.; Carlsen, P. N.; Frontier, A. J.; Eisenberg, R. *Org. Lett.* **2014**, *16*, 800. (l) Rao, W.; Koh, M. J.; Li, D.; Hirao, H.; Chan, P. W. H. *J. Am. Chem. Soc.* **2013**, *135*, 7926.

(3) Selected examples of asymmetric Nazarov cyclizations: (a) Wang, C.-S.; Wu, J.-L.; Li, C.; Li, L.-Z.; Mei, G.-J.; Shi, F. *Adv. Synth. Catal.* **2018**, *360*, 846. (b) Wang, G.-P.; Chen, M.-O.; Zhu, S.-F.; Zhou, Q.-L. *Chem. Sci.* **2017**, *8*, 7197. (c) Yang, B.-M.; Cai, P.-J.; Tu, Y.-Q.; Yu, Z.-X.; Chen, Z.-M.; Wang, S.-H.; Wang, S.-H.; Zhang, F.-M. *J. Am. Chem. Soc.* **2015**, *137*, 8344. (d) Kitamura, K.; Shimada, N.; Stewart, C.; Atesin, A. C.; Atesin, T. A.; Tius, M. A. *Angew. Chem., Int. Ed.* **2015**, *54*, 6288. (e) Takeda, T.; Harada, S.; Nishida, A. *Org. Lett.* **2015**, *17*, 5184. (f) Zi, W.; Wu, H.; Toste, F. D. *J. Am. Chem. Soc.* **2015**, *137*, 3225. (g) Raja, S.; Nakajima, M.; Rueping, M. *Angew. Chem., Int. Ed.* **2015**, *54*, 2762. (h) William, R.; Wang, S.; Ding, F.; Arviana, E. N.; Liu, X.-W. *Angew. Chem., Int. Ed.* **2014**, *54*, 10742. (i) Jolit, A.; Walleser, P. M.; Yap, G. P. A.; Tius, M. A. *Angew. Chem., Int. Ed.* **2014**, *53*, 6180. (j) Flynn, B. L.; Manchala, N.; Krenske, E. H. *J. Am. Chem. Soc.* **2013**, *135*, 9156. (k) Hutson, G. E.; Turkmen, Y. E.; Rawal, V. H. *J. Am. Chem. Soc.* **2013**, *135*, 4988. (l) Basak, A. K.; Shimada, N.; Bow, W. F.; Vicić, D. A.; Tius, M. A. *J. Am. Chem. Soc.* **2010**, *132*, 8266. (m) Huang, J.; Frontier, A. J. *J. Am. Chem. Soc.* **2007**, *129*, 8060. (n) Dhoro, F.; Kristensen, T. E.; Stockmann, V.; Yap, G. P. A.; Tius, M. A. *J. Am. Chem. Soc.* **2007**, *129*, 7256. (o) Rueping, M.; Ieawsuwan, W.; Antonchick, A. P.; Nachtsheim, B. J. *Angew. Chem., Int. Ed.* **2007**, *46*, 2097. (p) Liang, G.; Trauner, D. *J. Am. Chem. Soc.* **2004**, *126*, 9544. (q) Aggarwal, V. K.; Belfield, A. J. *Org. Lett.* **2003**, *5*, 5075.

(4) Selected examples of achiral DNE: (a) Martin, M. C.; Sandridge, M. J.; Williams, C. W.; Francis, Z. A.; France, S. *Tetrahedron* **2017**, *73*, 4093. (b) Wang, Z.; Xu, X.; Gu, Z.; Feng, W.; Qian, H.; Li, Z.; Sun, X.; Kwon, O. *Chem. Commun.* **2016**, *52*, 2811. (c) Lempenauer, L.; Dunach, E.; Lemièrre, G. *Org. Lett.* **2016**, *18*, 1326. (d) Seema, D.; Ramasastry, S. S. V. *Org. Lett.* **2015**, *17*, 5116. (e) Riveira, M. J.; Mischne, M. P. *Chem. - Eur. J.* **2012**, *18*, 2382. (f) Usanov, D. L.; Naodovic, M.; Brasholz, M.; Yamamoto, H. *Helv. Chim. Acta* **2012**, *95*, 1773. (g) Hastings, C. J.; Backlund, M. P.; Bergman, R. G.; Raymond, K. N. *Angew. Chem., Int. Ed.* **2011**, *50*, 10570. (h) Rieder, C. J.; Winberg, K. L.; West, F. G. *J. Org. Chem.* **2011**, *76*, 50. (i) Smith, C. D.; Rosocha, G.; Mui, L.; Batey, R. A. *J. Org. Chem.* **2010**, *75*, 4716. (j) Hastings, C. J.; Pluth, M. D.; Bergman, R. G.; Raymond, K. N. *J. Am. Chem. Soc.* **2010**, *132*, 693. (k) Cordier, P.; Aubert, C.; Malacria, M.; Lacote, E.; Gandon, V. *Angew. Chem., Int. Ed.* **2009**, *48*, 8757.

(5) Examples of other chiral Brønsted acid-catalyzed asymmetric 4*π* electrocyclizations: (a) Li, H.; Tong, R.; Sun, J. *Angew. Chem., Int. Ed.* **2016**, *55*, 15125. (b) Cai, Y.; Tang, Y.; Atodiresse, I.; Rueping, M. *Angew. Chem., Int. Ed.* **2016**, *55*, 14126. (c) Sun, F.-L.; Zeng, M.; Gu, Q.; You, S.-L. *Chem. - Eur. J.* **2009**, *15*, 8709.

(6) Selected reviews on chiral Brønsted acid catalysis: (a) Merad, J.; Lalli, C.; Bernadat, G.; Maury, J.; Masson, G. *Chem. - Eur. J.* **2018**, *24*, 3925. (b) James, T.; van Gemmeren, M.; List, B. *Chem. Rev.* **2015**, *115*, 9388. (c) Akiyama, T.; Mori, K. *Chem. Rev.* **2015**, *115*, 9277. (d) Zhu, C.; Saito, K.; Yamanaka, M.; Akiyama, T. *Acc. Chem. Res.* **2015**, *48*,

388. (e) Parmar, D.; Sugiono, E.; Raja, S.; Rueping, M. *Chem. Rev.* **2014**, *114*, 9047. (f) Mahlau, M.; List, B. *Angew. Chem., Int. Ed.* **2013**, *52*, 518. (g) Cheon, C. H.; Yamamoto, H. *Chem. Commun.* **2011**, 47, 3043. (h) Terada, M. *Synthesis* **2010**, 2010, 1929. (i) Terada, M. *Chem. Commun.* **2008**, 4097.

(7) Selected examples: (a) Oh, D. C.; Williams, P. G.; Kauffman, C. A.; Jensen, P. R.; Fenical, W. *Org. Lett.* **2006**, *8*, 1021. (b) Clegg, N. J.; Paruthiyil, S.; Leitman, D. C.; Scanlan, T. S. *J. Med. Chem.* **2005**, *48*, 5989. (c) Blizzard, T. A.; Morgan, J. D., II; Mosley, R. T.; Birzin, E. T.; Frisch, K.; Rohrer, S. P.; Hammond, M. L. *Bioorg. Med. Chem. Lett.* **2003**, *13*, 479. (d) Cosenzi, A. *Cardiovasc. Drug Rev.* **2003**, *21*, 1. (e) Lin, W. H.; Fang, J. M.; Cheng, Y. S. *Phytochemistry* **1995**, *40*, 871.

(8) See Figures S100 and S101 in the SI for the ORTEP drawings of the crystal structures for **4j** and **4n**.

(9) Wheland, G. W. *J. Am. Chem. Soc.* **1942**, *64*, 900.

(10) Wohlfarth, C. In *Supplement to IV/6. Landolt-Börnstein-Group IV Physical Chemistry (Numerical Data and Functional Relationships in Science and Technology)*; Lechner, M., Ed.; Springer: Berlin, Heidelberg, 2008; Vol. 17.

(11) (a) Kong, L. M.; Han, X. Y.; Jiao, P. *Chem. Commun.* **2014**, 50, 14113. (b) Rueping, M.; Nachtsheim, B. J.; Koenigs, R. M.; Ieawsuwan, W. *Chem. - Eur. J.* **2010**, *16*, 13116. (c) Nakashima, D.; Yamamoto, H. *J. Am. Chem. Soc.* **2006**, *128*, 9626.

(12) (a) Zhang, X.; Kang, J.; Niu, P.; Wu, J.; Yu, W.; Chang, J. *J. Org. Chem.* **2014**, *79*, 10170. (b) Chang, M. Y.; Chen, Y. C.; Chan, C. K. *Tetrahedron* **2014**, *70*, 2257.